2015

Zircon Geochronology and Tectonic Evolution of Eclogites from the Beishan and Qinling Orogens, China

Wanchese M. Saktura

Zircon Geochronology and Tectonic Evolution of Eclogites from the Beishan and Qinling Orogens, China

Abstract

Central Asia is host to some of the best examples of ultra-high pressure metamorphic rocks in the world. The study sites located in Beishan and Qinling Orogens contain examples of these high pressure rocks, called eclogites. They are an evidence of ancient continental collisions and their age and composition provide invaluable information about tectonic mechanics during collisions. This study focuses on geochronology of eclogites sampled from Beishan and Qinling Orogens. The Beishan eclogite, occurs as small mafic pods within highly deformed gneisses. The geological context and geochemistry of these eclogites determined in this study suggests they were originally rift-related MORB-type basalts rather than discrete fragments of oceanic crust, as previously thought.

Zircon dates obtained from the Beishan eclogite reveal peak metamorphism at 466 ± 27 Ma, which is concordant with the literature. However, U/Th ratios in zircon cores (ca. 880 Ma) are too low to have crystallized from mafic magma and therefore represent xenocrystic cores or previous metamorphic event rather than age of the protolith. The maximum age of the eclogite protolith is constrained by the crystallization age of the country rock orthogneiss at 920 ± 14 Ma. The end of retrogression metamorphism in the studied terrane was constrained by granitic vein that intruded the eclogite at 424 ± 8.6 Ma. This study provides the age for this rock for the first time. From evidence gathered for Beishan Orogen, this study proposes new tectonic model for initial stage of orogen development.

The Qinling eclogites did not yield significant amount of zircons, so they could not be dated with certainty. One zircon was dated at 490 ± 83 Ma which is consistent with metamorphic age established in literature, but statistically they cannot be used as a reliable age. However, its remarkably well-preserved eclogite facies mineral assemblage, that is contrary to Beishan eclogite, suggest diversity of dynamics during high pressure terrane exhumation.

Lastly, this study has found possible connection between extrusive tectonics of India- Eurasia collision and its long distance (~600 km) effects on Beishan terrane. Here named, “Cenozoic Thermal Event”, led to reset of metamict zircons in the eclogite, where new ages correspond to major tectonic developments in Tibetan Plateau. This finding provides a new, previously undocumented relationship between tectonism and reset of the zircon geochronometers, which may have significant implications for future geochronology of crustal-scale fault systems.

Degree Type

Thesis

Degree Name

BSc Hons

Department

School of Earth & Environmental Science

Advisor(s)

Solomon Buckman

Keywords

Metamorphism, geochemistry, garnet, omphacite

Zircon Geochronology and Tectonic Evolution of Eclogites from the Beishan and Qinling Orogens, China

By

Wanchese Mateusz Saktura

A thesis submitted in part fulfilment of the requirements of the Honours degree of Bachelor of Science in the School of Earth and Environmental Sciences

University of Wollongong, 2015

The information in this thesis is entirely the result of investigations conducted by the author, unless otherwise acknowledged, and has not been submitted in part, or otherwise, for any other degree or qualification.

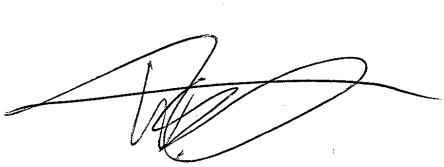

Wanchese Mateusz Saktura

14th October 2015

“This thesis is dedicated to my parents for their never ending support”

Abstract

Central Asia is host to some of the best examples of ultra-high pressure metamorphic rocks in the world. The study sites located in Beishan and Qinling Orogens contain examples of these high pressure rocks, called eclogites. They are an evidence of ancient continental collisions and their age and composition provide invaluable information about tectonic mechanics during collisions. This study focuses on geochronology of eclogites sampled from Beishan and Qinling Orogens. The Beishan eclogite, occurs as small mafic pods within highly deformed gneisses. The geological context and geochemistry of these eclogites determined in this study suggests they were originally rift-related MORB-type basalts rather than discrete fragments of oceanic crust, as previously thought.

Zircon dates obtained from the Beishan eclogite reveal peak metamorphism at 466 ± 27 Ma, which is concordant with the literature. However, U/Th ratios in zircon cores (ca. 880 Ma) are too low to have crystallized from mafic magma and therefore represent xenocrystic cores or previous metamorphic event rather than age of the protolith. The maximum age of the eclogite protolith is constrained by the crystallization age of the country rock orthogneiss at 920 ± 14 Ma. The end of retrogression metamorphism in the studied terrane was constrained by granitic vein that intruded the eclogite at 424 ± 8.6 Ma. This study provides the age for this rock for the first time. From evidence gathered for Beishan Orogen, this study proposes new tectonic model for initial stage of orogen development.

The Qinling eclogites did not yield significant amount of zircons, so they could not be dated with certainty. One zircon was dated at 490 ± 83 Ma which is consistent with metamorphic age established in literature, but statistically they cannot be used as a reliable age. However, its remarkably well-preserved eclogite facies mineral assemblage, that is contrary to Beishan eclogite, suggest diversity of dynamics during high pressure terrane exhumation.

Lastly, this study has found possible connection between extrusive tectonics of India-Eurasia collision and its long distance (~600 km) effects on Beishan terrane. Here named, “Cenozoic Thermal Event”, led to reset of metamict zircons in the eclogite, where new ages correspond to major tectonic developments in Tibetan Plateau. This finding provides a new, previously undocumented relationship between tectonism and reset of the zircon geochronometers, which may have significant implications for future geochronology of crustal-scale fault systems.

Acknowledgements

I would like to thank my supervisors Dr. Solomon Buckman and Prof. Allen Nutman for their advice, expertise and reviews throughout the year. For the project you helped me run that thought me so much, and the knowledge and skills that will serve me throughout my career, and lastly, for the patience and understanding.

I would like to show my gratitude to Prof. Yan Zhen for warm welcoming and the teachings during our field work in China.

I would like to thank José Abrantes, for everything you taught me over the years, for allowing me to use your lab and for everything you have done for me, your help is greatly appreciated. Special appreciation and gratitude is dedicated to Penny Williamson, for all your help throughout the undergraduate years and for your reviews during honours, your kindness will never be forgotten.

Special thanks also go to Associate Professors Brian G. Jones and Chris Fergusson for your teachings throughout the years and conversations that guided me through my honours. Many thanks are also dedicated to Dr. Alexandru Codilean and Dr. Tony Dosseto for your advices and inspiration.

I thank Dr. Mitchell Nancarrow for your help with EDS and CL data acquisition, and answering my never ending questions.

I would like to thank Prof. Richard Roberts for permission to use Raman and Luc Bordes for introducing me to the technique and help with the data acquisition and interpretation.

I am grateful to whole staff and students of School of Earth and Environmental Sciences, for creating this fantastic and motivational environment that I had a chance to work in.

I owe my deepest gratitude to my family, for understanding and supporting me with any decision that I have made throughout my degree.

I would like to thank Jessica Walsh for companionship through this year, this wouldn't be the same without you.

I would also like to thank my fellow "salt mine" workers, Catherine Bowie and Nick van Lijf for their companionship and help throughout this year and making honours an enjoyable experience.

Table of Contents

Chapter Five

Chapter Six

Chapter Seven

List of Figures

List of Tables

Chapter One

Introduction

1.1 Introduction

Eclogites are rare high grade metamorphic rocks that carry significant implications for geologists who study the tectonic evolution of the orogens and deep lithospheric conditions. Central Asia is geologically very complex region, where over millions of years frequent tectonic collisions led to formation of many ultra-high pressure (UHP) rocks such as eclogites. These provide valuable insights into dynamics of the deep continental subduction through their rare mineral assemblages that only form in so-called "forbidden zone (Zhang *et al.* 2003). The minerals such as coesite, K-cymrite or even possibly stishovite will occur only at very high pressures and low temperature conditions. That are only achievable on Earth in the subductions zones during deep continental subductions (Schreyer 1988, Chopin 2003, Liu *et al.* 2007, Mikhno *et al.* 2013). These implications is what attracts many researchers to study UHP rocks, as they provide indirect insight into these unreachable regimes that occur deep within the lithosphere.

Two examples of eclogite rocks from central Asia and central China are the main focus of this study. The first site near Gubaoquan village (Figure 1.1 and 1.2) in the Beishan Orogen is the core of this investigation. It is associated with a long inactive mountain belt that is a part of much larger tectonic assembly, the Central Asian Orogenic Belt that stretches across central Asia. The second eclogite studied is located near Kanfenggou village (Figure 1.1 and 1.3) and formed during assembly of the Qinling Orogen that is part of different tectonic formation, the Central Orogenic Belt of China. Eclogites studied in this project will be referred to by the name of the nearest village where they were found, that is Gubaoquan and Kanfenggou eclogites, respectively.

The eclogites are known to occur in three different geologic modes: as xenoliths in deep-suited igneous intrusions such as kimberlites, as blocks in serpentinite mélanges and lenses/boudins in metamorphic terranes (Coleman 1965, Qu *et al.* 2011, Nutman *et al.* 2013, Nikitina *et al.* 2014). The latter is the mode of occurrence for both eclogites studied. This

setting implies *in situ* metamorphism of large rock masses (e.g. a whole terrane), where only compositionally distinct rocks record the eclogite facies metamorphism. Other modes represent allochthonous type, as they formed deep within the lithosphere and were brought to the current site by carrier rocks, such as kimberlites or serpentinites and are largely unrelated to the country rock (Nutman *et al.* 2013, Nikitina *et al.* 2014). Such eclogites provide insight into deep lithospheric conditions but have no or little implication in orogenesis.

Figure 1.1 Map of China showing study sites as well as provinces explored. Outlines were obtained by tracing Google Earth © 2015 satellite imagery.

Since eclogite facies metamorphism is a high grade event, the mineralogical changes that occur in the process are significant. The deep crustal emplacement implies complex changes during prograde metamorphism, as well as at the time of retrogression during eclogite exhumation (Ernst 2001). The petrographic examination in this study will focus on tracing these changes to determine peak metamorphic assemblages that are indicatory of the conditions. This is often masked by subsequent retrogressive metamorphism facies overprinting the primary mineralogy, providing challenges in deciphering the order of changes. Once determined, it will reveal the evolution the rock that is representative of collisional evolution of the orogen.

The protolithic aspect of the studied rocks is based on petrographic examinations and is further explored by geochemical analyses. It is necessary to derive the general protolithic identity of the rock as it can have significant implications about the origin or setting of formation. However, geochemistry at eclogite facies can be a source of many uncertainties that can lead to misinterpretation. At this metamorphic grade, many elements become mobile and the rock loses its distinctive geochemical signatures. The rare earth elements have been proven to be the most immobile and therefore any conclusions derived in this study are mainly based on discrimination obtained from this suite of elements.

The study of the Gubaoquan and Kanfenggou eclogites are complemented by geochronology to obtain time constraints on the events observed in the petrographic examination and to determine the time of formation for the suite of rocks studied at Gubaoquan site. Many different rocks types were obtained from this site which will aid in establishing the complete series of geological events that took place in this study area. The array of data collected from the sample analysis, as well information gathered from the literature will be used to interpret the geological evolution of the studied sites.

1.2 Location and Overview

Gubaoquan Site

The main study site of this project is located near Gubaoquan in Beishan (Orogen) Mountains, Gansu Province in north western China (40°59′21.75″N, 95°02′25.27″E). As shown on Figure 1.2 this region is under dry climatic regime with very little vegetation. Abundant rock outcrops separated by loose alluvium allow easy mapping and therefore

general geological interpretations can be attempted from satellite imagery, as shown in Figure 1.2. However, the dry conditions have not contributed to good preservation, as rocks at this site show advanced weathering. The rock ages at this location range from Precambrian to Triassic of a diverse types; which include high grade metamorphic such as eclogites and gneisses, igneous of an intrusive and extrusive sort as well as sedimentary from variety of environments such as deep marine, shelf-derived, arc-derived *etc*. (Liu *et al.* 2010, Xiao *et al.* 2011).

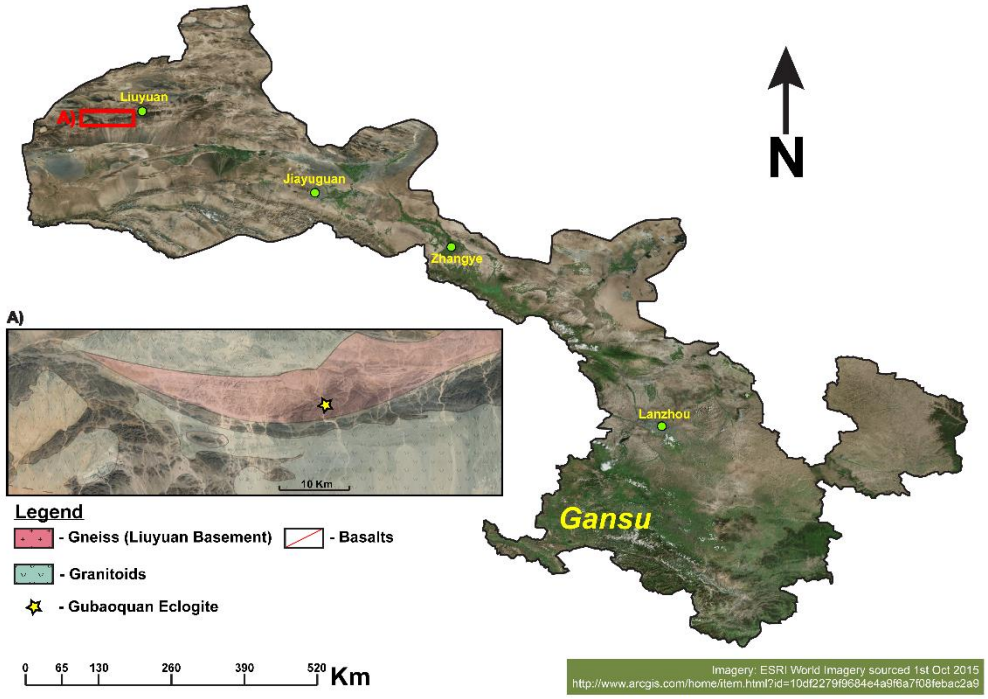

Figure 1.2 Satellite image of Gansu Province displaying location of study area and landscape characteristics. A) Close up of the site showing Gubaoquan eclogite location and high percentage of outcrop area. This figure shows how well exposed the rocks are in this region and that the basic relationships can be obtained from satellite imagery. Contact relationships were solely obtained from image whereas rock types were sourced from Liu *et al.* (2010), inset image was acquired from GoogleEarth (10/11/2014).

The Beishan Orogen was studied by many authors to target various aspects of its evolution, however only Liu *et al.* (2010) and Qu *et al.* (2011) focused on the eclogites and their implications. The former author has conducted detailed field work and produced well defined geological map shown in the next chapter from which lithology types mapped on the satellite image were derived. Both authors provided geochronological data for the eclogite metamorphism which was replicated in this study and it equates to *ca.* 466 Ma. The protolith age derived from zircon cores was established at ca. 886 – 881 Ma by both authors,

this was also attempted to be replicated and similar age was acquired. However, the U/Th ratios of analyzed cores were too low for a mafic body, therefore they were interpreted to be xenocrystic. This means that the protolithic age of the eclogite is unknown but the maximum age is constrained by the country rock. At this locality variety of rock types were analyzed in this project, and the major ones were successfully dated allowing for construction of model of the events that affected this area. Although these authors provided fulfilling data on the metamorphic conditions and evolution of the eclogite, their classification of the protolith is not satisfactory. Their geochemical work has identified oceanic crust to be best suited protolith for this rock. However, the sole appearance and field relationships indicate that this might be unlikely and therefore one of the main scopes of this project is to provide evidence for an alternative origin.

Kanfenggou Site

The second study site of this project is located in Qinling (Orogen) Mountains, near Kanfenggou village in Henan Province, central China (33°50'2"N 110°51'27"E) (Figure 1.3). At this locality two main rocks where studied, the eclogite and host rock paragneiss (Figure 1.4). The eclogite is present in form of large block or lens (~7 metres wide, exposure

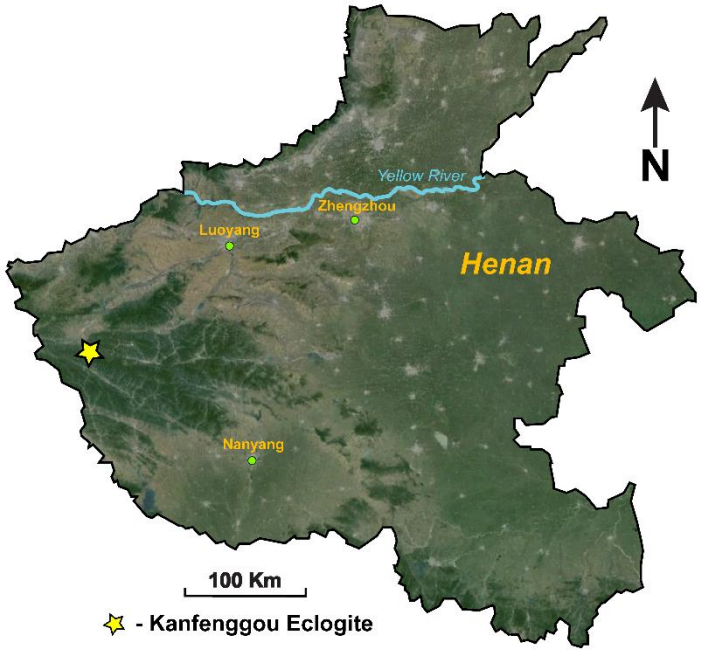

Figure 1.3 Satellite image of Henan Province displaying major cities and location of Kanfenggou village where the eclogite was found. Image acquired from GoogleEarth (4/10/2013)

limited by vegetation). Single eclogite outcrop was found, in contrast to the Gubaoquan eclogite where belt of eclogite bodies is present. As shown on Figure 1.3, this area is well-vegetated in comparison to the Gubaoquan site, what makes accurate mapping and field interpretations significantly harder to achieve.

Eclogites associated with Qinling orogenesis have been intensively studied because of the ultra-high pressure conditions to which they have been subjected. This has resulted in formation of coesite (high pressure polymorph of quartz) and more importantly, metamorphic microdiamonds which are very rare (Yang *et al.* 2003). This attracted many workers, who studied various aspects of the eclogites and their implications. They were reported in several locations, where Kanfenggou eclogite has not received as much focus as the other occurrences. This provides an opportunity to complement scarce information about this eclogite and to determine if it complies with the others in the orogen. These eclogites were also originally classified as metamorphosed oceanic crust, however Wang *et al.* (2013) argued that their protolith must be continental in origin what offers more logical explanation, however additional evidence must be gathered in order to determine which hypothesis provides the most plausible explanation.

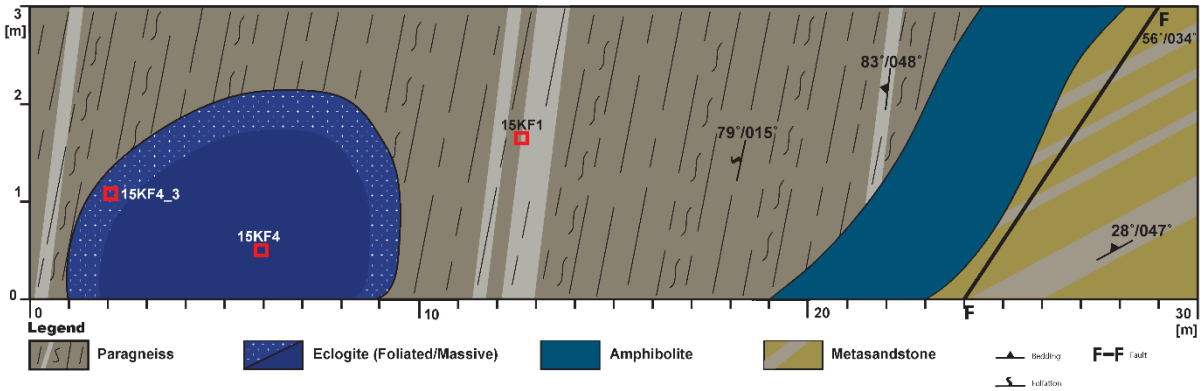

Figure 1.4 Sketch of Kanfenggou eclogite outcrop showing field relationships with strikes and dips for foliation and protolithic bedding.

1.3 Aims and Objectives

The aim of this study is to describe eclogites and associated lithologies at Gubaoquan (Beishan Orogen) and Kanfenggou (Qinling Orogen) sites, through their mineralogy, geochemistry and geochronology in order to investigate metamorphic members in scope of their protolithic nature and metamorphic history. This will be supported by examinations of

other rock types, what will aid in deciphering geological history of the studied terranes. These aims will be accomplished through the following objectives:

i. Petrography – Determine mineralogical assemblage, texture, mineral relationships and equilibria. Study prograde and retrograde mineral assemblages as well as alteration products.
ii. Geochemistry – Quantify whole-rock major and trace element composition of eclogites to determine their protoliths and tectonic setting to verify feasibility of geochemical classification techniques on studied eclogites.
iii. Geochronology – Determine the age of the eclogites and associated lithologies and the time of metamorphism through zircon U-Pb dating of xenocrystic cores and metamorphic rims.
iv. Comparative study – basic analytical and literature based study of Qinling eclogite to determine similarities and differences between the two eclogites.

1.4 Methodology

This section presents methods used in this project to prepare samples for data acquisition and the general procedures that were followed to assure precision and consistency throughout the project and with the literature. The principles and theory involved for each of the analysis is further explored in the Introduction section in every chapter in order to provide a theoretical overview of the analysis and how the data was acquired to meet the requirements of the project. The aim of this section is to reveal the procedures used to assure reproducibility of the results.

Sample collection

The ten samples from Gubaoquan have been collected during Dr. Solomon Buckman's initial expedition to Beishan in 26th June 2014 and are listed in Table 1.1. They have been left at the Chinese Academy of Geological Sciences, Beijing, China for zircon extraction and mounting and thin section preparation. Additional samples from Kanfenggou site were collected during field work to Qinling Orogen in Central Orogenic Belt of China in April 2015. The samples were acquired *in situ*, directly from the outcrop using hammers. The weathered parts were cleared from the rock to sample only the fresh rock. The date and GPS co-ordinates of collected samples were recorded with any additional information of the

outcrop that were available such as dip and strike, foliation, contact zones, faults, sedimentary structures, bedding orientation, etc. Field descriptions and site locations and sketches are included in Appendix A.

(Table 1.1 on the next page)

Table 1.1 Samples collected from Gubaoquan and Kanfenggou sites, showing conducted analyses.

Sample/Site	Rock Type	Petrography	Geochemistry	Geochronology	Location	Date
Gubaoquan						
14GBQ1	Eclogite	✓	✓	✓		
BS02	Eclogite	✓	-	-		
14GBQ2	Granitic Vein	✓	✓	✓		
14GBQ3	Eclogite-Jadeite	-	✓	-	40°59′21.75″N 95°02′25.27″E	26/06/2014
14GBQ4	Eeclogite-Amphibolite	✓	-	-		
14GBQ5	Eclogite-Garnet rich	-	✓	✓		
14GBQ6	Gneiss	✓	-	-		
14GBQ7	Dolerite	✓	-	(attempted)		
14GBQ8	Augen gneiss	✓	-	-		
BS04	Gneiss	✓	-	-		
14GBQ9	Lamprophyre	✓	-	✓	40°58′51.25″N 95°02′38.07″E	
14GBQ10	Augen K-spar gneiss	✓	-	✓		
Kanfenggou						
15KF1	Gneiss	✓	✓	-	33°50'2"N 110°51'27"E	15/04/2015
15KF4_1	Eclogite	✓	✓	✓		
15KF4_3	Eclogite	✓	✓	-		

Petrography

Fourteen polished thin sections from Gubaoquan and Kanfenggou were made by the Chinese Academy of Geological Sciences, Beijing, China and University of Wollongong, Australia. They were made to ~30 micron thickness. The petrographic examination was conducted using Lecia DM2500 petrographic microscope with photographic instrumentation at University of Wollongong. Polished/uncovered thin section were chosen as it allows for *in situ* analysis in the future if ever required; in this project energy-dispersive X-ray spectrometry was used to analyse chemical composition of the phases of interest to complement petrographically acquired data.

Geochemistry

Several geochemical analyses were performed in order to better constrain protoliths of the metamorphic rocks, their degree of peak metamorphism and to determine rock settings in broader tectonic context. The following three analyses were used to provide invaluable information regarding these concepts:

Whole-rock Geochemistry

The analysis required rock to be pulverized; for this purpose rocks were cut into smaller pieces to improve crushing and to remove any altered parts, so only the fresh rock was analysed. Then the rock was washed and dried prior to crushing. Approximately 20-40 grams of rock were crushed in Chrome-Steel ring TEMA. The Gubaoquan samples were processed at Chinese Academy of Geological Sciences in Beijing, China; whereas Kanfenggou samples were processed at University of Wollongong, NSW, Australia and then sent to Australian Laboratory Services Pty Ltd. in Brisbane for the analysis.

Major and Trace Elements

The trace elemental analysis was performed prior to the major oxide, as it provides accurate abundances of the trace elements and general indication of major oxide content. Information obtained from this analysis is used to determine the appropriate flux for the majors and if oxidation of sulfides procedure is needed. For the analysis, approximately 5 g of rock powder is needed which is then thoroughly mixed with ~10 drops of Polyvinyl Acetate (PVA-binding agent) and then pressed in aluminium caps into the pellet, which is then dried in the oven at 60° C overnight.

Major oxide analysis required approximately 1 g of rock sample powder that was mixed with a Lithium Meta- or Tetra-borate flux to facilitate melting in platinum crucibles. The mixture was heated progressively at a rate of approximately 70° C/10 minutes until the temperature of 970° C was reached and the sample was molten. The liquid samples were poured onto a clean graphite disk and pressed into glass disks using an aluminium plunger. The disks were then left on a hot plate at approximately 240° C for 2 hours and then transferred to hot plate set for 100°C and were left for slow cooling and annealing overnight. The XRF analysis was then performed for major elemental concentrations on the aluminium pressed side. This procedure was performed by Australian Laboratory Services Pty. Ltd. Brisbane under code ME-XRF260 and ME-GRA05 for the Loss of Ignition (LOI).

Rare Earth Elements

The analysis for rare earth elements (REE) was conducted using Inductively Coupled Plasma Mass Spectrometry (ICP-MS) by the Australian Laboratory Services Pty Ltd. in Brisbane under code ME-MS61r which analyses base metals and REE. The samples were analysed for 48 elements + REEs by HF-HNO_3-$HClO_4$ acid digestion and HCl leach followed by ICP-AES and ICP-MS analysis. This process quantitatively dissolves nearly all elements in the majority of geological materials, however most resistive minerals such as zircons were only partially digested. Obtained results were received as parts per million.

Energy-Dispersive X-Ray Spectrometry (EDS)

This analysis was performed on thin sections and zircon inclusion in order to verify or determine mineralogy. The instrument used was Scanning Electron Microscope (SEM) JEOL JSM-6490LV at Innovation Campus, University of Wollongong. The analysis was performed under low vacuum to avoid ionization of the sample. The working distance was set to 10 mm to avoid collision with the analyser. The accelerating voltage was set to 15 kV in order to achieve spectrum count rate between 52 000 and 60 000 counts per second (cps). For the zircon inclusions this method was used in conjunction with cathodoluminescence (CL) imaging add-on on the SEM. The instrument Gatan MonoCL4 was used to acquire CL image of the zircon with inclusion to verify its association, then EDS analysis was performed at selected sites. Always one control site of known mineralogy was analyzed, the zircon background.

Geochronology

The zircon-derived ages for 5 selected samples (4 from Gubaoquan and 1 from Kanfenggou) were obtained using zircon U-Pb dating technique with Sensitive High Resolution Ion Microprobe Reverse Geometry (SHRIMP-RG) instrument at Australian National University (ANU). For this analysis, samples had to be adequately prepared to form mounts which were inserted into the machine. This was conducted in accordance to the following procedure:

1. The zircons were obtained by crushing 10-15 kilograms of rock sample to grain size range of 100 to 400 microns. Then the sample was deslimed using Wilfley Table to remove fine powder and retain the heavier and coarser mineral fraction. The sample was then dried and highly magnetic minerals were removed using hand and rare earth magnets. These processes reduce the amount of material used in order to limit amounts of consumables used in the later processes.
2. The achieved concentrate was then processed using a Frantz Magnetic Separator. It was run through multiple times, progressively increasing the magnet's amplitude, each time the non-magnetic fraction was re-run.
3. The concentrate was then placed in a heavy liquid to remove the lighter fraction further. Heavy liquid used was Di-iodomethane with specific gravity of 3.3. The light fraction was washed and retained, but the heavy fraction is the one containing zircon and was further processed.
4. Once again, the concentrate was processed by Frantz, but this time at constant amplitude of 1.50 and the tilt was decreased in five steps from 5° to 1°, by one degree at the time.
5. At this stage, the concentrate was ready for hand-picking and mounting.
6. The zircon mounts were made by placing double-sided tape on perfectly flat glass, then where possible ~150 zircon grains of each sample were arranged in rows on the sticky tape (keeping the row arrangement asymmetrical). After all the samples have been placed on the tape, the TEMORA-2 and OG-1 standards were added, approximately 20 and 10 grains of each respectively.
7. Once all the zircons have been set, the mould was placed above them and they were encased in a low vapour pressure epoxy resin and left for 2 days to harden.
8. The hardened mount was ground on #600 grit emery paper in "figure 8" fashion to assure even wear down. This was done until almost all zircon cores were exposed, then polishing was performed on nylon pad with 1 micron diamond paste until the majority

of scratches were removed and smooth surface was attained. This process was completed in stages, one minute of polishing followed by inspection under reflected light microscope; time taken: 4-5 minutes per mount.

The zircon mounts G5772, G5773, G5774, G5775 and G5776 were made at Chinese Academy of Geological Sciences in Beijing, China. Mounts W39 and W41 were made at University of Wollongong, NSW, Australia.

The received zircon mounts were photographed using Lecia DM2500 microscope in the reflected light setting to produce mount maps which were necessary for efficient navigation during Cathodoluminescence (CL) imaging and SHRIMP dating. The CL images were produced using JEOL-6610A SEM at ANU. These images revealed internal structures within zircons such as cores and rims, as well as mineral inclusions which were then identified using EDS. The main purpose of these images was to determine which zircons can provide relevant information for the project and to find suitable spot for microprobe analysis.

The SHRIMP-RG U-Pb zircon dating procedure:

1. The zircon mount was gold coated to allow electrical conductivity and grounding of non-conductive epoxy material in order to stop overheating and isotope disturbance during analysis.
2. Once the mount was inserted, laboratory standard sample SL13 was analysed prior to dating to verify the precision of the instrument, followed by analysis of reference material on the mount (Temora-2 or OG-1)
3. When standards provided satisfactory results, dating could commence and three sample analyses were conducted followed by the standard to verify that the precision of the instrument has not been affected.
4. Ideally 16 analyses were conducted per sample where it was possible.
5. The procedures for raw data reduction and common lead corrections are outlined in Chapter Five.

Chapter Two

Regional Geology

2.1 Introduction

The Beishan and North Qinling metamorphic terranes and eclogites within them have been the focus of research for the past 20 years. Many contrasting models have been proposed, but with ongoing research and new data becoming available, the understanding of these orogens recently began to reach consensus. Many workers researching different aspects of the same lithologies led to a scattered array of information available for each of the eclogites. However, in the Beishan region many workers classified the Gubaoquan eclogite as originally being part of an ophiolite, which has significant tectonic implications. This classification is thought to lack significant evidence to support it, *ergo* this study will focus on revising its classification. Similarly, the Kanfenggou eclogite protolith was also classified as part of simatic crust (Tang *et al.* 2014), but this view has already been challenged (Wang *et al.* 2013), therefore the scope of studying this site will be to acquire additional evidence to determine which hypothesis provides most logical interpretation.

2.2 Geological Settings

2.2.1 Beishan Orogen – Gubaoquan Site

The Beishan Orogen is located in the southern-most region of Central Asian Orogenic Belt (CAOB), also referred to as Altaids. The Altaids extent is marked by Baltica Craton in the west, Siberian Craton to the north and Tarim and North China Cratons to the south (Sino-Korean Craton) (Figure 2.1). The Beishan Orogen consists of amalgamated island arc complexes, ophiolites and microcontinents (Figure 2.2). Its western boundary is marked by Tianshan Orogen and Mongolia-Xing'anling Orogen to the east and separated by Ruoqiang-Xingxingxia and Altyn Tagh–Alxa faults, respectively. In the north, the Beishan orogenic collage is bounded by the Southern Mongolian Accretionary System and in the south by Dunhuang Block, that is often referred to as a north-eastern extension of Tarim craton.

However its true association is unknown due to desert top cover that occupies the majority of the craton's area. Outcrops are only present around the collisional margins of the Traim craton and Dunhuang Block (Zong *et al.* 2012).

The Beishan Orogen formed as a consequence of long lasting subduction-accretion processes that were operating from Neoproterozoic until Late Palaeozoic-Early Mesozoic what led to amalgamation of discrete terranes (Liu *et al.* 2010, Song *et al.* 2013a). However, collisional processes did not operate as "one-by-one" terrane accretion, but as multi-stage inter-terrane agglomeration, with final synthesis in Late Permian to Early Triassic (Xiao *et al.* 2011). The resulting collage consists of island arcs, arc-derived sedimentary packages, ophiolitic mélanges and gneissic units, interpreted as microcontinents due to their Precambrian basement type characteristics (Song *et al.* 2013b). Their tectonic evolution remains ambiguous, but current understanding of accretionary orogens allows for division into four major terranes according to Liu *et al.* (2010) which are separated by suture zones and marked by ophiolites (Figure 2.2). From the north to south, the first terrane is

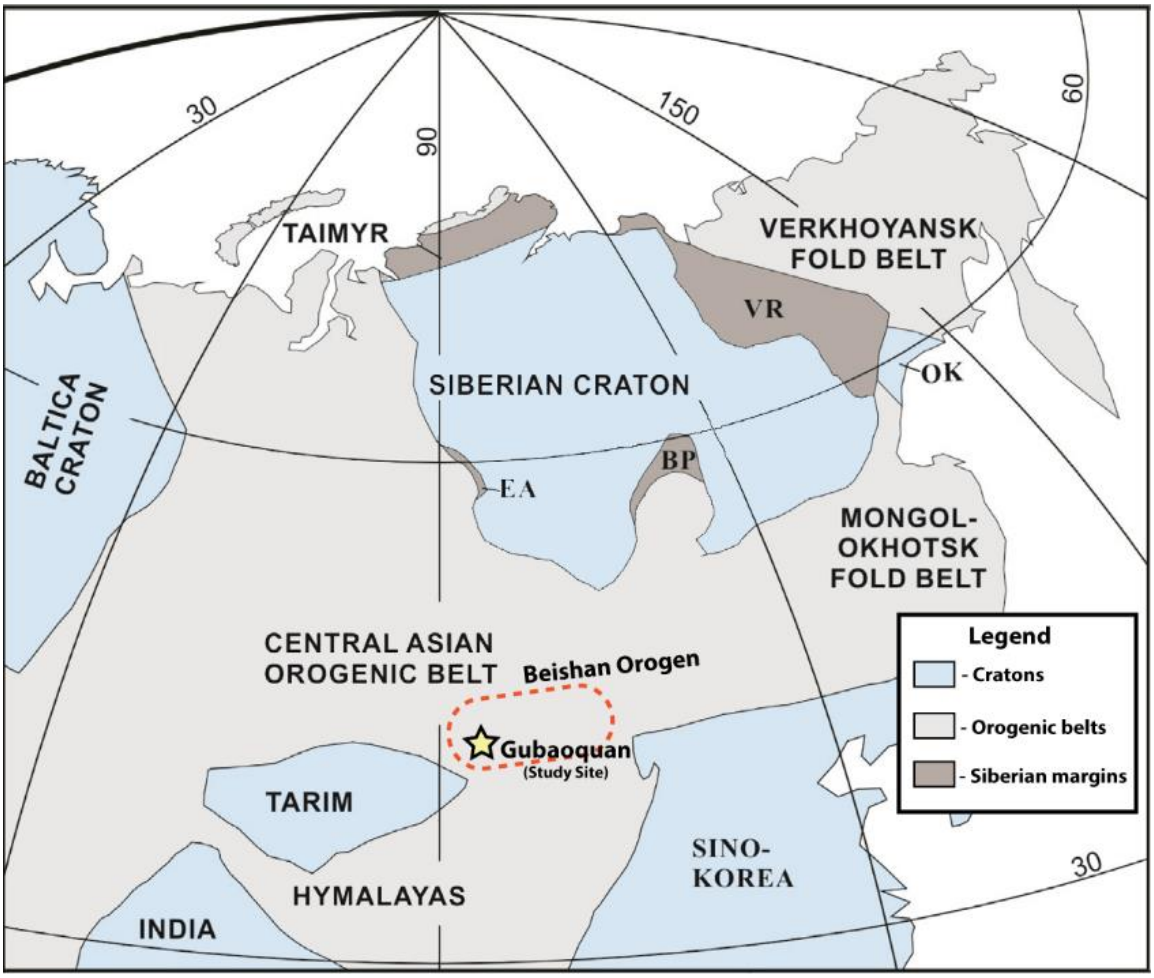

Figure 2.1 Tectonic map of Central Asian Orogenic Belt; modified after Powerman *et al.* (2015)

Yuanbaoshan Arc which is separated from the Mingshui-Hanshan microcontinent by Hongshishan-Baiheshan suture. The southern margin of the Mingshui-Hanshan microcontinent is marked by the Shibanjing –Xiaohuangshan suture between it and the Dongqiyishan Arc. The last terrane is the Liuyuan microcontinent separated from previous terrane by the Hongliuhe-Xichanjing suture. It belongs to the Huaniushan Group which accounts for Precambrian basements in the southern regions of the Beishan Orogen and hosts the eclogite bodies (Liu *et al.* 2010, Song *et al.* 2013a).

Throughout the literature there are additional suites or lithological divisions not mentioned above. Some authors describe Palaeozoic plutonism in the Dunhuang Block as traces of a volcanic arc that is referred to as the Shibanshan Arc (Mao *et al.* 2011). On the other side of an acclaimed Liuyuan Ocean (branch of Palaeo-Asian Ocean) is a subduction zone with northern polarity, leading to the development of Huaniushan Arc on or at the margin of the

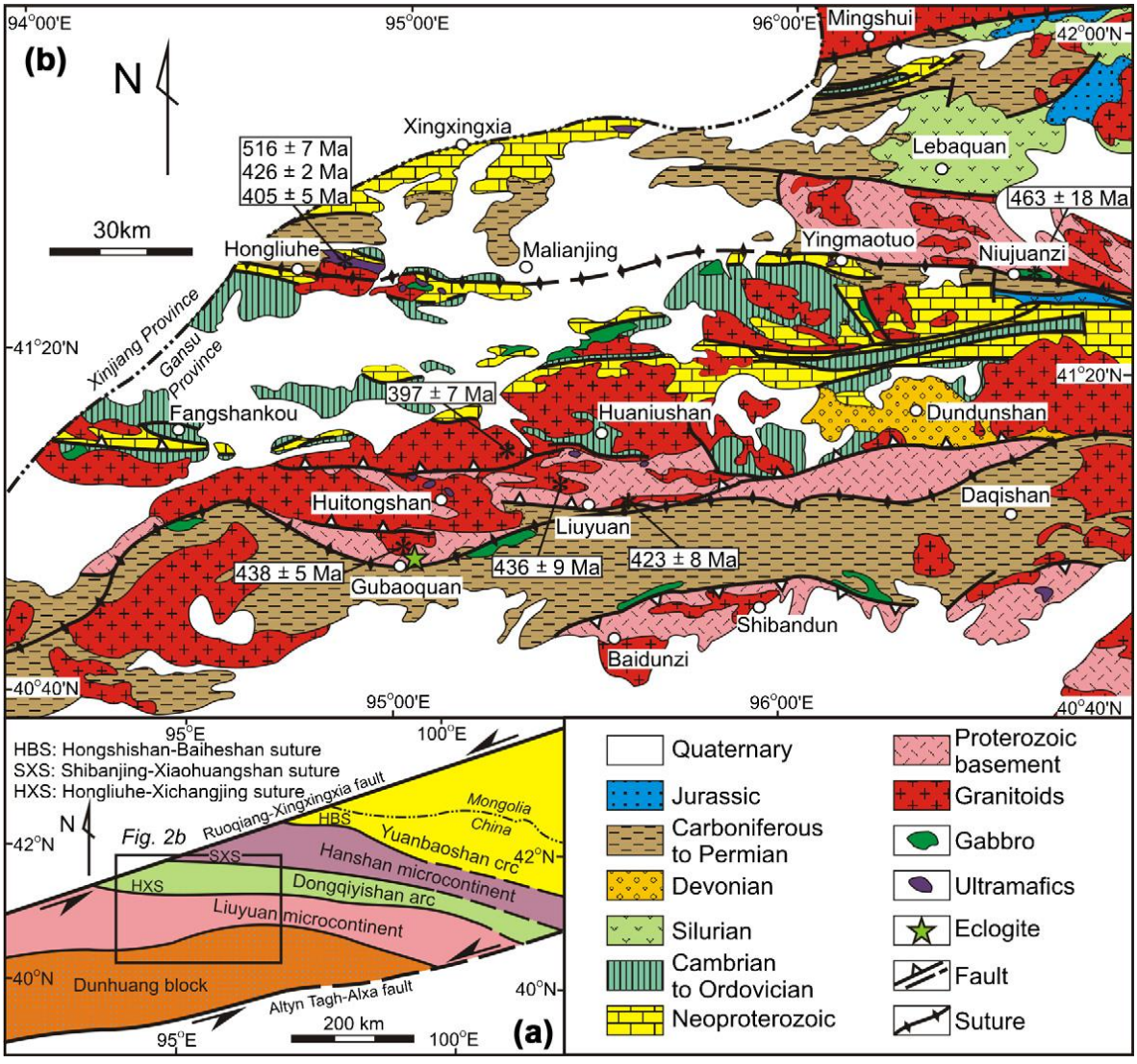

Figure 2.2 Geological map of Beishan Orogen from Liu *et al.* (2010)

Liuyuan Microcontinent (Mao *et al.* 2011, Xiao *et al.* 2011). Within this collage, other terranes or suites have been recognized such as the Mazongshan continental block or arc and Hongliuhe, Xingxingxia and Hongshishan mélanges. There are inconsistencies in the literature about the origin and affiliation of these terranes. For the simplicity of studying larger scale tectonic processes all these local terranes from the Shibanshan Arc to the Queershan Arc (last arc in Southern Mongolian Accretionary system) have been named Gongpoquan Composite Arc-accretionary System (Qu *et al.* 2011, Xiao *et al.* 2011, Cleven *et al.* 2013).

Gubaoquan Eclogite

The eclogite in the Beishan Orogen was first discovered sixteen years ago by Mei (1999) and was mainly described in Chinese literature, but in more recent years work conducted by Liu *et al.* (2010) and Qu *et al.* (2011) brought knowledge about this region to the broader scientific community worldwide. Earlier work done by Yang *et al.* (2006) provided the first U-Pb SHRIMP metamorphic ages for the Gubaoquan eclogite indicating Neoproterozoic metamorphism at 819 ± 21 Ma. This was a starting point for further research in this region, as subsequent workers did not agree with these ages and interpretation, what resulted in more detailed studies.

Liu *et al.* (2010) provided the most reliable U-Pb SHRIMP ages for the eclogite and host gneisses, which are now commonly cited throughout the literature. They reported 886 ± 4 Ma for the core and 465 ± 10 Ma for the metamorphic rim in the zircons from the eclogite body, and *ca.* 1450 Ma and 900 Ma for the core and rim respectively for the host gneiss. Their work provided essential ages for the major lithologies within this area, providing a constraint on geological events. Lack of geochronological data throughout this region was a major problem, therefore recent works mainly concentrated on geochronological studies and tectonic reconstructions widely supported by geochemical data. However this broad approach doesn’t provide enough information about lithological relationships on smaller scale. Liu *et al.* (2010) strongly emphasized that closer relationships between eclogite and its country rock and their metamorphic linkage needs more detailed study.

Additional work on the Gubaoquan eclogite was conducted by Qu *et al.* (2011) who reattempted dating eclogite zircons and achieved an Ordovician age of 467 ± 16 Ma for the metamorphic rim and 881 ± 12 Ma for the protolith core. Their results are in line with Liu

et al. (2010) as they fall within margin of error and therefore provide a reliable age for the eclogite facies metamorphism. However, uncertainty still remains regarding age of the protolith for eclogitic body as Yang *et al.* (2006) reports Mesoproterozoic age of 1007 ± 20 Ma for the zircon cores whereas Liu *et al.* (2010) and Qu *et al.* (2011) report Neoproterozoic ages; therefore a significant gap of >100 Ma of difference remains. Hence, further investigation regarding the protolith age is needed to clarify inconstancy in the results.

Qu *et al.* (2011) were the first to undertake estimation of pressure (P) and temperature (T) paths using NCFMASHTO system in THERMOCALC software for the Gubaoquan eclogite body. Their petrological and phase relationship study revealed a clockwise pattern for the P-T path, with close to isothermal decompression during retrograde metamorphism. According to their work, peak eclogite facies metamorphism was reached at a pressure >15.5 kbar and temperature at 700-800° C, which is partially inconsistent with Ti-in-zircon thermometer used by Liu *et al.* (2010), who report temperature range of 623° to 792° C for the same eclogite body. Therefore, lower limit may have been overestimated. Next stage of metamorphism occurred at P=12-14 kbar and T=700-750° C and is characterised by the first appearance of plagioclase within mineral assemblage indicating retrogression metamorphism to HP granulite facies stage. This further declined to granulite facies at P = 8-9.5 kbar and T ~700° C. The retrogression metamorphism has concluded on amphibolite facies stage, with conditions estimated to P = 5-7 kbar and T = 600-700° C. Occurrence of this stage is most conspicuous as eclogite lenses have garnet-free amphibolite facies retrogression rims, which can be easily distinguished from garnet-bearing eclogitic cores. However, cores are only preserved in larger bodies, as smaller lenses have completely retrograded to amphibolite.

Liu *et al.* (2010) and Qu *et al.* (2011) both agree on the protolith of the Gubaoquan eclogite which is reported to be oceanic crust. This is not an unusual occurrence as numerous eclogites have simatic affiliation, but the actual source was not investigated. Previous works on eclogites throughout the world have reported various sources of protoliths such as pillow basalt, ocean plateau or even ocean island basalts, indicating complexity of dynamics during plate subduction to a point of eclogite formation and emplacement. The entrapment of ocean floor and its edifices within lower crust or upper mantle is poorly understood, due to the inaccessibility of that zone, but it is crucial in understanding eclogite emplacement and exhumation. The signatures of these processes can be modelled through mineralogical assemblage changes which have been documented and processed by Qu *et al.* (2011) in

pseudosection calculations. The determined clockwise P-T path indicates progressive subduction of simatic crust to eclogite facies metamorphic stage at 467 ± 16 Ma, followed by exhumation through retrograde metamorphism at 428.9 ± 3.8 Ma. This age was obtained from $^{39}Ar/^{40}Ar$ dating of biotite in an augen gneiss, a country rock hosting the eclogite that is a dominant member of this metamorphic suite. It is assumed that they underwent exhumation synchronously, possibly as one terrane.

Although P-T estimations using pseudosections provide crucial information for metamorphic suites, they have varying degrees of uncertainty. They are based on the establishment of 'perfect equilibrium' among minerals within the rock which can be easily modified during post-peak metamorphic events. Many high pressure rocks often undergo post-collisional heating or multi-stage retrogression during exhumation, resulting in modifications to equilibrium of peak metamorphic mineral assemblage (Aoya *et al.* 2003, Cao *et al.* 2011). Therefore a careful approach is needed when interpreting THERMOCALC pseudosection results.

2.2.2 Qinling Orogen – Kanfenggou Site

The Qinling Orogen is part of a larger geologic complexity, the Central Orogenic Belt (COB) of China, which stretches for more than 4000 km. The orogens that constitute COB from east to west are: Dabie-Sulu, Qinling-Tongbai, Qilian, Qaidam, Altun and Kunlun (Yang *et al.* 2005). The Qinling-Tongbai-Dabie orogenic belt formed as a result of continental collision and amalgamation of terranes between North China Block (NCB) and South China Block (SCB). This orogen is further divided into North (NQ) and South Qinling (SQ) terrane that are separated by the Shangdan Fault, which is also referred to as Shangdan Suture (Figure 2.3) (Yang *et al.* 2003, Wang *et al.* 2011, Wang *et al.* 2013).

This project will focus on the NQ terrane as it is where high grade metamorphic rocks are preserved, including high pressure to ultra-high pressure eclogites. This terrane is further divided into three main groups: Kuanping, Erlangping and Qinling, that correspond to back-arc basin, island arc to back-arc basin-related setting and depositionally unrelated Palaeoproterozoic Complex, respectively (Figure 2.3 and 2.4) (Dong *et al.* 2011, Wang *et al.* 2013, Tang *et al.* 2014). However, the latter is of particular importance as it contains the metamorphic rocks that underwent eclogite facies metamorphism, preserving timing of the collision. Therefore acquiring accurate U-Pb zircon age of the metamorphism from the

Kanfenggou eclogite will be the key component during study of this site. Acquired results can be correlated with other ages that were obtained along this suture zone to constraint the collision.

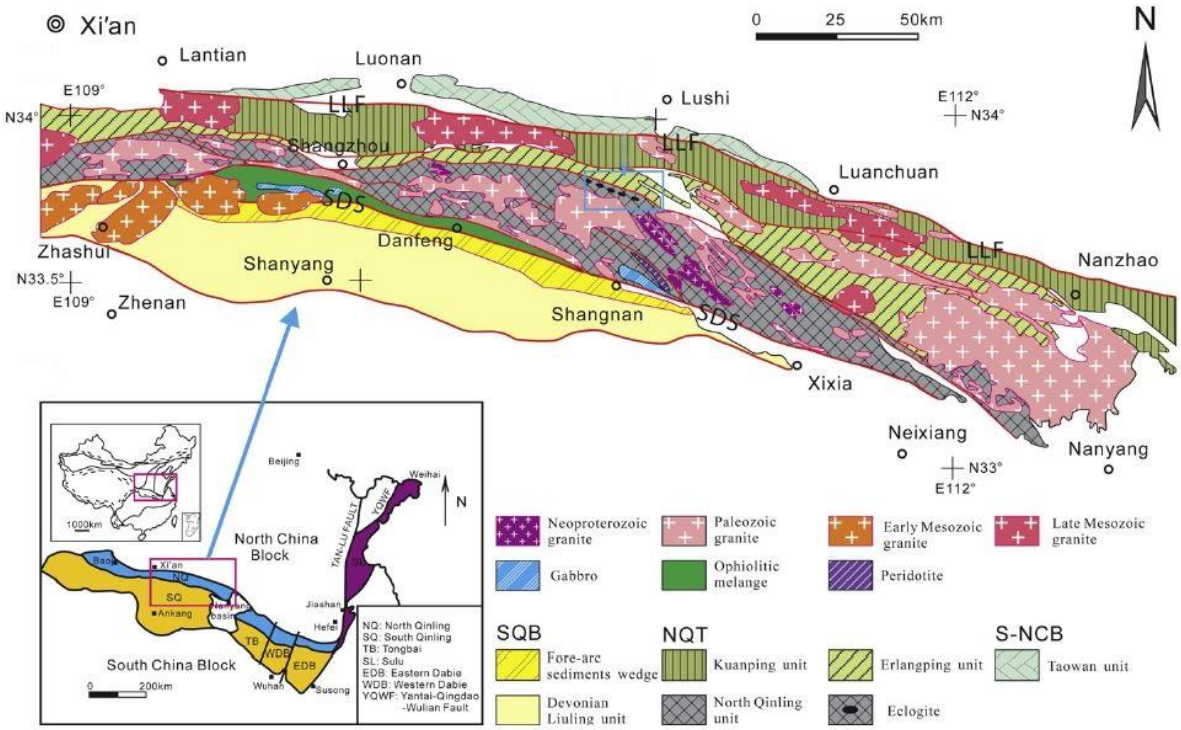

Figure 2.3 Map of Qinling orogen indicating eclogite localities within UHP metamorphic belt of North Qinling unit. SDS – Shangdan Suture/Fault from (Wang *et al.* 2013)

Qinling Eclogites

The amalgamation processes that led to the assembly of the Qinling-Tongbai-Dabie Orogen produced three separate episodes of HP-UHP metamorphism. The first stage occurred in the Early Palaeozoic, when Neoproterozoic mafic rocks in North Qinling terrane underwent UHP eclogite facies metamorphism. A subsequent stage took place in the Carboniferous where Silurian MORB-like protolith thought by Wu *et al.* (2009) to be Palaeo-Tethyan oceanic crust, was subjected to eclogite facies metamorphism at 309 ± 2 Ma and is now present in Hong'an terrane. The final stage occurred in the Triassic in Dabie-Sulu Orogen, when Neoproterozoic simatic crust underwent UHP metamorphism during the termination of continent-continent collision between SCB and NCB. The resulting eclogitic UHP and HP metamorphism produced rare partial melting of the eclogite-producing felsic melt that was still preserved within melt channels (Wang *et al.* 2013, Wang *et al.* 2014).

The UHP eclogites from Early Palaeozoic metamorphic event in North Qinling were studied by many workers as consensus regarding the age of the protolith and eclogite facies metamorphism was difficult to reach. Different authors provided ages with high uncertainty or their data was contradicting general understanding of tectonic setting of this region. However, recent work conducted by Cheng *et al.* (2012) and Wang *et al.* (2013) provided concordant and conclusive zircon U-Pb ages that allow for reliable tectonic interpretation of the events in northern Qinling. Cheng *et al.* (2012) reported 496.6 ± 5.7 Ma for eclogite facies metamorphism and *ca.* 800 Ma for the protolith, and similarly Wang *et al.* (2013) reports 490 ± 12 Ma and 798 ± 23 Ma, respectively. The NQ terrane has received much attention since the discovery of metamorphic microdiamonds and coesite in eclogite bodies and hosting country rocks (Yang *et al.* 2003, Cheng *et al.* 2012). This led to further studies regarding metamorphic conditions to which these UHP rocks were subjected, using mineral equilibria and pseudosections authors determined pressure range of 2.6-2.8 GPa and temperature 660°-710° C at peak metamorphic stage (Cheng *et al.* 2012).

The NQ terrane is of particular interest as it contains eclogite bodies but there are still uncertainties about its affinity and geological setting, whereas the SQ terrane is well understood. The eclogites were reported in several locations in the NQ unit; they occur as lenses, blocks and layers scattered throughout the UHP metamorphic belt that is 2-5 km wide and stretches east-west for 30 km along the northern boundary. Within the belt main lithologies include orthogneisses, paragneisses and schists, which all host eclogitic bodies (Wang *et al.* 2013). The emplacement of eclogites is attributed to early stages of the amalgamation process between SCB and NCB that occurred in Early Palaeozoic. However there are two conflicting scenarios regarding protolith origin and eclogite formation; Dong *et al.* (2011) proposed E-MORB or OIB protolith for the eclogite from a back-arc setting of Erlangping Basin that was subducted beneath Qinling island arc (now NQ terrane) in southward orientated subduction zone. On the contrary, Ratschbacher *et al.* (2003) and

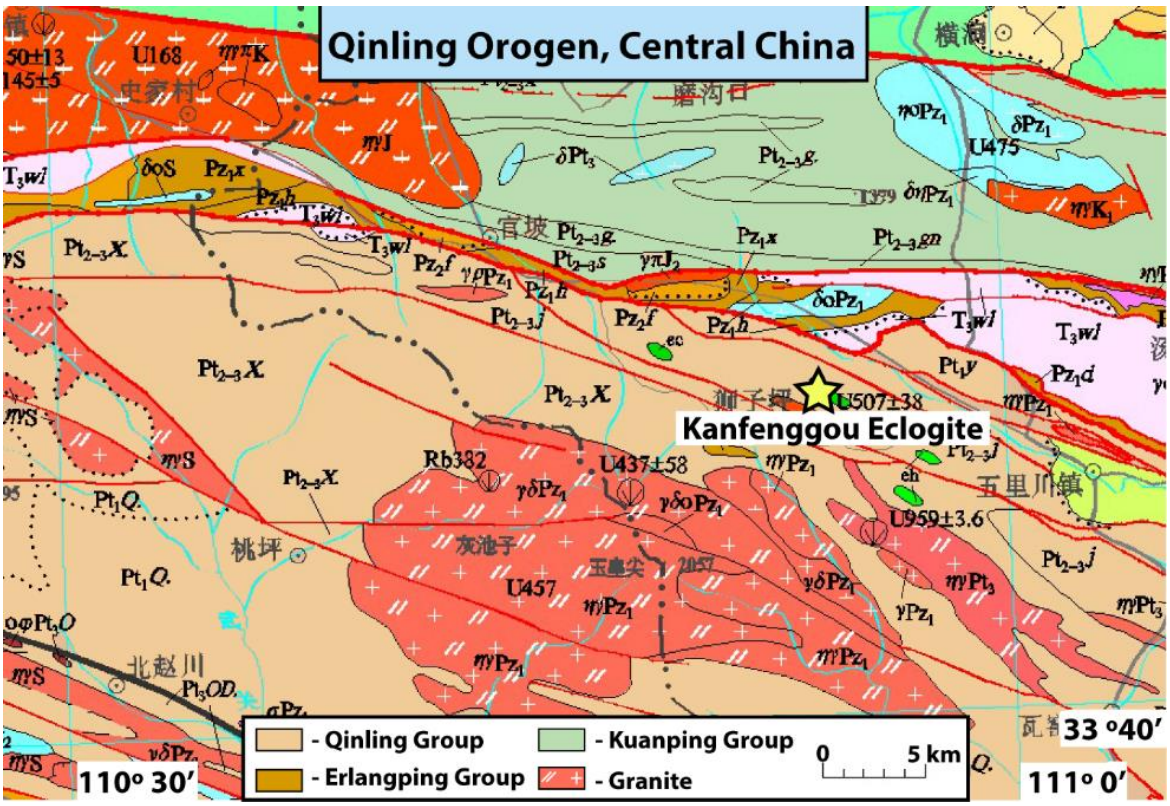

Figure 2.4 Geological map of Kanfenggou site and adjacent units. Green boudins represent eclogite sites. Modified after Geological Survey of China, 2009.

Wang *et al.* (2011) proposed northward subduction zone within an arc-continent collisional setting, where the protolith was suggested to be continental in origin. The empirical evidence presented by Wang *et al.* (2013) support this scenario, where whole rock geochemical analysis revealed a tholeiitic trend for the eclogite and plotting trace element data on discrimination diagrams such as Ta/Yb–Th/Yb and Hf–Th–Ta overlap in areas of E-MORB and Within-plate tholeiite. There are also systematic discrepancies in geochemical composition between NQ eclogite and Erlangping basaltic rocks, which contradict the scenario proposed by Dong *et al.* (2011) which was under assumption that NQ eclogite and Erlangping basalts were produced from the same source.

Since NQ unit's tectonic affinity remains unresolved, the origin of eclogite's protolith has to be determined, as it has important role in understanding the tectonic evolution of this region. Meng and Zhang (1999) proposed that the North Qinling unit formed as magmatic arc with back-arc basin at the southern margin of NCB. The NQ unit was always viewed as an isolated terrane due to its lack of direct stratigraphical correlation with adjacent terranes, as its sedimentary cover is very different to the one of SQ and it also lacks characteristic Late Archean to Paleoproterozoic basement of NCB and widespread Late Neoproterozoic

magmatism of SCB. However some similarities have eventually been found and Ratschbacher *et al.* (2003) proposed that NQ unit has SCB basement and NCB related upper unit, which was inconsistent with currently available data. These developments still have not led to consensus, as many authors favoured isolated setting for the NQ terrane, until thorough investigation by Wang *et al.* (2013) provided convincing evidence regarding the affiliation and eclogite protolith. They proposed that the NQ unit was part of SCB that rifted in Neoproterozoic before the widespread magmatism occurred and that tholeiitic basalts that formed during this rifting episode is the protolith for NQ eclogite. This is further supported by the presence of tholeiitic basalts at the northern margin of SCB and their Pb isotopic signatures that indicate similarities between SCB and NQ terranes and strong distinctiveness from NCB (Wang *et al.* 2013). Therefore discrepancies in sedimentary cover and lack of Late Neoproterozoic magmatism can be clarified by the eclogite protolith itself. Its formation is attributed to rifting magmatism when the NQ terrane separated from the SCB at *ca.* 800 Ma, the age of the eclogite protolith. The isolated NQ unit therefore will not be affected by a later magmatism episode and its isolation will result is different sedimentation modes, explaining its distinctiveness from surrounding terranes (Wang *et al.* 2013).

The array of evidence presented by Wang *et al.* (2013) supports NQ terrane affiliation to SCB and favours northward subduction setting, showing that south orientated subduction of back-arc basin is improbable as a mechanism for eclogite formation and emplacement. However, the foundation of this scenario is based on eclogite protolith being continentally-derived during a rifting episode, therefore strong evidence supporting this hypothesis is needed. Wang *et al.* (2013) have shown that the protolith might be a within-plate tholeiite or E-MORB, indicating that further geochemical work is required to determine its tectonic affinity.

Chapter Three

Petrography

3.1 Introduction

This chapter will present the petrographic examination of 14 polished thin sections from the Gubaoquan and Kanfenggou sites. The petrography was used in this study to verify the accuracy of classification of rocks in the field, to determine mineral assemblages *via* textural relationships, and, to derive information about sequential events that affected rocks studied. This analysis also provided valuable information about the degree of the alteration and weathering that will assist in interpretation of the geochemical data.

The examination was conducted using a Leica DM2500 petrographic microscope with mounted camera through which all the figures were obtained. The mineral abbreviations used in this chapter were based on Kretz (1983) symbol system.

3.2 Petrography of the Gubaoquan Site

The Gubaoquan site is largely composed of the metamorphic units such as paragneiss and orthogneiss that make up the Proterozoic Liuyuan basement, within which eclogite blocks are hosted. Other lithologies present includ granitic veins, dolerite and lamprophyre dykes that seem to be syn- to post-metamorphic intrusions as they are undeformed and retain igneous mineralogy (Figure 3.1). Thin section examination revealed that the development of peak metamorphic assemblages and subsequent retrogression is strongly dependant on rock bulk composition.

The petrographic study of sampled lithologies revealed that alteration effects are widely present in all rock types. It was observed that the degree of alteration and weathering is associated with mineralogical composition and fluid content. As more hydrous rocks (lamprophyre) or those affected by alteration during retrogression (eclogite) display the strongest weathering and alteration effects from all rock types studied at this site

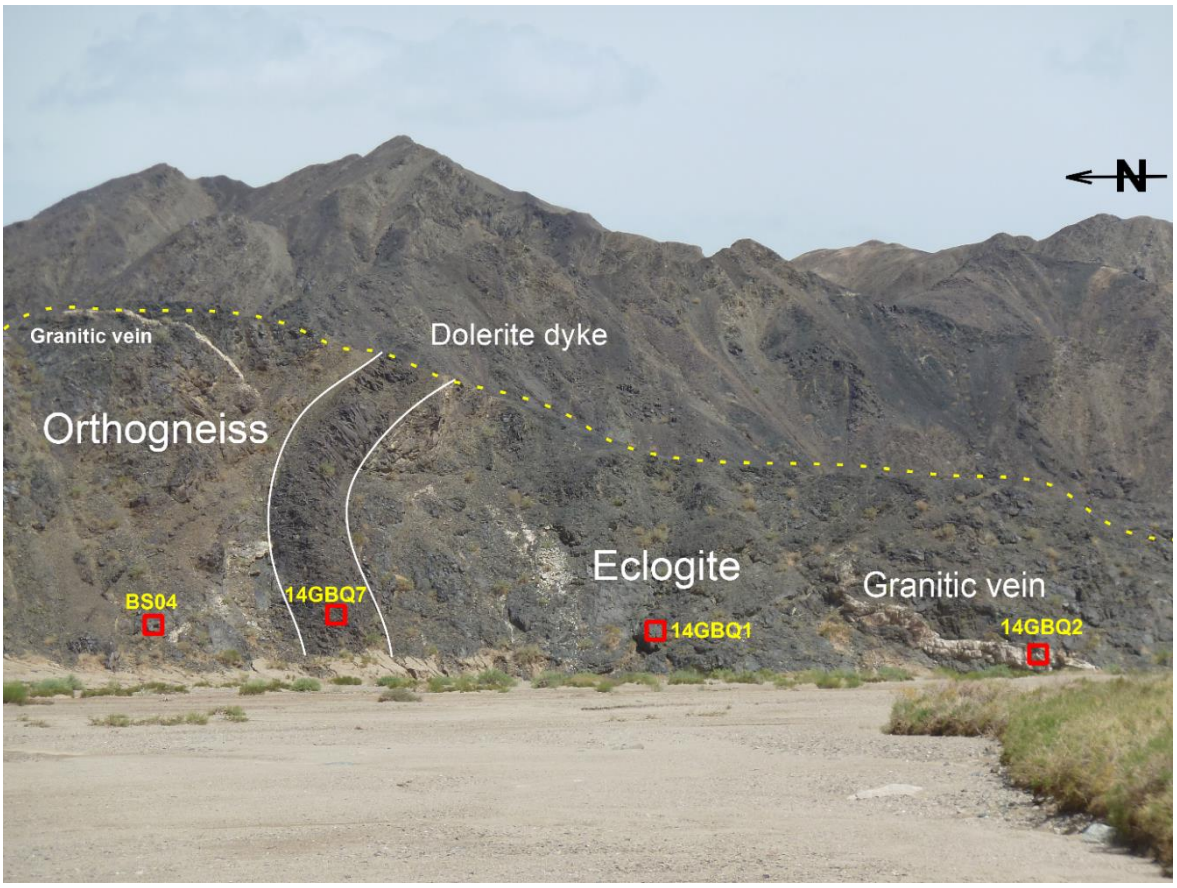

Figure 3.1 Image of Gubaoquan site outcrop along the river bed. It shows most of the lithologies from the site and from where the samples were collected. The lamprophyre and orthogneiss outcrop is ~100 m south from this location. Site location: 40° 59' 17.80"N, 95° 02' 20.29"E.

3.2.1 Eclogite

Several samples have been collected across a petrologically zoned eclogitic body. From the centre to the margin the effects of retrogression metamorphism become more pronounced, to the point where the margin of the eclogite has reverted completely to an amphibolite with none or very scarce garnet preserved. All acquired samples were collected from the largest eclogitic body in Beishan area, because only the cores of largest blocks have actual the eclogite facies garnet + omphacite mineral assemblage preserved in them. In most eclogitic bodies in the area the omphacite has inverted into amphibole and plagioclase forming symplectite textures. Additionally during the regressive stage amphibolite facies metamorphic event overprinted pre-existing mineral assemblage with amphibole and plagioclase.

The sample 14GBQ1 was collected from the main exposed section of the eclogite body (40° 59' 17.80"N, 95° 02' 20.29"E) (Figure 3.1). The overall macroscopic texture of the sample is granoblastic and medium grained, with garnet and amphiboles easily identifiable in hand specimen. In thin section major minerals are: amphibole (40%), garnet (30%) and plagioclase (25%). Also present are relict omphacite and quartz, rutile, secondary chlorite, opaque minerals and zircons that are common as inclusions in garnets. The garnets range from subidioblastic to xenoblastic and are 0.5 to 2 mm in size. The amphibole + plagioclase symplectite is mostly xenoblastic but some exist as pseudomorphs after omphacite or augite maintaining subidioblastic form. The majority of plagioclase within this sample is part of the symplectite as pseudomorph after omphacite, however occasional crystals have been observed, especially within veins and often associated with amphiboles suggesting association to the later stage amphibolite facies metamorphism. The sample does not show strong signs of alteration, the chloritization is restricted to microfractures. Several large amphibole crystals show dusty texture to their cores and more pronounced cleavages indicating slight effects of the alteration.

Sample BS02 was collected from near the granitic vein, it has the same mineral composition and very similar mineral content and crystal size to the sample 14GBQ1. In thin section this sample shows widespread evidence of later stage amphibolite facies event, with a 2 cm veinlet composed of amphibole and plagioclase intruding into the eclogitic body. In this section grain size is 2 to 6 mm with a subidioblastic to idioblastic crystal habit.

The textural relationships between preserved original phases and secondary mineral replacements show complex series of metamorphic episodes that have affected the eclogite facies assemblage. The garnets have proven to be most useful in unravelling this series of events as they were able to preserve mineral assemblages from different stages and were not strongly affected by later retrogressive processes or alteration. The first metamorphic episode (M_1) recognized, was the eclogite facies metamorphic event in which garnet and omphacite have crystallized. However mainly garnet remains as definite evidence of this episode as omphacite has been recrystallized into plagioclase and amphibole symplectite in the subsequent hydrous retrogressive episode (M_2) (see Figure 3.2). Small inclusions of omphacite have been persevered in many garnet cores and some fragments still remain in the groundmass, often surrounded by other minerals like quartz or opaque that protected them from expanding symplectite domains. Therefore presence of omphacite in equilibrium with garnet provides evidence that this rock underwent eclogite facies metamorphism, even

though it was almost erased by the subsequent M_2 episode. The evidence of M_2 event are clearly visible by micro-veinlet intrusions within eclogite body as described in sample BS02, and were also visible in sample 14GBQ1 where a fine-grained vein of interlocking plagioclase and amphibole cross-cuts garnet grains. The retrogression metamorphism of eclogites observed here is most likely associated with exhumation of the metamorphic terrane (Ernst 2001).

The evidence gathered in thin section show that anhydrous eclogitic body underwent saturation with fluids at the time of retrogression metamorphism. This was suggested by well-developed texture of some of the amphibole + plagioclase symplectites that form in hydrous environments. The symplectites after omphacite that commonly develop in eclogites consist of clinopyroxene + plagioclase in form of thin worm-like textures, where individual minerals are often hard to distinguish under petrographic microscope. However in sample 14GBQ1 some symplectites had thick and well-developed intergrowths of amphibole + plagioclase with multiple twinning present. This is indicates advanced recrystallization at amphibolite facies regime.

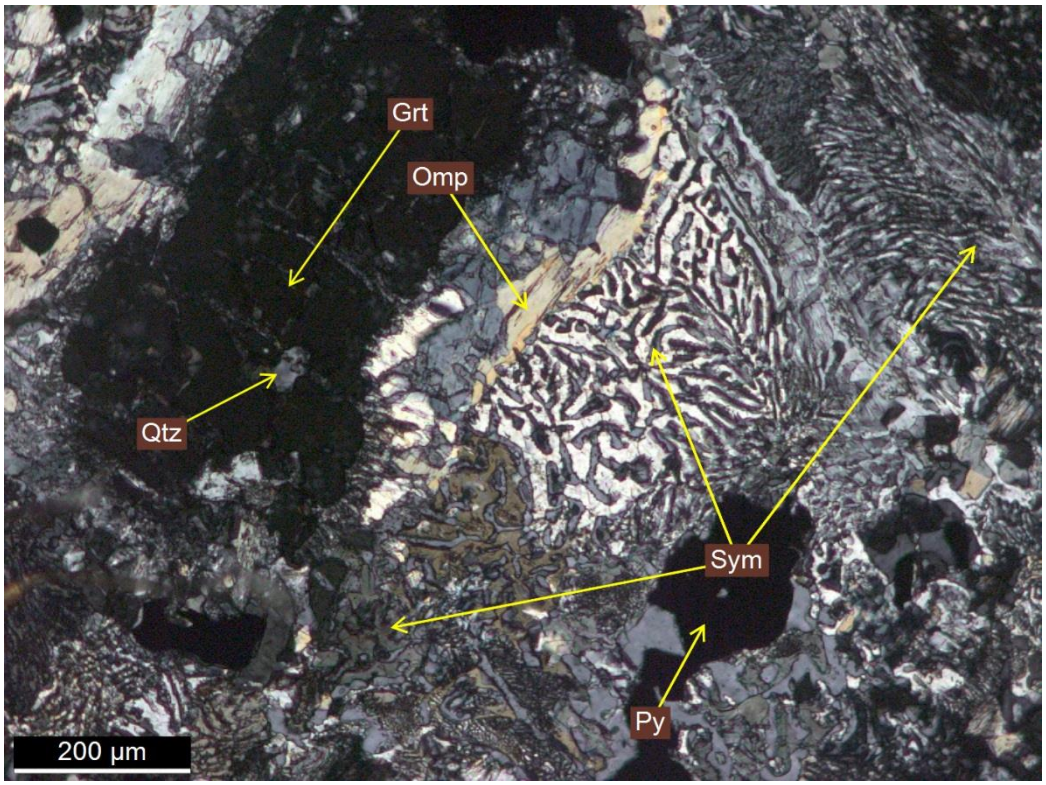

Figure 3.2 Photomicrograph in cross polarized light of the sample 14GBQ1 showing remnants of eclogite facies mineral assemblage and symplectite (Sym) replacing omphacite.

3.2.2 Amphibolite

The amphibolite sample 14GBQ4 was collected from the rim of the large eclogite body (40° 59' 17.80"N, 95° 02' 20.29"E). In thin section mineralogical composition of the sample is dominated by amphiboles (94%), other minerals present include plagioclase (3%), orthoamphibole (< 1%), quartz (< 1%) and opaque (< 1%). The sample is medium-grained and has granoblastic texture defined by the abundant amphiboles which are randomly orientated and show subidioblastic to xenoblastic crystal shape, several simple twins have been observed within the interlocking mass. The minor orthoamphiboles have been observed within the sample showing xenoblastic grain shape (Figure 3.3). The majority of opaque minerals have been identified to be pyrite, it commonly occurs as disseminated cluster of blebs, sometimes intergrown with amphibole resembling a symplectite texture. The effects of alteration on the sample are pronounced, strong dusty texture has been observed on the plagioclase and to a lesser degree on the amphiboles (Figure 3.4). The latter also shows more prominent cleavage planes what signifies a minor alteration.

From the field relationships between where this sample was taken and the core of the eclogite body indicate that this part might have been eclogitized at the peak stage of the metamorphism but then was retrogressed to amphibolite facies during exhumation. Examination of the thin section has not revealed any eclogite facies remnants, the mineralogical composition evidently points to amphibolite facies assemblage of amphibole + orthoamphibole + plagioclase + quartz indicating complete recrystallization in the margin of the mafic body.

(Figure 3.3 and Figure 3.4 on the next page)

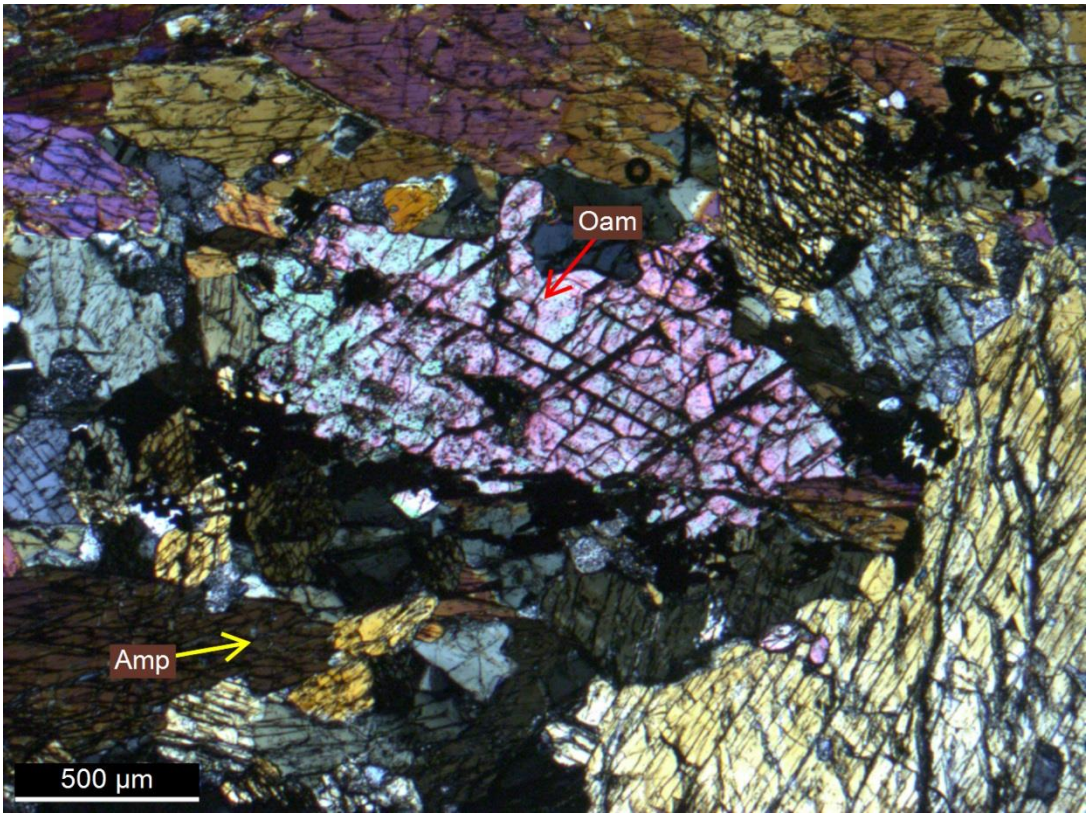

Figure 3.3 Photomicrograph in cross polarized light of the sample 14GBQ4 showing common amphibole and rare orthoamphibole.

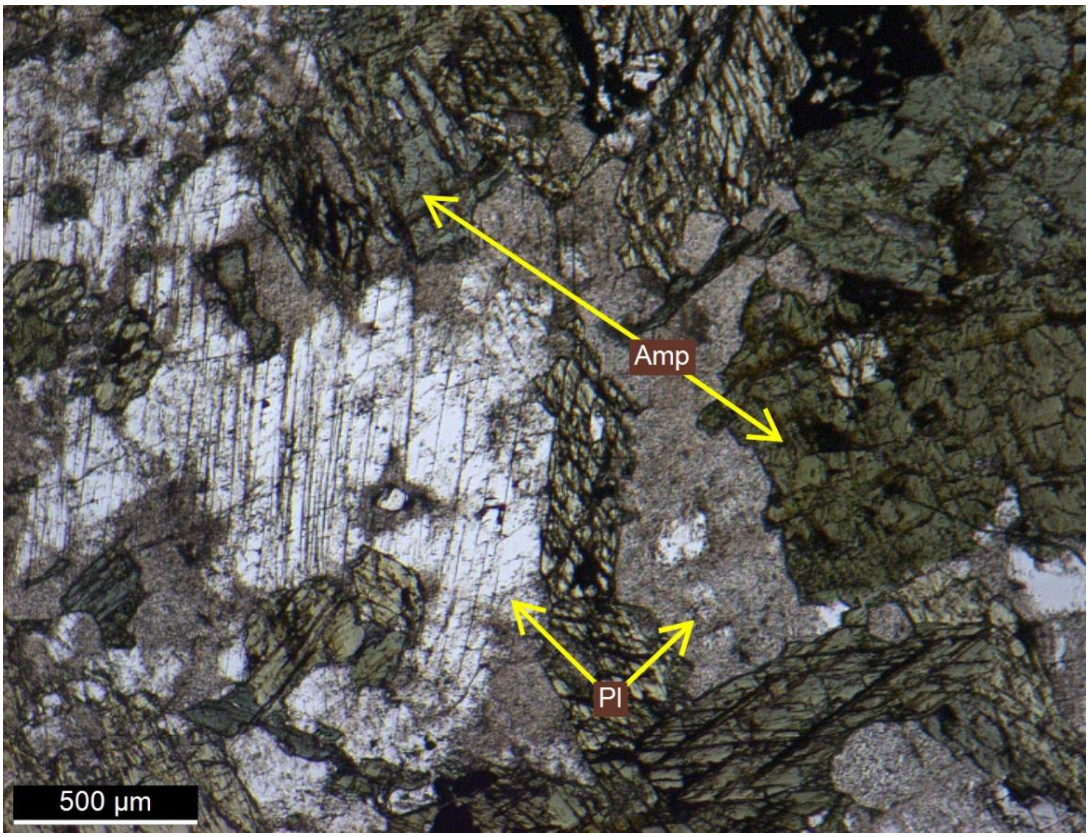

Figure 3.4 Photomicrograph in plane polarized light of the sample 14GBQ4 showing an amphibolite facies mineral assemblage and strong effects of alteration.

3.2.3 Orthogneiss

The four gneiss samples (14GBQ10, 14GBQ8, 14GBQ6 and BS04) were collected about 100 metres south from eclogite body (40° 59' 9.49"N, 95° 02' 19.14"E). This lithology has developed augen texture but augen size is highly variable. The major minerals in sample 14GBQ10 are quartz (40%), microcline (30%) and plagioclase (25%) and minor biotite (1%), muscovite and secondary chlorite (3%) with accessory opaques and zircon (many large prismatic zircons have been identified within this sample). Other two samples 14GBQ8 and BS04 show very similar mineral composition and textures, the only difference being the degree of alteration and mica content (varying from 1% to 5%). The augen are composed of microcline feldspar that contains occasional inclusions of other minerals like quartz or plagioclase that usually are more altered than the enclosing feldspar. Within the augen pressure shadows ellipsoidal agglomerates of quartz with granoblastic texture have been observed, which can be quite common within mylonitized rocks with rigid porphyroclasts. Myrmekite of quartz + plagioclase occurs in sample 14GBQ10 and 14GBQ8 (Figure 3.5). This might be an additional indicator of the tectonic deformation to which this rock has been subjected. The matrix mineralogy of the gneiss has overall xenoblastic texture and is composed of quartz, finer microcline, porphyroclastic plagioclase and fine micas that define the foliation. Quartz is found as elongate “ribbons” that have recrystallized into subgrain domains. The mineralogy and textures support that this gneiss had an igneous protolith that was probably a granitic, therefore it is referred to as an orthogneiss.

The samples display apparent signs of alteration, especially in feldspars where dusty textures have been observed (Figure 3.7). The most affected are plagioclase crystals where almost whole grains have been overprinted by sericite to the point that phase could not be identified. However, small cores of few crystals have been preserved displaying multiple twinning what led to their successful identification. The microcline does not display as strong alteration, only slight dusty texture that occurs as patches in parts of the crystals. The secondary minerals such as chlorite occur mainly along microfractures cross-cutting the feldspar crystals and along foliation planes. These zones are preferential paths for any potential fluid to penetrate the rock, and where exposed crystal faces can undergo the alteration reactions that lead to formation of secondary minerals; in this way several veins of chlorite were produced (Figure 3.7). However overall effects of chloritization and sericitization are evident throughout the sample but their products are extremely fine

grained, whereas within veins these minerals precipitate as larger crystals due to space availability. This strong and uniform alteration of feldspars and presence of myrmekite might indicate some metasomatic activity during exhumation of this unit. The textures and mineralogy indicate high temperature assemblages were slightly retrogressed with fluid ingress during greenschist facies retrogression (M_3).

The mineralogical composition of sample BS04 consists of quartz (70%) and orthoclase (30%) with other minor minerals such as plagioclase (3%), muscovite (1%), tourmaline and secondary chlorite. This sample also has augen texture, where augen are composed of orthoclase and orthoclase + quartz, with muscovite developing the foliation around the augen. All phases present in the rock have been arranged into layers during deformation and metamorphism producing xenoblastic grain shapes. The quartz is the dominant matrix mineral. It is fine-grained and granoblastic and commonly exists as layers or ribbons in pressure shadows between the augen. Throughout the sample small localised sites of tourmaline clusters have been observed. The effects of alteration are evident within the sample in the form of dusty textures in feldspars and precipitation of secondary minerals (Figure 3.6). The sericitization has affected all feldspars, but plagioclase were most affected to the point of some being unidentifiable. Orthoclase crystal are less altered and show only slight dusting in plane polarized light (Figure 3.6). The effects of chloritization can be recognized along microfractures and foliation planes that are adjacent to the plagioclase crystals. Such sites were favourable for precipitation of chlorite and it is the most common mode of occurrence, however small chlorite laths are also present within some plagioclase crystals alone.

(Figure 3.5 and Figure 3.6 on the next page)

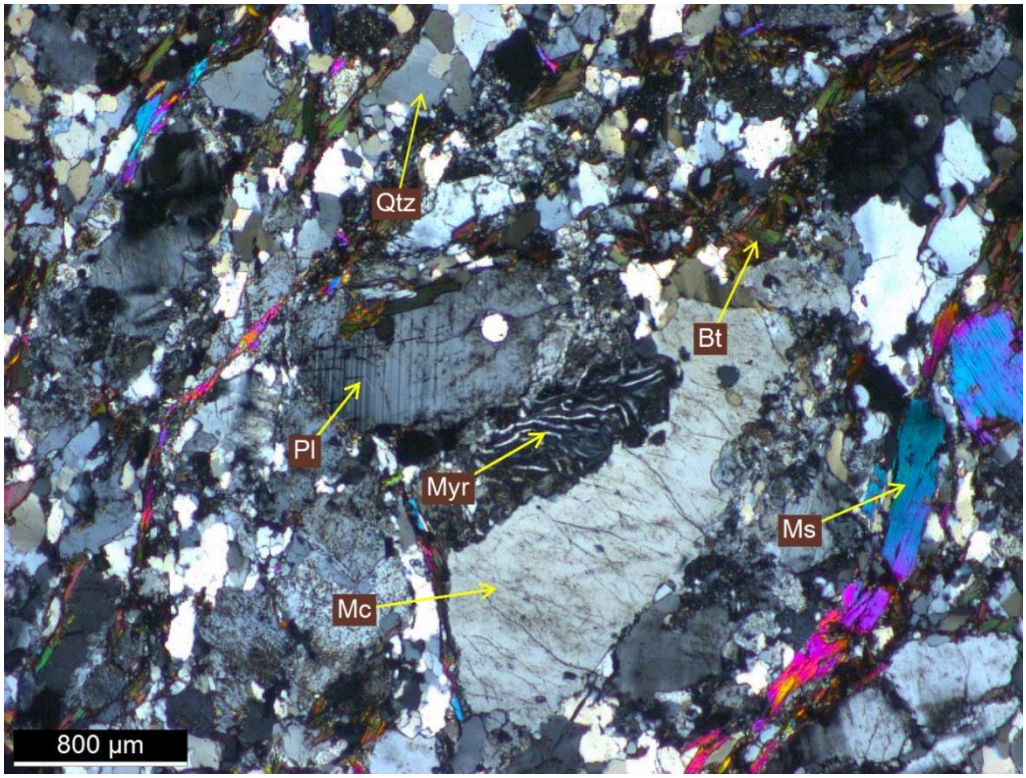

Figure 3.5 Photomicrograph in cross polarized light of the sample 14GBQ8 showing the general mineral assemblage and textures. The texture of interest is the myrmekite (Myr) shown in the centre. (Mc – microcline, Ms – muscovite)

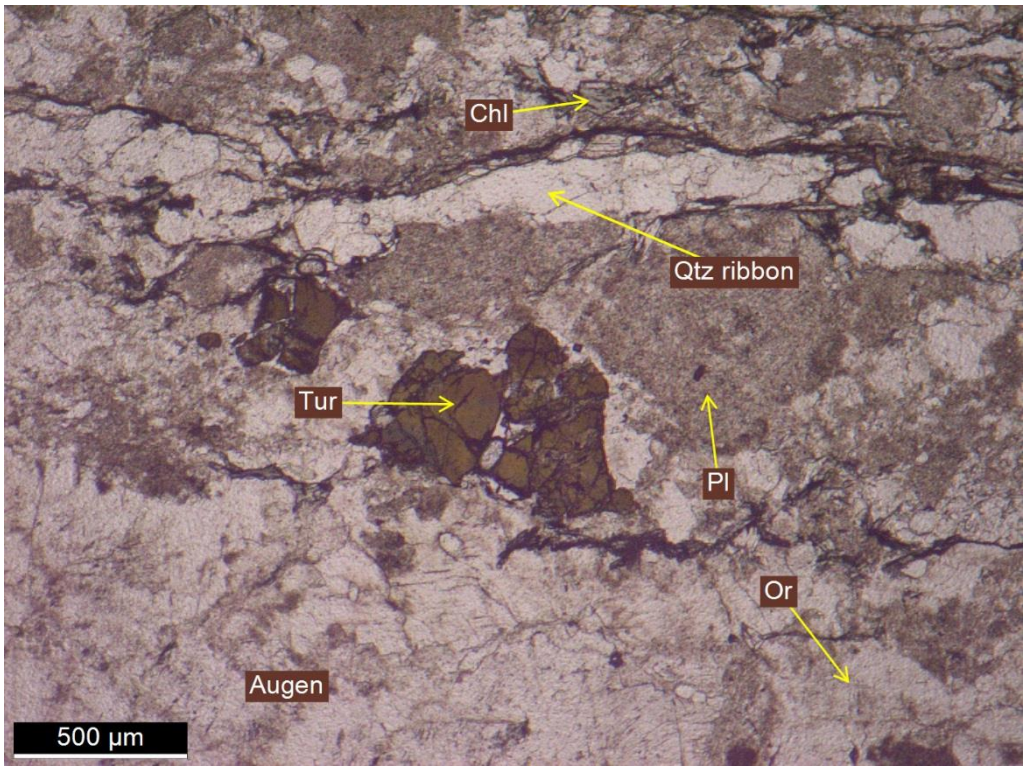

Figure 3.6 Photomicrograph in plane polarized light of the sample BS04 showing part of larger augen, common minerals and accessory tourmaline. The alteration effects of feldspars are well displayed in this image.

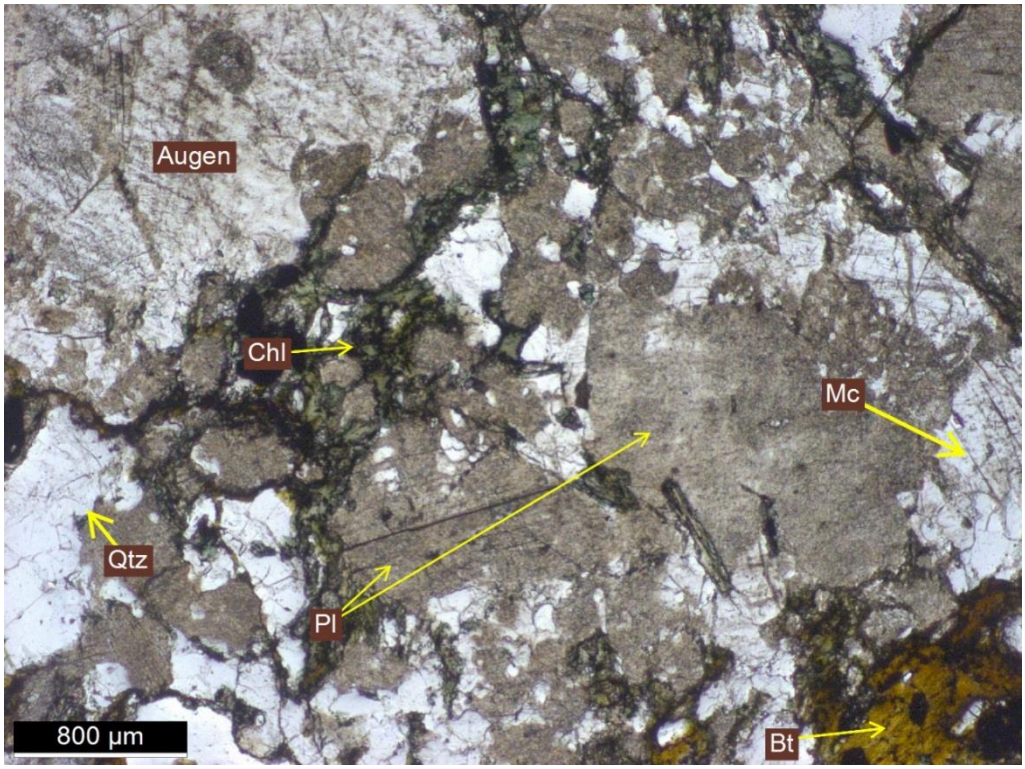

Figure 3.7 Photomicrograph in plane polarized light of the sample 14GBQ10 shows part of microcline augen and matrix mineral assemblage. The effects of chloritization and sericitization on feldspars are clearly visible in PPL.

3.2.4 Granitic vein

The sample 14GBQ2 was collected from the granitic vein intruding the eclogite (Figure 3.1). It shows overall equigranular texture formed by plagioclase (40%) and quartz (40%) and some potassium feldspar (15%). The muscovite occurs as laths along junctions between grain boundaries of other minerals (Figure 3.8). Sporadic biotite laths have also been spotted, their pleochroic colours were very weak, what suggests iron deficiency within the rock. The plagioclase crystals are subhedral and display multiple twinning in majority of the grains, some crystals and crystal clusters also show grid twinning. Whereas quartz and potassium feldspar are anhedral and are infilling among the plagioclase. The potassium feldspar is sparse and only few crystals shown simple twins. Some large plagioclase crystals have inclusions of the smaller grains, they are rounded therefore lost their euhedral shape. This is likely due to remelting of the crystallized phases during secondary or multiple magma injections into the chamber or violent magma mixing during initial stages of plutonism.

This sample shows signs of alteration, especially in feldspars where almost all grains have dusty alteration texture that is clearly visible in both plane and polarised light in thin section.

Another alteration feature identified within plagioclase was exsolution lamellae that formed orthogonally to the direction of twinning within 3% of the crystals. However the most widespread process that effected all feldspars within this granite sample was breakdown of feldspars to sericite and minor chlorite. The sericite did not affect the grain boundaries to high degree, it mainly overprinted across all feldspar phases in preferential direction of each grain. However chlorite alteration in contrast to sericite is more common at the grain boundaries where it displays intergrowth patterns with muscovite and sericite, indicating that sericitization and chloritization occurred at the same time (Figure 3.8).

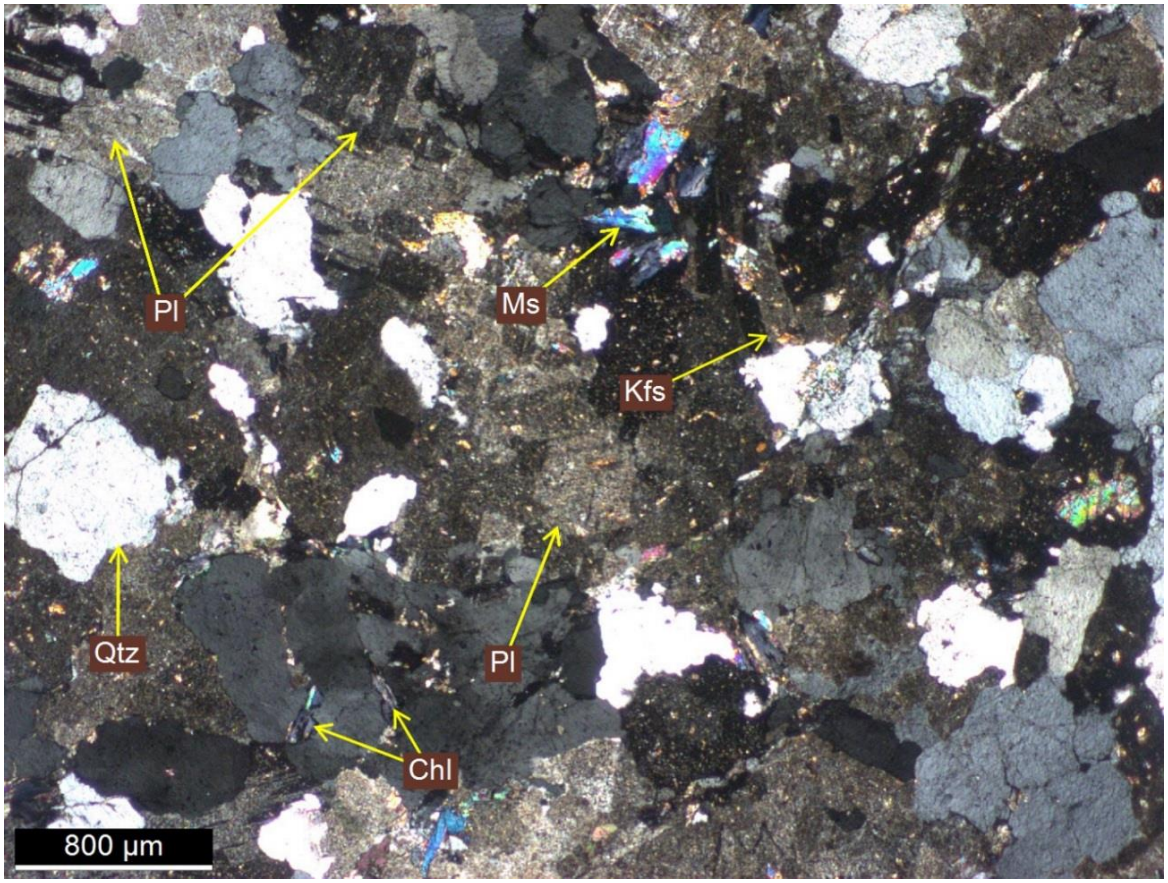

Figure 3.8 Photomicrograph in cross polarized light of the sample 14GBQ2 shows mineral assemblage of the granitic vein. The effects of sericitization and chloritization are clearly visible. Inclusion of rounded feldspar can observed in top left corner under "Pl" label.

3.2.5 Dolerite

The sample 14GBQ7 was collected from the mafic dyke adjacent to the eclogite body (Figure 3.1). The dolerite is fine grained and has holocrystalline ophitic texture composed of plagioclase (40%), clinopyroxene (35%), orthopyroxene (10%) and amphibole (5%), other minor minerals include: opaque phases (mostly pyrrhotite 5%), biotite (4%) and quartz (≤1%). The rock has poikilitic texture of the rock is defined by plagioclase as chadacrysts

within oikocrystic pyroxenes (Figure 3.9). The opaque minerals vary in shape, ranging from euhedral to anhedral. The anhedral crystals often display ameboidal shape sporadically containing inclusions of other minerals where most of them have been identified as pyrrhotite (Figure 3.10). Whereas euhedral to subhedral crystals have been identified as different sulfide phase, but they require chemical analysis for accurate phase determination as its soft nature resulted in strongly abraded surface making it hard to identify in reflected light.

The alteration mainly affects the amphiboles and biotite, it is evident through the dusty texture on the crystals. The sericite alteration is mainly present on plagioclase crystals, especially along cleavage planes and microfractures but general overprint is also visible. The chloritic alteration is more profound and it affects both plagioclase and pyroxenes, its strongest effects occur along grain boundaries and microfractures. Small reaction rims have been observed between plagioclase and pyroxenes, however the small scale of this occurrence made the products unidentifiable.

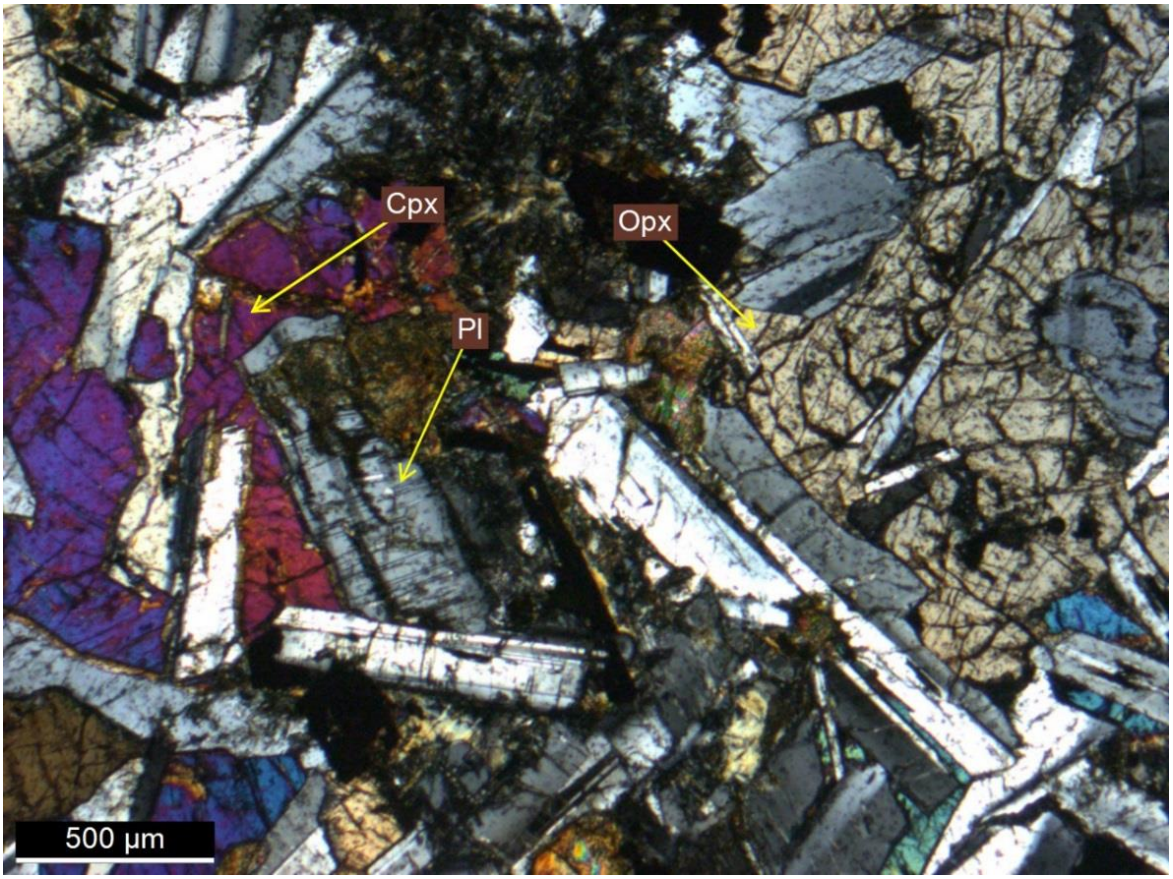

Figure 3.9 Photomicrograph in cross polarized light of the sample 14GBQ7 showing mineral assemblage of the dolerite dyke with poikilitic texture shown to the left from the centre.

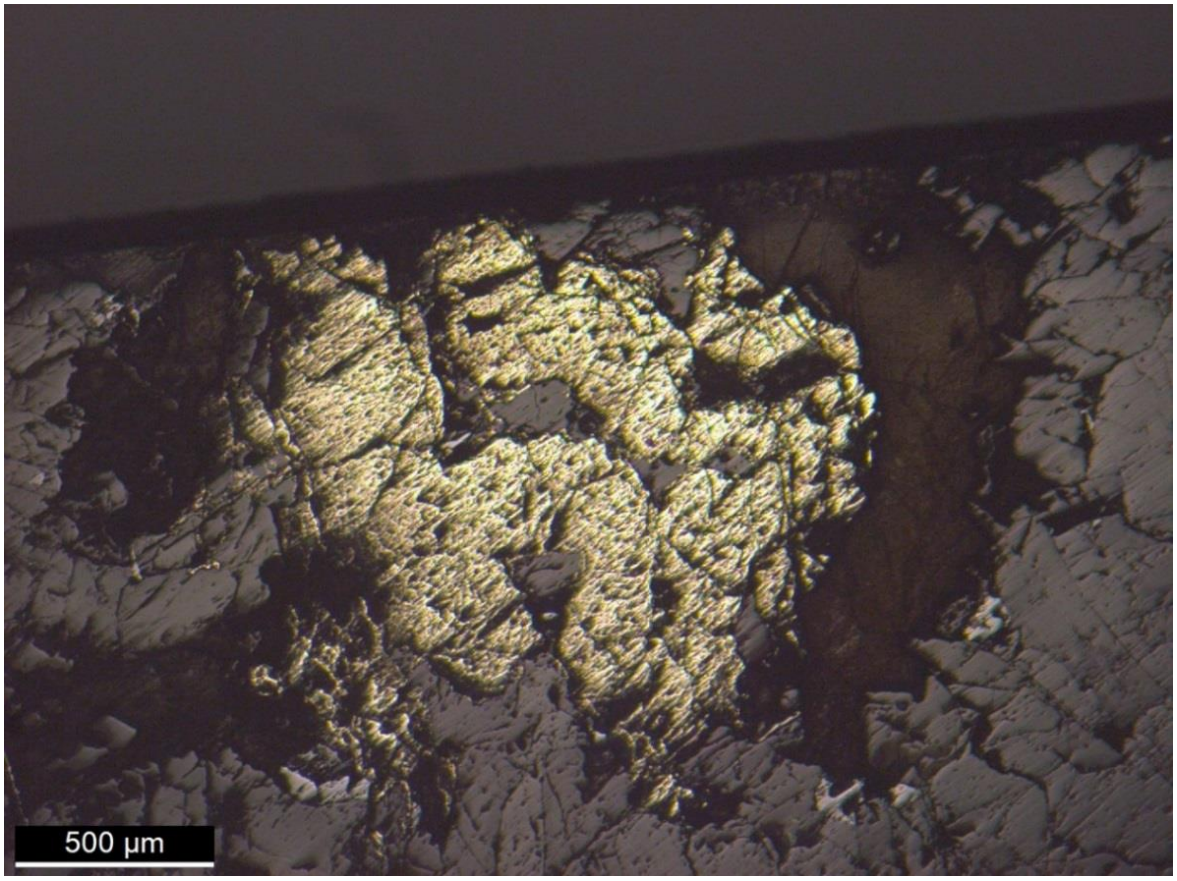

Figure 3.10 Photomicrograph in reflected light of the sample 14GBQ7 showing large anhedral pyrrhotite crystal with inclusions.

3.2.6 Lamprophyre

The sample 14GBQ9 was collected from the lamprophyre dyke that was cross-cutting the orthogneiss. In the outcrop, like most lamprophyres it was heavily weathered and eroded in comparison to surrounding strata. The effects of alteration were strongly evident in thin section, as majority of phases (~90%) show alteration of their primary mineralogy.

In thin section fine grained (0.1-0.5 mm) porphyritic texture has been observed where phenocrysts consist of olivine pseudomorphs (0.05-0.44 mm), pyroxenes (0.05-0.30 mm) and phlogopite (0.05-0.50 mm). The groundmass is hypocrystalline and aphanitic, however minor phases were possible to identify and consist of phlogopite, pyroxenes, sericite and chlorite. The olivine pseudomorphs constitute ~20% of the mass, there is very little olivine present as majority has been completely replaced by alteration products, however the phase was identified due to its characteristic crystal habit (Figure 3.11). The pyroxenes also have been completely replaced by the alteration minerals what made further identification impossible (Figure 3.12). Small olivines and pyroxenes have not been observed as most

likely they have been completely altered, and now are indistinguishable from the groundmass. Some minor plagioclase was also identified but like the rest of the sample it was heavily altered to sericite and chlorite, therefore it is believed that sericite and chlorite within the groundmass is purely a product of altered olivine, pyroxene, plagioclase and other minerals.

Interesting relationship seen throughout the sample was that all olivine and pyroxene crystals have thin and brown corona around it, what could suggest reaction between those phases and hydrous melt as magma cooled. Some opaque minerals are also present within the lamprophyre; they are not sulfides as the have silicate-like internal reflections in reflected light. They constitute 1-2% of the groundmass as small nodules and can also be large and abundant in the olivine and pyroxene phenocryst rims.

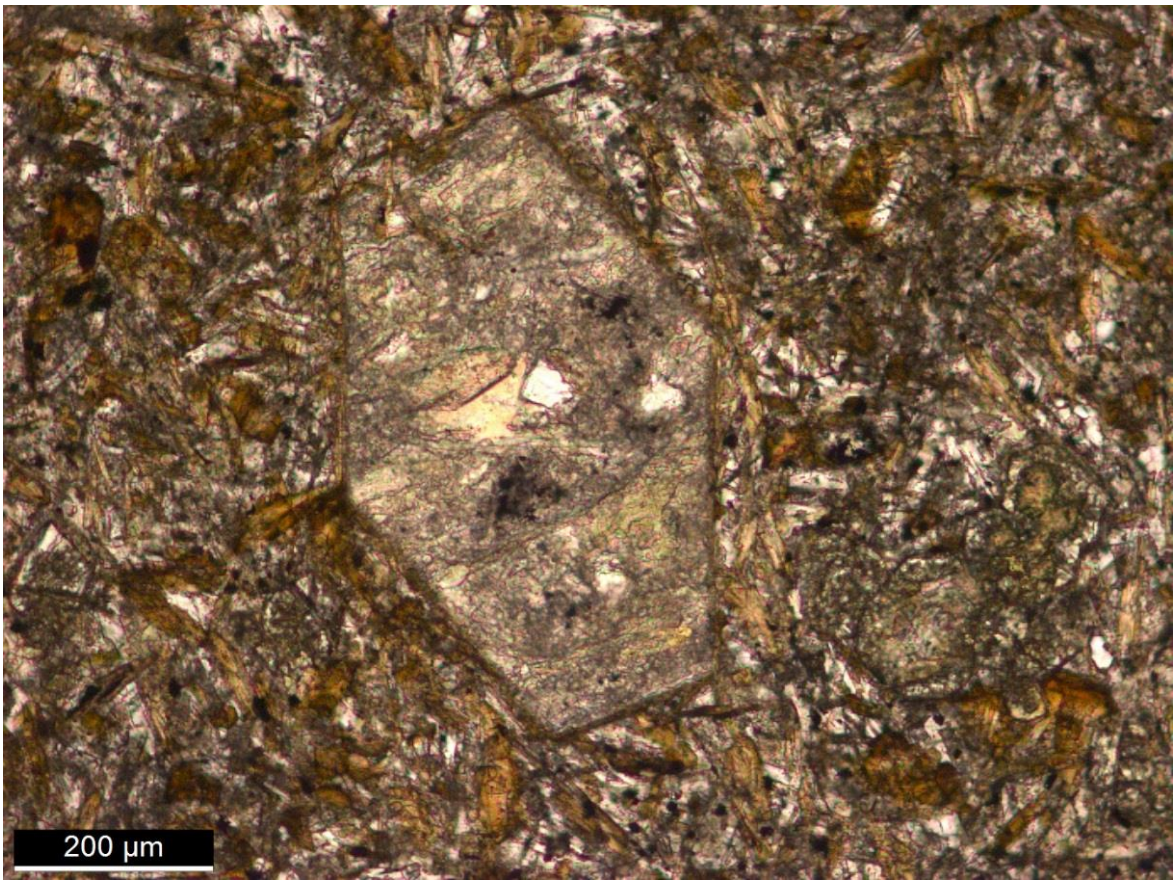

Figure 3.11 Photomicrograph in plane polarized light of the sample 14GBQ9 displaying pseudomorph after olivine phenocryst within fine-grained micaceous matrix.

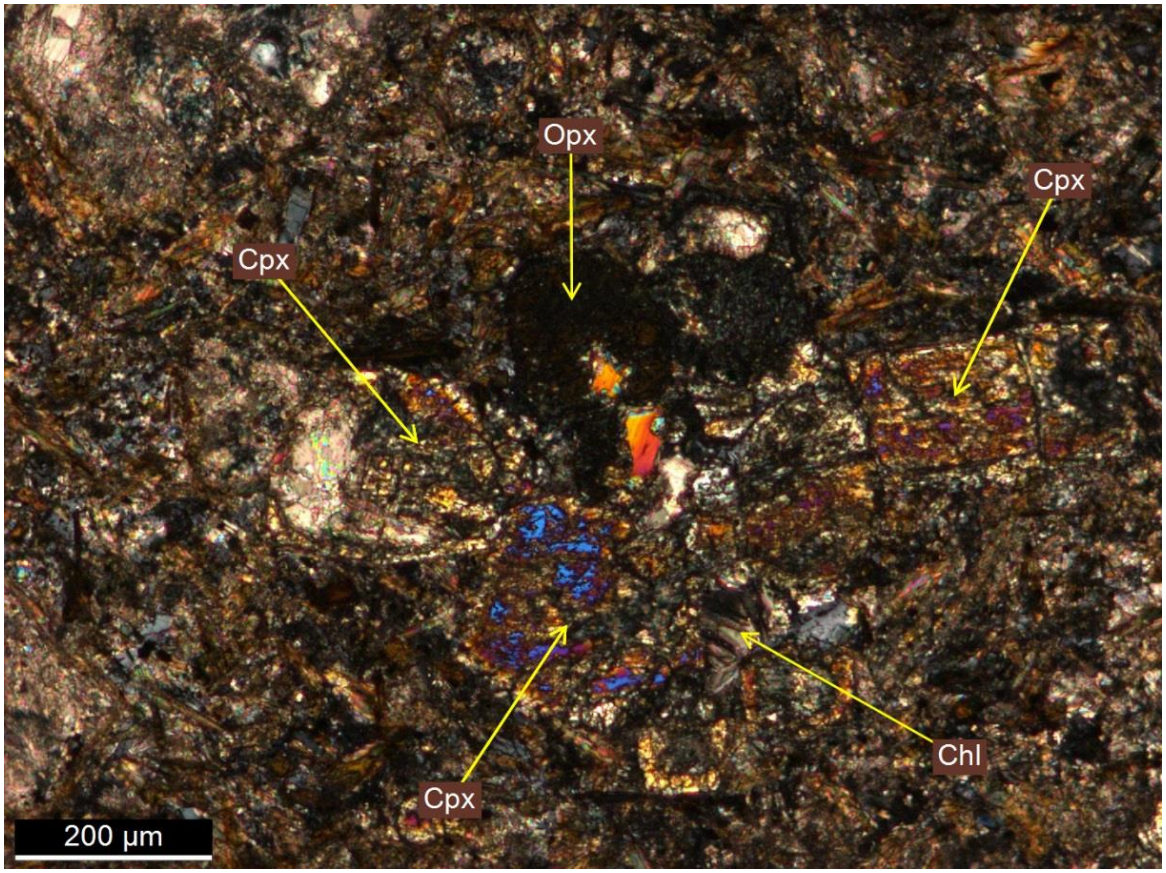

Figure 3.12 Photomicrograph in cross polarized light of the sample 14GBQ9 displaying strongly altered cluster of pyroxenes with large chlorite laths.

3.3 Petrography of the Kanfenggou Site

The samples used for petrography of Kanfenggou site were collected from 33°50'2"N 110°51'27"E. The lithology hosting the eclogites is the paragneiss (metagreywacke). Other lithologies encountered are metasandstone and amphibolite. All those rocks have been assigned to the Lower Proterozoic Qinling Group (Wang *et al.* 2011). The rock outcrops are only exposed along a country road and stream bed as these poorly exposed rocks are covered by alluvium and vegetation. Two main rock types sampled were eclogite (15KF4) and paragneiss (15KF1) (Figure 3.13a and 3.13b, respectively). The outcrop of the latter is fresh, with very little fracturing and weathering. On the other hand, the eclogite is slightly fractured, along which weathering is noted.

Similar to the Gubaoquan site, the metamorphic evolution of the terrane is best preserved within the eclogite due to its competence during subsequent exhumation and hydration events. In contrast, the paragneiss displays the overall high degree of the ductile deformation that has affected these rocks. Therefore those two units have complement each other providing insight into the geological history of this area through the petrographic

investigation. The effects of the alteration were clearly visible during petrographic examination and the degree of its intensity corresponds to macroscopic features noted in the field. Microfractures were the main loci of alteration and it mainly occurred in three following modes: epidotization, chloritization and sericitization. However, sections distant from those fractured zones remained unaltered.

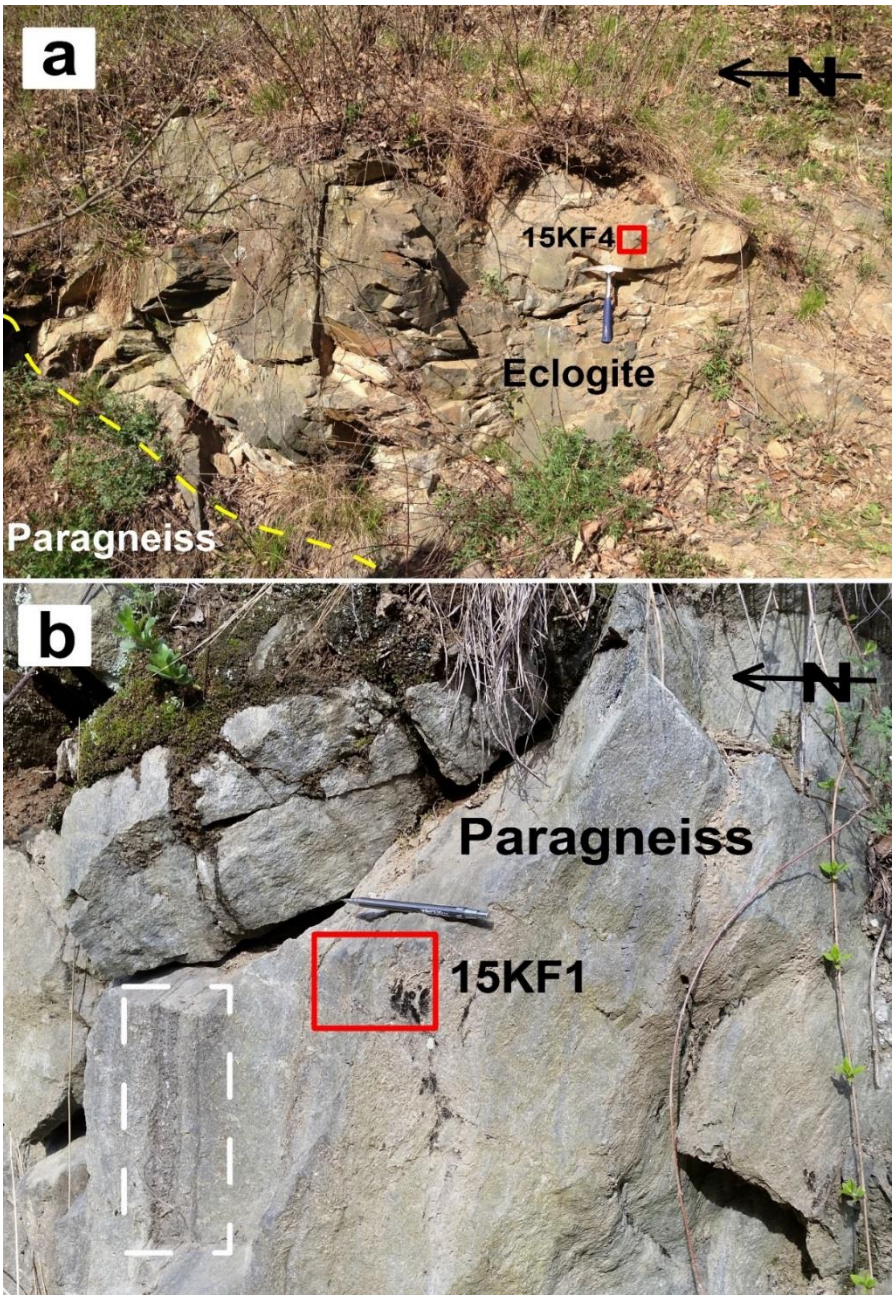

Figure 3.13 Rock outcrops near Kanfenggou from which individual sample were taken are shown by the red squares. (a) Shows the eclogite block (15KF4), the exact contact with paragneiss could not be determine due to vegetation cover. Around 30 meters south from this location the photograph of paragneiss (b) was taken. (b) Shows outcrop of the paragneiss (15KF1), the white dashed square shows original sedimentary layering present within the rock. To the right of centre of the photograph crenulation fabric can be observed.

3.3.1 Eclogite

A suite of samples was collected from the eclogite and they are labelled as 15KF4. Sample 15KF4_1a is sourced from the core of the block and shows porphyroblastic texture. Garnets form xenoblastic porphyroblasts in a granoblastic matrix of the rock. Their distribution is non-uniform and their grain size varies from 1 to 15 mm. However microscopic examination reveals that porphyroblasts consist of small garnet grains intergrown with quartz in form of clusters displaying a skeletal texture. Sample 15KF4_3b collected from the margin of the eclogite has consistent mineralogy to the core sample but it is texturally different. It is equigranular and weakly foliated, where elongated amphiboles, quartz-ribbon and needle-like omphacite crystals define a foliation (Figure 3.16).

The petrographic examination of eclogite sample 15KF4_1a revealed that mineral assemblage consists of garnet (40%), omphacite (30%), amphibole (10%), quartz (10%), titanite (5%) and other minor minerals such as clinozoisite, plagioclase, apatite and opaque minerals (Figure 3.14 and 3.15). The garnet grains range from 0.1 to 0.6 mm and their shape is idioblastic to xenoblastic. The omphacite appears to be dominated by jadeite, determined from its first order birefringence colours. Its crystals are generally subidioblastic and their size ranges between 0.05 and 0.3 mm. The amphiboles present within the sample were identified as glaucophane due to its characteristic blue-green pleochroic colours. They displayed subidioblastic grain shape and ranged in size between 0.05 to 0.3 mm. Titanite occurs as vein-like clusters of overlapping grains that are subidioblastic to xenoblastic and ranges in size between 0.08 to 0.2 mm. The opaque minerals encountered within the samples are mainly ameboidal sulfides such as chalcopyrite and pyrite. Generally minor alteration products are concentrated along microfractures, where chloritization of pyroxenes is most pronounced. Sericitization and epidotization of accessory plagioclase crystals has also occurred, but majority of minerals within the rock remain unaltered.

Thus eclogite facies mineral assemblage of garnet + omphacite + quartz + titanite is well preserved (Figure 3.15), but it has been slightly altered by late stage retrogressive amphibole overprint. The major minerals do not contain any signs of prior metamorphic events, therefore eclogite facies metamorphism is recognized as the first event (M_1). The omphacite crystals do not show strong evidence of retrogression in the form of symplectites as seen in the Gubaoquan eclogite. However appearance of glaucophane and intrusions of plagioclase + quartz microveins indicate that a retrogression event occurred (M_2). Nevertheless retrogression is not as pronounced as in Gubaoquan eclogite or other eclogites in the vicinity

described in the literature. Some effects at the rims of the Kanfenggou eclogite block were associated with deformational events of the terrane, which are well imprinted on the paragneiss and are further explored in section 3.3.2. After eclogitization this terrane had to be exhumed and cooled rapidly, preventing prolonged exposure to retrogressive high temperature decompression reactions.

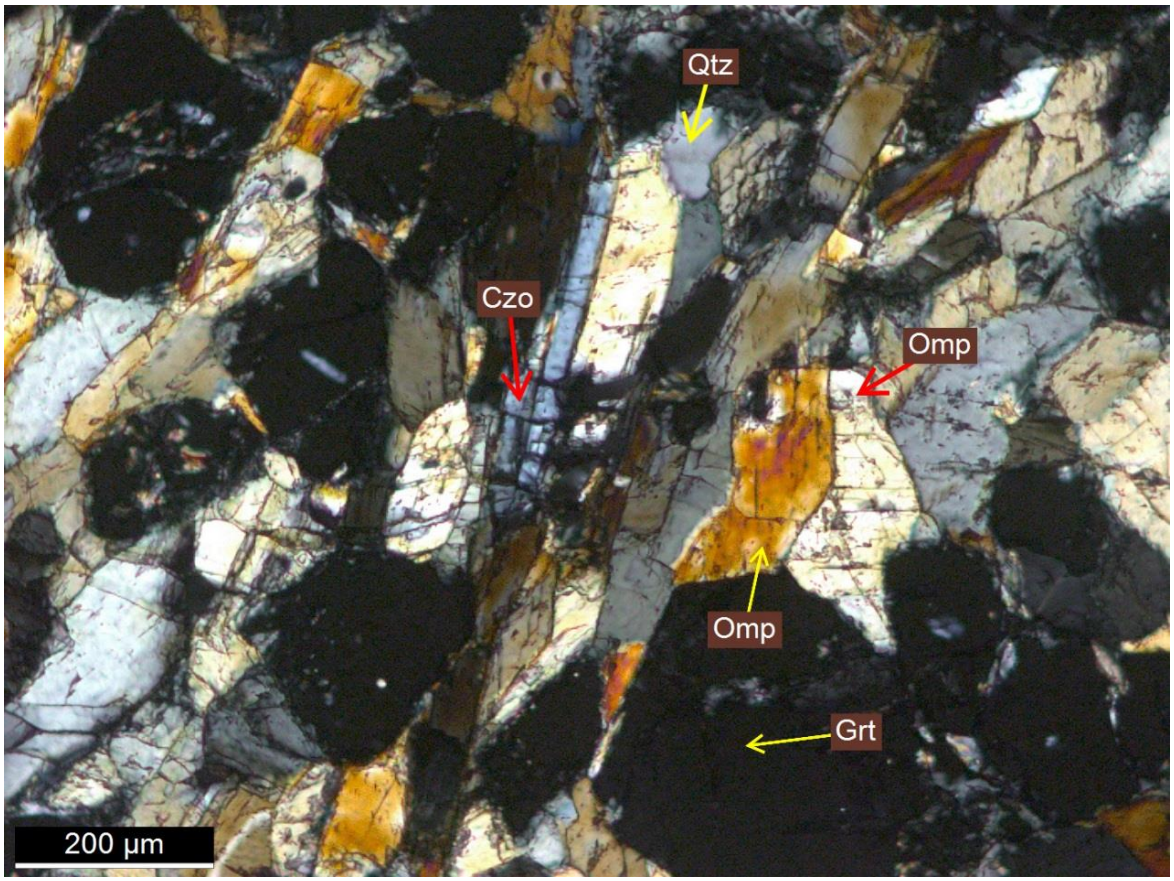

Figure 3.14 Photomicrograph in cross polarized light of the sample 15KF4_1a showing M_1 and M_2 mineral assemblages.

(Figure 3.15 and Figure 3.16 on the next page)

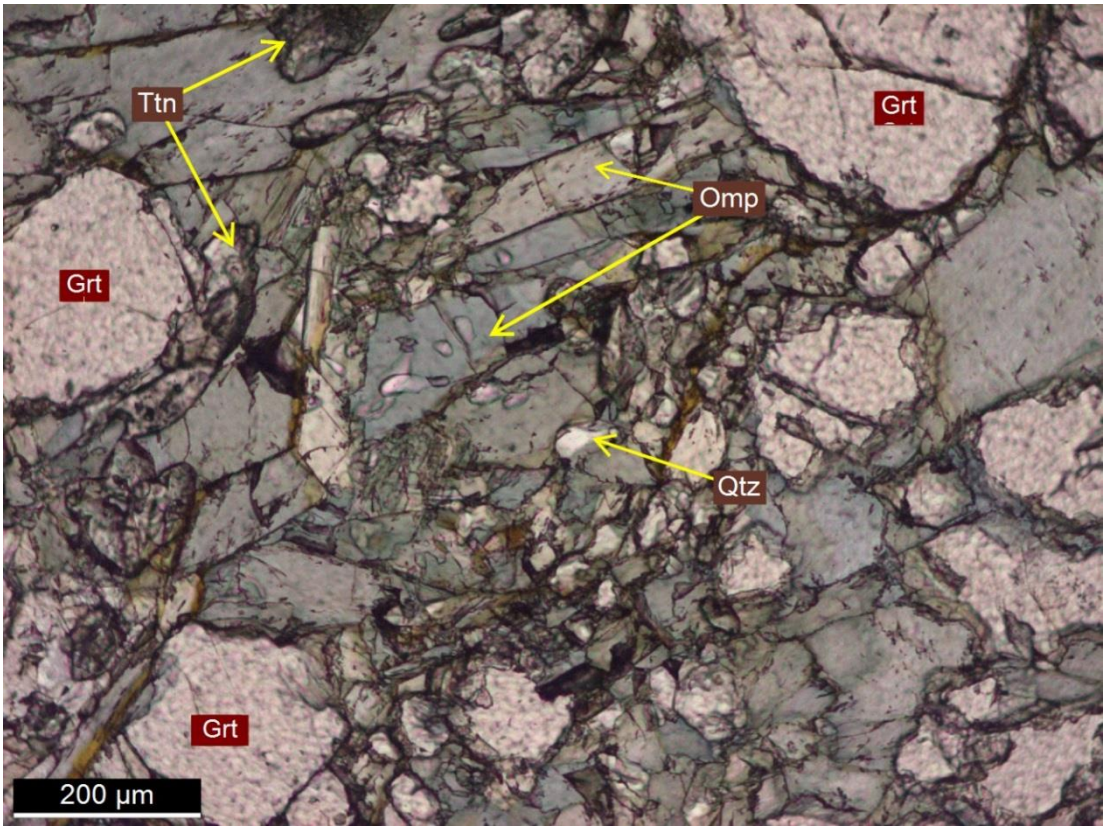

Figure 3.15 Photomicrograph in plane polarized light of the sample 15KF4_1a showing well preserved eclogite facies mineral assemblage.

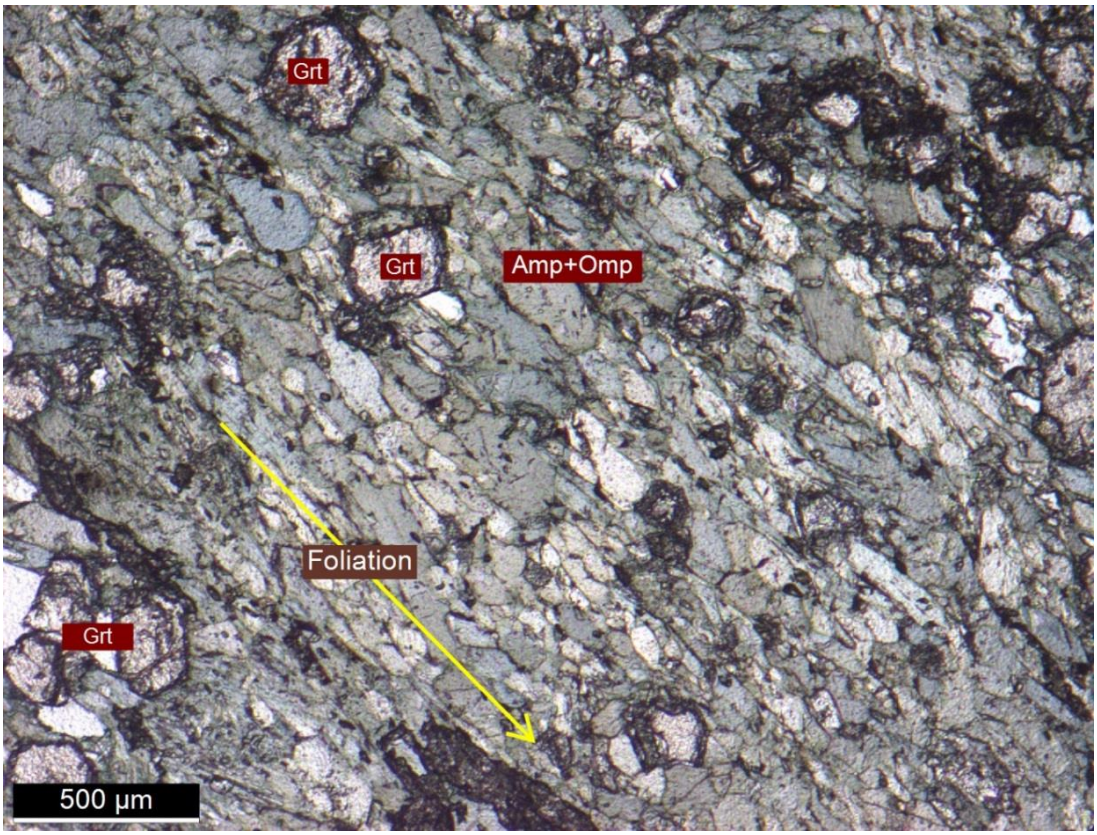

Figure 3.16 Photomicrograph in plane polarized light of the sample 15KF4_3b showing gentle foliation fabric produced mainly by amphiboles and sporadic omphacite.

3.3.2 Paragneiss

The sample 15KF1_a was collected from gneissic country rock to the eclogite, in literature it is often referred to as schist (Wang *et al.* 2013), but its mineralogical composition and texture indicates gneiss grade. Its mineralogical composition consist of quartz (40%), feldspar (orthoclase; 30%), biotite (15%) and muscovite (5%) with other minor minerals such as titanite, clinozoisite, tourmaline, chlorite and opaque minerals. The gneiss is fine-grained and foliated with biotite visible in macroscale along the foliation planes. This sample displays two metamorphic textures, a porphyroclastic augen (Figure 3.17) and granoblastic (Figure 3.18) due to its two distinct layers preserved within the rock. The augen range 0.2-0.7 mm in size and are mainly composed of feldspar that has poikiloblastic texture with small quartz inclusions, and commonly displays simple twinning. The metamorphic quartz have been observed within pressure shadows where two augen are close together, otherwise the augen are surrounded by foliation composite (biotite ± muscovite). Other rare minerals encountered were idioblastic tourmaline preserved within feldspar augen, idioblastic to subidioblastic titanite crystals and sporadic clinozoisite crystals within the foliation matrix.

From the macroscale observations this lithology is interpreted as paragneiss due to its well preserved original sedimentary layering and its richness in micaceous minerals (Figure 3.13b). The observed layered structure within the rock can be separated into two types of protolith's original material. The dominant Layer Type 1 (LT1) is the bulk composition of the rock, it consists of quartz and feldspar grains within muddy matrix (current micas) (Figure 3.20). The Layer Type 2 (LT2) is composed of quartz, feldspar and opaque minerals, muddy material (no or very little micas) is not present in this layer what could suggest higher energy event at the time of deposition (Figure 3.18). Based on the mineralogical composition and sedimentary structures found in this sample it is suggested that protolith of this rock could be a greywacke.

From both macro- and microscale observations two deformation events have been recognized. The first deformation event (D_1) was sheared, which led to development of augen texture and distinctive foliation in LT1 due to soft nature of the material. The LT2 was more rigid and resistant to deformation due to its compositional material and interlocking texture, therefore it remained unaffected. The second event (D_2) was of a compressional mode and lesser intensity but its σ_1 was imposed at different orientation, what

produced crenulation fabric throughout the rock with slight kink bending in LT2 creating tension gashes that were infilled by calcite (Figure 3.20).

The sample 15KF1_b is comprised of LT1 (Figure 3.20) that had the same augen texture and mineral composition as described above. However, it was observed that tourmalines were a lot more abundant and it is believed that this variation was caused by chemical diversity of proposed muddy matrix of the sedimentary protolith. The soft nature of this material prevented preservation of D_2 event macroscale deformational features. However thin section examination reveal that at microscale small effects of crenulation have been imposed on micaceous minerals (Figure 3.19).

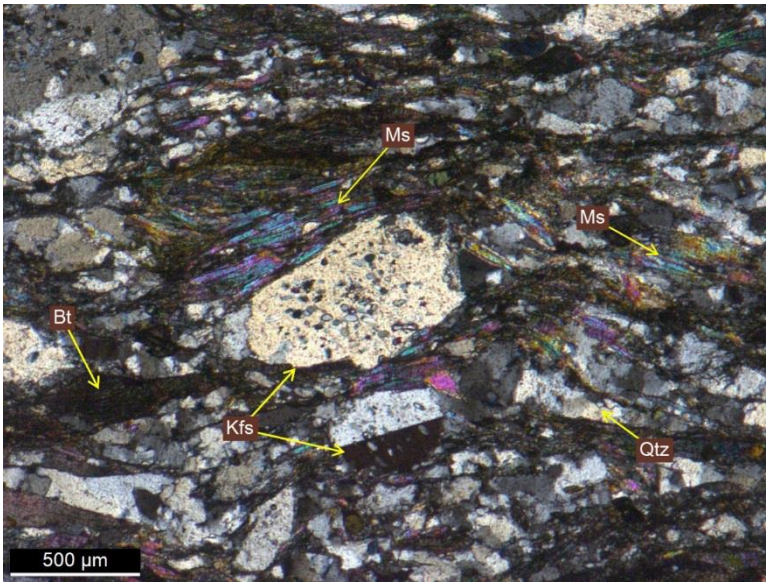

Figure 3.17
Photomicrograph in cross polarized light of the sample 15KF1_a showing part of LT1 with twinned K-feldspar augen in the centre. This part of thin section shows only muscovite + biotite foliation composite.

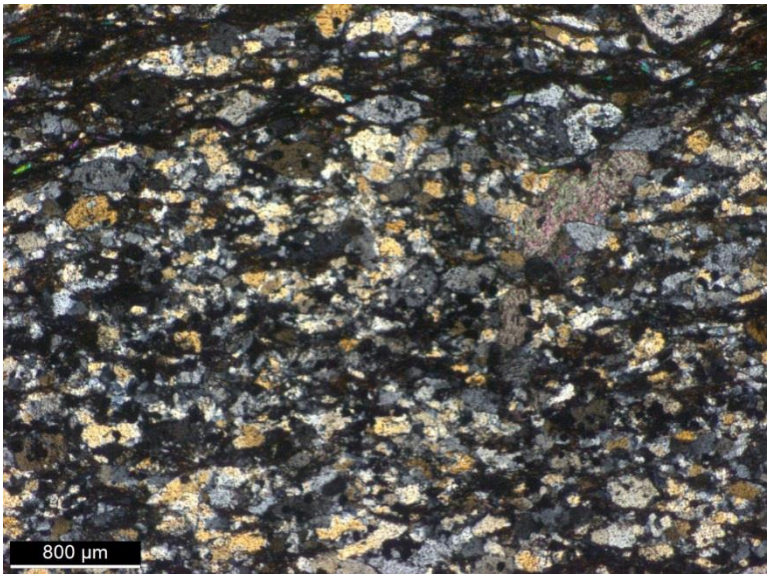

Figure 3.18
Photomicrograph in cross polarized light of the sample 15KF1_a showing LT2. Uniformly distributed components of the layer consists of quartz, k-feldspar and opaque phase. The upper part of the photograph shows boundary with LT1.

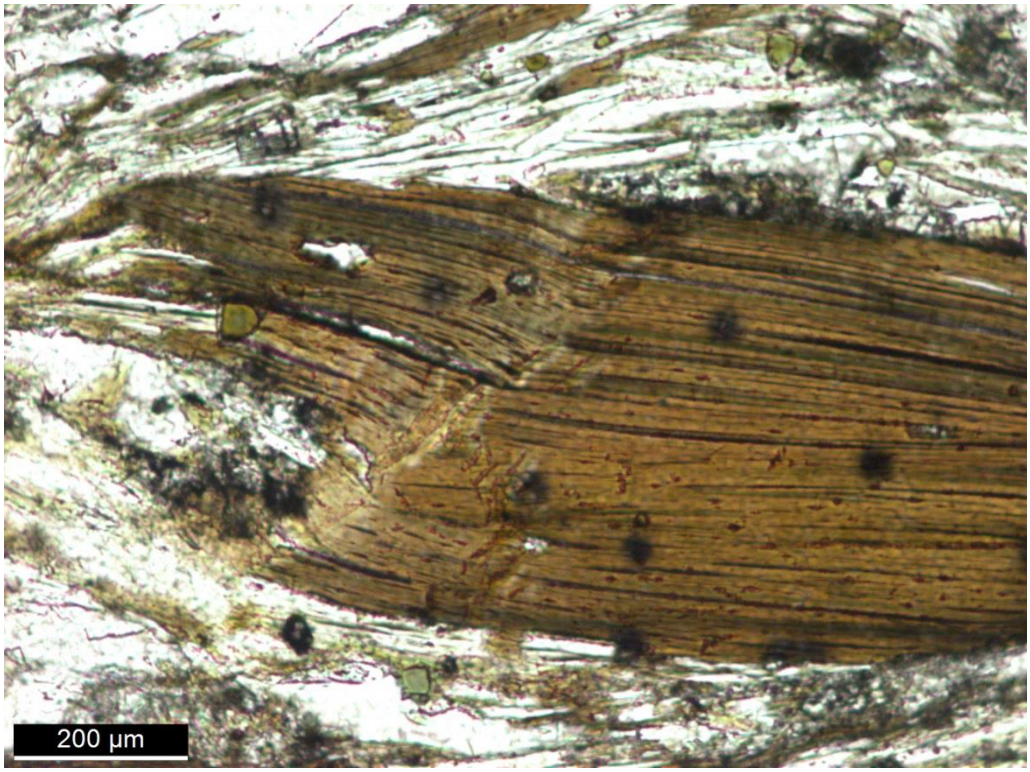

Figure 3.19 Photomicrograph in plane polarized light of the sample 15KF1_b showing slight effects of crenulation being imposed on biotite crystal. The black spots scattered throughout the biotite lath are radiation damage aureoles from zircon inclusions (metamictization of biotite's crystal lattice).

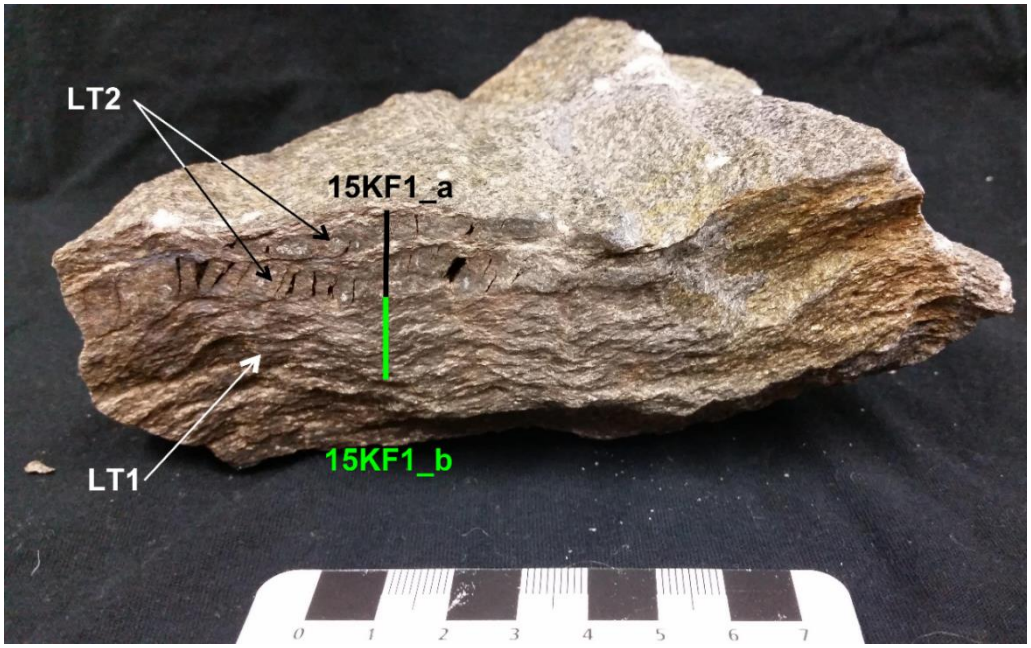

Figure 3.20 A photograph of the sample 15KF1 shows from where each thin section was taken and the original sedimentary layering (LT1 and LT2). The gentle folding of the rock is defined as crenulation imprinted during D_2 event. The cavities present within the LT2 are tension gashes that were originally infilled by calcite but it has been weathered out.

Chapter Four

Geochemistry

4.1 Introduction

This chapter will present and evaluate geochemistry data from the collected samples. The methods used to acquire the results were presented in Methodology section in Chapter One, here each section will present principles of each analysis to provide an overview of theoretical background and possible sources of uncertainty. At first, it is necessary to outline that use of geochemical data in study of eclogite facies rocks has to be approached with great caution and reserve. As at such high pressures and temperatures element mobility becomes a significant issue which can't be accounted for. The protolith will undergo considerable geochemical changes during prograde metamorphism that is associated with dehydration followed by rehydration during retrogressive stage driven by exhumation (Jahn 1998). This causes significant fluid movements that lead to element mobilization. For this reason authors such as Rollinson (1993) suggests use of geochemical data for classification and discrimination of metamorphic rocks only up to green schist facies, however the element mobility is still highly dependent on element itself, phase in which it is hosted as well as fluid content of the rock. Therefore in this study interpretation of major and minor oxide data is treated with reserve and obtained results were attempted to be reproduced using trace and rare earth element (REE) data, especially the REE and high field strength elements (HFSE) as they are considered to be largely immobile providing robust results.

The geochemical methods applied in this project include X-ray fluorescence analysis for major elements and the Inductively-Coupled Plasma Mass Spectrometry for base metals, trace and rare earth elements to characterize the rock types and their possible geotectonic settings. At last, Energy-Dispersive X-Ray Spectrometry was used to identify mineralogy of inclusions in zircons, which had to be supplemented by Raman Spectroscopy in order to differentiate polymorphic species.

The whole rock geochemical data for Gubaoquan and Kanfenggou sites is presented in Table 4.1. The acquired data was presented and manipulated using GeoChemical Data Toolkit v.3 to produce classification and discrimination diagrams and plots that are presented in this chapter. The two samples from Kanfenggou site were collected from the eclogite core and margin, as it was shown in Chapter Three. They were texturally different with slight differences in mineral concentrations, however as it will be shown they are compositionally very similar. The Gubaoquan eclogite however had zoning imposed by the retrogression. The sample 14GBQ1 is the fresh least retrogressed core of the eclogite, sample range of 14GBQ5 (1-4) that show garnet enrichment with more pronounced retrogressive effects and correspond to eclogite's mantle, whereas sample 14GBQ3 that was initially classified in field as jadeite-rich eclogite is actually an amphibolite (retrogressed eclogite) that corresponds to the block's margin and is the most retrogressed and altered sample from the array.

4.2 Whole-rock Geochemistry

Major and Minor Elements

Principles of XRF

The X-Ray Fluorescence spectrometry (XRF) is based on elicitation of secondary X-rays from analysed sample of the specific wavelength corresponding to particular elements *via* primary X-ray beam. This beam originates as electron cloud produced by current passing through the tungsten filament (cathode) that is then directed through the X-ray tube into the anode where the X-rays are generated. Produced X-ray beam is aimed at the sample to produce X-ray fluorescence that is then used to determine elemental composition and concentration with reference to calibration standard. The only limitation of this technique is that it can't measure elements that are lighter than Na, but it is still able to analyse up to 80 elements with concentration range from 100% to few parts per million (Jenkins and Vries 1970, Rollinson 1993).

Table 4.1 Whole rock major and trace element data for Gubaoquan and Kanfenggou sites.

sample	14GBQ1	14GBQ2	14GBQ3	14GBQ5	14GBQ5-1	14GBQ5-2	14GBQ5-3	14GBQ5-4	15KF1	15KF4_1	15KF4_3
rock type	Eclogite	Granite	Eclogite (Jd)	Eclogite (Grt)	Eclogite (Grt)	Eclogite (Grt)	Eclogite (Grt)	Eclogite (Grt)	Paragneiss	Eclogite	Eclogite
description	core	vein	Jadite			Garnet-rich				core	margin
age (Ma)	≥466	≥424	≥466	≥466	≥466	≥466	≥466	≥466		*ca.* 480	*ca.* 480
lat. (N)					40° 59′ 21.75″					33° 50' 2″	
long. (E)					95° 02′ 25.27″					110° 51' 27″	
SiO_2	46.8	76.56	46.75	45.81	50.57	46.81	46.15	47.53	68.53	41.27	46.67
TiO_2	1.59	0.07	1.68	1.67	1.81	1.4	1.57	1.58	0.73	2.01	2.93
Al_2O_3	14.79	13.38	13.55	14.22	14.18	13.93	14.4	13.81	12.9	16.42	13.9
Fe_2O_3	3.04	0.25	4.99	2.18	2.44	2.92	2.42	2.68	5.8	21.27	17.75
FeO	11.8	0.2	10.87	14.06	15.07	11.87	12.16	12.09	n/a	n/a	n/a
MnO	0.22	0.01	0.25	0.26	0.26	0.18	0.25	0.21	0.08	0.43	0.28
MgO	7.16	0.2	7.21	6.96	5.59	8.02	7.14	7.96	2.43	4.77	5.94
CaO	10.16	1.02	11.57	10.85	7.46	10.75	11.82	10.6	1.46	12.3	10.65
Na_2O	2.78	5.03	2.09	1.95	1.5	2.49	2.53	2.33	2.14	1.18	1.64
K_2O	0.42	2.54	0.11	0.27	0.09	0.22	0.18	0.21	3.2	0.27	0.31
LOI	0.53	0.86	0.1	0.71	-0.2	0.43	0.47	0.12	2.23	0.4	0.13
P_2O_5	0.14	0.04	0.12	0.16	0.39	0.12	0.13	0.15	0.14	0.43	0.27
total	99.43	100.16	99.29	99.1	99.16	99.14	99.22	99.27	99.64	100.75	100.47
trace elements											
Cr	138	1.9	133	139	124	177	127	137	98	117	182
Ni	75.1	2.03	88.5	99.2	48.3	105	71.1	109	24.4	41.3	63.1
Rb	19.5	79.8	4.71	10.2	4.31	4.8	8.43	5.73	131.5	8.9	8.9
Sr	176	88	149	99.2	108	192	148	158	101	216	146
Ba	93.2	184	18.1	25.9	19.4	47.1	33.9	36	420	30	40
Nb	8.49	8.71	6	8.73	18.8	6.99	8.41	9.59	12	11.8	14
Zr	115	30.3	14.8	19.9	33	20.8	18.9	16.7	34.3	17.3	21.9
Hf	2.83	1.28	0.67	0.8	4.1	0.98	0.86	0.86	1.1	0.7	0.8
Ta	0.63	1.44	0.35	0.47	1	0.37	0.46	0.49	0.9	0.88	0.92
Th	0.3	10.3	0.15	0.06	0.16	0.13	0.11	0.2	10.7	2	1.8
U	0.49	4.27	0.13	0.1	0.21	0.27	0.12	0.16	1.8	0.5	0.5
Y	29.4	11	20.3	27.6	43.4	28.7	29.4	28.3	26.2	44.5	38.5

Table 4.1 (continuation) Whole rock major and trace element data for Gubaoquan and Kanfenggou sites.

sample	14GBQ1	14GBQ2	14GBQ3	14GBQ5	14GBQ5-1	14GBQ5-2	14GBQ5-3	14GBQ5-4	15KF1	15KF4_1	15KF4_3
rock type	Eclogite	Granite	Eclogite (Jd)	Eclogite (Grt)	Eclogite (Grt)	Eclogite (Grt)	Eclogite (Grt)	Eclogite (Grt)	Paragneiss	Eclogite	Eclogite
description	core	vein	Jadite			Garnet-rich				core	margin
age (Ma)	≥466	≥424	≥466	≥466	≥466	≥466	≥466	≥466		*ca.* 480	*ca.* 480
lat. (N)					40° 59′ 21.75″					33° 50' 2″	
long. (E)					95° 02′ 25.27″					110° 51' 27″	
La	6.39	3.73	3.76	4.35	7.1	8.3	7.48	6.63	30	17.2	15.8
Ce	16.4	7.8	9.94	11.7	19	22.8	18.3	18	64.9	43.8	40.7
Pr	2.48	0.82	1.56	1.82	3.04	3.48	2.63	2.57	8.22	6.44	5.75
Nd	12.2	3.11	7.99	8.99	15.6	16.3	12.4	12.1	31.9	30.6	27.3
Sm	3.55	0.95	2.39	3.02	5.4	4.22	3.32	3.45	5.64	6.87	6.41
Eu	1.35	0.26	0.89	1.04	1.96	1.27	1.07	1.27	1.19	2.33	2.27
Gd	4.69	1.08	3.29	4.48	7.88	4.83	4.44	4.77	5.21	7.57	7.29
Tb	0.77	0.23	0.57	0.75	1.31	0.79	0.78	0.82	0.79	1.19	1.13
Dy	5.02	1.74	3.78	4.8	8.42	5.13	5.32	5.24	4.8	7.68	6.95
Ho	1.09	0.37	0.79	1.06	1.73	1.1	1.16	1.06	0.94	1.65	1.36
Er	3.11	1.17	2.36	2.99	5.04	3.21	3.28	3.06	2.76	4.82	3.71
Tm	0.44	0.18	0.34	0.43	0.72	0.46	0.47	0.45	0.39	0.63	0.47
Yb	2.86	1.34	2.29	2.87	4.69	3.09	2.93	2.79	2.74	3.94	2.93
Lu	0.42	0.21	0.34	0.41	0.73	0.46	0.44	0.42	0.42	0.58	0.43

Gubaoquan and Kanfenggou Eclogites

The results of whole rock geochemical analysis of eclogites are presented in Table 4.1. The analysis has revealed that Gubaoquan eclogite's SiO_2 wt% content ranges between 45% and 47% indicating that the protolith of the rock was mafic in composition. The Kanfenggou eclogite's SiO_2 wt.% was slightly lower ranging between 41% and 46% suggesting ultramafic to mafic protolith for this rock. On the TAS classification diagram (SiO2 *vs.* Na_2O+K_2O) by Le Bas *et al.* (1986) both eclogites plot in basalt field with one ultramafic (ultrabasic) sample plotting in picrobasalt field (Figure 4.1). These were also attempted to be classified using AFM scheme of Irvine and Baragar (1971) and all show characteristic trend of iron enrichment driven by fractionation of magma in the chamber by precipitation of forsterite (Figure 4.2). Using major element composition data to determine tectonic setting of the eclogite was attempted. However as expected highly mobile elements used in such discrimination diagrams do not provide reliable indication as variable results were obtained. In the $MnO-TiO_2-P_2O_5$ Mullen (1983) classification diagram Gubaoquan eclogite plots in Island Arc Tholeiite field and Kanfenggou eclogite in MORB (Figure 4.3), whereas on $MgO-FeO^T-Al_2O_3$ diagram of Pearce *et al.* (1977) Gubaoquan eclogite plots in Ocean Island field; in this classification Kanfenggou eclogite is disregarded due to lack of the FeO data (not pictured).

The use of the geochemical data of major and minor elements in eclogite facies rocks proves poor quality of the results especially with the minor elements. However, major oxides that exist in higher concentrations such as SiO_2, Al_2O_3 and $FeO_{(total)}$ are suspected not to undergo considerable changes.

It is most likely due to their role and abundance in major rock forming minerals as any mobilisation imposed by high grade metamorphism will not have high enough impact to cause significant changes to those element concentrations, unless partial melting occurs; which has not occurred at either of the studied sties. This is based on geochemical data observations of eclogite protoliths determined above and is in line with literature (Liu *et al.* 2010, Qu *et al.* 2011).

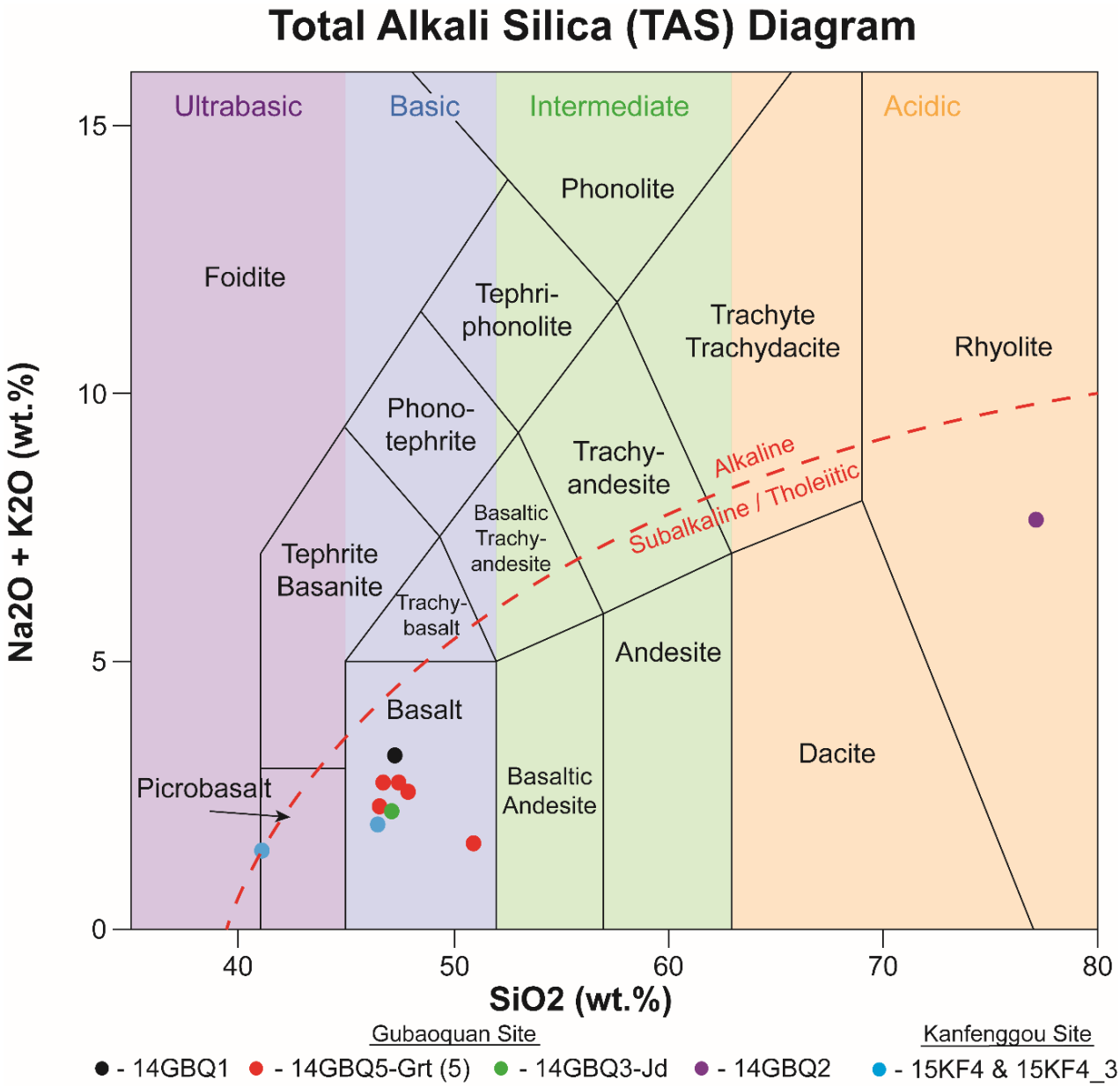

Figure 4.1 Whole-rock composition classification diagram after Le Bas *et al.* (1986). Black, red and green points correspond to Gubaoquan eclogite, whereas blue points represent Kanfenggou eclogite; Pink point corresponds to granitic vein.

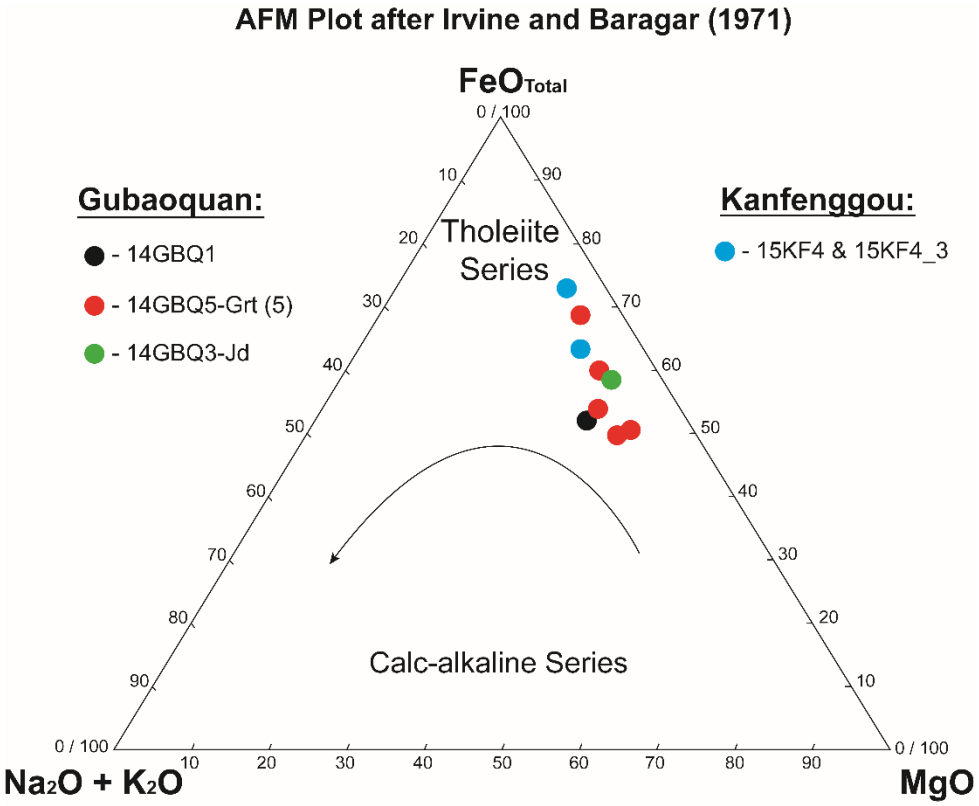

Figure 4.2 The AFM classification diagram after Irvine and Baragar (1971) showing tholeiitic trend for both eclogites.

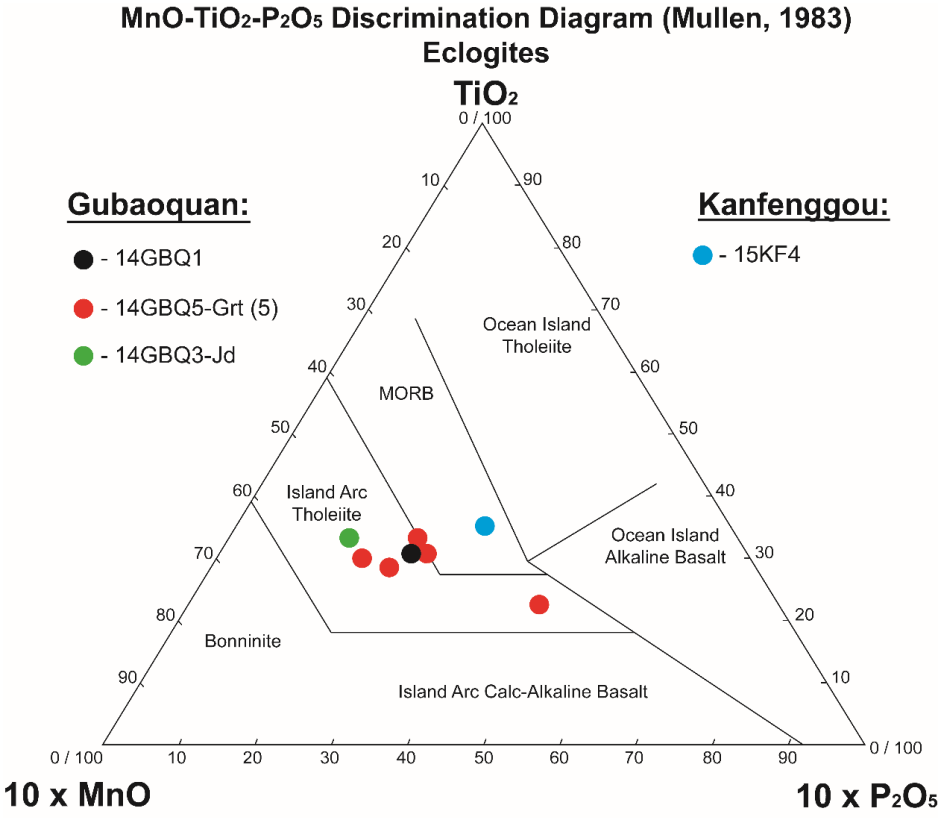

Figure 4.3 Geotectonic classification diagram for basalts after Mullen (1983).

Gubaoquan Granitic Vein

The results of whole rock geochemical analysis of sample 14GBQ2 the granitic vein are presented in Table 4.1. The analysis has revealed that SiO2 wt% content of the sample is 76% with elevated alkali content what resulted with sample plotting in the rhyolite field on TAS diagram (Figure 4.1) by Le Bas *et al.* (1986) proving its granitic affinity. Based on granite's major and minor oxide content sample is classified as calc-alkaline and strongly peraluminous granite according to Sylvester (1989) classification scheme (not pictured). The major and minor cations were further used in attempt to determine tectonic setting at which this granite has formed. The R_1-R_2 geotectonic classification scheme of Batchelor and Bowden (1985) was used in this attempt and it revealed that granite sample plots at transition between syn-collisional and post-orogenic fields (Figure 4.4). Further evidence regarding granites affinity and tectonic setting were gathered from trace element data and are presented in section 4.3.

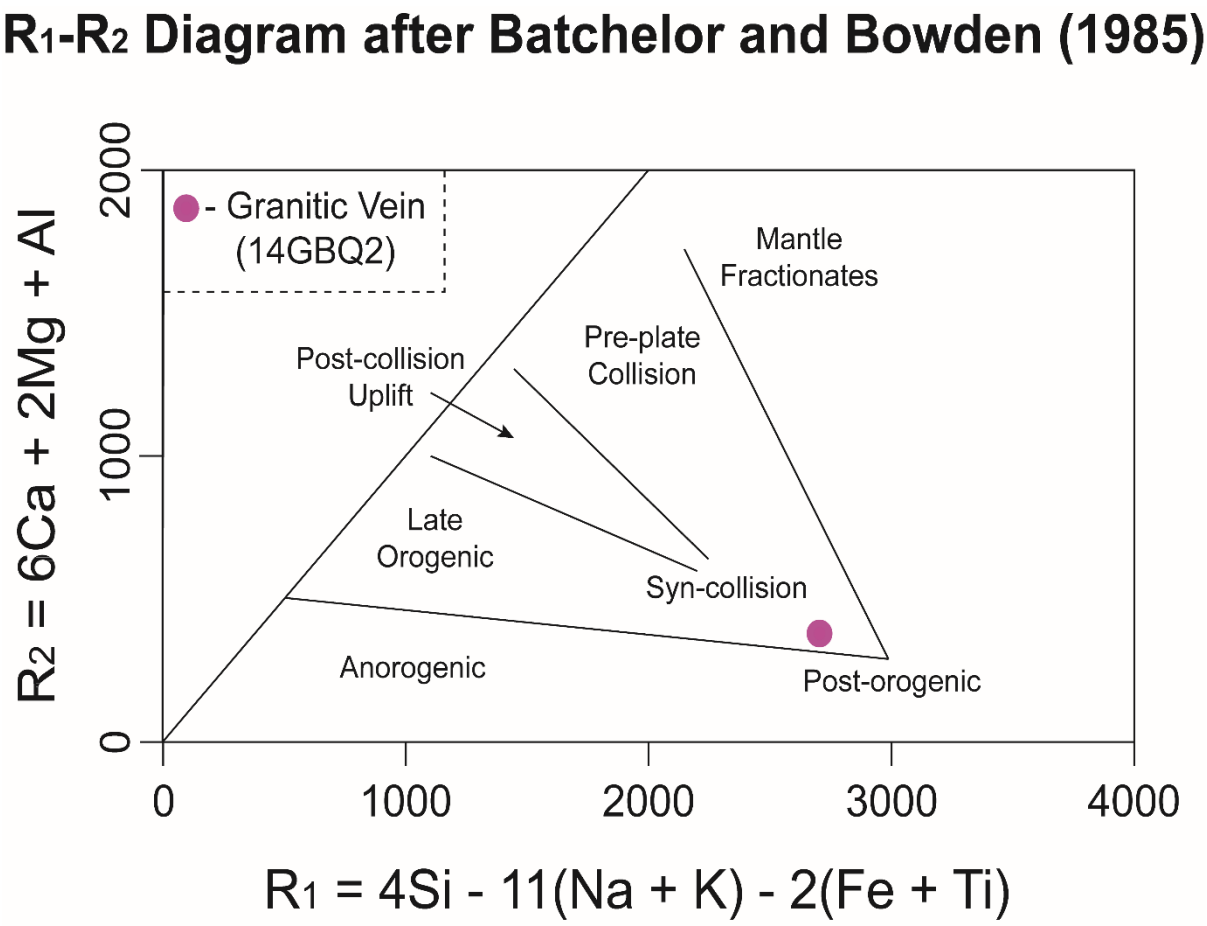

Figure 4.4 Geotectonic classification diagram for granites after Batchelor and Bowden (1985).

4.3 Trace and Rare Earth Elements

Principles

The group of Rare Earth Elements (REE) comprises of the Lanthanide Series metals ranging from La to Lu with Y often added to the group due to its ionic radius compatibility with the group. The characteristic feature of REE is that they have very similar chemical and physical properties, they show small and steady decrease in ionic radius with increasing atomic number and have stable 3+ oxidation state (with exception of Ce^{4+} and Eu^{2+}). These similarities lead to strong association between them and common mode of occurrence. However subtle differences in their properties lead to fractionation in the rock forming minerals (Rollinson 1993). This phenomenon has been used in geochemistry to study genesis of rocks and petrological processes. The REE group have been divided into 2 or 3 sub-groups based on the size of the atomic radius to simplify the notation of the results. The elements from La to Sm are termed light rare earths (LREE) and those from Gd to Lu are called heavy rare earths (HREE), sometimes additional division to middle rare earth (MREE) is also used, it accounts for elements from Pm to Ho (Henderson 1984).

The presentation of REE geochemical data requires normalization as concentrations and abundances of these elements are variable in the environment and universe, therefore standard reference material is needed to derive information from the data. Most commonly used material for REE distribution patterns is chondrite meteorite, as it is thought that chondritic meteorites are remnants of original unfractionated material from which solar system formed. The REE abundance and variability in them, arises from binding energy and stability that is determined by whether the number of protons and neutrons is odd or even (even atomic number elements are more stable and therefore more abundant than odd atomic number elements) (Henderson 1984). Therefore use of chondrite normalization allows removal of this obscuring trend and reveals fractionation patterns within the sample with reference to the chondritic standard. The REE patterns are derived from direct plotting of normalized concentration *vs.* atomic number. This visual representation allows for quick identification of anomalies, depletions or enrichments of the particular element or a group of elements what will aid in the geological processes assessment. Additionally to chondritic-normalization, primitive mantle normalization is often used for multi-element diagrams (spiderplots). Those include broader array of elements in order of increasing compatibility that show deviation trends from primordial mantle before formation of continental crust (Rollinson 1993).

Gubaoquan and Kanfenggou Eclogites

The trace and rare earth element data from both sites is presented in Table 4.1. Analysed samples have been normalized against chondrite (Figure 4.6) and primitive mantle (Figure 4.7) and are displayed in form of spidergrams so their concentration patterns can be revealed. The investigation was undertaken for the protolith type discrimination using trace element data under Pearce (1996) discrimination scheme of Nb/Y *vs*. Zr/Ti (Figure 4.5). All samples were plotted in basalt field assuring the classification obtained by major oxide data.

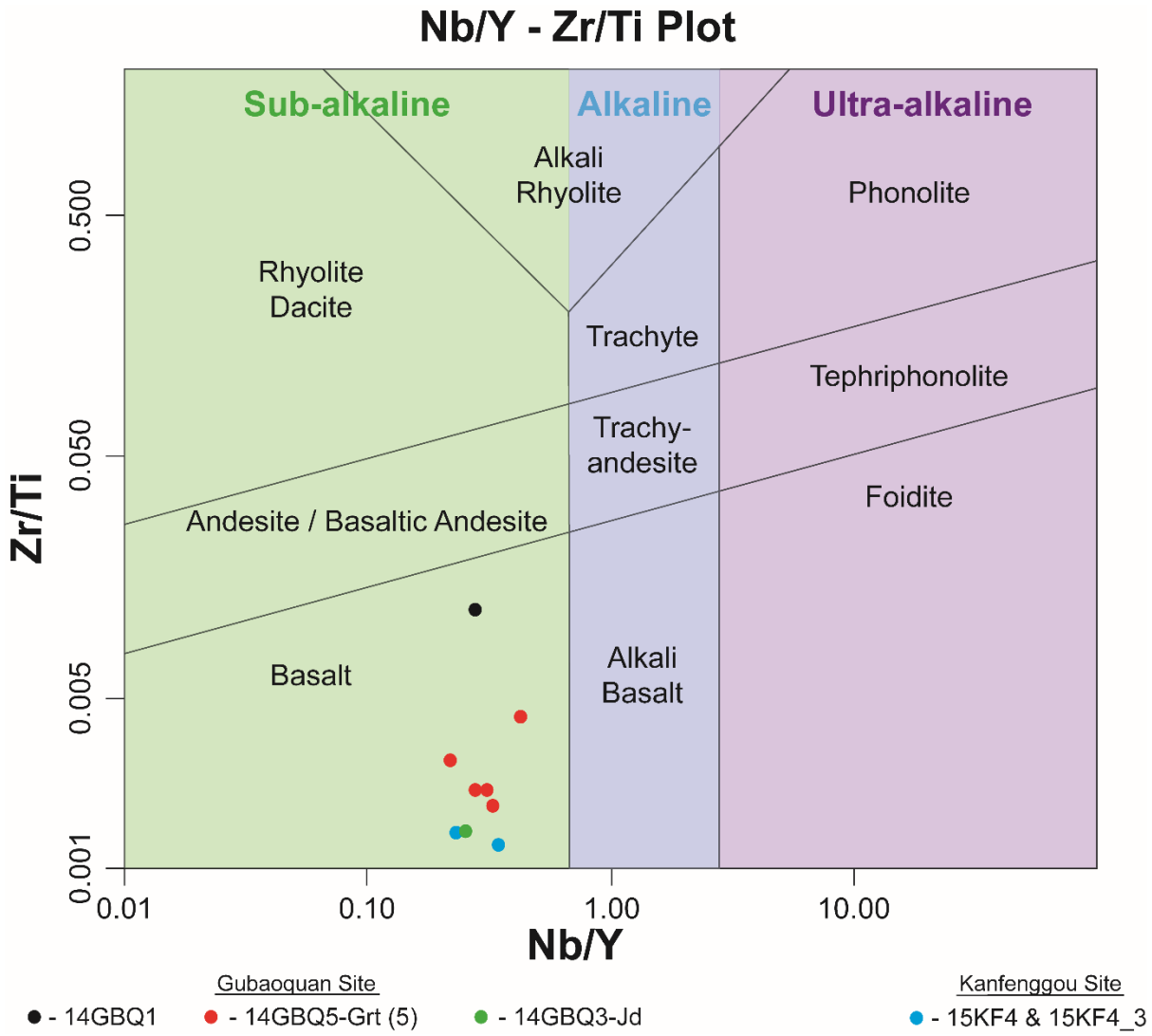

Figure 4.5 Trace element discrimination diagram for basalts modified by Pearce (1996).

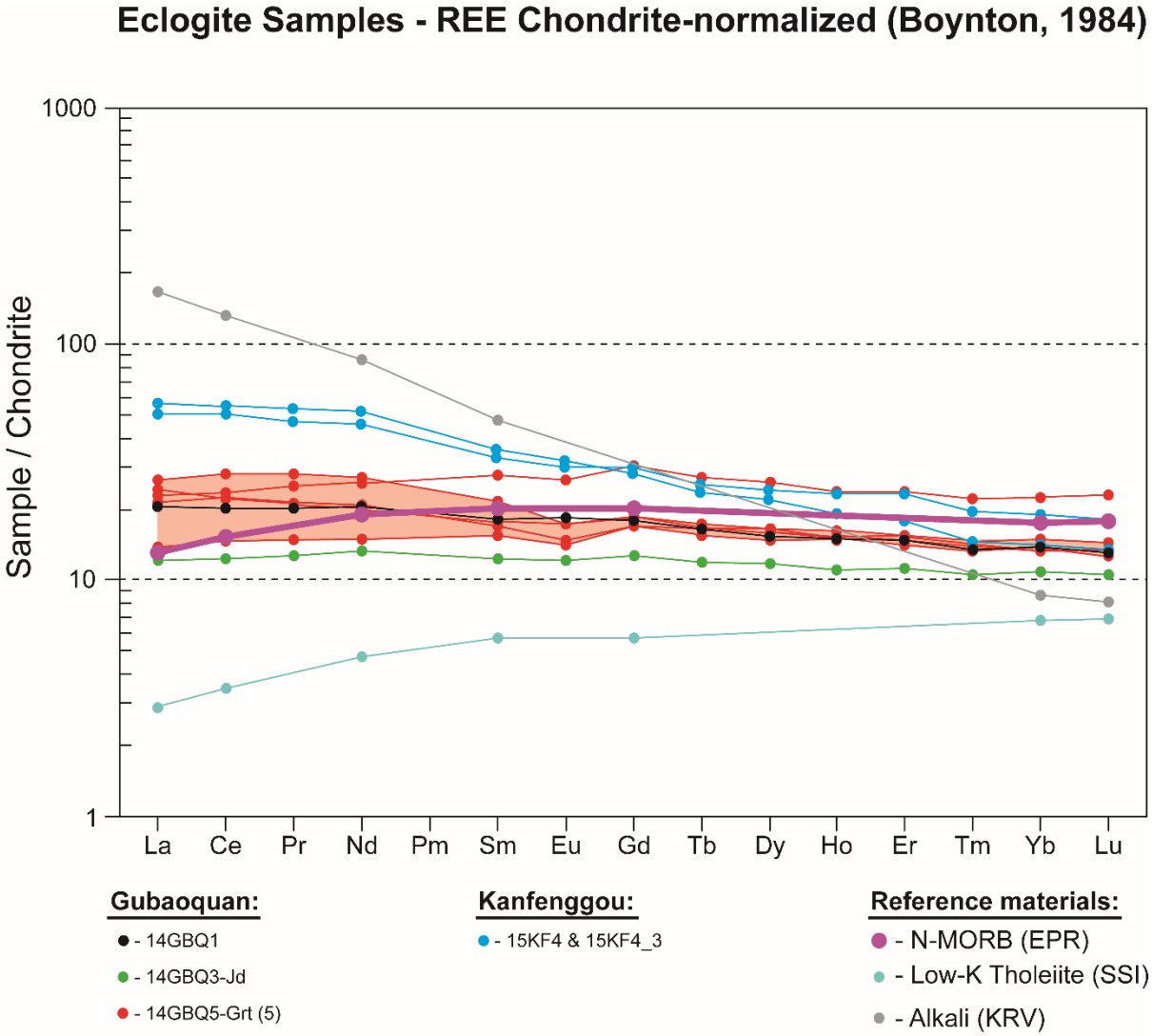

Figure 4.6 Whole-rock chondrite-normalized REE patterns for Gubaoquan (black, red and green) and Kanfenggou (blue) eclogites after Boynton (1984). Additional Alkali basalt, Tholeiite and N-MORB sample were added for modern analogue comparison. Red shaded area represents array of garnet-rich eclogite, displayed because it is thought to represent average for the Gubaoquan eclogite.

The chondrite normalized samples from Gubaoquan (Figure 4.6) generally show flat patterns with slight LREE and MREE enrichment with gentle negative Eu anomaly observable in garnet-rich eclogite samples, whereas in eclogite core the anomaly is not present. The Kanfenggou samples show stronger enrichment in LREE and moderate in HREE relative to chondrite standard creating negatively sloping pattern without Eu anomaly. The samples show parallel and closely spaced patterns indicating lack of variation in REE composition between the core and the margin. Besides analyzed samples, several reference basaltic material were plotted in order to determine geochemical association of studied samples. Three following reference materials were chosen to explore potential source of the rock:

Alkali basalt from Kenya Rift Valley, Low-K Tholeiite from South Sandwich Islands and Tholeiite basalt (N-MORB) from East Pacific Rise (EPR); the geochemical data was sourced from Gill (2010). The Gubaoquan samples show same pattern as N-MORB (pink) reference material, which is consistent with literature (Liu *et al.* 2010, Qu *et al.* 2011). The Kanfenggou samples partially resemble the N-MORB pattern as their LREE enrichment is the only feature that deviates their concordance. It also differs significantly from other reference materials, therefore N-MORB is the best suited candidate for the protolith of Kanfenggou eclogite. In the primitive mantle normalized spidergrams (Figure 4.7), the Gubaoquan eclogite garnet-rich samples show strong depletion in Ba, Th and Zr and moderate depletion of K and Sr. Sample 14GBQ1 displays similar patter to the rest of the analyzed samples with exception of the two anomalies. All Gubaoquan eclogite samples have distinctive K and Zr relative depletion, whereas the eclogite core sample is actually showing slight enrichment in those elements. This anomaly could have been caused by activity of retrogression; possibly a fluid ingress for which

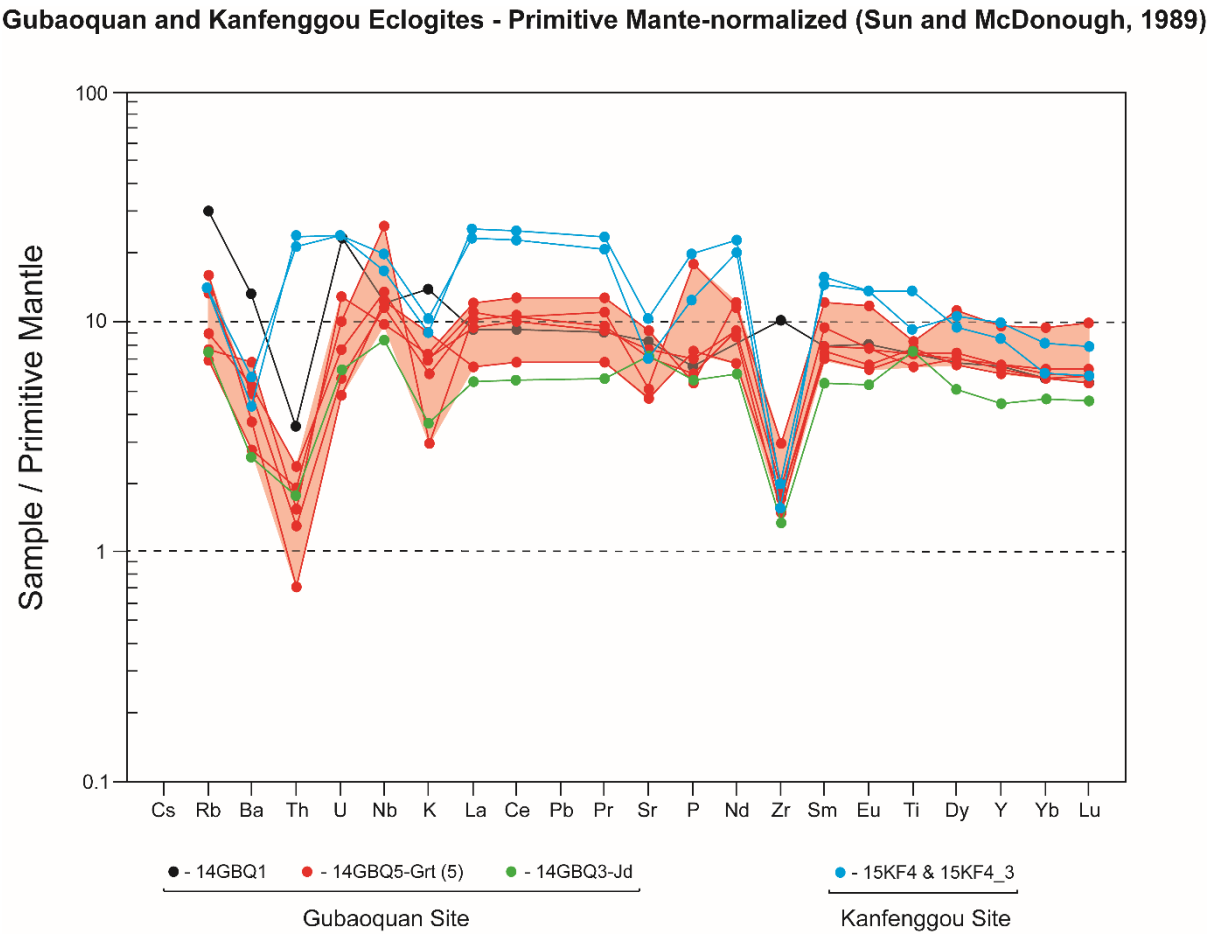

Figure 4.7 W hole-rock primitive mantle normalized trace element patterns for Gubaoquan (black, red and green) and Kanfenggou (blue) eclogites after Sun and McDonough (1989). Red shaded area represents array of garnet-rich eclogite, displayed because it is thought to represent average for the Gubaoquan eclogite.

evidence were observed in thin sections; this could have led to mobilisation and therefore depletion of those elements in affected marginal sections of eclogite body, leaving the core unaffected to some degree. The Kanfenggou eclogite shows similar patterns as Gubaoquan that is described as characteristic for the MORB-type protolith by Qu *et al.* (2011). Theses samples are slightly more enriched in selected trace elements in comparison to eclogite from the Beishan but they share comparable degree of Ba, K and Zr depletion expect Th, as this anomaly is not present. Use of reference materials in this classification was shown to be redundant, as suit of chosen elements lacked comparability and therefore no similarities in pattern were revealed. The complete lack of similarity between the reference material and sample patterns contributes to the questionability of use of the geochemistry data from high grade metamorphic rocks.

Through use of trace elements both eclogites were shown to have MORB characteristics, the Gubaoquan eclogite very well matches REE concentrations and distributions of N-MORB from EPR. The Kanfenggou eclogite has revealed similar pattern with slight enrichment especially in LREE, that could interpreted as transitional form between N-MORB and E-MORB. However classification diagram by Pearce (2008) that uses Yb-normalized Th-Nb proxy for geotectonic nature of basalts has revealed that it could be crustal-contaminated (Figure 4.8).

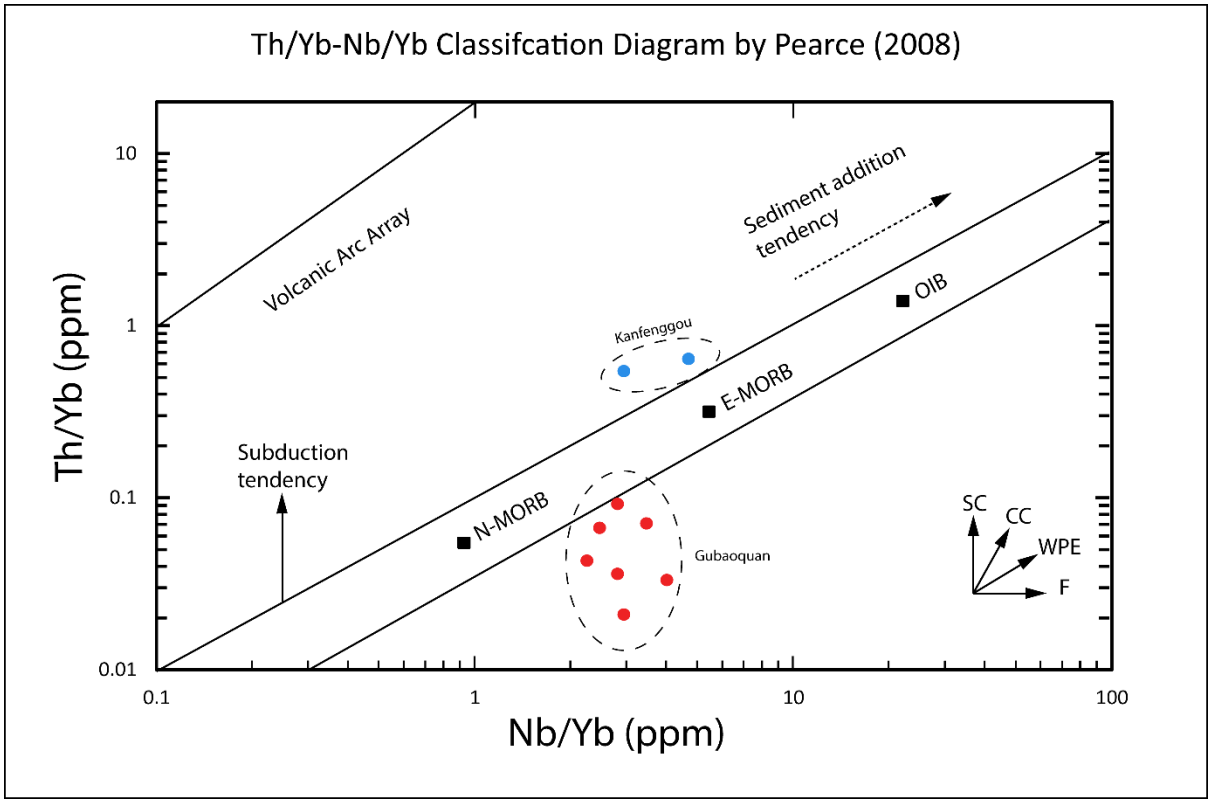

Figure 4.8 Trace element classification diagram for basalts and associated trends. Modified after Pearce (2008). SC – subduction component; CC – crustal contamination; WPE – within-plate enrichment; F - fractionation

This trend is consistent with observed field relationships, as assumption of protolith being a dyke persists, therefore intrusion of basaltic magma into hydrous sedimentary sequence has high chance of being contaminated by country rock fluid absorption (Frost and Frost 1987). The Gubaoquan eclogites are also interpreted as basaltic dykes, however they intruded into granite that is relatively less hydrous than sedimentary rocks, therefore within-plate enrichment or crustal contamination signatures have less influence as they have been masked by pre-intrusion fractionation which has shown to be the most dominant characteristic for this suite of samples, and was previously observed on AFM diagram (Figure 4.2).

Gubaoquan Granitic Vein

The trace element data was used in granite tectonic discrimination scheme of Pearce *et al.* (1984) to further verify geotectonic setting for this rock. Plotting of the results has revealed that this sample lies in syn-collisional and volcanic arc granite fields. The former is in line with previous major element based classification whereas here presented classification of the former is questionable as volcanic arc setting is contradictory to the rock field relationships. This led to re-evaluation of results with the conclusion that granitic vein has been contaminated with crustal material. As according to Pearce *et al.* (1984) crustal contamination can occur at the margins of the intrusions and in those rich in enclaves, where in case of this granitic vein both these common sources are present due to narrow nature of the body and country rock inclusions seen in the outcrop. Such contaminated samples are most likely to plot in syn-collisional and volcanic arc granite fields (Pearce *et al.* 1984), therefore results from this tectonic discrimination should be interpreted with caution.

4.4 Zircon Inclusions (EDS & Raman)

Principles

The Energy Dispersive X-ray Spectrometry (EDS) technique utilises electron beam of the Scanning Electron Microscope (SEM) to generate X-ray photons by bombardment of solid sample. Similarly, to XRF this technique has detection limitations, usually with appropriate instrumentation elements with atomic numbers as low as 4 and as high as 92 (Be and U) can be detected and quantified. Such detection range satisfies requirements for study of geological materials such as rocks in thin section and zircon mounts. Important aspect of the analysis to

consider is the acceleration voltage, as it should be high enough to exceed critical excitation energy of the studied material (should at least be doubled in order to allow accurate quantification) but it can't be too strong as it will increase penetration depth and create additional background 'noise' lowering the accuracy and detection limits. For this reason accelerating voltage of approximately 15 kV was used, as it assures accurate detection of Fe which is the heaviest element among studied major oxides that will be needed to correctly identify unknown phases. Another precaution considered was avoiding sites that are close to the grain boundary or where overlapping of minerals occurs. As electrons not only affect surface area of the material, they also penetrate and scatter inside of it. Therefore if analysing too close to the boundary, the obtained results can be contaminated by adjoining or underlying grain. Alternatively, analysis can be run as a site average, selecting polygonal area to be analysed rather than spot analysis; both approaches were used depending on accuracy need from the analysis (University of California 2014).

Procedure

The instruments used in this technique were SEM-JEOL JSM-6490LV and CL detector Gatan MonoCL4. The analysis was performed under low vacuum to prevent ionisation of the samples with acceleration voltage set to 15kV. For routine CL imaging voltage is usually set to 5 kV on this instrument, but it had to be increased to match the energy needed for EDS. This resulted in lower resolution images, especially under higher magnification. These two detectors were used in conjunction, where CL detector was used to acquire image of the zircon, when inclusion was spotted the analysis sites were marked; always adding control site on zircon host to assure that EDS analysis is operating correctly. Here are presented final outcomes of the analyses, the individual spectra are presented in Appendix C.

Results

Gubaoquan Eclogite (14GBQ1)

The analysis of many zircon grains from eclogite sample revealed moderate abundance of inclusions in zircon domains. The most significant inclusion are the ones enclosed in metamorphic rim of the zircon as they can provide insight into metamorphic regime at the time of crystallization or growth, however these have been proven to be rare. The most abundant inclusion was apatite, here it is considered to be an additional indicator of a protolith for Gubaoquan eclogite. As it was shown by Schandl *et al.* (1990) that P_2O_5 is highly soluble in basic magmas and most commonly will precipitate as apatite when its anion concertation

reaches 3-4 wt%. These authors described that basalts with abundant apatite are most likely to be generated in previously enriched mantle; once temperature-dependent P_2O_5 concertation was reached. This high apatite abundance in zircon reveals high P_2O_5 saturation in the protolith, however any traits of it in the groundmass have been removed during high degree of metamorphism and remobilized P was absorbed by garnet due to its affinity for phosphorous (Konzett and Frost 2009). This could be used a minor indication of eclogite's basic protolith and possible linkage to low degree partial melting of the mantle (Schandl *et al.* 1990).

Other, less abundant but the more significant inclusions were omphacite, quartz, garnet and rutile (Figure 4.9, Figure 4.12 and Figure 4.13, respectively) that represent characteristic eclogite facies mineral assemblage as seen in thin section. However, the plagioclase (albite) inclusion was also found in the core of the other zircon (Figure 4.14) what could indicated that zircon growth took place in pre- or post-eclogite granulite or amphibolite facies metamorphic event as described by Qu *et al.* (2011), alternatively it could be a preserved component of protolithic igneous assemblage.

High Pressure Quartz

The cathodoluminescence imaging in conjunction with EDS has revealed quartz inclusion in one of the zircons. The intriguing feature observed around that inclusion is the radial fracturing of the hosting zircon (Figure 4.9). Such feature is usually characteristic of the coesite (high-pressure polymorph of quartz). When coesite inverts back to quartz its condensed crystal lattice will undergo expansion with decrease in confining pressure. This often results in fracturing of the surrounding minerals, this is a characteristic feature used to verify previous presence of coesite after inversion is complete. This is a common occurrence during exhumation of rare ultra-high pressure eclogites (Chopin 2003). Since coesite is a polymorph of quartz, both minerals have exactly the same chemical composition therefore they can't be distinguished geochemically, *ergo* EDS analysis is incapable to differentiate between the two minerals and alternative method of identification has to be applied. For this reason Raman Spectroscopic technique was used, as it provides insight into the bonding between the elements allowing to determine the difference between quartz and coesite. The analysis was conducted using green Diode Solid-State Laser with wavelength of 532 nm and output power of 42 mW; the spot size of each analysis was within 0.5-1 μm range. The analysis has revealed that inclusion consist entirely of quartz, not coesite. However, some inconsistency exist between normal quartz spectra band and the one acquired. As main diagnostic band of quartz has peak at 464-466 cm^{-}

[1] (Parkinson and Katayama 1999, Schmidt and Ziemann 2000) and the spectra acquired from the inclusion has main peak at 468 cm^{-1} (Figure 4.11). There were several studies conducted on degree of Raman shift of coesite and quartz with relation to pressure conditions (Parkinson and Katayama 1999, Sobolev *et al.* 2000, Enami *et al.* 2007). The general trend observed implied positive correlation between degree of the shift to the changing pressure conditions. However, Enami *et al.* (2007) has shown that shift in quartz spectra can also be attributed to mode of occurrence, physical properties of host mineral and process of sample preparation, therefore caution has to be exercised when interpreting the results. Nevertheless pressure-dependant Raman band shift in coesite has been proven to be a viable technique and previous study of Parkinson and Katayama (1999) has shown that shift in coesite spectra is always accompanied with corresponding shift in quartz. Therefore this may imply that Gubaoquan eclogite underwent higher pressure condition than it was previously estimated, as similar degree of shift has been recorded by previous studies (Parkinson and Katayama 1999, Enami *et al.* 2007).

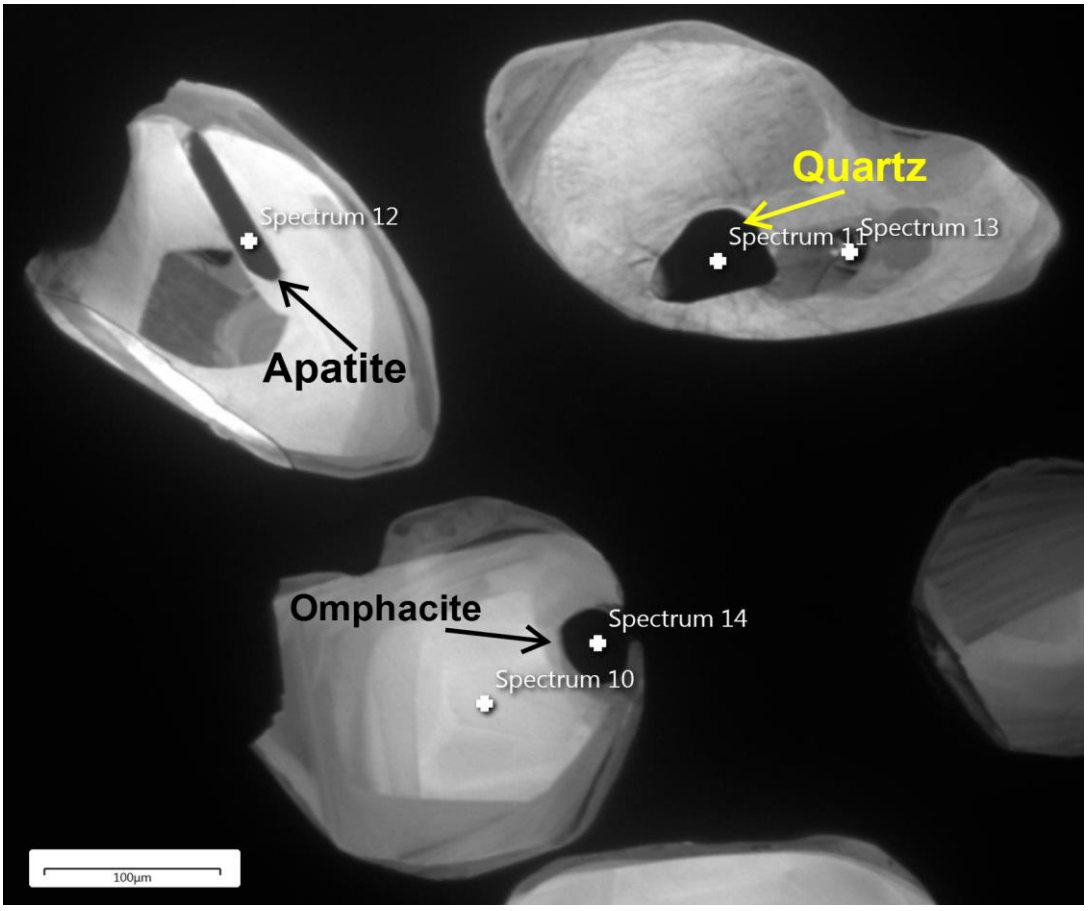

Figure 4.9 The CL image of zircons from the eclogite sample 14GBQ1 showing apatite, quartz and omphacite inclusions. The results of Spectrum 10-14 are attached in Appendix C with results in wt%.

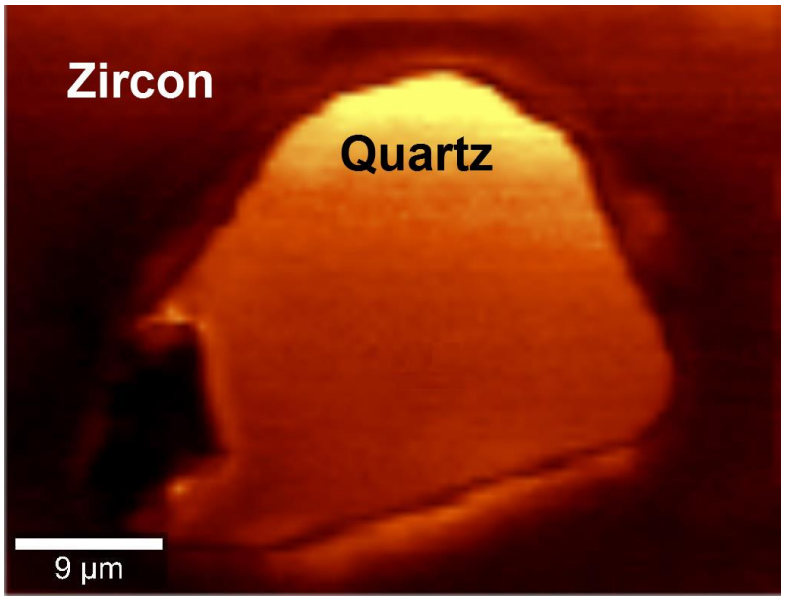

Figure 4.10 Raman spectroscopy mapping of the quartz inclusion from Figure 4.9. Showing gentle concentric zoning in intensity of the signal for the selected filter band. The intensity is increasing towards the core, indicating progressive decompression changes to the structure of the quartz grain.

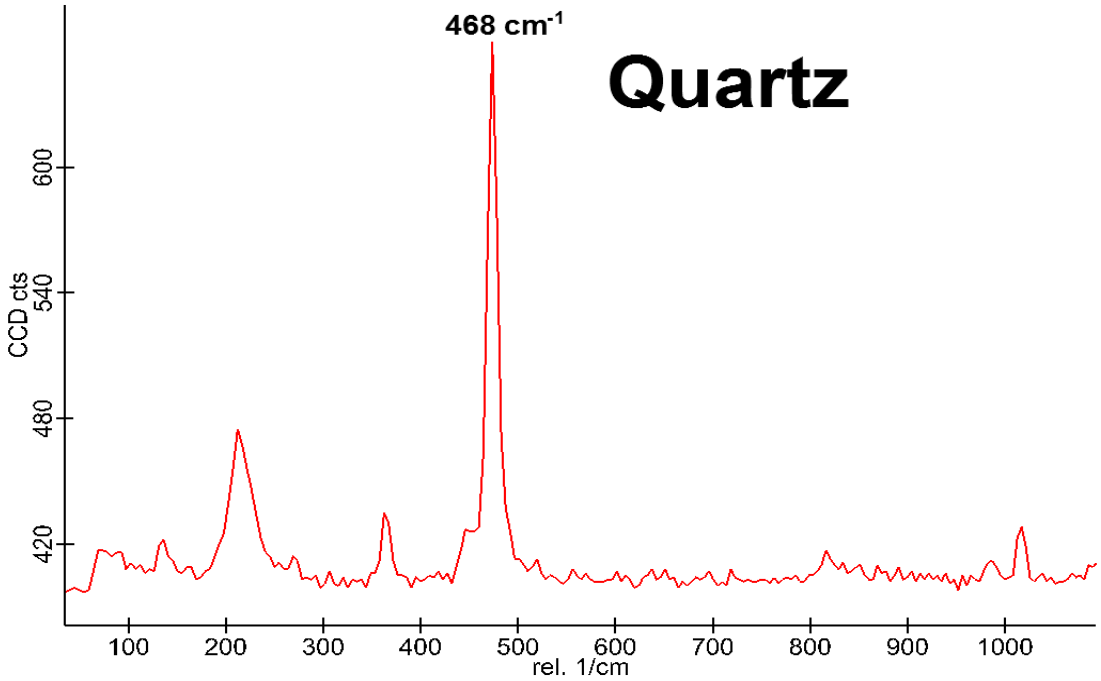

Figure 4.11 Raman spectra for the zircon quartz inclusion from Figure 4.9 and Figure4.10.

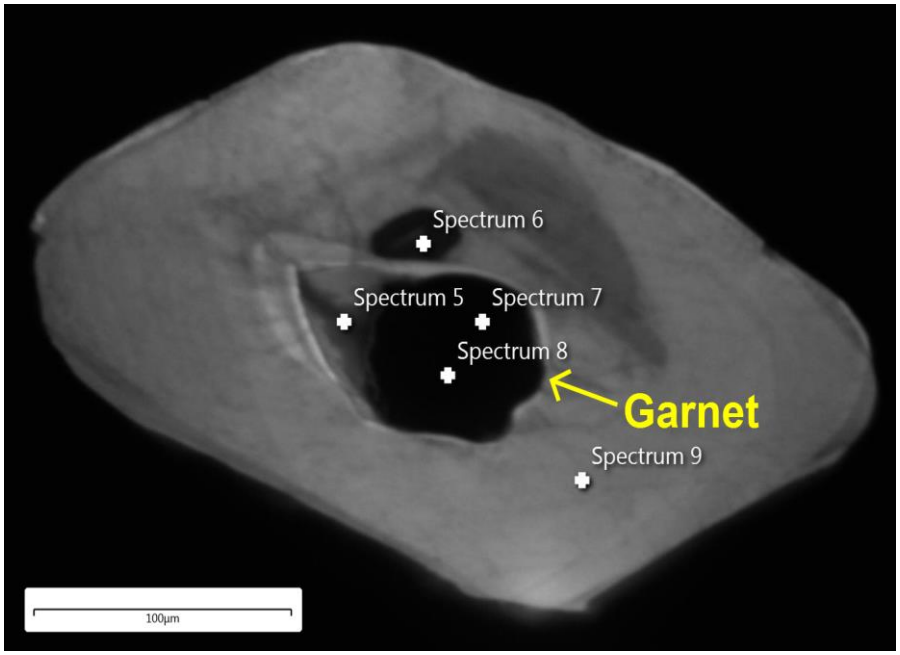

Figure 4.12 The CL image of zircon from the eclogite sample 14GBQ1 showing garnet inclusion. The results of Spectrum 5-9 are attached in Appendix C with results in wt%.

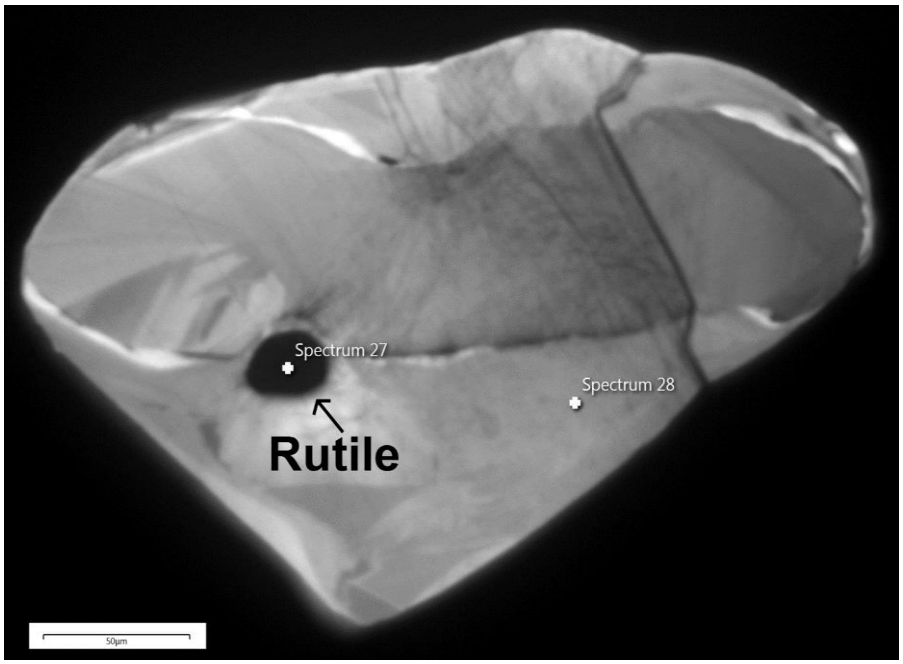

Figure 4.13 The CL image of zircon from the eclogite sample 14GBQ1 showing rutile inclusion. The results for Spectrum 27 and 28 are attached in Appendix C with results in wt%.

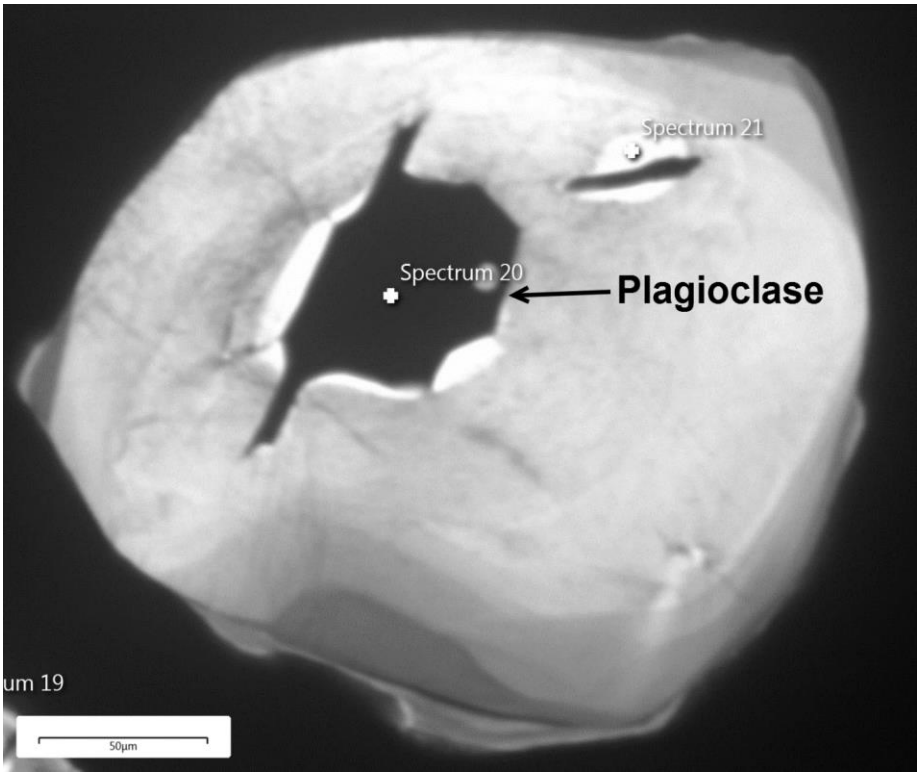

Figure 4.14 The CL image of zircon from the eclogite sample 14GBQ1 showing plagioclase (albite) inclusion. The results for Spectrum 20 and 21 are attached in Appendix C with results in wt%.

Chapter Five

Zircon Geochronology

5.1 Introduction

This chapter will present SHRIMP U-Pb dating of zircons from studied rocks at Gubaoquan and Kanfenggou sites. For the former site, the zircon ages were acquired for the eclogite (14GBQ1), orthogneiss (14GBQ10), granitic vein (14GBQ2) and lamprophyre dyke (14GBQ9). For the Kanfenggou site, a zircon concentrate was produced for eclogite (15KF4) only. The aim of this part of the study is to verify the metamorphic and protolithic ages of the metamorphosed rocks (Wang *et al.* 2011, Cheng *et al.* 2012), as well as provide new ages for igneous rocks that were not previously dated; the granitic vein and lamprophyre dyke.

Zircon is a very useful mineral in geological studies due to its qualities. In terms of geochronology, the main attribute is that during formation its crystal lattice will incorporate and retain uranium and other trace elements, but it will not absorb lead. This allows for precise U-Pb dating of the mineral, as in theory, all lead detected within the grain will be a product of *in situ* decay of U to Pb. However, this phenomenon is not as simple in practice, as contamination with common rock lead still occurs during natural alteration of zircons at time of weathering and during the sample preparation processes, and therefore corrections for it have to be performed in order to achieve accurate age results. The physical resistance of zircon to external process such as weathering, erosion and high temperature and pressure conditions of metamorphism is another and probably most important of its attributes (Corfu *et al.* 2003). Its longevity and resistance preserves the zircon's origin signature and therefore allows geologists to track its evolution as it is being transferred between geological environments.

Zircons have highly diverse external morphologies and internal textures that are driven by the environment they crystallize from or the external processes which are imposed on them. It is therefore important to understand their implications in order to correctly decipher the geological history of the rock from which the zircon was derived (Corfu *et al.* 2003). For this purpose, methods of reflected light microscopy and cathodoluminescence imaging have been

widely applied in studying these features. In this study, reflected light images were acquired to produce maps of the zircon mounts which were used for navigation during the U-Pb dating process and to determine textural features of the grains. This approach prevented dating of sites that have mineral inclusions or were strongly affected by fractures. Such features should be avoided as they could have disturbed isotopic ratios or contain excess amounts of common lead, what would produce unreliable results. The use of cathodoluminescence imaging is primarily used to differentiate between metamorphic growth and protolithic core domains on zircon crystals, and to detect domains or grains with recrystallized internal textures so they can be avoided. Use of these methods allowed for efficient acquisition of reliable age data which are used to create models of geological evolution for the studied sites.

5.1.1 Cathodoluminescence Imaging

Cathodoluminescence (CL) imaging is only one of many techniques where luminescence of the material is achieved by excitation of an atom within the material to its upper energy state, followed by relaxation to ground state. In the CL process, this is attained by high energy electrons derived from the cathode which are then used to bombard the material as a focussed, rastered beam which during relaxation produces photons that are captured by the detector (McFarlane 2014). The luminesce within zircons is produced by trace element impurities that become activators during the process; the most common are rare earth elements (REE) and those in actinides series elements (commonly U and Th). The intensity and wavelength of electromagnetic spectrum produced is dependent on the element present. Therefore this technique can be used to estimate what group of elements are present and their relative abundance. This information can be used further to distinguish between igneous and metamorphic zircons (or igneous zircon core *vs.* metamorphic rim), especially for those formed at eclogite facies (Rubatto 2002). During growth zircon will incorporate the chemistry of the environment it is in. This information becomes locked in the grains and can be studied to determine the origin and age of the zircon, temperature at the time of crystallization and geological setting at which it formed. Therefore analysing the zircon's growth zoning seen in CL images and elemental distribution can provide insight into the geological history of studied rocks (Rubatto 2002, Corfu *et al.* 2003, McFarlane 2014).

Based on the above information, it is possible to distinguish between magmatic and metamorphic zircons using CL imaging purely from zircon luminesce. The

cathodoluminescence intensity is inversely proportional to the Uranium content; the higher U abundance the lower the luminesce (McFarlane 2014). Therefore igneous zircons are usually less luminescent as they are enriched in U and the metamorphic zircons are depleted in this element and therefore they appear brighter. However this is not always the case, as other elements such as RREs contribute to the zircon luminescence patterns through their distribution and relative magnitude of abundance which can radically differ between samples, leading to misinterpretation.

5.1.2 U-Pb Geochronology

The Uranium-Lead (U-Pb) isotopic system used for dating is based on the same principles as any other radioisotope geochronological system. The main concept behind these systems is the radioactive decay of the unstable isotope (parent) to the stable isotope (daughter), usually of a different element. This can be accomplished in a single step or a chain of decays until the stable form is reached. The radioactive decay occurs as emission of alpha or beta particles from the nucleus of an unstable isotope, and the rate of decay is distinctive for each isotope. In the U-Pb isotopic dating system, there are two decay series used, where ^{238}U and ^{235}U are main parental isotopes and ultimately decay to ^{206}Pb and ^{207}Pb respectively.

The rates have been proven to be constant and independent of external factors such as temperature, pressure, chemical state, etc. (see review by Williams 1998). This relationship made it possible to use these rates to calculate the ages of studied material; however this requires satisfaction of certain criteria in order to achieve accurate and reliable result. As the decay rate (λ) remains constant, then for each unstable parent isotope (P_o) there will be one daughter isotope (D) produced for a given amount of time, which can be expressed in form of following equation:

$$D = P_o\,(1 - e^{-\lambda t})$$

where D is amount of daughter isotopes produced after "t" amount of time from P_o amount of original parent material at "λ" decay constant rate.

In radioisotope geochronology, the relationship between parent and daughter isotopes is often expressed in ratios. Therefore the equation can be rewritten in the following form:

$$\frac{D}{P} = e^{\lambda t} - 1$$

In order to determine the age of the rock using radioisotopes an appropriate isotopic system has to be used, as many naturally occurring isotopes have different decay rates. An ideal system will have a half-life (measurement of time taken for half of original parent material to decay to its daughter product) that will allow for some parent material to be preserved and will produce enough daughter material so it can be measured. Also choosing an appropriate radioisotope is dependent on many other factors that have been summarised by Williams (1998) and Schoene (2014) but mainly it should have a half-life that is comparable to the age of the rock studied. The half-life ($T_{1/2}$) and decay constant relationship can be express in the form of the following equation:

$$T_{1/2} = \frac{\ln 2}{\lambda}$$

Half-lives of the decay series in U-Pb dating system:

^{238}U to ^{206}Pb in $T_{1/2}$ = 4470 Ma

^{235}U to ^{207}Pb in $T_{1/2}$ = 704 Ma

The use of U-Pb isotope system in geochronology has numerous advantages. The key benefit is that the system is paired, meaning that both U isotopes decay to different Pb isotopes at different rates. This allows for independent age determination using daughter isotopes $^{207}Pb/^{206}Pb$, providing an internal check whether the isotopic system has been disturbed, and therefore if calculated ages are correct (review by Williams 1998). Due to the paired nature of this system, the obtained data can be very well expressed on concordia diagrams, allowing to determine if the isotopic ratios remained unchanged (concordant) or disturbed (discordant). The diagram used in this study is Tera-Wasserburg concordia that compares $^{238}U/^{206}Pb$ against $^{207}Pb/^{206}Pb$. This diagram is advantageous over the Wetherill concordia ($^{207}Pb/^{235}U$ – $^{206}Pb/^{238}U$), because it allows one to plot measured isotopic values without calculation of ^{235}U content from measured ^{238}U and the modern uranium isotopic composition, which therefore minimizes the uncertainty of the results (Williams 1998). However, before the U-Pb age can be derived, correction for common Pb has to be performed. In this study, corrections for common lead were performed using "Lead" software.

Method

The zircons were dated using the SHRIMP RG instrument at the Australian National University (Canberra). Analytical procedures followed those described by Williams (1998). The analytical spot size was ~20 μm; the reduction of the raw data was conducted using the ANU software 'PRAWN' and 'Lead'. The $^{206}Pb/^{238}U$ ratio of the unknowns was calibrated using measurements of the Temora-2 reference material (U–Pb ages concordant at 417 Ma Black *et al.* (2003)) after every 3 analyses of the unknowns. U and Th abundance was calibrated using measurement of the reference zircon SL13 (U=238 ppm) located in a set-up mount prior to the commencement of the analytical session. The reduced and calibrated data were assessed and plotted using the ISOPLOT Excel software add-in of Ludwig (2003). The uncorrected and corrected isotopic ratios and ages for Gubaoquan and Kanfenggou sites are presented in Tables 5.1 and 5.2, respectively.

(Table 5.1 on the next page)

Table 5.1 SHRIMP U-Pb zircon data for Gubaoquan Site

Labels	site	U/ppm	Th/ppm	Th/U	$^{204}Pb/^{206}Pb$	$^{238}U/^{206}Pb$	$^{207}Pb/^{206}Pb$	age $^{206}Pb/^{238}U$	age $^{207}Pb/^{206}Pb$	%conc
14GBQ1 Eclogite										
Metamorphic rims										
3.1	r,hd,ov	31.45	0.08	0.00266	0.0074 ± 0.0025	12.50 ± 0.59	0.0805 ± 0.0805	483 ± 19		
4.1	r,hd,ov	30.13	0.18	0.00583	0.0127 ± 0.0034	13.51 ± 0.81	0.1034 ± 0.1034	435 ± 23		
5.1	r,hd,eq	32.71	0.06	0.00187	0.0069 ± 0.0029	12.52 ± 0.62	0.1015 ± 0.1015	470 ± 22		
Protolithic cores										
1.1	c,h,eq	37.08	4.86	0.13	0.0030 ± 0.0018	9.62 ± 0.45	0.0802 ± 0.0046	623 ± 23		
2.1	e,h,ov	42.99	5.24	0.12	0.0017 ± 0.0008	7.15 ± 0.43	0.0791 ± 0.0049	832 ± 35		
6.1	e,h,ov	33.16	3.81	0.11	0.0048 ± 0.0014	7.38 ± 0.37	0.0932 ± 0.0051	794 ± 29		
7.1	e,osc, q	49.71	8.44	0.17	0.0018 ± 0.0011	6.70 ± 0.27	0.0787 ± 0.0022	887 ± 27		
9.1	r,hd,eq	73.95	7.93	0.11	0.0006 ± 0.0008	7.28 ± 0.26	0.0797 ± 0.0033	817 ± 55		
10.1	r,hd,eq	38.5	0.41	0.01	0.0050 ± 0.0029	11.75 ± 0.46	0.0753 ± 0.0054	516 ± 18		
11.1	r,hd	36.13	0.83	0.02	0.0074 ± 0.0041	11.33 ± 0.62	0.1266 ± 0.0065	502 ± 40		
12.1	r,hd,ov	32.88	1.41	0.04	0.0043 ± 0.0027	11.48 ± 0.68	0.0852 ± 0.0088	522 ± 27		
13.1	e,h,ov	28.63	4.19	0.15	0.0017 ± 0.0020	6.65 ± 0.32	0.0909 ± 0.0058	880 ± 55		
14.1	r.hd	87.57	8.7	0.10	0.0038 ± 0.0016	7.04 ± 0.32	0.0819 ± 0.0031	843 ± 29		
15.1	c,h	27.13	4.21	0.16	0.0056 ± 0.0019	6.71 ± 0.33	0.1039 ± 0.0041	860 ± 34		
16.1	c,h	61.91	14.72	0.24	0.0059 ± 0.0015	7.02 ± 0.35	0.0942 ± 0.0047	832 ± 32		
5.2	c,h,eq	34.92	5.54	0.16	0.0031 ± 0.0020	6.23 ± 0.29	0.0988 ± 0.0058	929 ± 42		
5.3	r,hd,eq	30.56	0.06	0.00	0.0104 ± 0.0036	12.19 ± 0.64	0.0912 ± 0.0912	488 ± 22		
4.2	c,h,ov	21.34	2.88	0.14	0.0135 ± 0.0069	6.38 ± 0.38	0.1343 ± 0.0100	869 ± 65		
11.2	c,h	12.05	2.82	0.23	0.0061 ± 0.0035	22.14 ± 81.85	0.1260 ± 0.0100	260 ± 800		
10.2	c,h	44.77	7.79	0.17	0.0044 ± 0.0018	6.77 ± 0.31	0.0854 ± 0.0026	871 ± 32		
17.1	c,h,ov	279.24	73.56	0.26	0.0004 ± 0.0002	6.79 ± 0.29	0.0726 ± 0.0014	881 ± 27		
12.2	c,h,ov	33.6	4.64	0.14	0.0011 ± 0.0012	6.85 ± 0.34	0.0927 ± 0.0074	854 ± 80		
3.2	c,h,ov	55.01	9.46	0.17	0.0008 ± 0.0006	6.49 ± 0.38	0.0826 ± 0.0027	910 ± 60		
18.1	m,h	6	4.29	0.71	0.0072 ± 0.0030	133.30 ± 40.18	0.1134 ± 0.0094	44 ± 10		
19.1	e,h,ov	24.23	2.62	0.11	0.0083 ± 0.0032	7.31 ± 0.45	0.1057 ± 0.0073	789 ± 41		
20.1	m,h,eq	4.41	9.09	2.06	0.0071 ± 0.0035	436.62 ± 525.69	0.1028 ± 0.0081	14 ± 12		
21.1	c,h,ov	61.04	9.17	0.15	0.0007 ± 0.0004	6.39 ± 0.26	0.0825 ± 0.0021	924 ± 48		

Table 5.1 (continuation) SHRIMP U-Pb zircon data for Gubaoquan Site

Labels	site	U/ppm	Th/ppm	Th/U	$^{204}Pb/^{206}Pb$			$^{238}U/^{206}Pb$			$^{207}Pb/^{206}Pb$			age $^{206}Pb/^{238}U$			age $^{207}Pb/^{206}Pb$			%conc
22.1	e,h,ov	21.82	2.8	0.13	0.0089	±	0.0026	6.89	±	0.38	0.1002	±	0.0050	841	±	38				
23.1	c,h,eq	6	4.24	0.71	0.0098	±	0.0063	137.54	±	55.92	0.1429	±	0.0119	41	±	13				
24.1	c,h,ov	36.89	4.42	0.12	0.0031	±	0.0022	6.89	±	0.34	0.0869	±	0.0044	855	±	35				
25.1	e,h	24.93	2.79	0.11	0.0083	±	0.0043	6.77	±	0.42	0.1593	±	0.0126	795	±	80				
14GBQ5 Eclogite (Garnet)																				
1.1	r,hd,ov	3.67	0.1	0.026	0.0387	±	0.0247	41.95	±	11.69	0.2449	±	0.0293	117	±	60				
2.1	c,sz,ov	105.76	18.04	0.171	0.0011	±	0.0007	7.00	±	0.26	0.0794	±	0.0025	849	±	27	743.9	±	411.6	113.8
3.1	m,h,ov	18.59	0.09	0.005	0.0172	±	0.0076	13.18	±	1.05	0.1447	±	0.0143	423	±	41				
4.1	m,h,eq	232.15	164.68	0.709	0.0024	±	0.0007	12.04	±	0.64	0.0680	±	0.0018	508	±	20				
5.1	e,h,ov	262.38	72.61	0.277	0.0004	±	0.0002	6.38	±	0.37	0.0737	±	0.0013	934	±	37	866	±	92.82	107.6
14GBQ10 Orthogneiss																				
1.1	e,osc,p	867.5	250.69	0.29	0.0002	±	0.0001	6.31	±	0.25	0.0692	±	0.0005	950	±	65	833	±	36.42	113.6
2.1	e,osc,p	982.69	383.77	0.39	0.0003	±	0.0001	6.46	±	0.21	0.0708	±	0.0007	927	±	23	838.7	±	56.58	110.2
3.1	m,osc,p	659.7	406.36	0.62	0.0014	±	0.0002	6.51	±	0.27	0.0867	±	0.0011	903	±	32	831.3	±	97.89	108.3
4.1	m,osc,fr	490.8	262.21	0.53	0.0000	±	0.0000	6.45	±	0.21	0.0687	±	0.0008	931	±	130	875.7	±	26.28	106.1
5.1	e,osc,p	662.84	342.05	0.52	0.0001	±	0.0001	6.40	±	0.24	0.0704	±	0.0008	936	±	28	905.2	±	33.65	103.3
6.1	e,osc,eq	1133.85	355.6	0.31	0.0001	±	0.0001	6.53	±	0.24	0.0703	±	0.0007	918	±	24	881.2	±	36.56	104.1
7.1	m,osc,eq	1285.67	247.49	0.19	0.0000	±	0.0000	6.48	±	0.30	0.0696	±	0.0006	925	±	60	898.9	±	23.81	102.8
8.1	e,osc,eq	750.98	401.84	0.54	0.0002	±	0.0001	6.55	±	0.26	0.0706	±	0.0010	916	±	24	879.3	±	53.75	104
9.1	e,osc,p	1040.99	299.91	0.29	0.0001	±	0.0001	6.58	±	0.21	0.0700	±	0.0007	911	±	22	904	±	38.42	100.8
10.1	m,osc,fr	764.89	273.07	0.36	0.0004	±	0.0001	6.68	±	0.29	0.0701	±	0.0007	898	±	30	735.4	±	56.69	121.4
11.1	m,osc,p	1182.63	364.89	0.31	0.0001	±	0.0001	6.62	±	0.27	0.0701	±	0.0007	906	±	25	872.7	±	42.65	103.7
12.1	e,osc,p	1227.12	389.71	0.32	0.0001	±	0.0001	6.38	±	0.19	0.0692	±	0.0006	940	±	48	850.3	±	34.73	110.1
13.1	e,osc,p	1287.87	654.53	0.51	0.0028	±	0.0002	7.22	±	0.27	0.1043	±	0.0020	801	±	28	761	±	133.3	105.1
14.1	m,osc,ov	681.8	343.68	0.50	0.0002	±	0.0001	6.67	±	0.24	0.0702	±	0.0006	900	±	22	845.8	±	54.71	106.2
15.1	e,sz,fr	848.19	536.17	0.63	0.0001	±	0.0001	6.53	±	0.25	0.0692	±	0.0008	918	±	49	874.1	±	38.21	104.9
16.1	m,osc,fr	843.42	330.18	0.39	0.0001	±	0.0001	6.49	±	0.28	0.0688	±	0.0008	925	±	65	837.2	±	47.28	110.1
2.2	e,rex,p	1010.07	403.66	0.40	0.0001	±	0.0000	6.42	±	0.26	0.0697	±	0.0005	933	±	48	868.3	±	26.56	107.2
17.1	e,rex,ov	732.38	243.19	0.33	0.0002	±	0.0002	6.45	±	0.21	0.0695	±	0.0005	930	±	34	814.4	±	87.75	113.7

Table 5.1 (continuation) SHRIMP U-Pb zircon data for Gubaoquan Site

Labels	site	U/ppm	Th/ppm	Th/U	$^{204}Pb/^{206}Pb$			$^{238}U/^{206}Pb$			$^{207}Pb/^{206}Pb$			age $^{206}Pb/^{238}U$			age $^{207}Pb/^{206}Pb$			%conc
18.1	e,rex,p	715.51	623.22	0.87	0.0001	±	0.0001	6.47	±	0.19	0.0704	±	0.0010	926	±	20	884.2	±	52.15	104.5
19.1	c,h,ov	125.58	158.14	1.26	0.0009	±	0.0005	6.51	±	0.27	0.0725	±	0.0021	918	±	29	579.4	±	343.9	156.6
14GBQ2 Granitic Vein																				
1.1	m,osc,eq	898.77	377.87	0.42	0.0004	±	0.0001	15.03	±	0.60	0.0561	±	0.0008	415	±	13				
2.1	m,osc,p	576.06	340.71	0.59	0.0005	±	0.0003	14.76	±	0.55	0.0595	±	0.0013	420	±	11				
3.1	e,osc,p	450.57	157.27	0.35	0.0006	±	0.0004	14.76	±	0.61	0.0590	±	0.0013	421	±	12				
4.1	e,osc,fr	570.28	215.44	0.38	0.0005	±	0.0002	14.61	±	0.44	0.0605	±	0.0009	424	±	9				
5.1	e,osc,eq	685.09	223.46	0.33	0.0005	±	0.0002	14.26	±	0.62	0.0591	±	0.0009	435	±	13				
6.1	m.osc,p	628.29	282.44	0.45	0.0002	±	0.0001	14.58	±	0.50	0.0585	±	0.0008	426	±	12				
7.1	e,osc,eq	784.62	256	0.33	0.0002	±	0.0002	15.00	±	0.71	0.0586	±	0.0010	414	±	19				
8.1	c,h,eq	627.34	152.7	0.24	0.0001	±	0.0001	6.71	±	0.33	0.0712	±	0.0008	893	±	160	942	±	38.35	95
9.1	m,osc,eq	760.76	419.64	0.55	0.0002	±	0.0001	6.59	±	0.28	0.0703	±	0.0005	910	±	27	850.5	±	44.08	106.7
10.1	m,osc,fr	1131.57	359.39	0.32	0.0003	±	0.0002	14.35	±	0.45	0.0592	±	0.0010	432	±	11				
11.1	m.osc,p	576.09	252.18	0.44	0.0008	±	0.0003	14.93	±	0.67	0.0591	±	0.0013	416	±	14				
12.1	c,h,fr	569.02	84.48	0.15	0.0002	±	0.0001	6.60	±	0.22	0.0728	±	0.0011	906	±	30	910.3	±	52.49	99.6
13.1	m,h,p	439.2	161.39	0.37	0.0005	±	0.0003	14.26	±	0.48	0.0610	±	0.0011	434	±	12				
14.1	m,osc,p	724.09	227.79	0.31	0.0002	±	0.0002	14.68	±	0.55	0.0599	±	0.0011	422	±	34				
15.1	e,osc,eq	524.17	177.82	0.34	0.0013	±	0.0003	14.14	±	0.46	0.0680	±	0.0027	434	±	11				
16.1	e,hd,eq	828.66	257.92	0.31	0.0006	±	0.0002	6.97	±	0.61	0.0775	±	0.0018	855	±	85	899.9	±	121.8	95.2
14GBQ9 Lamprophyre																				
1.1	e,p	129.76	189.54	1.46	0.0048	±	0.0018	25.82	±	1.17	0.0810	±	0.0065	236	±	9				
1.2	e,p	308.77	420.51	1.36	0.0037	±	0.0014	27.19	±	1.19	0.0628	±	0.0054	229	±	8				
2.1	e,ov	1695.4	2676.21	1.58	0.0003	±	0.0001	7.47	±	0.35	0.0717	±	0.0007	804	±	43	831	±	48.94	96.9
3.1	e,rex	789.18	547.14	0.69	0.0003	±	0.0001	6.34	±	0.24	0.0709	±	0.0008	944	±	30	840.7	±	72.63	111.8
3.2	c,rex	554.41	445.93	0.80	0.0006	±	0.0002	7.09	±	0.31	0.0720	±	0.0008	846	±	25	717	±	95.75	117.5
4.1	e,h	90.85	35.27	0.39	0.0030	±	0.0017	7.86	±	0.30	0.0762	±	0.0030	761	±	23				

Site grain type and analysis location: p=prism, ov=oval, eq=equant, fr=fragment, e=end, m=middle, c=core, r=rim/overgrowth
Site CL imagery: osc=oscillatory zoned, h=homogeneous, hd=homogeneous dark, low luminescence, sz=sector zoned, rex=recrystallised
All analytical errors are given a 1σ
Concordance and $^{207}Pb/^{206}Pb$ ages only given for Precambrian sites

5.2 The Gubaoquan Site

5.2.1 Eclogite

Zircon Morphology

Zircons in eclogite sample 14GBQ1 exhibit typical characteristics of those found in high pressure metamorphic rocks (Corfu *et al.* 2003). Grains are mostly equant with some displaying gently irregular shapes, their length ranges from 70 μm to 250 μm with general length to width ratios of 2:1. The CL imaging revealed that several zircons have two domains, a core and overgrowth rim (Figure 5.1). The sub-rounded to rounded and irregular shapes of the zircon cores implies that these grains were subjected to corrosion prior to eclogite facies metamorphism, as characteristic prismatic morphology cannot be seen in any of the grains. Both cores and rims are homogenous and were only distinguishable by their luminescence as cores appear light-coloured in contrast to rims that are darker. The difference in luminesce can be attributed to thorium concentration that is elevated in cores in comparison to the rims, as a major contributing factor such as uranium content is approximately uniform between the two domains. Homogenous zircon textures are dominant throughout the sample, but several grains display oscillatory zoning mainly in core domains. However, one zircon crystal a had dark rim with oscillatory zoning present, suggesting the possibility of a rare and controversial occurrence of such internal structure in metamorphic overgrowth (Corfu *et al.* 2003). Unfortunately, the rim was too narrow to be analysed, and therefore its true nature could not have been determined.

The metamorphic rim development is limited, and therefore protolith cores constitute the majority of the grain mass. The process of corrosion is evident by etched cavities within cores, across which overgrowth became the widest, providing enough surface area for microprobe analysis (zircon 4 in Figure 5.1), otherwise the rims were too narrow to be analysed.

U-Pb Dating Results

Overall, 31 analyses were performed on eclogite sample 14GBQ1. Only 3 (3.1, 4.1, and 5.1) of these provide genuine ages of metamorphism (Figure 5.1 and Table 5.1). Another set of 5 analyses (1.1, 5.3, 10.1, 11.1, and 12.1) were also aimed at the metamorphic rim, but due to its narrow size the microprobe beam could not entirely fit on the rim and some core domain was included in the analysis, resulting in elevated ages. Therefore these ages are excluded from further interpretation. An additional 5 analyses were performed on sample 14GBQ5 in order to

determine if similar trends exist among those two eclogite samples. Obtained results revealed that trends are most likely to exist, however it cannot be determined with certainty due to the low count rates of these analyses and very low U content (Table 5.1). Interestingly, the analysis 4.1 on the core of the grain provided an age of 508±20 Ma, that overlaps with metamorphic age range determined in this work and previous works (Liu *et al.* 2010, Qu *et al.* 2011), indicating that this may be the first zircon in this study that has entirely grown in an eclogite facies metamorphic event (M_1).

A further 3 analyses (18.1, 20.1 and 23.1) gave ages of 44±10 Ma, 14±12 Ma and 41±13 Ma respectively and 117±60 Ma (site 1.1) in sample 14GBQ5. These very young ages are interpreted to be a result of a Late Mesozoic to Cenozoic thermal event that caused resetting of the U-Pb isotopic system (Nutman 2015, pers. comm., 08/07).

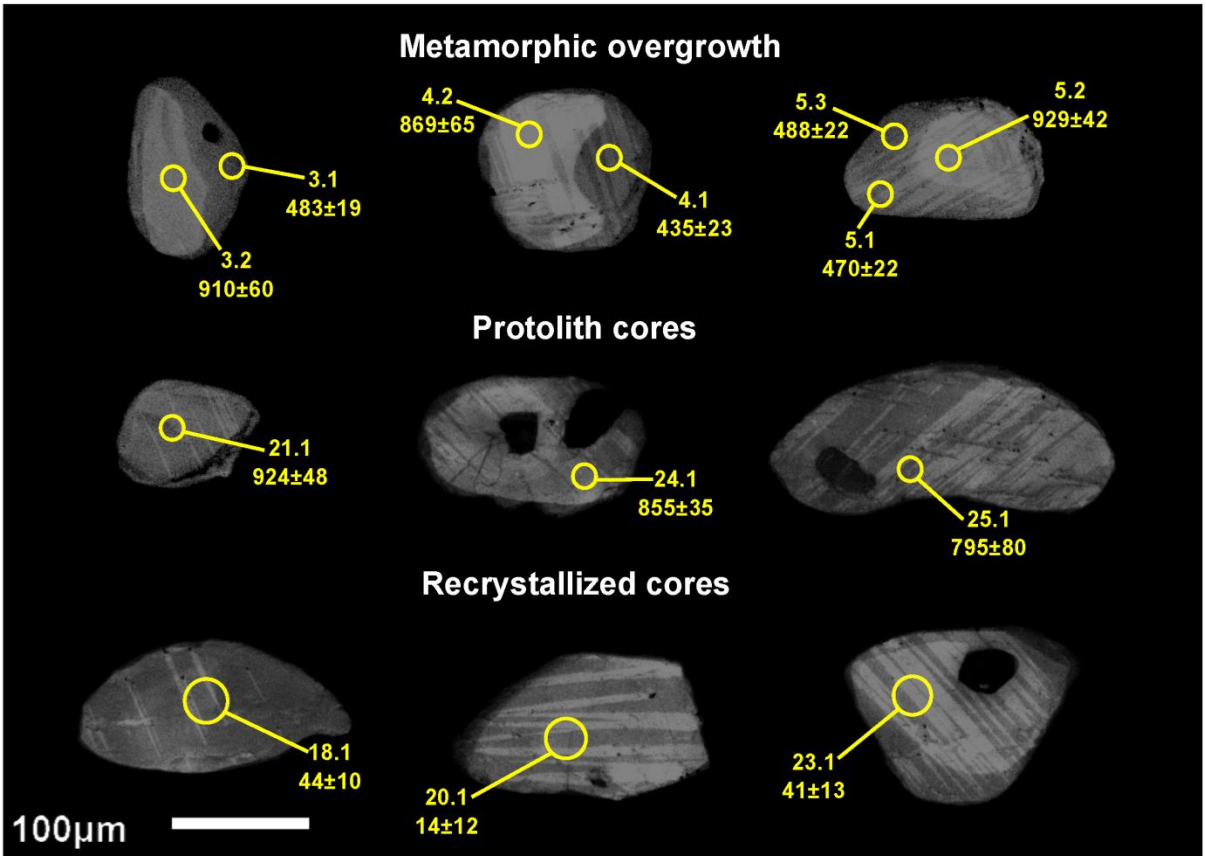

Figure 5.1 The 3 representative zircons from each category for eclogite sample 14GBQ1. The circles represent spots where analysis was undertaken, with ages (in Ma) for each individual spot. The textural striations should be ignored, as they are not endemic, they are a result of gold coating disturbance.

Metamorphic Rims

The 3 analyses (3.1, 4.1 and 5.1) performed on zircon metamorphic domains in sample 14GBQ1 give Cambrian to Ordovician ages 483 ± 19 Ma, 435 ± 23 Ma and 470 ± 22 Ma, respectively. These analyses revealed that new rims have very small amounts of uranium and radiogenic lead. In such instances, use of ^{204}Pb common lead correction method can lead to overcorrection and generation of too young ages. In order to avoid this effect, modelled common Pb composition was used to execute the correction. For the purpose of this study the ratio of Zartman and Doe (1981) for orogene lead composition for Ordovician age was used (^{207}Pb/^{206}Pb=0.85). In this data manipulation technique, uncorrected values (^{238}U/^{206}Pb and ^{207}Pb/^{206}Pb) for those 3 points plus the model common Pb composition were used to regress the data in Tera-Wasserburg space. The lower intercept of concordia of this regression is at 466 ± 27 Ma with 95% confidence (MSWD=0.95), this is interpreted as the age of metamorphism (Figure 5.2). The robustness of this approach was tested by input of significantly increased and decreased ^{207}Pb/^{206}Pb ratio and observation of the effect on the results. The test revealed that ratios such as 0.90 and 0.80 lead to ages of 467 ± 27 Ma and 464 ± 27 Ma respectively, indicating that radical changes in ^{207}Pb/^{206}Pb common lead composition has very little effect of the final age, confirming the robustness and reliability of this technique. The quality of the result was further explored by determination of the weighted mean for the acquired ages (Figure 5.3). The obtained mean age was exactly the complete confidence and satisfaction for obtained ages.

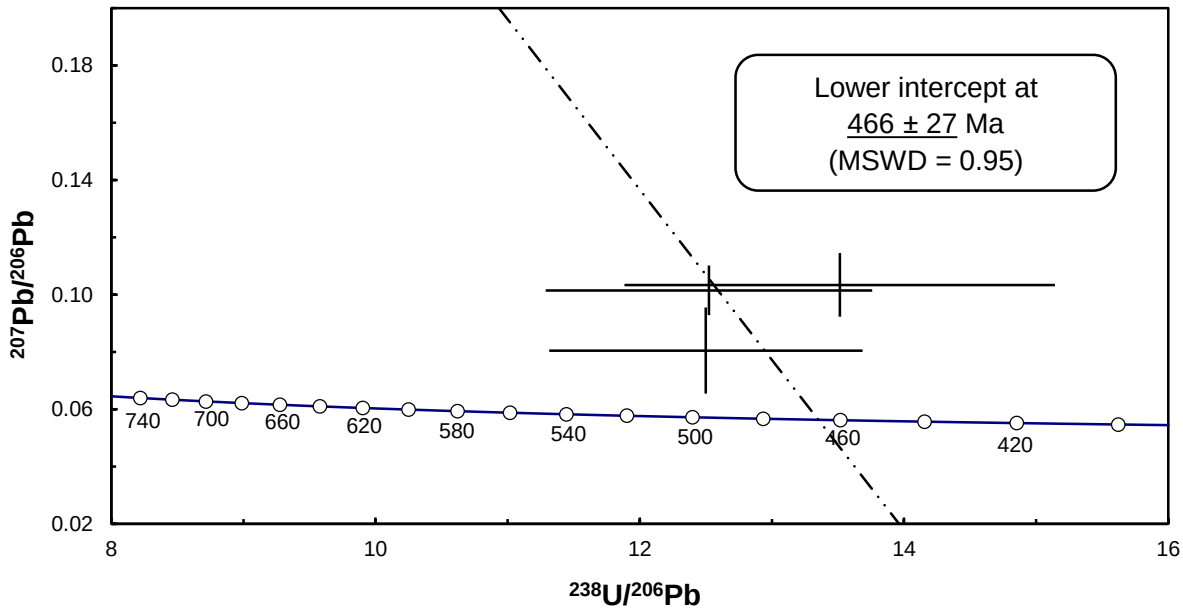

Figure 5.2 Tera-Wasserburg plot for eclogite sample 14GBQ1, metamorphic rims only.

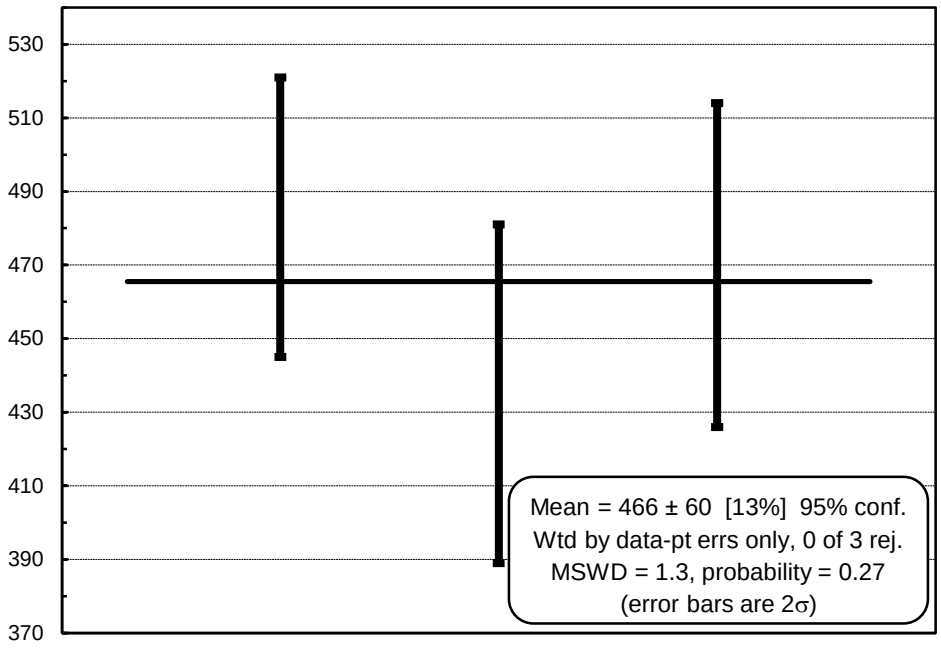

Figure 5.3 The weighted mean plot with standard deviation for eclogite sample 14GBQ1, metamorphic rims only, when data are regressed to concordia individually, using the model common Pb composition

Protolithic Cores

The remaining 19 analyses from sample 14GBQ1 were aimed at protolithic cores of the zircons to determine the timing of its magmatic crystallization prior to the metamorphism. The analysis revealed that points cluster together around 900 Ma; however none of them actually coincide with concordia (Figure 5.4). This is believed to be caused by the same low U and Pb factor as described above. The same correction method used for metamorphic rims was applied for the cores. The "unanchored" results provided an age of 874 ± 30 Ma, whereas "anchored" gave an age of 860 ± 18 Ma. Therefore, in this case, use of this technique also allows for a better constraint of the age and lowers the margin of error. The quality of the result was further explored by determination of the weighted mean for the acquired ages that was established at 855 ± 17 Ma when regressed individually to concordia (Figure 5.5). This revealed that ages obtained by two different methods produce results within error providing the confidence in the acquired data. However, the Th/U ratios of analysed protolithic cores is less than expected for mafic magmas, and therefore they are proposed to be xenocrystic cores of the country rock to the mafic body.

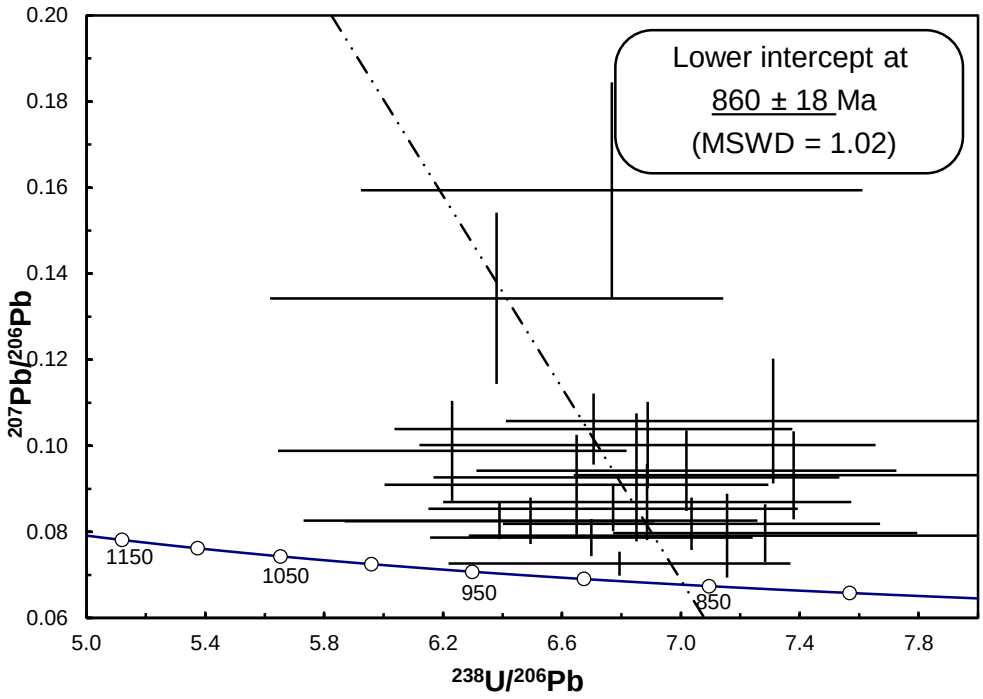

Figure 5.4 Tera-Wasserburg plot for eclogite sample 14GBQ1, protolithic cores only.

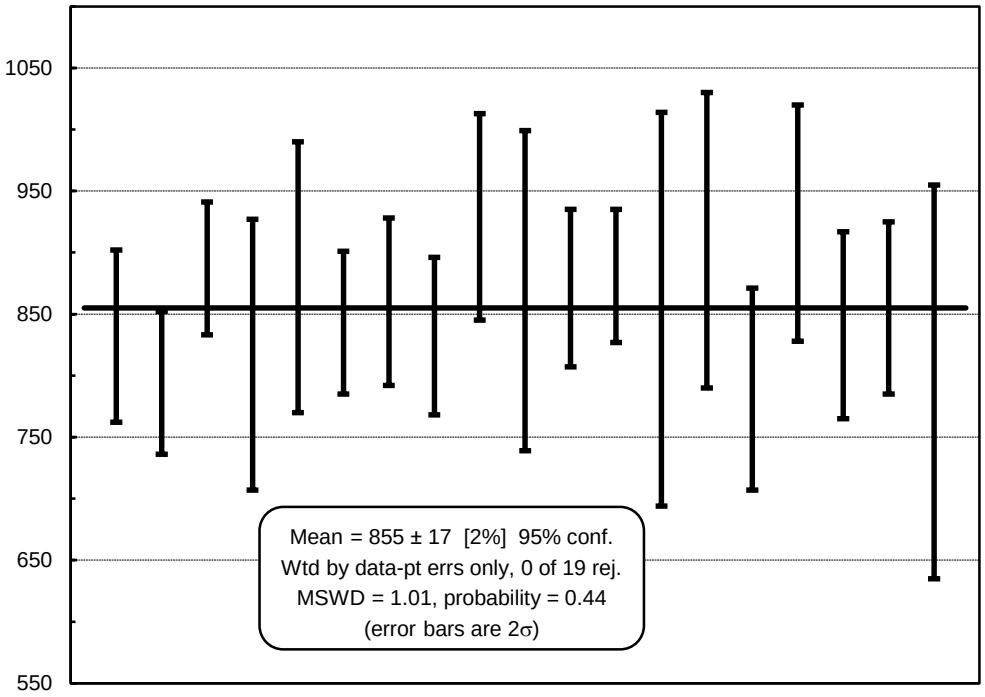

Figure 5.5 The weighted mean plot with standard deviation for eclogite sample 14GBQ1, protolithic cores only

5.2.2 Orthogneiss

Zircon Morphology

Zircons from orthogneiss sample 14GBQ10 show characteristic features of igneous zircons, indicating little modification during metamorphism. The grain lengths range from 80 μm to 350 μm with little variation in length to width ratios ranging from 1:1 to 3:1, where 2:1 is the most dominant.

The CL imaging has revealed a high diversity of internal textures in orthogneiss zircons, but igneous oscillatory zoning is most abundant (Figure 5.6). However, many display modifications in the form of convolution banding and homogenization of oscillatory zoning that was caused by late magmatic recrystallization (Nutman 2015, pers. comm., 08/07). Corfu *et al.* (2003) also described these modifications as a result of late and post-magmatic cooling driven by magmatically derived fluids. This process often results in a shift of trace elements across the zircon crystal domains, resulting in zones of trace element enrichment and depletion. This form of recrystallization produced light and dark patches within affected zircon domains that are most likely a result of those elemental shifts. Therefore internal textures indicate that these zircons were affected by late- or post-magmatic event and not a metamorphic event as it was originally thought.

Several zircons display core-rim textures where cores commonly are homogenous and rims are oscillatory zoned, *ergo* not related to metamorphism. This is further supported by U-Pb dating results (Table 5.1). The intensity of luminescence of homogenous zircons and domains of the heterogeneous ones is highly variable throughout the sample. It ranges from completely dark cores and grains to very bright domains, patches and single zones (Figure 5.6). It is most likely attributed to trace element content and its redistribution caused by recrystallization. Zircons do not show metamorphic overgrowth rims, however any thin growth could have been masked by oscillatory zoning texture of the grains, but it is unlikely due their appearance and therefore it is concluded that zircons have not experienced growth during metamorphism.

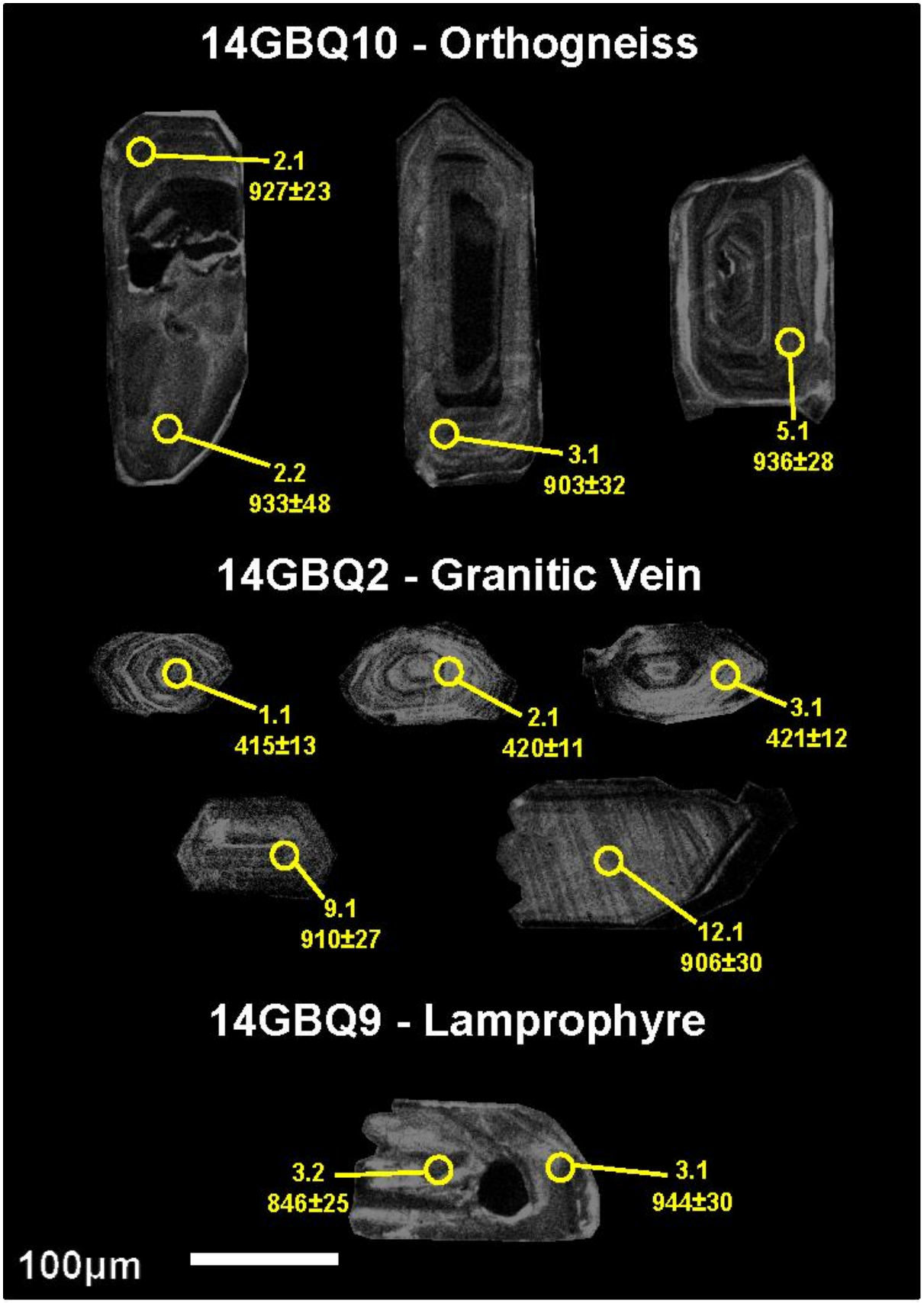

Figure 5.6 The representative zircons for granitic vein, orthogneiss and lamprophyre samples. The circles represent spots where analysis was undertaken, with ages (in Ma) for each individual spot. The textural striations should be ignored as they are not endemic, they a result of gold coating disturbance.

U-Pb Dating Results

For the orthogneiss sample 14GBQ10, 20 analyses were performed on 19 zircon grains (Table 5.1). Since a lack of metamorphic growth was revealed in CL imaging, the analysis was mainly aimed at conformable oscillatory zoning of igneous protolith zircons. Several analyses were also performed on homogenous domains of varied luminesce intensity and on recrystallized zones with convoluted textures. The aim of this attempt was to determine possible disturbance effects on U-Pb isotopic system changes during recrystallization and trace element redistribution.

Form the 20 analyses performed, all gave Precambrian ages ranging from 799 Ma to 946 Ma forming cluster within error of concordia (Figure 5.7). Derived ages have elevated but consistent standard deviation. However, the final weighted mean was established at 920 ± 14 Ma with 95% confidence (MSWD=0.19) giving a reliable and satisfactory result with acceptable standard deviation (Figure 5.8). This age is interpreted as the crystallization time of igneous protolith. There were 4 analyses (2.2, 17.1, 18.1 and 19.1) performed on recrystallized domains to determine age of that event. However, the results indicate that this event had no significant influence on the isotopic system and thus occurred within error of the magmatic crystallization age.

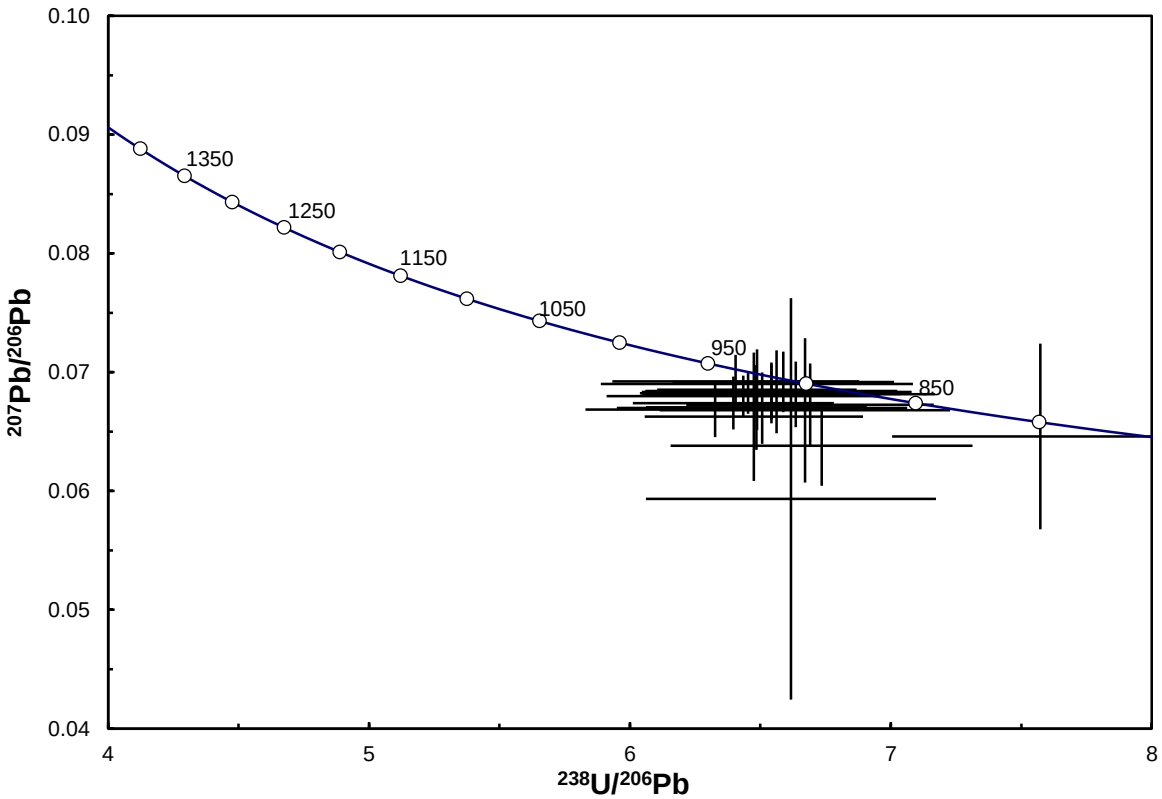

Figure 5.7 Tera-Wasserburg plot for orthogneiss sample 14GBQ10

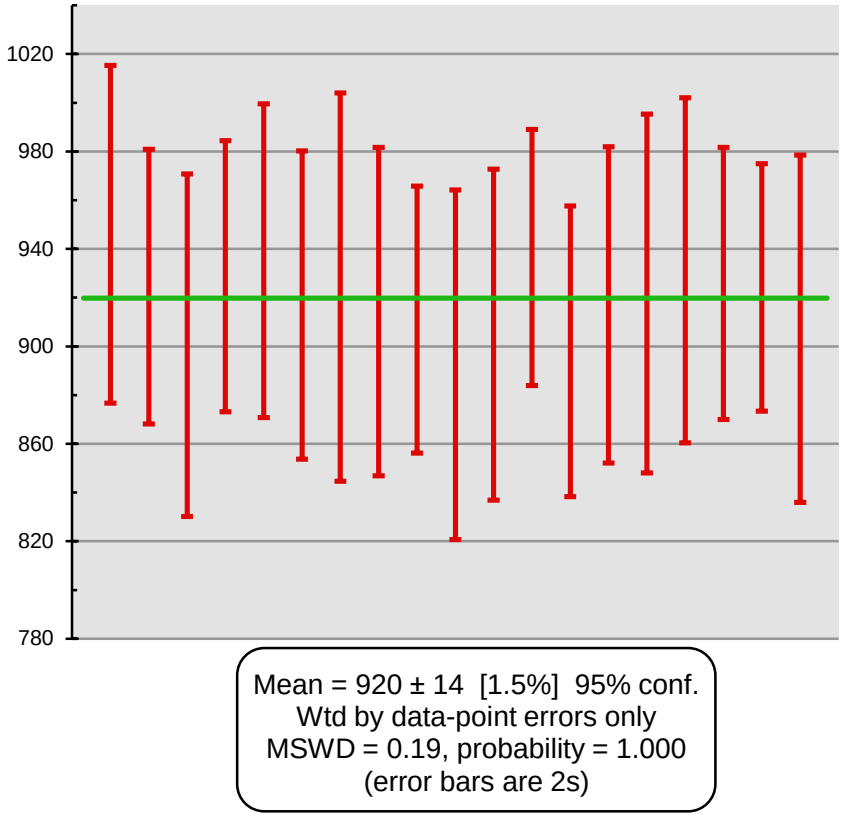

Figure 5.8 The weighted mean plot with standard deviation for orthogneiss sample 14GBQ10

5.2.3 Granitic Vein

Zircon Morphology

Zircons from granitic vein 14GBQ2 display characteristic morphology of prismatic to equant with oscillatory zoning of an igneous zircon. The grain length ranges between 40 μm and 300 μm, which results in highly diverse length-to-width ratios among the grains; they vary between 1:1 and 5:1, giving a sample average of 3:1. The CL imaging has revealed oscillatory zoning to be a dominant internal texture within zircon grains. Several inherited zircons have homogenous cores and some grains also display broad zoning as an internal texture (Figure 5.6). A highly variable factor noted within this sample was luminescence intensity, as some grains were extremely dark with slight evidence of zoning, whereas others were intensely light masking any internal structures. The same variability was also noted between individual zones within the grain; however this is a characteristic occurrence that leads to development of oscillatory, zoning which is produced by variation in rare earth element content (McFarlane 2014).

Within 23 zircon grains disturbance to oscillatory zoning was observed, having irregular shapes, convoluted zones and highly luminescent patches. This is thought to be attributed to the similar processes discussed in section 5.2.2.

U-Pb Dating Results

For the sample 14GBQ2, 16 zircons were chosen for analysis on the basis of their internal textures determined by cathodoluminescence imaging. Sections that were affected by slight modifications to internal textures or were partially recrystallized were avoided. The analysis spots were aimed at conformal oscillatory zoning and homogenous sectors to avoid the risk of dating disturbed isotopic system. Following these precautions resulted in accurate and reliable ages (Table 5.1).

From the performed analyses, 12 gave Middle Silurian to Early Devonian ages ranging from 435 to 414 Ma. Derived ages are concordant and form a cluster on within error of concordia (Figure 5.9). The final weighted mean age of this population at 424 ± 8.6 Ma with 95% confidence (MSWD=0.25) (Figure 5.10). Another 4 analyses (8.1, 9.1, 12.1 and 16.1) gave Precambrian ages ranging from 910 to 855 Ma; these are interpreted to be inherited zircons from country rocks that were assimilated during the granitic vein intrusion. The analysis 16.1 that provided the lower age limit inherited zircons is overestimated because of high uranium content, which also resulted in high margin of error.

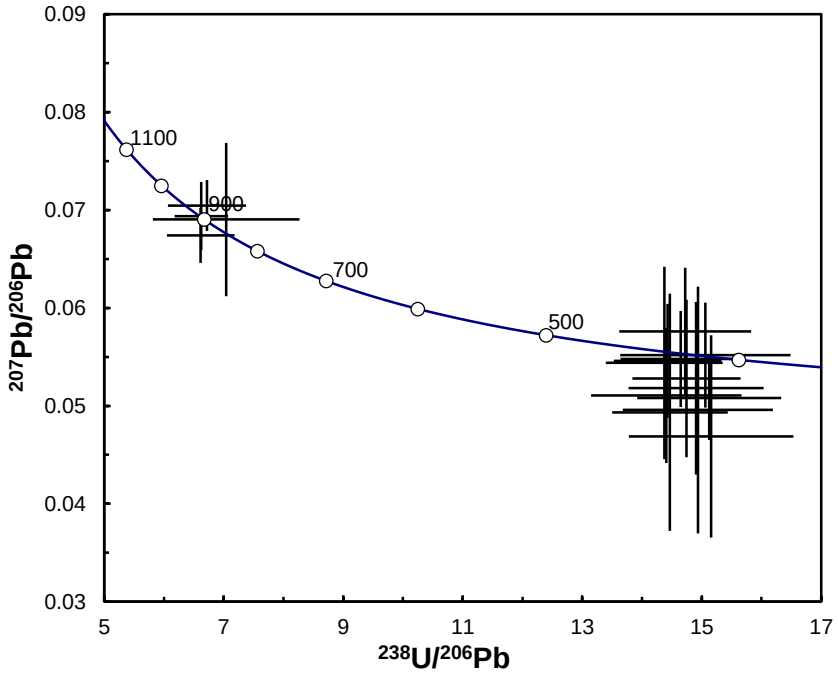

Figure 5.9 Tera-Wasserburg plot for granitic vein sample 14GBQ2, shows distribution of ages for its magmatic and inherited zircons.

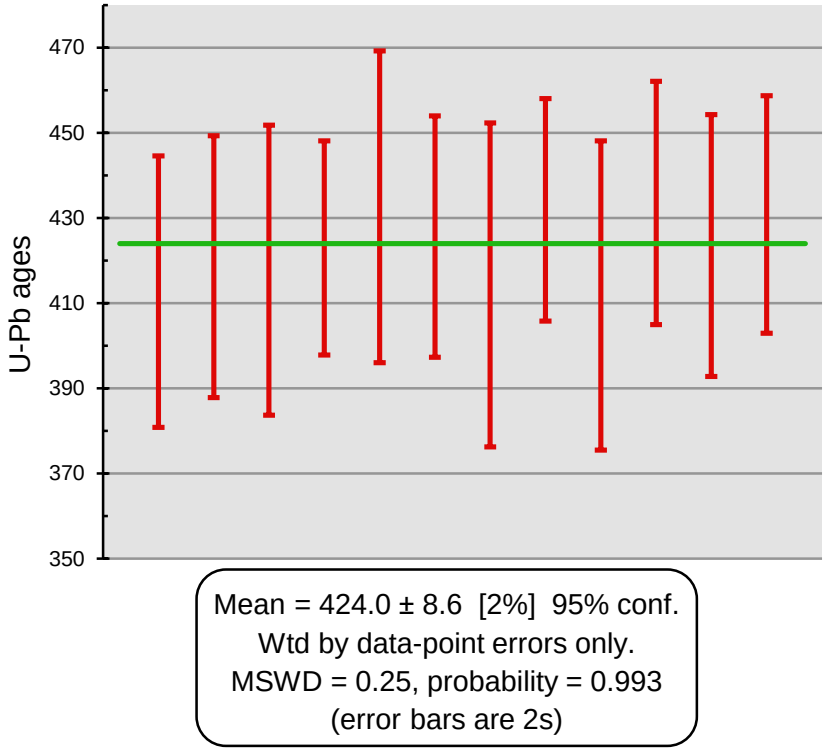

Figure 5.10 The weighted mean plot with standard deviation for granitic vein sample 14GBQ2; excluding inherited zircons.

5.2.4 Lamprophyre

Zircon Morphology

The lamprophyre sample 14GBQ9 has produced very little zircons, only 4 grains were detected and analysed. Their grain length is approximately 200 μm and length-to-width ratio is 2:1. The CL image of the zircons reveal a strongly disturbed texture. The zircon no. 3 (Figure 5.6) has gentle oscillatory zoning disturbed by recrystallization, possibly by the process similar to that discussed in section 5.2.2. The other zircons are strongly luminescent, appearing completely bright, masking any internal structures.

U-Pb Dating Results

Due to the low abundance of zircons recovered from the lamprophyre dyke and only 6 analyses performed, it is not possible to determine a definite age of this intrusion; however it can provide general information of what can be expected in further studies. Some grains were spotted prior to the analysis, whereas others were directly targeted with the microprobe ion beam in order to find zirconium peak so that an analysis could be conducted. Secondly, identified zircons have been affected by recrystallization processes and some had high uranium and low lead content,

resulting in extremely high and low $^{238}U/^{206}Pb$ and $^{207}Pb/^{206}Pb$ ratios respectively. This produces some discordance on Tera-Wasserburg diagram what further affected the credibility of achieved ages (Figure 5.11).

Nevertheless, obtained ages provide certain indication of the timing of the intrusive event, as on the timescale of the events studied in this project, this still provides credible information for modelling. Two sets of ages were obtained where the first set consisted of analyses 1.1 and 1.2 giving Triassic ages of 236 ± 9 and 229 ± 8 Ma respectively, with a weighted mean of 232 ± 12 Ma with 95% confidence (MSWD=0.34) (Figure 5.12). These ages are interpreted as the timing of the crystallization of the lamprophyre dyke, which is further supported by high Th/U ratios characteristic of mafic rock. Whereas the second set provided Precambrian ages ranging from 944 to 804 Ma. These are interpreted to be inherited zircons from the country rock, as their Th/U ratios and ages are similar to those from orthogneiss into which this dyke intrudes. The CL image and two analyses performed on zircon 3 (3.1 and 3.2; Figure 5.6) show the effects of recrystallization through internal textures and highly deviated ages. The analysis 4.1 was rejected from the calculations because it contained significantly more common lead and less uranium; additionally its high luminescence masked the internal texture of the zircon, increasing probability of analysing a disturbed site.

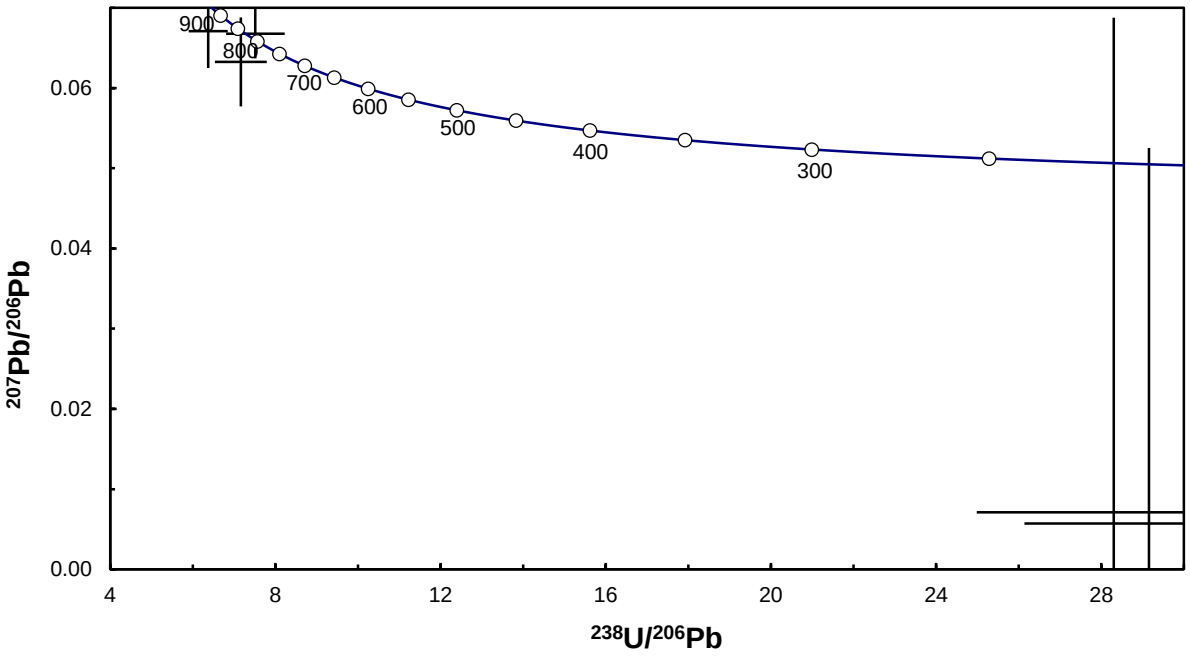

Figure 5.11 Tera-Wasserburg plot for lamprophyre sample 14GBQ9, shows distribution of ages for its magmatic and inherited zircons.

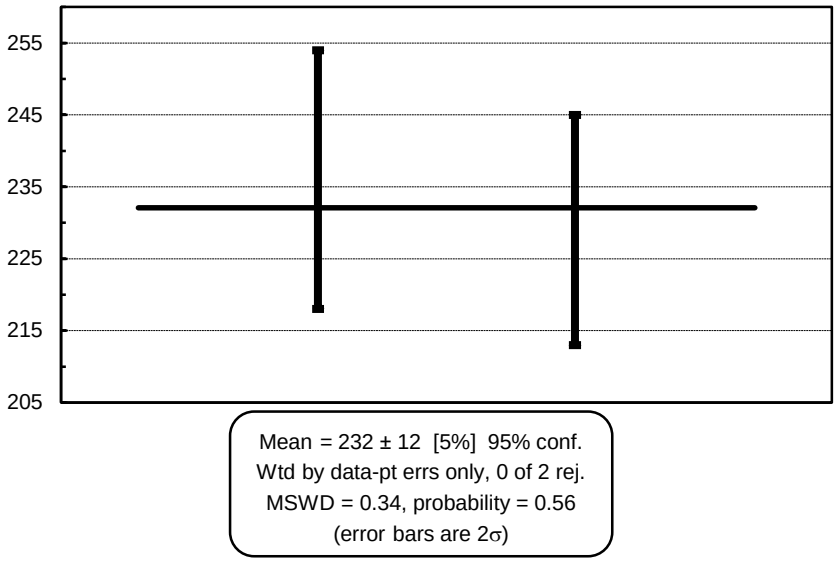

Figure 5.12 The weighted mean plot with standard deviation for lamprophyre sample 14GBQ9; for its magmatic zircons excluding the inherited ones.

5.3 The Kanfenggou Site

5.3.1 Eclogite

Zircon Morphology and U-Pb Dating Results

The early stages of examination have revealed that zircons are very scarce in this sample. From ~ 150 grains selected, only one was determined to be a zircon and rest of the selection constituted of apatite. The abundance of apatite prevented acquisition of CL images as their strong remnant luminesce obstructed the field of view. A single zircon grain was spotted using microprobe beam ablation to determine zirconium peak in the grains. The zircon grain found was approximately 100 μm in diameter and oval in shape.

Since only two analyses were performed on one zircon, there is no certainty in the result, especially when conventional method of ^{207}Pb correction gave age of 499 ± 580 Ma (Table 5.2). However, when the data were regressed using appropriate Zartman and Doe (1981) common Pb composition, the age and its uncertainty were reduced to 490 ± 83 Ma (Figure 5.13), which is a peak age of the metamorphism described in the literature (Wang *et al.* 2013). Therefore, obtained geochronological results for the Kanfenggou site do not provide usable ages for the modelling, but they provide an indication of probability of consistency with previous studies.

Table 5.2 SHRIMP U-Pb zircon data for Kanfenggou eclogite.

Labels	site	U/ppm	Th/ppm	Th/U	$^{204}Pb/^{206}Pb$			$^{238}U/^{206}Pb$			$^{207}Pb/^{206}Pb$			age $^{206}Pb/^{238}U$		
15KF4 Eclogite																
Metamorphic grains																
1.1	ov	2.49	0.02	0.00776	0.0055657	±	0.0056113	9.0844	±	0.91157	0.28269	±	0.0299	499	±	580
1.2	ov	0.82	0.02	0.02154	0.0000001	±	0.0042312	6.85073	±	0.82131	0.41989	±	0.03262	n/a	±	n/a

Site grain type and analysis location: p=prism, ov=oval, eq=equant, fr=fragment, e=end, m=middle, c=core, r=rim/overgrowth
Site CL imagery: osc=oscillatory zoned, h=homogeneous, hd=homogeneous dark, low luminescence, sz=sector zoned, rex=recrystallised
All analytical errors are given a 1σ

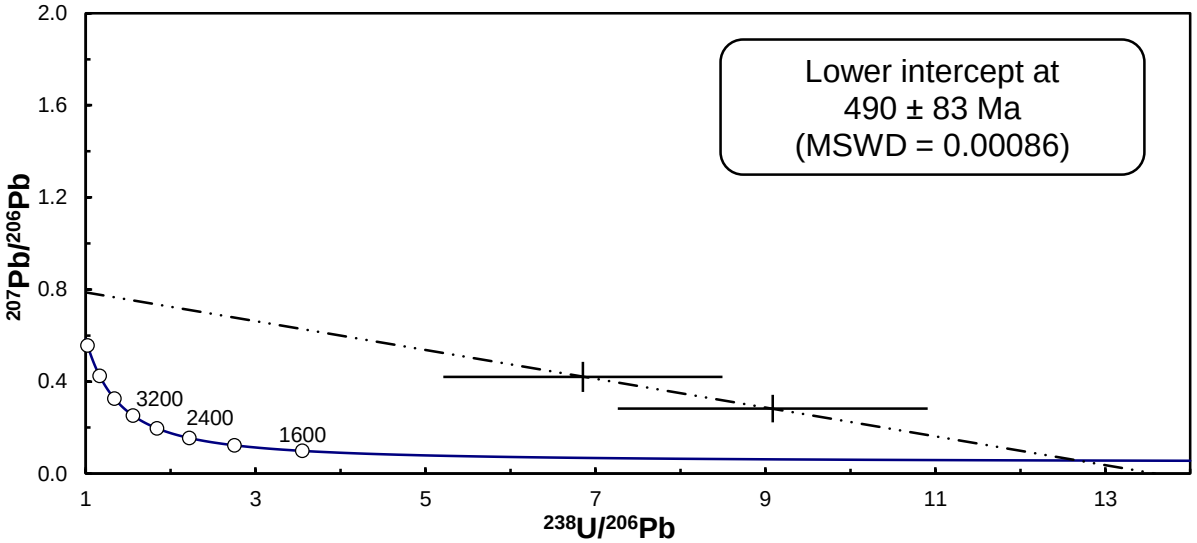

Figure 5.13 Tera-Wasserburg plot for eclogite sample 15KF4.

Chapter Six

Synthesis and Discussion

6.1 Introduction

This chapter will present synthesis of data collected in this study and information acquired from the literature. The data from Kanfenggou site in Qinling Orogen will not be discussed here in great detail as it was done with result report in previous chapters. The aim of Kanfenggou site was to provide comparison and contrast to the Gubaoquan site. As studied eclogites at these sites formed in separate events and under different conditions gaving an opportunity to study realm of the eclogite formation on broader scale. The lack of necessary data to undertake this detailed comparative study of Kanfenggou site has impeded this part of the project. Nevertheless, significant results were obtained, and provide an opportunity for future research.

For the reasons stated above, focus of this study was aimed at geological history of the Gubaoquan site and evolution of the Beishan Orogen. Next section discussed here will explore former aspect of the research, whereas Broader Concept will provide alternative model for the latter. In previous works main focus in this area was aimed at the determination of ocean closure between northern (Baltica and Siberian) and southern (Tarim and North China) cratons and final amalgamation of the Altaids. Two main concepts were favoured by various authors, the Early Palaeozoic and Late Permian-Early Mesozoic. In early stages of this project it was revealed that the closure took form of the multi-stage process, which is generally favoured by the scientific community. However, data indicates that there were not as many stages in this process as some authors tend to believe. The following synthesis of the data obtained in this project and acquired from the literature is aimed at evaluation of current tectonic models and discussion of anomalies encountered throughout the study.

6.2 Beishan Local Model

The geological events associated with assembly of Central Asian Orogenic Belt, including the Beishan Orogen represent 800 million years of history from assembly of a

Paleoproterozoic supercontinent to Early Palaeozoic breakup and dispersal of peri-Gondwanan microcontinents, followed by their amalgamation and accretion with younger oceanic terranes in Triassic. The oldest unit encountered at the Gubaoquan site are Neoproterozoic granitoids that are now part of the Beishan Basement Complex. It hosts the Gubaoquan eclogite as well as post-metamorphic igneous intrusions that have been studied in this project. This collection of different lithologies encountered in a small area of *c.* 900 m^2 represents long lasting geological activity since the Neoproterozoic until Late Mesozoic. The petrological, geochemical and geochronological data described in previous chapters will be brought together and integrated with existing data to explain better the tectonic evolution of Gubaoquan site and the surrounding terrane. Therefore, this part of discussion focuses on Ordovician-Silurian collision between Dunhuang Block and Liuyuan Basement.

Previous studies interpreted the eclogite body at Gubaoquan as a remnant of oceanic crust (Liu *et al.* 2010, Qu *et al.* 2011), mainly due to its mafic composition and its geochemical signatures. However, based on field relationships observed in this study, it is considered unlikely that this eclogite has been derived from simatic crust and therefore an alternative origin and model of tectonic events that led to its development are proposed.

6.2.1 Evolution of Southern Beishan Terranes

In the scope of local model of tectonic evolution in Southern Beishan terranes two key components are investigated, the Dunhuang Block and Liuyuan Basement. Multiple microcontinents have been identified in Beishan Orogen, based on their high grade metamorphic appearance, Precambrian ages, faulted bounded contacts and isolated field relationships (Xiao *et al.* 2011, Song *et al.* 2013c). However, commonly microcontinents are slivers of large cratons that have rifted during subduction related tectonism or mantle plume emplacement proximal to craton's margin (Muller *et al.* 2001). Thus microcontinents will be sourced from adjacent more extensive cratons that are the hinterland to the amalgamating orogen or were previously in proximity. This was investigated by Song *et al.* (2013c) through detrital zircon study of metasedimentary rocks of Beishan Basement Complex to determine the source provenances of these terranes. It revealed that these microcontinents are not rifted slivers of Siberia, North China and Tarim cratons as it was previously thought; instead their age populations suggested association with supercontinent Columbia indicating allochthonous origin; most likely juxtaposed by major tectonic thrusting (Song *et al.* 2013c). For this reason,

so-called microcontinents will be referred to as basement as they might be part of single microcontinental basement that is dissected by faults and partially covered by overlying rocks to form appearance of discrete terranes; this concept will be further explored in section 6.3.

Liuyuan Basement and Gubaoquan Eclogite

The Liuyuan Basement consists of orthogneisses and paragneisses of the Precambrian age. The age of the orthogneiss was determined in this study to be 920 ± 14 Ma by U-Pb zircon dating and previous studies obtained detrital zircon ages of 1446 ± 39 Ma and 2090 ± 100 Ma constraining depositional age of the paragneisses to be < 1446 Ma (Liu *et al.* 2010). Therefore, this rock suite represents sedimentary sequence sourced from Palaeoproterozoic rocks that was intruded by granitoids in Neoproterozoic. The ages obtained from these rocks suggest association with Rodinia.

As it was shown in Chapter Three, the orthogneiss has well-developed augen texture which is also present in paragneisses (Qu *et al.* 2011). The degree of deformation was observed to be variable, as both large well-defined augen and small elongated to ribbons augens (mylonitized) were present indicating mild and strong shearing. These gneissic rocks are host to the Gubaoquan eclogite that occurs as a dismembered assemblage of lenses of boudins varying size (centimetre to hundred metre scales). This indicates that the eclogites suffered strong deformation, most likely in the same event that developed augen texture in gneisses. The areal extent of eclogite occurrence in Gubaoquan is small (5 x 1 km as determined by Liu *et al.*, 2010) in comparison to other ophiolitic eclogite-bearing assemblages like Dora Maira, Italy (225 x 60 km as determined by Ernst, 2001). The host lithologies within which eclogite boudins are imbedded are typical crustal (granitic) rocks, and there is lack of any evidence that could indicate their ophiolitic association to support the hypothesis of an oceanic crust protolith for the eclogites. As it is highly unlikely to encounter completely allochthonous eclogites without direct fault contact such as those in Syros Island, Greece (Brady *et al.* 2000) or being carried in subduction-related rocks like serpentinites in mélange at Port Macquarie, Australia (Nutman *et al.* 2013). Therefore, implying an oceanic crust affinity solely based on geochemical signature of high grade metamorphic rock is not convincing, and their origin must be re-evaluated. Based on the information discussed above such as field relationships with the host rocks, mylonitized mode of occurrence, size of eclogite boudins, re-evaluation of geochemical data and additional information produced by previous studies (Liu *et al.* 2010, Qu *et al.* 2011)

it is herein proposed that Gubaoquan eclogite represents metamorphosed and dismembered mafic dyke or a sill that has intruded Proterozoic strata during or after Neoproterozoic, as constrained by the crystallization age of the orthogneiss. This would indicate the eclogites formed during transient high pressure in a microcontinent during Paleozoic terrane assembly. A similar origin for Paleozoic eclogites has been documented in the Caledonian orogen in northeast Greenland (Gilotti *et al.* 2004).

Dunhuang Block and HP Granulite

The Dunhuang Block consists of Archean basement rocks covered by Dunhuang Group that comprises sedimentary rocks and tonalite-trondhjemite-granodiorite (TTG) intrusions of Palaeoproterozoic age that have been metamorphosed to medium-high grades and were suggested to represent active margin of Tarim Craton (Zong *et al.* 2012). The Dunhuang Group and Block are of a particular importance in evolution of Southern Beishan terranes as they contain high pressure granulite facies rocks and are in inferred contact with Liuyuan Basement. This suite of rocks has undergone ductile deformation where gentle bending of strata was observed by Zong *et al.* (2012), however its intensity wasn't as severe as in Liuyuan Basement where dismembering of rocks was caused by mylonitization. Importantly, because of this low degree of deformation the original relationships between the rock types are preserved, *ergo* the nature of their protolith can be determined with higher certainty. This HP granulite of mafic composition exist as continuous body of various widths within the gneisses, resembling a series of dykes or sills what led to the conclusion that it is most suited protolith for this metamorphic rock.

6.2.2 Liuyuan and Dunhuang Terrane Collision and Orogeny

Presence of high pressure or ultra-high pressure rocks in the non-igneous environment carries undisputed implication for tectonic setting, as such rocks will only form in subduction and continental collision environments, therefore occurrence of these rocks provides proxy for relict orogenic processes from which key information about the operating conditions can be obtained and geological history of the region can be interpreted more accurately (Ernst 2001, Zhang *et al.* 2003). However, this truth bearing assumption has been significantly overused, especially in Beishan Orogen, as every occurrence of high pressure rock or an ophiolite led to

instant conclusion of existence of new subduction zone, suture and/or exotic microcontinent. This overly complicated approach to the tectonic setting of Altaids is a probable response to the oversimplified model of single and curved subduction zone between Siberia and Baltica Cratons proposed by Sengor *et al.* (1993), which has been invalidated in more recent literature.

The Dunhuang Block is believed to be leading margin of the north approaching Tarim Craton in the continental collision with current Beishan terranes (Liu *et al.* 2010, Qu *et al.* 2011, Zong *et al.* 2012). The site of the high pressure granulite is located in the northern marginal section of that continental body and it is the highest grade of metamorphic rock in this area and therefore it could represent its previous emplacement in the orogenic core setting. Similarly, Gubaoquan eclogite site is located in the southernmost marginal section of Liuyuan Basement also representing highest metamorphic grade in this localised area that could be interpreted as frontal terrane subjected to collisional orogenic regime. These field relationships could possibly indicate participation of these high pressure rocks in the same collisional event due their proximity. It is also inferred that the Dunhuang Block's oceanic crust was subducting to the north under the Liuyuan Basement from their corresponding metamorphic facies (further discussed below) and presence of Nb-enriched basalts and adakites within the Liuyuan Basement with crystallization ages ranging from *ca.* 451 to 374 Ma that correlate with timing of the subduction and the post-collisional magmatism (Mao *et al.* 2012).

HP granulite from the Dunhuang Group was studied in detail by Zong *et al.* (2012) and He *et al.* (2014). Their work concluded that peak granulite facies metamorphism conditions reached pressure of 14-17 kbar and temperature of ~800° C. This estimation is comparable to the P-T conditions of Gubaoquan eclogite, however with elevated temperature. These conditions shifted mineral equilibrium from the eclogite facies of jadeite + quartz stability field to the HP granulite facies where albite is present (clinopyroxene + garnet + plagioclase + quartz). This metamorphic event was dated by U-Pb zircon method at 444 ± 5 Ma and 431 ± 2 Ma respectively, by the authors above. HP granulite assemblages are a hallmark of a transient high pressure metamorphism deep in tectonically thickened crust in collisional orogens (O'Brien and Rötzler 2003). Conditions for HP granulite facies metamorphism is never realized in subduction channel and ophiolitic assemblages. The Gubaoquan eclogite metamorphism occurred at 466 ± 27 Ma, at least 22 Ma earlier than the granulite facies in Dunhuang Block. Alternatively, these episodes could have been synchronous if margin of error is to be considered. In this model however, these events are treated as separate, as up to date there were three U-Pb dating studies of the Gubaoquan eclogite; 465 ±10 Ma by Liu *et al.* (2010), 467 ±

16 Ma by Qu *et al.* (2011) and 466 ± 27 Ma this study, and they all indicate concordance at *ca.* 466 Ma. Concurrently the HP granulite metamorphism was dated at 444 ± 5 Ma and 431 ± 2 Ma showing either long-lasting metamorphism or two zircon growth stages. Therefore, eclogite and high pressure granulite forming events are considered as a separate metamorphic episodes associated with the same collisional event, but on opposite sides of the inferred suture.

Based on information above, the precursory metamorphism of Gubaoquan eclogite and orthogneiss could be considered a localised event in frontal terrane of the collision, such as continental shelf which during the collision was detached from the crust by the subducting plate and was forced into the deeper lithospheric levels where eclogite facies metamorphism of crustal rocks occurred (as demonstrated in Figure 6.1).

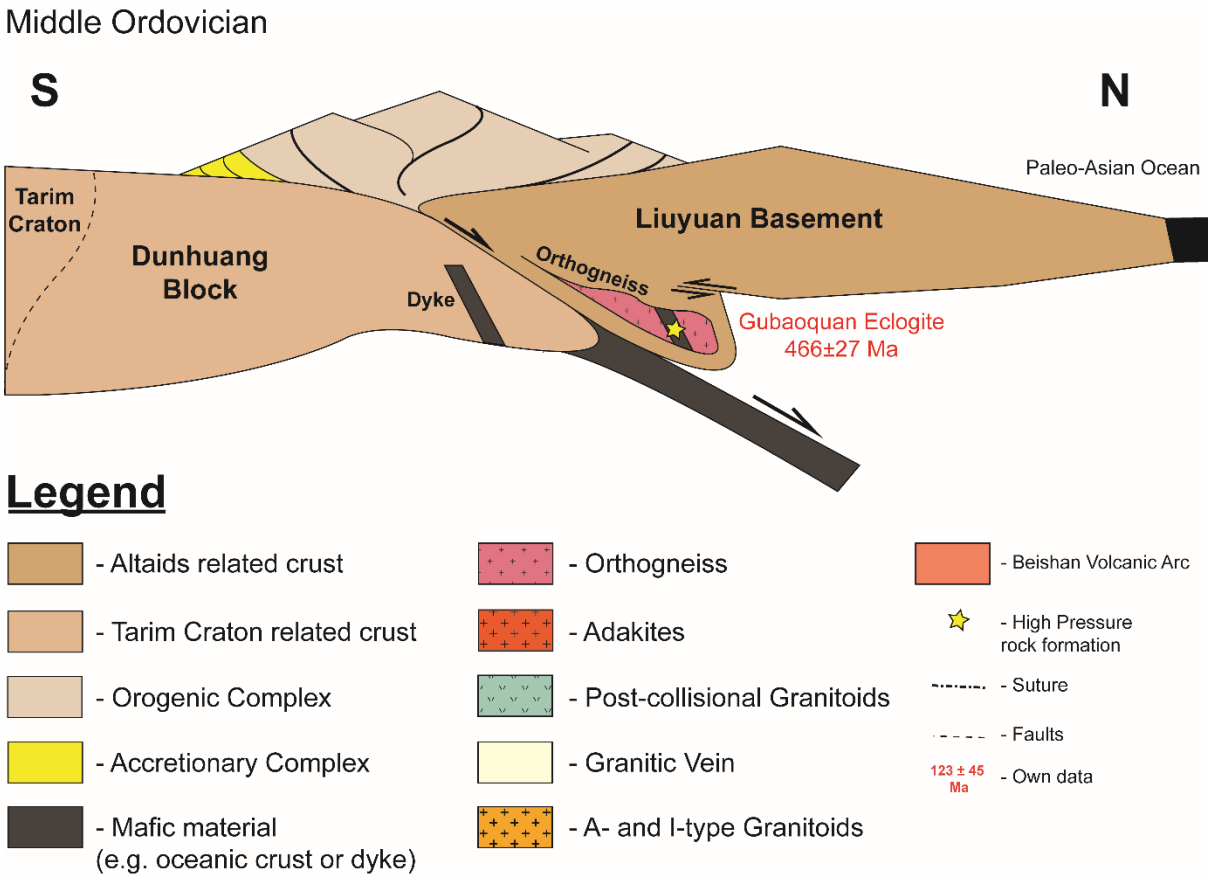

Figure 6.1 Schematic diagram of initial collision and eclogite metamorphism between Dunhuang Block and Liuyuan Basement.

The Gubaoquan site is considered to be a detached crustal fragment from the hanging-wall in the subduction zone (Liuyuan Basement). It is most likely to remain at lower levels while oceanic crust is still descending but once Dunhuang Block continental crust starts to descend into the subduction channel, the process is likely to slow down and the less dense material will

start to force the hanging-wall upwards. This form of emplacement and displacement relationship can be observed in this collision, as the end of peak metamorphism in down-going Dunhuang Block is thought to coincide with the retrogressive stage of Gubaoquan eclogite (as demonstrated in Figure 6.2 and 6.3).

The $^{40}Ar/^{39}Ar$ dating of biotite in augen gneiss conducted by Qu *et al.* (2011) revealed a well-defined plateau at age 428.9 ± 3.8 Ma with diffusion closure temperature of ~300° C. This constrains the cooling history related to exhumation, following the eclogite event. This provides strong evidence for synchronous prograde (in Dunhuang) and retrograde (in Liuyuan) metamorphism (as demonstrated in Figure 6.3). The HP granulite formation is thought to occur just prior to cessation of the subduction. Therefore, the youngest age of high pressure metamorphism in Dunhuang Block and Liuyuan Basement collision is considered an end of this event, as these metamorphic events are thought to take place soon after collision stops (Nutman *et al.* 2008); in this orogeny it occurred at 431 ± 2 Ma.

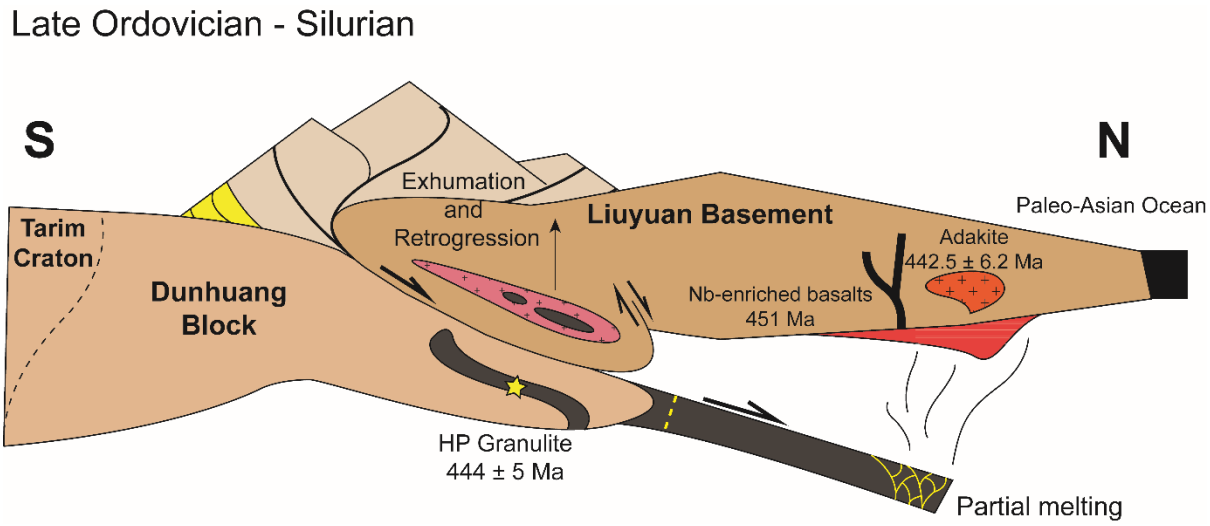

Figure 6.2 Schematic diagram showing late stage collision, where emplacement of a mafic dyke in the Dunhuang Block into HP granulite facies conditions was a driving force of exhumation and retrogression of previously metamorphosed eclogite. (HP granulite metamorphic age from Zong *et al.* (2012); Basalt and adakite ages from Mao *et al.* (2012))

Exhumation and retrogressive events are often accompanied by magma production, for which evidence are abundant throughout this area; ranging from plutons to felsic dykes where all share the age that is concurrent with retrogression. The break-off of dense oceanic crust and lithospheric mantle allows magmatism regime to take place. This is caused by open path access (slab window) that was left after slab break-off which allows fertile mantle move into

depressurized zone (aesthenospheric flow) initiating partial melting and melt ponding at the base of the crust producing chemically diverse magmas (Dilek and Altunkaynak 2009). This magmatism has provided an upper age constraint on the metamorphism at Gubaoquan site. As at this stage, the undeformed and non-metamorphosed granitic vein intruded the eclogite and this study provides first age for this event, which occurred at 424 ± 8.6 Ma (as demonstrated in Figure 6.3).

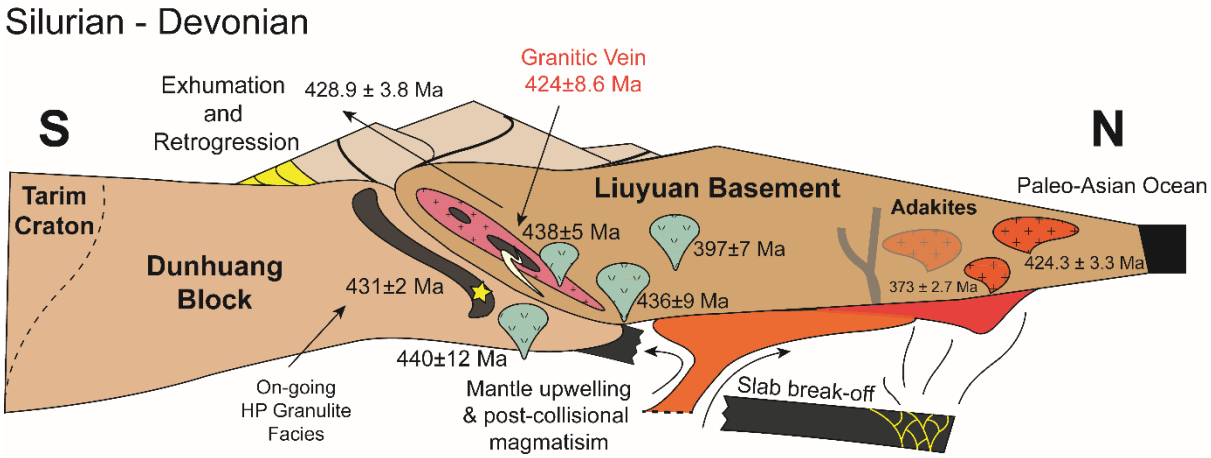

Figure 6.3 Schematic diagram showing end of metamorphism and post-collisional magmatism between the terranes. (Granitic vein age from this study; Granitoid (cyan colour) ages from Liu *et al.* (2010); Adakite ages from Mao *et al.* (2012); HP Granulite age from He *et al.* (2014)).

As presented in Chapter Four, geochemical discrimination diagrams revealed that the dated granitic vein formed in syn- to post-collisional setting, in accordance with the orogenic processes between the Dunhuang Block and Liuyuan Basement were coming to an end at this time. A granitic dyke swarm of very similar mineralogical and geochemical composition, with the same field relationships were also documented near South Central Tianshan Suture (Gao *et al.* 2011). Their presence was interpreted to be indicatory of partial melting of overthickened crust in high pressure post-collisional setting similar to the current Himalayan collision. Therefore, presence of almost identical dyke within Gubaoquan site could indicated that this collision exposed the crustal rocks to high temperature regimes at the time of convergence, resulting in intensive magmatism producing numerous granitoids that account for 30% of rocks in the Beishan Orogen (Liu *et al.* 2010).

Post Orogeny

Since cessation of orogenic processes between Dunhuang Block and Liuyuan Basement the tectonic activity was minimal until the Triassic. At deeper crustal levels ongoing magmatism

was persisting until Mesozoic. Further to the north, volcanism, plutonism and highly active tectonics were still in operation as Paleo-Asian Ocean was still open but progressing towards closure, which eventually occurred in the Late Permian-Triassic (Tian *et al.* 2014). This final closure of ocean basin and amalgamation of terranes between the Southern Mongolian Accretionary System and Tarim Craton led to formation of complete Beishan Orogen. It is expected to find some repercussions of this event in the area studied, as it is proximal.

Widespread Triassic magmatic activity and tectonic thrusting have been reported within Beishan Orogen (Zheng *et al.* 1996, Li *et al.* 2012, Tian *et al.* 2015). These are suspected to have been caused by final collisional accretion of the terranes. However, forces leading to formation of those deformations and magmatic intrusions are thought to be diverse. As areas involved in the collision will undergo compressional-type setting effects, whereas areas that are more distant such as Gubaoquan study site are expected to undergo extensional effects. Li *et al.* (2012) and Li *et al.* (2013) investigated many I-type, A-type granitoids adjacent to Dunhuang Block and Liuyuan Basement suture. Based on their geochemical signatures they concluded that magmatism must have been triggered by underplating within an extensional regime. These granitoids are associated with mafic-ultramafic dykes that are very common in this area. One of the studied intrusions, the lamprophyre dyke (14GBQ9) was examined in this research project, its U-Pb zircon dating revealed age of 232 ± 12 Ma which is interpreted as timing of crystallization, and is thought to be associated with this extensional regime described by these authors (as demonstrated in Figure 6.4). The accretion of Dunhuang Block and Liuyuan Basement led to formation of major crustal body referred to as Beishan Basement Complex, where Liuyuan Basement is its main component and Dunhuang Block is a smaller southern extension.

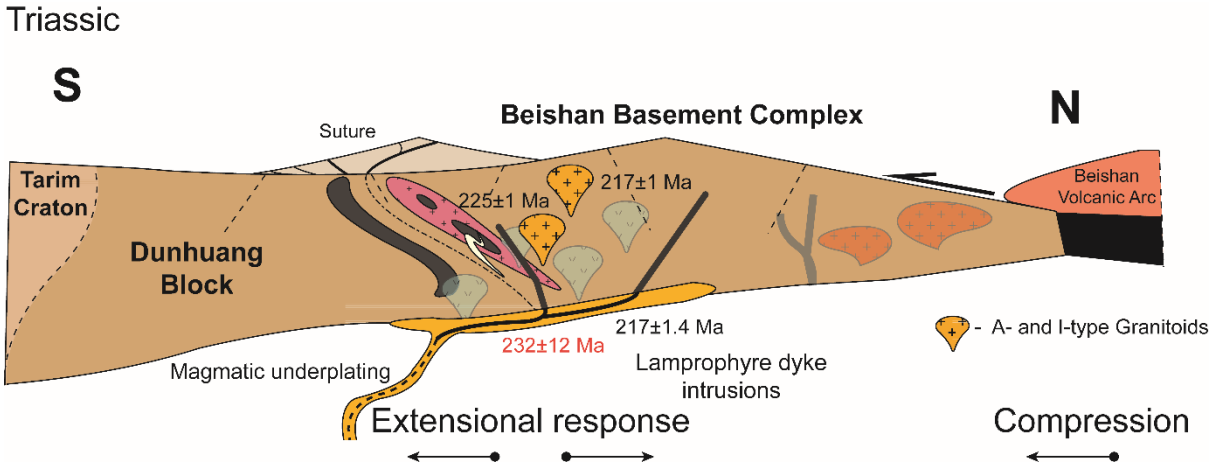

Figure 6.4 Schematic diagram rift magmatism resulting from extensional regime imposed by distant compressional force from arc obduction (discussed in section 0). (Lamprophyre age 232 Ma from this study and 217 from Mao *et al.* (2012); A- & I-type pluton ages from Li *et al.* (2012))

Summary

The constructed model is summarized alongside of geological time scale (Figure 6.5). The presented series of events associated with assembly of Beishan terranes has revealed extensive disturbance to tectonic realm in form of episodic magmatism over a long period. The short-lived Dunhuang and Liuyuan terrane collision event had a long-lived aftermath in form of emplacement of multiple intrusions. This has produced the highly diverse igneous bodies that are scattered throughout the Beishan Basement Complex.

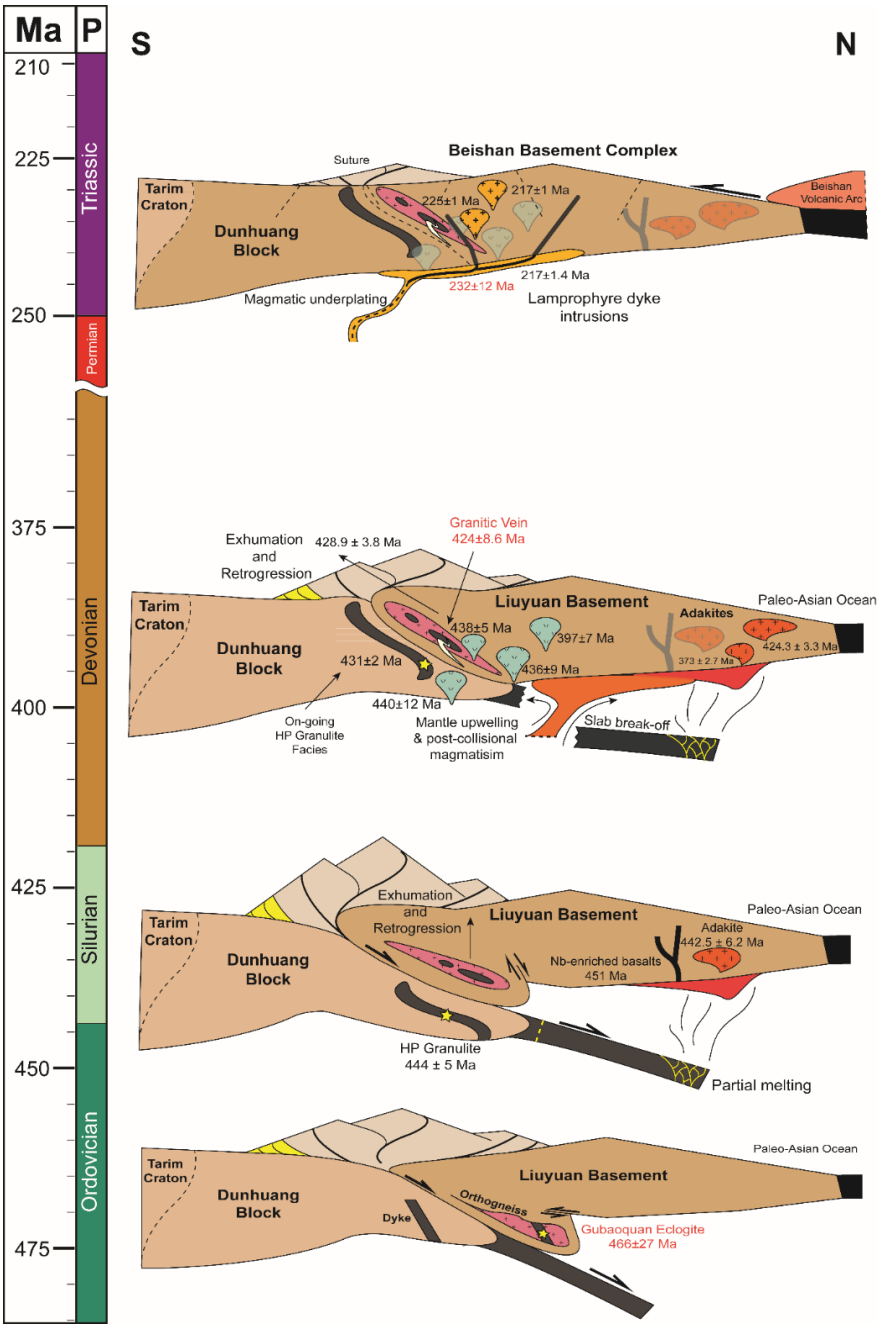

Figure 6.5 Summary of events studied in this project that are thought to occur in Beishan Orogen

6.2.3 Cenozoic Thermal Event

The U-Pb dating of eclogite sample (14GBQ1) has revealed age resetting of few zircons, as it was presented in Chapter Five and it was thought to be caused by Cenozoic Thermal Event (Nutman 2015, pers. comm., 08/07). However, there is no evidence of any magmatic or volcanic activity in this area as most orogenic and post-orogenic activities have ceased before the end of Mesozoic, therefore there must have been different external force acting upon this terrane to cause this resetting.

The only proximal tectonic activity that could correlate with this event is the India and Eurasia collision. The extrusion tectonics model proposed by Tapponnier *et al.* (1982) has shown that this collision could be responsible for formation of major central and eastern Asian faults such as active sinistral Altyn Tagh Fault, which bounds the Beishan Orogen. The Altyn Tagh Fault in near Himalayan region marks the boundary of Tibetan Plateau and it is one of the biggest faults in the world which extends for more than 600 km causing continental-scale displacements (Yin *et al.* 2002, Tian *et al.* 2015). Therefore, since it is possible for the Himalayan collision to exert strong enough forces to fracture and displace such large and distant land masses, then it can be assumed that the same compressional and frictional forces could have result in heat build-up that led to selective resetting of U-Pb zircon geochronometers in zircon domains most damaged by radioactive decay. Study conducted by Leloup *et al.* (1999) has shown that shear heating on its own can lead to temperature increase of up to 100° C at 5 km depth and 200° C at 35 km (Moho), therefore tectonic deformation could be considered a significant contributing factor. Additionally, Hoskin and Black (2000) has shown that trace element impurities within zircon crystal lattice increase zircon's susceptibility to recrystallization or resetting, lowering the temperature range for these changes to occur. Furthermore, Hoskin and Schaltegger (2003) have shown that metamict areas of zircon are very susceptible to recrystallization, which was recorded to occur at temperatures as low as 120-200° C in the presence of aqueous fluids. In such event affected zircon will lose some of the Zr, Si and all radiogenic Pb and will be heavily enriched in Ca, Al, Fe, Mn, LREE and water species. Therefore, impurities content in affected zircons should be investigated to verify if it had any contribution to creation of reset favourable regime, as combined with shear heating and local geothermal gradient there is high possibility for the causality of zircon geochronometer reset. The maximum temperature needed for this reset was constrained by $^{40}Ar/^{39}Ar$ dating of biotite in augen gneiss and was determined to be < 300° C (Qu *et al.* 2011).

Since the Beishan Orogen is bounded by two faults (the Ruoqiang-Xingxingxia Fault to the north and Altyn Tagh-Alxa Fault to the south), thus a lot of strain is acting on this terrane and therefore higher potential for heat production that could be responsible for resetting of zircon geochronometers. Furthermore, if this assumption is correct, it could be further deduced that obtained *ca.* 44 Ma, 41 Ma and 14 Ma ages could correspond to peak and high intensity strain and thermal energy build-up just prior to release in form of the major tectonic displacements.

Since zircons haven't been used for such purpose, there is no literature to support this finding. However, these events are expected to produce vast repercussions which can be used to correlate certain changes in the environments with the resets, if the chronological data is available. The study of fault activity in Annapurna region, Nepal conducted by Coleman and Hodges (1995) has shown evidence of E-W extensional regime in the Tibetan Plateau. Their $^{40}Ar/^{39}Ar$ dating of hydrothermal micas from the Thakkhola fault system gave ages of *ca.* 14 Ma. This extensional faulting was interpreted as onset of an accelerated uplift in the Tibetan Plateau. This work was further supported by Sun *et al.* (2005), as they identified significant change in sedimentation since 13.7 Ma in northern Tibetan Plateau along the Altyn Tagh Fault. At this locality mudstones were suddenly overlayed by conglomerates with addition of new sediment source. These authors concluded that this drastic change was also influenced by onset of uplift in north region of the plateau that is believed to occur significantly later than in its southern regions.

Both of these finding show evidence of increased tectonic activity in Tibetan Plateau and Altyn Tagh Fault at *ca.* 14 Ma which correlates with the youngest zircon reset. Therefore, there is a possibility that this uplift and associated extension have exerted enough of energy along the fault and onto the distant terranes to cause the reset of the zircon geochronometer. The earlier dates so far were found not to have any correlation in this region. However, as it was outlined by Yin *et al.* (2002) the activity along Altyn Tagh has commenced at *ca.* 49 Ma, therefore analyzed Middle Eocene ages could still relate to this onset tectonic activity but any obvious evidence along the fault zones have been erased by more recent reworking, as these faults are active to this date. Additionally, there is high probability that evidence for significant tectonic advancements in the Himalayan Orogen and Tibetan Plateau are more distant, as they had to develop in earlier stages of the collision. This is indicated by diachronous uplift of the plateau (Yin *et al.* 2002, Sun *et al.* 2005), so the correlating tectonic events to ages 44 Ma and 41 Ma could have occurred in the southern regions of Tibetan Plateau.

6.3 Broader Concept

Across the Beishan Orogen many arcs have been proposed, such as Shibanshan, Huaniushan, Dundunshan, Dongqiyshan and Yuanbaoshan, interlaced with microcontinent slivers such as Liuyuan and Hanshan. These arcs have been commonly referred to as the Gongpoquan Arc Accretionary System (Song *et al.* 2013a). However, they all have one common feature, their oldest recorded age is Cambrian-Ordovician and youngest from the end of Permian (Xiao *et al.* 2011, Song *et al.* 2013a, Guo *et al.* 2014). Therefore, it is acceptable to assume that the Cambrian-Ordovician age is the initiation of the arc activity and Permian to be its cessation. This however, raises a question for the probability that all the arcs in this long-lived and complex collision-accretionary system commenced and ceased their activity at the same time, especially when collision has taken form of multi-stage process (Xiao *et al.* 2011, Song *et al.* 2013a).

Present model for evolution of Beishan Orogen proposes ongoing subduction-accretion and rifting of several terranes until final agglomeration by the end of Permian (Xiao *et al.* 2011). This model infers involvement of several microcontinents separated by multiple subduction zones and associated volcanic arcs. Such concept has arisen from the abundance of ophiolites, high grade metamorphic rocks and arc-related sequences. Dissatisfaction with the proposed complexity in the model for the evolution of the Beishan Orogen has led to idea that simpler and more concise model should be developed. Based on literature review of the Beishan Orogen as well as other orogens with similar tectonic settings an alternative perspective for regional geology is proposed.

Here it is suggested that all these proposed arcs could be part of one arc system, here named Beishan Volcanic Arc. This assumption is based on common timing of initiation and cessation of volcanic activity for all these arcs as well as commonalities in their associated lithologies that have been described in detail in the literature (Xiao *et al.* 2011, Song *et al.* 2013a). This arc is interpreted to have been obducted onto the Beishan Basement Complex at the time of Paleo-Asian Ocean closure and final agglomeration of the terranes. Such occurrences have been previously documented; in Greenland, a Palaeoproterozoic magmatic arc was thrust over an Archean terrane (Nutman *et al.* 2008); The Cambrian Macquarie Arc in Eastern Australia was thrust onto passive margin of Australia in Ordovician (Aitchison and Buckman 2012); and more recently (Eocene) during closure of Tethys Sea, a classical example of obduction is Samail ophiolite, which was thrusted over the Arabian continental margin in Oman (Coleman

1981). For this obduction to occur an appropriate rock suite is required in the underlying base, commonly a carbonate-rich rock. The carbonates, evaporates or shales are soft and easily deformable rocks and they are key component in obduction events as their soft nature provides little friction and resistance in the collision what allows large rocks masses to be thrusted for substantial distances (Coleman and Lopez 1986). These rocks were shown to be present in the above mentioned Greenland, Eastern Australia and Oman settings, and are also present in abundance in the Beishan Orogen, displaying strong deformation and medium to high grade metamorphism (Xiao *et al.* 2011). After the obduction was completed it is believed that the subducting slab broke off, leading to buoyancy-driven uplift synchronous with relaxation that led to the fragmentation. This would have caused normal faulting with development of horst and graben relationships between faulted basement blocks. This brittle post-orogenic deformation is believed to main cause for fragmentation of overlying obducted Beishan Volcanic Arc. Thus it is hypothesised that this volcanic arc was dismembered into smaller components, that are divided by outcropping parts of Beishan Basement Complex as now exposed. Consequently, the current appearance would now resemble slivers of microcontinents interlaced with arcs. This is permissive of interpretation of a single dismembered arc or of many separate arc systems accreted progressively.

The following is the proposed series of events that took place during Beishan Orogen formation and is summarized in Figure 6.6:

A) After Silurian collision between Dunhuang Block and Liuyuan Basement and Closure of Liuyuan Ocean, the Beishan Basement Complex was formed. To the north was the Paleo-Asian Ocean that was subducting to the north, leading to development of the Beishan Volcanic Arc.
B) The final Beishan Orogen forming collision occurred between the Late Permian and Middle Triassic, and led to closure of the Paleo-Asian Ocean. In this event Beishan Volcanic Arc activity ceased, as it started to be obducted onto Beishan Basement Complex.
C) After the arc was obducted and subduction has ceased with slab break-off and the post-orogenic relaxation would have caused normal faulting of the terrane with basement complex block starting to uplift, dismembering overlying arc sequence.
D) Erosional activity has eroded large parts of the arc and unroofed parts of underlying basement, leaving the impression of separate microcontinents and arcs in fault contact, making it appear as multiple arcs and exotic terranes separated by sutures.

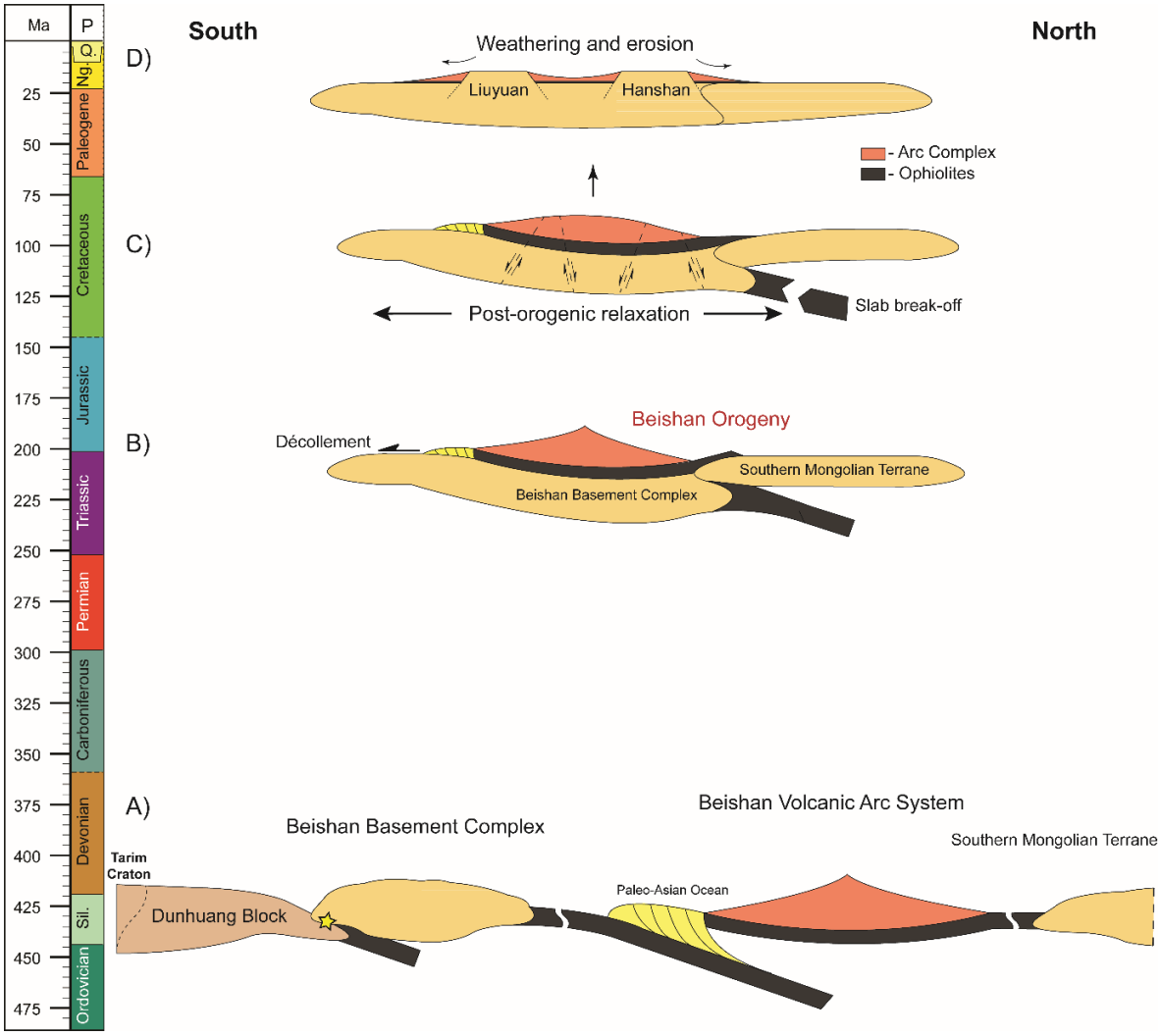

Figure 6.6 Broad scale model for the evolution of Beishan Mountain belt.

6.4 Comparisons

The comparative study that was aimed to be achieve at the final stage of this project was proven to be non-feasible due to lack of data from the Qinling Orogen, and the focus of the study was shifted towards the evolution of the Beishan Orogen. The low yield of zircons from the eclogite and lack of access to the data for the other lithologies has impeded the viable comparisons between the sites. For the same reason, appropriate discussion can't be achieved and therefore the results were discussed throughout the previous chapters and the drawn conclusions are presented in the Chapter Seven.

Chapter Seven

Conclusions and Recommendations

7.1 Beishan Orogen Conclusions

Based on the results from previous chapters, data from the literature and discussion above, the following array of conclusions can be drawn:

1) The protolith of the Gubaoquan eclogite was a mafic dyke or a sill emplaced into Precambrian crust on the basis of field relationships and its geochemical fingerprints that indicate tholeiitic signature. This was further supported by the Th/Yb-Nb/Yb diagram of Pearce (2008), which reveals some modest crustal contamination of the magma. Such trends are characteristic of magma ponding at the base of the crust followed by the crustal emplacement.
2) The U-Pb dating of zircons from rocks in Huaniushan Group at Gubaoquan site revealed high grade metamorphism in Middle Ordovician (466 ± 27 Ma) that led to formation of augen orthogneiss from host Neoproterozoic granite (920 ± 14 Ma) and eclogite from a cross cutting mafic dyke/sill. The high pressure metamorphic event was initiated by subduction-collision between Dunhuang Block and Liuyuan Basement during which part of the latter was dragged into subduction channel where eclogite facies metamorphism occurred.
3) Subsequent emplacement of Dunhuang crust into the subduction zone by slab-pull led to high pressure granulite metamorphism in the block on the other side of the suture. Low density sialic crust forced into the subduction channel forced exhumation of overlying crust, what led to synchronous prograde and extensive retrograde metamorphism in corresponding terranes during Early Silurian.
4) The end of retrogression within Liuyuan Basement was marked by post-collisional magmatic event during which numerous granitoids have been emplaced across Liuyuan and Dunhuang terranes; including granitic vein that intruded the largest boudin within eclogite belt at 424 ± 8.6 Ma.

5) The Late Permian to Late Triassic was a period of tectonic activity and magmatic reactivation within southern Beishan terranes. This time marks the closure of Paleo-Asian Ocean in northern Beishan area and its repercussions are recognised on the regional scale. The Gubaoquan area was subjected to extensional regime, what resulted in faulting and lamprophyritic as well as A- and I-type granitoid intrusions. This extensional reactivation and collision further in the north marks the end of Beishan orogenesis as well as the finalisation of Central Asian Orogenic Belt assembly.
6) Interpretation of the data from this study and from the literature, is in disagreement with model of multiple microcontinental collisions and favours long-lived arc accretionary model as favoured by Song *et al.* (2013c) with possible arc obduction (proposed in this study).
7) Subsequent episode of tectonism was introduced in this region during Cenozoic, when Indian continent collided with Eurasia leading to formation of major faults in the process of extrusion tectonics (Tapponnier *et al.* 1982). This event is recorded for the first time in the study area by resetting of the U-Pb system in metamict zircons.

7.2 Qinling Orogen Conclusions

Based on the information obtained in this study and discussions of the eclogite and paragneiss in previous chapters following conclusions can be drawn:

1) Kanfenggou eclogite yielded scarce zircons with low U content, meaning the data obtained from them did not yield precise ages. However, one of the obtained ages is in agreement with literature, and it corresponds to eclogite facies metamorphism at 490 ± 83 Ma. The petrographical examination of Kanfenggou eclogite has revealed that retrogression is minimal.
2) This remarkable preservation leads to more questions, as exhumation generally leads to severe retrogression to the peak eclogite facies mineral assemblage. Therefore its preservation is very important as it can have vast implications for the dynamics of the evolution of the Qinling orogen. This could have been achieved by remarkably fast or simply anhydrous exhumation and therefore time-independent exhumation.
3) On the bases of geochemical results and field relationships it is concluded that Kanfenggou eclogite and paragneiss represent dyke or sill intrusion and country rock

relationship, as at the Gubaoquan site. The tholeiitic fraction trend and crustal contamination effect are thought to represent mafic-ultramafic magma ponding at the bottom of the crust prior to intrusion that led to tholeiitic fractionation.

4) Petrographical examination of several eclogite and paragneiss thin sections has not revealed minerals that would provide evidence for ultra-high pressure metamorphism.

7.3 Recommendations

The eclogite studies conducted on the Gubaoquan eclogite in this project provided indicatory evidence that the protolith for this rock may have been misidentified. In order to verify the origin of the eclogite more analytical work should be performed. It is recommended to carry out more zircon analysis in attempt to find protolithic zircons, as none have been found. The Neoproterozoic zircons dated here and those studied by other workers are believed to inherited ones, as they provide ages comparable to those of a host rocks. Therefore, it is recommended to perform Laser Ablation-ICP-MS analysis for trace elements on new batch of zircons in order to find grains with mafic REE patterns, as these will correspond to protolith rock type determined here. This might be proven to be challenging as zircon yield from mafic rocks is generally low, this however could be facilitated by bulk CL imaging prior to laser ablation study. Once protolithic zircon is found, the nature of eclogite can be resolved by U-Pb dating, to provide crystallization age which will allow to correlate it with any know events (e.g. break up of Rodinia or Gondwana or oceanic crust generation *etc*.). Furthermore, the argument for continental origin of the Gubaoquan eclogite can be reinforced by Hf isotopic studies on zircons, as this data will be able to determine if a crustal component was added to the magma prior to the crystallization. This would be indicatory of continental origin as eclogite originating from the oceanic crust will not display any crustal contamination, its signature should be solely mantle derived.

Further research is recommended in regards to Cenozoic Thermal Event identified in this study, it is believed that cause for its occurrence can be solved by LA-ICP-MS analysis for trace elements and other metals outlined above. However, here proposed conjectures may not be an actual causes, therefore further research is needed. It is believed that this resetting event is important and could provide considerable implications for the evolution of the study area as well as broaden the understanding of external effects on zircons. As it was mentioned by Hoskin and Schaltegger (2003), many experimental studies have been conducted on fluid-induced recrystallization and isotopic resetting; these were considered to be important in nature

but experimentally derived results and textures were still not observed in natural environment, therefore these zircon require more study as they could provide opportunity to explore fluid induced recrystallization and isotopic resetting in collisional rocks at late stage of exhumation or during near surface processes or influences of distal tectonics on mineral modification.

At last, study of Kanfenggou eclogite could be expanded further; feasibility of this however, is dependent on zircon concentrate yields as this factor is what hampered this work. In contrast to Gubaoquan eclogite, controversy about protolith nature of the Kanfenggou eclogite has already been attempted to be subverted with continental origin. However in this study area argument for oceanic and crustal origin of the protolith is thought to be at stalemate, *ergo* further work is needed to provide more evidence for either of the hypothesis; consequently the same approach as for the Gubaoquan eclogite is recommended here.

References

Aitchison, J. C. and Buckman, S. 2012. Accordion vs. quantum tectonics: Insights into continental growth processes from the Paleozoic of eastern Gondwana. *Gondwana Research.* **22**(2), 674-680.

Aoya, M., Uehara, S.-I., Matsumoto, M., Wallis, S. R. and Enami, M. 2003. Subduction-stage pressure-temperature path of eclogite from the Sambagawa belt: Prophetic record for oceanic-ridge subduction. *Geology.* **31**(12), 1045-1048.

Batchelor, R. A. and Bowden, P. 1985. Petrogenetic interpretation of granitoid rock series using multicationic parameters. *Chemical Geology.* **48**(1), 43-55.

Black, L. P., Kamo, S. L., Allen, C. M., Aleinikoff, J. N., Davis, D. W., Korsch, R. J. and Foudoulis, C. 2003. TEMORA 1: a new zircon standard for Phanerozoic U–Pb geochronology. *Chemical Geology.* **200**(1), 155-170.

Boynton, W. V. 1984. Cosmochemistry of the rare earth elements: meteorite studies. *In. Rare earth element geochemistry.* **16:** 63-114.

Brady, J., Shiver, H., Grandy, A., Cheney, J. and Schumacher, J. (2000). Whole-rock geochemistry and metamorphism of blueschist/eclogite-facies mafic rocks on Syros, Cyclades, Greece. Geological Society of America, Abstracts with Programs.

Cao, Y., Song, S. G., Niu, Y. L., Jung, H. and Jin, Z. M. 2011. Variation of mineral composition, fabric and oxygen fugacity from massive to foliated eclogites during exhumation of subducted ocean crust in the North Qilian suture zone, NW China. *Journal of Metamorphic Geology.* **29**(7), 699-720.

Cheng, H., Zhang, C., Vervoort, J. D., Li, X., Li, Q., Wu, Y. and Zheng, S. 2012. Timing of eclogite facies metamorphism in the North Qinling by U–Pb and Lu–Hf geochronology. *Lithos.* **136-139**, 46-59.

Chopin, C. 2003. Ultrahigh-pressure metamorphism: tracing continental crust into the mantle. *Earth and Planetary Science Letters.* **212**(1-2), 1-14.

Cleven, N. R., Lin, S. and Xiao, W. 2013. The Hongliuhe fold-and-thrust belt: Evidence of terminal collision and suture-reactivation after the Early Permian in the Beishan orogenic collage, Northwest China. *Gondwana Research.* **27**(2), 796-810.

Coleman, J. and Lopez, J. 1986. Dolomite decollements-exception or rule. *Am. Assoc. Pet. Geol., Bull.;(United States).* **70**(CONF-860624-).

Coleman, M. and Hodges, K. 1995. Evidence for Tibetan plateau uplift before 14 Myr ago from a new minimum age for east-west extension. *Nature.* **374**(6517), 49-52.

Coleman, R. G. 1965. Eclogites and Eclogites: Their Differences and Similarities. *Geological Society of America bulletin.* **76**(5), 483-508.

Coleman, R. G. 1981. Tectonic setting for ophiolite obduction in Oman. *Journal of Geophysical Research: Solid Earth (1978–2012).* **86**(B4), 2497-2508.

Corfu, F., Hanchar, J. M., Hoskin, P. W. O. and Kinny, P. 2003. Atlas of zircon textures. *Reviews in mineralogy and geochemistry.* **53**, 469-500.

Dilek, Y. and Altunkaynak, Ş. 2009. Geochemical and temporal evolution of Cenozoic magmatism in western Turkey: mantle response to collision, slab break-off, and lithospheric tearing in an orogenic belt. *Geological Society, London, Special Publications.* **311**(1), 213-233.

Dong, Y., Zhang, G., Neubauer, F., Liu, X., Genser, J. and Hauzenberger, C. 2011. Tectonic evolution of the Qinling orogen, China: Review and synthesis. *Journal of Asian Earth Sciences.* **41**(3), 213-237.

Enami, M., Nishtyama, T. and Mouri, T. 2007. Laser Raman microspectrometry of metamorphic quartz: A simple method for comparison of metamorphic pressures. *AMERICAN MINERALOGIST.* **92**(8-9), 1303-1315.

Ernst, W. G. 2001. Subduction, ultrahigh-pressure metamorphism, and regurgitation of buoyant crustal slices — implications for arcs and continental growth. *Physics of the Earth and Planetary Interiors.* **127**(1–4), 253-275.

Frost, R. B. and Frost, C. D. 1987. Fluid Movements—Element Transport and the Composition of the Deep Crust. *In* D. Bridgwater. *Magmas as a source of heat and fluids in granulite facies metamorphism*, Springer Science & Business Media. **281:** 1-18.

Gao, J., Klemd, R., Qian, Q., Zhang, X., Li, J., Jiang, T. and Yang, Y. 2011. The collision between the Yili and Tarim blocks of the Southwestern Altaids: Geochemical and age constraints of a leucogranite dike crosscutting the HP–LT metamorphic belt in the Chinese Tianshan Orogen. *Tectonophysics.* **499**(1–4), 118-131.

Gill, R. 2010. Igneous rocks and processes: a practical guide. *In*, John Wiley & Sons**:** Chapter: Basalts and Related Rocks, p.44.

Gilotti, J. A., Nutman, A. P. and Brueckner, H. K. 2004. Devonian to Carboniferous collision in the Greenland Caledonides: U-Pb zircon and Sm-Nd ages of high-pressure and

ultrahigh-pressure metamorphism. *Contributions to Mineralogy & Petrology*. **148**(2), 216-235.

Googleearth (4/10/2013). Henan Province. Landsat, DataSIO, NOAA, U.S Navy, NGA, GEBCO

Googleearth (10/11/2014). Liuyuan Area, Gansu Province, DigitalGlobe; CNES/Spot Image; AutoNavi 2015

Guo, Q., Xiao, W., Hou, Q., Windley, B. F., Han, C., Tian, Z. and Song, D. 2014. Construction of Late Devonian Dundunshan arc in the Beishan orogen and its implication for tectonics of southern Central Asian Orogenic Belt. *Lithos.* **184-187**, 361-378.

He, Z., Zhang, Z., Zong, K., Xiang, H. and Klemd, R. 2014. Metamorphic P–T–t evolution of mafic HP granulites in the northeastern segment of the Tarim Craton (Dunhuang block): Evidence for early Paleozoic continental subduction. *Lithos.* **196–197**, 1-13.

Henderson, P. (1984). Rare earth element geochemistry, Amsterdam ; New York : Elsevier, 1984.

Hoskin, P. and Black, L. 2000. Metamorphic zircon formation by solid-state recrystallization of protolith igneous zircon. *Journal of metamorphic Geology.* **18**(4), 423-439.

Hoskin, P. W. O. and Schaltegger, U. 2003. The Composition of Zircon and Igneous and Metamorphic Petrogenesis. *Reviews in Mineralogy and Geochemistry.* **53**(1), 27-62.

Irvine, T. and Baragar, W. 1971. A guide to the chemical classification of the common volcanic rocks. *Canadian journal of earth sciences.* **8**(5), 523-548.

Jahn, B.-M. 1998. Geochemical and isotopic characteristics of UHP eclogites and ultramafic rocks of the Dabie orogen: implications for continental subduction and collisional tectonics. *In* B. Hacker and J. G. Liou. *When continents collide: geodynamics and geochemistry of ultrahigh-pressure rocks*, Springer**:** 203-239.

Jenkins, R. and Vries, J. L. D. (1970). Practical X-ray spectrometry, London : Macmillan, 1970. 2nd ed.

Konzett, J. and Frost, D. J. 2009. The High P–T Stability of Hydroxyl-apatite in Natural and Simplified MORB—an Experimental Study to 15 GPa with Implications for Transport and Storage of Phosphorus and Halogens in Subduction Zones. *Journal of Petrology.* **50**(11), 2043-2062.

Kretz, R. 1983. Symbols for rock-forming minerals. *The American mineralogist.* **68**(1-2), 277-279.

Le Bas, M. J., Maitre, R. W. L., Streckeisen, A., Zanettin, B. and Rocks, I. S. O. T. S. O. I. 1986. A Chemical Classification of Volcanic Rocks Based on the Total Alkali-Silica Diagram. *Journal of Petrology.* **27**(3), 745-750.

Leloup, P. H., Ricard, Y., Battaglia, J. and Lacassin, R. 1999. Shear heating in continental strike-slip shear zones: model and field examples. *Geophysical Journal International.* **136**(1), 19-40.

Li, S., Wang, T., Wilde, S. A., Tong, Y., Hong, D. and Guo, Q. 2012. Geochronology, petrogenesis and tectonic implications of Triassic granitoids from Beishan, NW China. *Lithos.* **134-135**, 123-145.

Li, S., Wilde, S. A. and Wang, T. 2013. Early Permian post-collisional high-K granitoids from Liuyuan area in southern Beishan orogen, NW China: Petrogenesis and tectonic implications. *Lithos.* **179**, 99-119.

Liu, L., Zhang, J., Green, H. W., Jin, Z. and Bozhilov, K. N. 2007. Evidence of former stishovite in metamorphosed sediments, implying subduction to> 350 km. *Earth and Planetary Science Letters.* **263**(3), 180-191.

Liu, X., Chen, B., Jahn, B.-M., Wu, G. and Liu, Y. 2010. Early Paleozoic (ca. 465 Ma) eclogites from Beishan (NW China) and their bearing on the tectonic evolution of the southern Central Asian Orogenic Belt. *Journal of Asian Earth Sciences.*

Ludwig, K. R. (2003). User's manual for Isoplot 3.00: a geochronological toolkit for Microsoft Excel, Kenneth R. Ludwig.

Mao, Q., Xiao, W., Fang, T., Wang, J., Han, C., Sun, M. and Yuan, C. 2012. Late Ordovician to early Devonian adakites and Nb-enriched basalts in the Liuyuan area, Beishan, NW China: Implications for early Paleozoic slab-melting and crustal growth in the southern Altaids. *Gondwana Research.* **22**(2), 534-553.

Mao, Q., Xiao, W., Windley, B. F., Han, C., Qu, J., Ao, S., Zhang, J. E. and Guo, Q. 2011. The Liuyuan complex in the Beishan, NW China: a Carboniferous–Permian ophiolitic fore-arc sliver in the southern Altaids. *Geological Magazine.* **149**(03), 483-506.

Mcfarlane, C. R. M. 2014. Trace element characterization of CL response in zircon by high spatial resolution LA-ICP-MS *Mineralogical Association of Canada.* **45**, 169-182.

Mei, H. 1999. The first discovery of eclogite and Palaeoproterozoic granitoids in the Beishan area, northwestern Gansu Province, China. *Chinese science bulletin.* **44**(4), 356-361.

Meng, Q.-R. and Zhang, G.-W. 1999. Timing of collision of the North and South China blocks: Controversy and reconciliation. *Geology.* **27**(2), 123-126.

Mikhno, A. O., Schmidt, U. and Korsakov, A. V. 2013. Origin of K-cymrite and kokchetavite in the polyphase mineral inclusions from Kokchetav UHP calc-silicate rocks: evidence from confocal Raman imaging. *European Journal of Mineralogy.* **25**(5), 807-816.

Mullen, E. D. 1983. MnO/TiO2/P2O5: a minor element discriminant for basaltic rocks of oceanic environments and its implications for petrogenesis. *Earth and Planetary Science Letters.* **62**(1), 53-62.

Muller, R. D., Gaina, C., Roest, W. R. and Hansen, D. L. 2001. A recipe for microcontinent formation. *GEOLOGY.* **29**(3), 203-206.

Nikitina, L. P., Korolev, N. M., Zinchenko, V. N. and Felix, J. T. 2014. Eclogites from the upper mantle beneath the Kasai Craton (Western Africa): Petrography, whole-rock geochemistry and UPb zircon age. *Precambrian Research.* **249**(0), 13-32.

Nutman, A. P., Buckman, S., Hidaka, H., Kamiichi, T., Belousova, E. and Aitchison, J. 2013. Middle Carboniferous-Early Triassic eclogite–blueschist blocks within a serpentinite mélange at Port Macquarie, eastern Australia: Implications for the evolution of Gondwana's eastern margin. *Gondwana Research.* **24**(3-4), 1038-1050.

Nutman, A. P., Kalsbeek, F. and Friend, C. R. L. 2008. The Nagssugtoqidian orogen in South-East Greenland: Evidence for Paleoproterozoic collision and plate assembly. *American Journal of Science.* **308**(4), 529-572.

O'brien, P. and Rötzler, J. 2003. High-pressure granulites: formation, recovery of peak conditions and implications for tectonics. *Journal of Metamorphic Geology.* **21**(1), 3-20.

Parkinson, C. D. and Katayama, I. 1999. Present-day ultrahigh-pressure conditions of coesite inclusions in zircon and garnet: Evidence. *Geology.* **27**(11), 979.

Pearce, J. A. 1996. A user's guide to basalt discrimination diagrams. *Trace element geochemistry of volcanic rocks: applications for massive sulphide exploration. Edited by DA Wyman. Geological Association of Canada, Short Course Notes.* **12**, 79-113.

Pearce, J. A. 2008. Geochemical fingerprinting of oceanic basalts with applications to ophiolite classification and the search for Archean oceanic crust. *Lithos.* **100**(1–4), 14-48.

Pearce, J. A., Harris, N. B. and Tindle, A. G. 1984. Trace element discrimination diagrams for the tectonic interpretation of granitic rocks. *Journal of petrology.* **25**(4), 956-983.

Pearce, T. H., Gorman, B. E. and Birkett, T. C. 1977. The relationship between major element chemistry and tectonic environment of basic and intermediate volcanic rocks. *Earth and Planetary Science Letters.* **36**(1), 121-132.

Powerman, V., Shatsillo, A., Chumakov, N., Kapitonov, I. and Hourigan, J. 2015. Interaction between the Central Asian Orogenic Belt (CAOB) and the Siberian craton as recorded by detrital zircon suites from Transbaikalia. *Precambrian Research.* **267**, 39-71.

Qu, J. F., Xiao, W. J., Windley, B. F., Han, C. M., Mao, Q. G., Ao, S. J. and Zhang, J. E. 2011. Ordovician eclogites from the Chinese Beishan: implications for the tectonic evolution of the southern Altaids. *Journal of Metamorphic Geology.* **29**(8), 803-820.

Ratschbacher, L., Hacker, B. R., Calvert, A., Webb, L. E., Grimmer, J. C., Mcwilliams, M. O., Ireland, T., Dong, S. and Hu, J. 2003. Tectonics of the Qinling (Central China): tectonostratigraphy, geochronology, and deformation history. *Tectonophysics.* **366**(1-2), 1-53.

Rollinson, H. R. (1993). Using geochemical data: evaluation, presentation, interpretation. England, Longman Scientific & Technical.

Rubatto, D. 2002. Zircon trace element geochemistry: partitioning with garnet and the link between U–Pb ages and metamorphism. *Chemical Geology.* **184**(1–2), 123-138.

Schandl, E., Gorton, M. and Wicks, F. (1990). Mineralogy and geochemistry of alkali basalts from Maud Rise, Weddell Sea, Antarctica. Proceedings of the Ocean Drilling Program, Scientific Results.

Schmidt, C. and Ziemann, M. A. 2000. In-situ Raman spectroscopy of quartz: A pressure sensor for hydrothermal diamond-anvil cell experiments at elevated temperatures. *American Mineralogist.* **85**(11-12), 1725-1734.

Schoene, B. 2014. 4.10 - U–Th–Pb Geochronology. *In* H. D. H. K. Turekian. *Treatise on Geochemistry (Second Edition)*. Oxford, Elsevier**:** 341-378.

Schreyer, W. 1988. Experimental studies on metamorphism of crustal rocks under mantle pressures. *Mineralogical magazine.* **52**(1), 1-26.

Sengor, A. M. C., Natal'in, B. A. and Burtman, V. S. 1993. Evolution of the Altaid tectonic collage and Palaeozoic crustal growth in Eurasia. *Nature.* **364**(6435), 299-307.

Sobolev, N. V., Fursenko, B. A., Goryainov, S. V., Shu, J. F., Hemley, R. J., Mao, H. K. and Boyd, F. R. 2000. Fossilized high pressure from the Earth's deep interior: The coesite-in-diamond barometer. *PROCEEDINGS OF THE NATIONAL ACADEMY OF SCIENCES OF THE UNITED STATES OF AMERICA.* **97**(22), 11875-11879.

Song, D., Xiao, W., Han, C., Li, J., Qu, J., Guo, Q., Lin, L. and Wang, Z. 2013a. Progressive accretionary tectonics of the Beishan orogenic collage, southern Altaids: Insights from zircon U–Pb and Hf isotopic data of high-grade complexes. *Precambrian Research.* **227**, 368-388.

Song, D., Xiao, W., Han, C. and Tian, Z. 2013b. Geochronological and geochemical study of gneiss–schist complexes and associated granitoids, Beishan Orogen, southern Altaids. *International Geology Review.* **55**(14), 1705-1727.

Song, D., Xiao, W., Han, C., Tian, Z. and Wang, Z. 2013c. Provenance of metasedimentary rocks from the Beishan orogenic collage, southern Altaids: Constraints from detrital zircon U–Pb and Hf isotopic data. *Gondwana Research.* **24**(3-4), 1127-1151.

Sun, J., Zhu, R. and An, Z. 2005. Tectonic uplift in the northern Tibetan Plateau since 13.7 Ma ago inferred from molasse deposits along the Altyn Tagh Fault. *Earth and Planetary Science Letters.* **235**(3-4), 641-653.

Sun, S.-S. and Mcdonough, W. 1989. Chemical and isotopic systematics of oceanic basalts: implications for mantle composition and processes. *Geological Society, London, Special Publications.* **42**(1), 313-345.

Sylvester, P. J. 1989. Post-Collisional Alkaline Granites. *The Journal of Geology.* **97**(3), 261-280.

Tang, L., Santosh, M., Dong, Y., Tsunogae, T., Zhang, S. and Cao, H. 2014. Early Paleozoic tectonic evolution of the North Qinling orogenic belt: Evidence from geochemistry, phase equilibrium modeling and geochronology of metamorphosed mafic rocks from the Songshugou ophiolite. *Gondwana Research.*

Tapponnier, P., Peltzer, G., Le Dain, A. Y., Armijo, R. and Cobbold, P. 1982. Propagating extrusion tectonics in Asia: New insights from simple experiments with plasticine. *Geology.* **10**(12), 611-616.

Tian, Z., Xiao, W., Sun, J., Windley, B. F., Glen, R., Han, C., Zhang, Z., Zhang, J. E., Wan, B., Ao, S. and Song, D. 2015. Triassic deformation of Permian Early Triassic arc-related sediments in the Beishan (NW China): Last pulse of the accretionary orogenesis in the southernmost Altaids. *Tectonophysics.*

Tian, Z., Xiao, W., Windley, B. F., Lin, L. N., Han, C., Zhang, J. E., Wan, B., Ao, S., Song, D. and Feng, J. 2014. Structure, age, and tectonic development of the Huoshishan–Niujuanzi ophiolitic mélange, Beishan, southernmost Altaids. *Gondwana Research.* **25**(2), 820-841.

University of California, R. (2014). Introduction to Energy Dispersive X-ray Spectroscopy (EDX) of bulk specimens. Concise introductory texts to the principles of electron microscopy and e-beam microanalysis. U. O. C. Central Facility for Advanced Microscopy and Microanalysis

Wang, H., Wu, Y.-B., Gao, S., Liu, X.-C., Liu, Q., Qin, Z.-W., Xie, S.-W., Zhou, L. and Yang, S.-H. 2013. Continental origin of eclogites in the North Qinling terrane and its tectonic implications. *Precambrian Research.* **230**, 13-30.

Wang, H., Wu, Y. B., Gao, S., Liu, X. C., Gong, H. J., Li, Q. L., Li, X. H. and Yuan, H. L. 2011. Eclogite origin and timings in the North Qinling terrane, and their bearing on the amalgamation of the South and North China Blocks. *Journal of Metamorphic Geology.* **29**(9), 1019-1031.

Wang, L., Kusky, T. M., Polat, A., Wang, S., Jiang, X., Zong, K., Wang, J., Deng, H. and Fu, J. 2014. Partial melting of deeply subducted eclogite from the Sulu orogen in China. *Nat Commun.* **5**, 5604.

Williams, I. S. 1998. U–Th–Pb geochronology by ion microprobe. *Reviews in Economic Geology.* **7**(1), 1-35.

Wu, Y.-B., Hanchar, J. M., Gao, S., Sylvester, P. J., Tubrett, M., Qiu, H.-N., Wijbrans, J. R., Brouwer, F. M., Yang, S.-H., Yang, Q.-J., Liu, Y.-S. and Yuan, H.-L. 2009. Age and nature of eclogites in the Huwan shear zone, and the multi-stage evolution of the Qinling-Dabie-Sulu orogen, central China. *Earth and Planetary Science Letters.* **277**(3-4), 345-354.

Xiao, W. J., Mao, Q. G., Windley, B. F., Han, C. M., Qu, J. F., Zhang, J. E., Ao, S. J., Guo, Q. Q., Cleven, N. R., Lin, S. F., Shan, Y. H. and Li, J. L. 2011. Paleozoic multiple accretionary and collisional processes of the Beishan orogenic collage. *American Journal of Science.* **310**(10), 1553-1594.

Yang, J.-S., Wu, C.-L., Chen, S.-Y. and Shi, R.-D. 2006. Neoproterozoic eclogitic metamorphic age of the Beishan eclogite of Gansu, China: Evidence from SHRIMP U-Pb isotope dating. *Geology in China.* **33**(2), 323-325.

Yang, J., Liu, F., Wu, C., Xu, Z., Shi, R., Chen, S., Deloule, E. and Wooden, J. L. 2005. Two Ultrahigh-Pressure Metamorphic Events Recognized in the Central Orogenic Belt of China: Evidence from the U-Pb Dating of Coesite-Bearing Zircons. *International Geology Review.* **47**(4), 327-343.

Yang, J., Xu, Z., Dobrzhinetskaya, L. F., Green, H. W., Pei, X., Shi, R., Wu, C., Wooden, J. L., Zhang, J., Wan, Y. and Li, H. 2003. Discovery of metamorphic diamonds in central China: an indication of a > 4000-km-long zone of deep subduction resulting from multiple continental collisions. *Terra Nova.* **15**(6), 370-379.

Yin, A., Rumelhart, P. E., Butler, R., Cowgill, E., Harrison, T. M., Foster, D. A., Ingersoll, R. V., Qing, Z., Xian-Qiang, Z., Xiao-Feng, W., Hanson, A. and Raza, A. 2002. Tectonic history of the Altyn Tagh fault system in northern Tibet inferred from Cenozoic sedimentation. *Geological Society of America Bulletin.* **114**(10), 1257-1295.

Zartman, R. E. and Doe, B. R. 1981. Plumbotectonics-the model. *Tectonophysics.* **75**(1-2), 135-162.

Zhang, L., Ellis, D. J., Arculus, R. J., Jiang, W. and Wei, C. 2003. 'Forbidden zone' subduction of sediments to 150 km depth— the reaction of dolomite to magnesite + aragonite in

the UHPM metapelites from western Tianshan, China. *Journal of Metamorphic Geology*. **21**(6), 523-529.

Zheng, Y., Zhang, Q., Wang, Y., Liu, R., Wang, S. G., Zuo, G., Wang, S. Z., Lkaasuren, B., Badarch, G. and Badamgarav, Z. 1996. Great Jurassic thrust sheets in Beishan (North Mountains) - Gobi areas of China and southern Mongolia. *Journal of Structural Geology*. **18**(9), 1111-1126.

Zong, K. Q., Zhang, Z. M., He, Z. Y., Hu, Z. C., Santosh, M., Liu, Y. S. and Wang, W. 2012. Early Palaeozoic high-pressure granulites from the Dunhuang block, northeastern Tarim Craton: constraints on continental collision in the southern Central Asian Orogenic Belt. *Journal of Metamorphic Geology*. **30**(8), 753-768.

Appendix A – Field Notes

Date: 14/04/2015

Nán Taí – Mo-Deposit

Coordinates: 33°55’15”N 110°03’16”E

Lithologies: Aplite, chert, limestone, shale, lamprophyre and phyllite

Minerals: molybdenite, magnetite, chalcopyrite, pyrite

Notes:

- Aplite (fine grain granite) has extensive quartz veining at 85°
- Mo found in veins most likely crystallized in late stage during fluid exsolving, Mo & other sulphides are also present in aplite mass, not only in veins
- Additionally to aplite mineralization also occurs in limestone (molybdenite, chalcopyrite, pyrite and magnetite)
- “Marbleized limestone” has contorted shale lenses, deformed by calcite crystal growth

Date: 15/04/2015

Kanfenggou Village – Eclogite locality

Coordinates: 33°50’02”N 110°51’27”E

Lithologies: eclogite, paragneiss, amphibolite, metasandstone, slate, diorite (deformed)

Minerals: garnets, omphacite, malachite

Notes:

- Eclogite block is ~7m in length and is hosted in paragneiss
- Eclogite’s exposed surface has malachite staining on it
- There are quartz veins present in the eclogite block
- Paragneiss displays compositional changes throughout, it is strongly deformed
- Metasedimentary rocks are part of the same sequence

Cross-section of the outcrop:

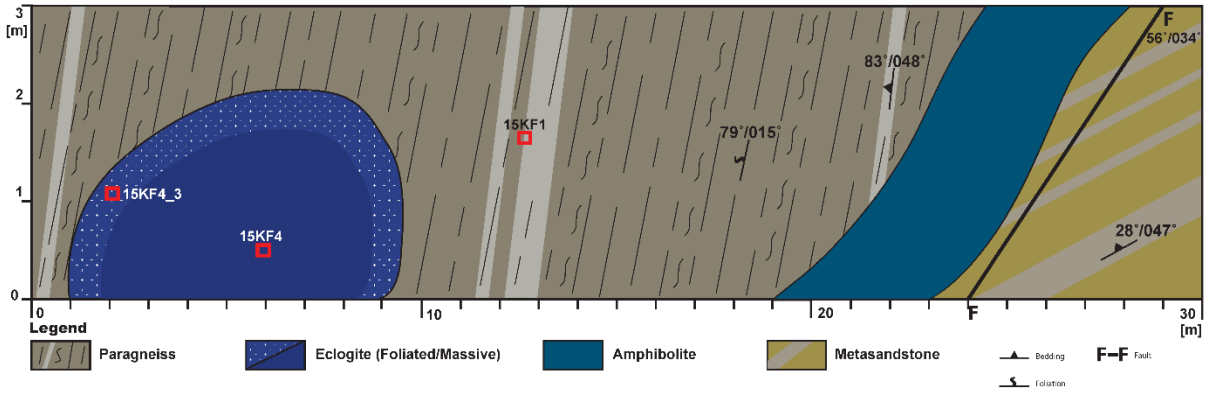

Date: 16/04/2015

Xiajiadian Mine – Au & V

Coordinates: 33°50’02”N 110°51’27”E

Lithologies: dolomite (Proterozoic & Cambrian), conglomerate, chert, shale

Metals mined: Au & V

Notes:

- Grades: Au: ~6g/t & V: ~0.97%
- Gold not visible, mainly mineralized along faults, shears and unconformities
- Hosting country rock: dolomite, conglomerate, cherts (black and red)
- Vanadium is hosted in shale with low grade but still gives strong metallic lustre, mineralization is concentrated along contact with Proterozoic dolomite
- Richest gold mineralization occurs along contact zone between Proterozoic and Cambrian dolomites
- Ore body is strongly silicified and fractured (crumbly)

Date: 16/04/2015

Liujiaxia Mine – Au

Coordinates: 33°50’02”N 110°51’27”E

Lithologies: phyllite, conglomerate,

Metals mined: Au

Notes:

- Average grade: 5-6 g/t, but highest recorded ~13g/t
- Proterozoic basement unconformably overlayed by Cambrian to Silurian sedimentary sequence. Dominant rock type is conglomerate, its clasts are also sedimentary in origin, and these rocks are interpreted to come from exposed accretionary prism that eroded into the fore-arc basin. Whole sequence is truncated by NE-SW steeply (85°-90°) dipping fault.
- Mineralization is concentrated along the fault within Early Devonian part of the sequence
- Mineralization is extremely fine and cannot be seen, it is thought to be hosted within pyrite which is very fine itself.
- Sequence is strongly silicified
- Along the road away from the mine shaft rock sequence consists of Proterozoic basalts interpreted to be ocean floor that is followed by massive sandstone with occasional shale layers interpreted as turbidite sequence overlying the ocean floor.

Liujiaxia Mine

- Gold mine, ave grade ~ 5-6 g/t but higest recorded ~ 13g/t

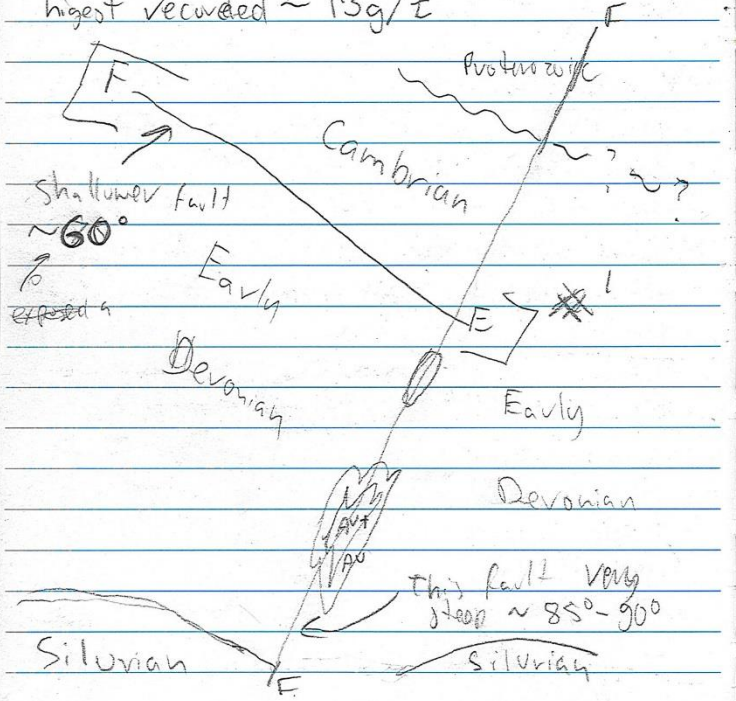

Lithologies present: phyllite (near entrance), conglomerate (probably from fore arc setting)

- Rocks present in this complex represent accretionary prism that was exposed above the surface and eroded into the fore arc basin
- Mineralisation not visible, but heavily saturated with quartz (from fluids)
- Gold most likely to be within sulphides such as pyrite, but pyrite is very fine

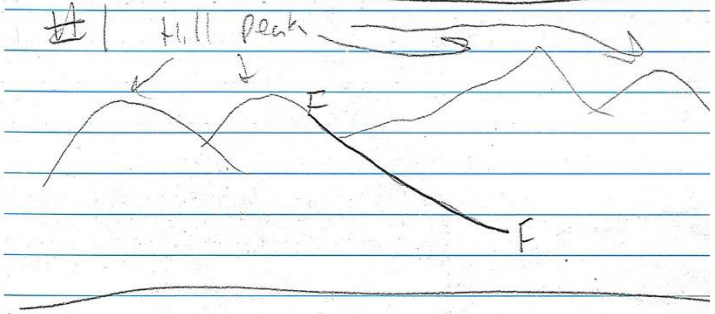

- Conglomerate clasts (mainly sedimentary rock) soaked up silicic fluids, very hard (silicified)

Date: 17/04/2015

Longtougou Mine – Au & W

Coordinates: (underground)

Lithologies: marls, siltstone, sandstone & conglomerate

Metals mined: Au & W

Notes:

- Average Au grade: ~4 g/t
- Tectonic setting: Accretionary complex and Fore-Arc
- Accretionary complex deformed to anticline, where fold axis is strongly faulted with E-W orientation with dip to the N
- 8 gold deposits developed along these faults. Mineralization hosted in quartz veins in pyrite crystals. Mineralization is syntectonic.
- Tungsten has developed din low temperature setting, what is unusual for this metal ast it usually develops in high temperatures; in this deposit it is associated with marls (carbonates) might have had some influence?!
- Veins are a main type of mineralization, they are often zoned. Country rock adjacent margin has concentrated pyrite whereas inner section of the veins constitutes of barite.

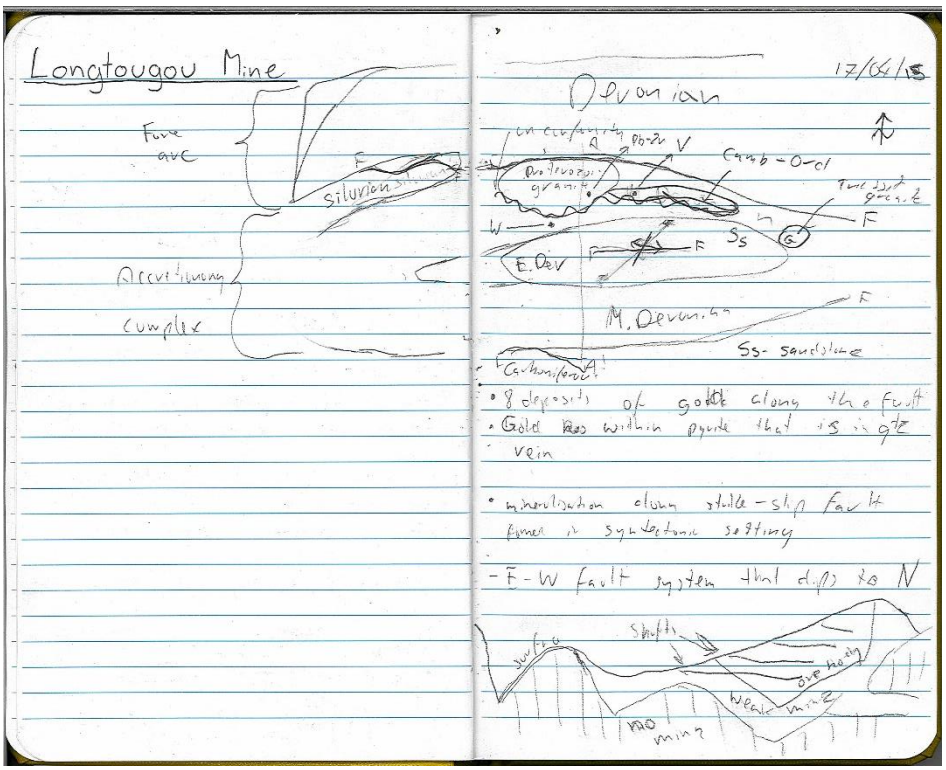

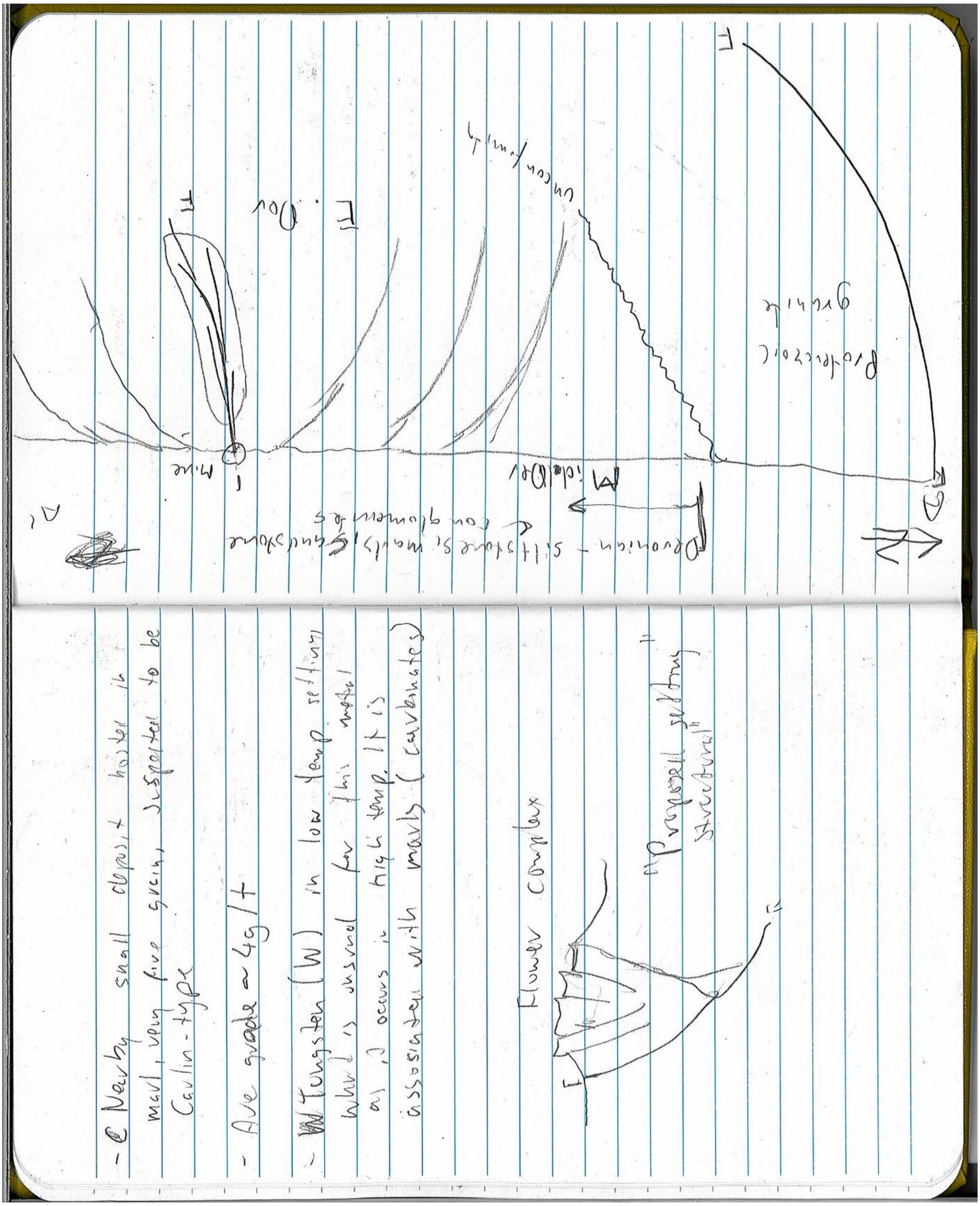
Devonian - siltstones, marls, sandstone & conglomerates
Proterozoic granite
unconformity
Mine
Nearby small deposit hosted in marl, very fine grain, suspected to be Carlin-type
Ave grade ~ 4g/t
Tungsten (W) in low temp setting which is unusual for this metal as it occurs in high temp. It is associated with marls (carbonates)
Flower complex

Date: 18/04/2015

Road Exposures near Xiaoshimen

Coordinates: 32°42’24”N 110°32’43”E

Lithologies: conglomerates, phyllite, chert, granite, basalt dyke, siltstone

Notes:

- First rock type found is conglomerate, its clasts consist of slate, phyllite and granite, probably sourced from Proterozoic core complex (granite). It is massive, as no bedding has been observed; clasts are suspended in fine quartz matrix and are well-rounded but it is not river conglomerate, it could be mass flow deposit.
- Next unit is muddy matrix conglomerate that has smaller gneiss and sandstone derived clasts, what implies different source area. This conglomerate is overlain by phyllite which has be Ar-Ar dated to 220 Ma, however this date is not accepted by local community.
- Phyllite has been intruded by granitic body that was further intruded by basaltic dyke
- This road side sequence exposure is approximately 1km in length
- **Collected samples:**
- MD01 – mafic rock with garnet (amphibolite-dyke) (32°42.858’N 110°34.655’E)
- MD02 – another mafic rock with garnet (32°43.304’N 110°35.015’E)

18/04/15

- Road exposure of mass flow deposit
- Clasts include: slate, phyllite, granites

Location: 32° 42' 24"N 110° 32' 43" E

- Conglomerate, highly deformed
- Probably source from Proterozoic core complex (granite)

- Conglomerate body is massive, no bedding observed. Clasts are suspended in fine grain rich matrix, and are well rounded. But it is not river conglomerate.

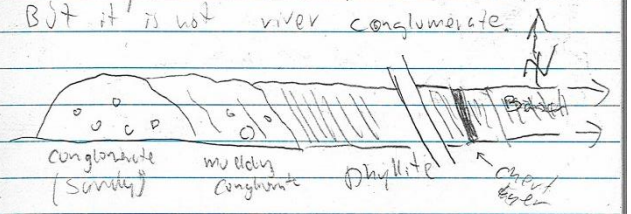

- Ar-Ar dating of phyllite revealed 220 Ma, which is not accepted by local community.

Clasts are: gneiss, sandstone.

- Second conglomerate body has smaller clasts from different source

- Basalt intrusive body

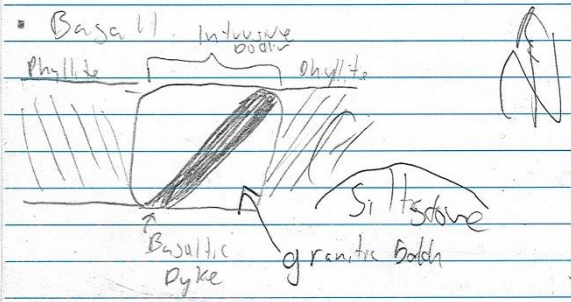

Lengthof cross-section ~ 1km

Mafic rock sample with garnet taken from:

32° 42.859' E Mafic Dyke =
110° 34.655' = MD01

Date: 19/04/2015

Road Exposures starting near Wo Long Gong

Coordinates: 30°34’24”N 110°44’29”E

Lithologies: sandstone, basalt dyke

Notes:

- Dyke was very thick and basaltic in composition
- Observed minerals: quartz, garnet, pyrite
- It contained granitic veins (veinlets) that were composed of quartz and feldspar implying partial melting at amphibolite facies. Most likely caused by decompression and was synchronous with shearing deformation as veins are aligned in one direction and usually infill fractures or tension gashes
- Dyke was dated at 220-250 Ma
- Next stop was at multiple thrust system where strong deformation was observed adjacent to the thrust fault and was becoming weaker inwards into the block.

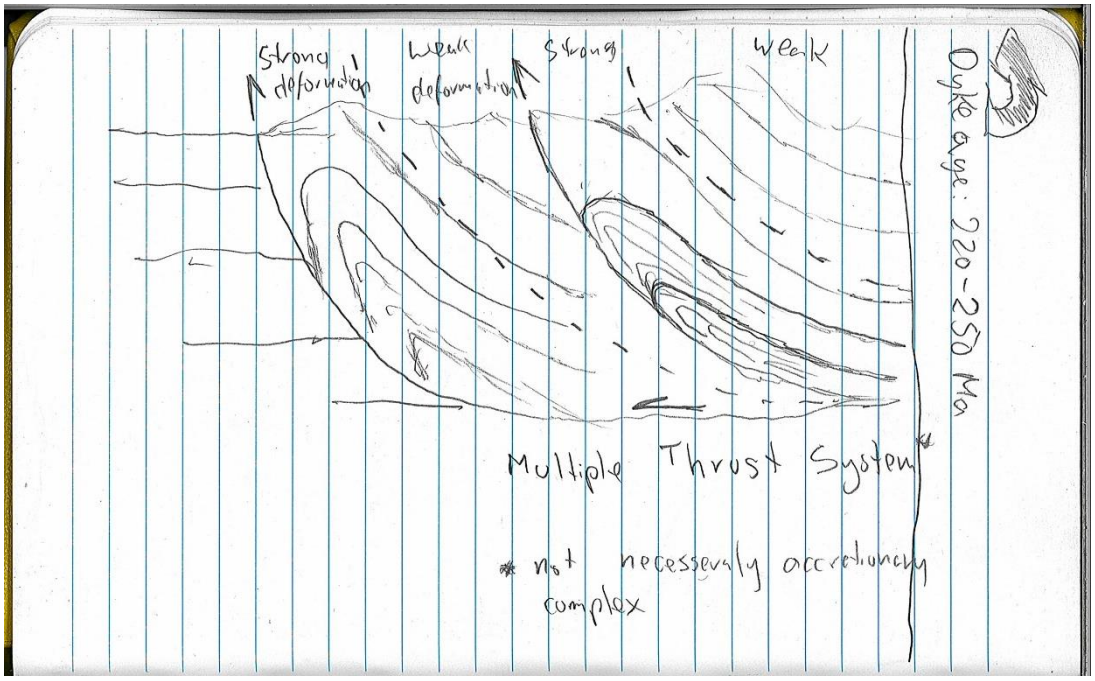

Date: 20/04/2015

Zhushan Melange

Coordinates: 32°08’09”N 110°08’02”E

Lithologies: shale, marl, limestone, chert

Notes:

- Limestone block has been seen in shale
- This wasn’t actual melange, most likely it was a sequence of shale and marl layers that has been dismembered during deformation
- Shale represents deep water succession, probably upper part of Bouma sequence as cross-bedding has been observed.
- Volcanic rocks in the area gave age of 260 Ma
- Further down the exposure black chert beds have been seen with ‘en echelon’ veins
- These beds have been deformed to almost isoclinal fold

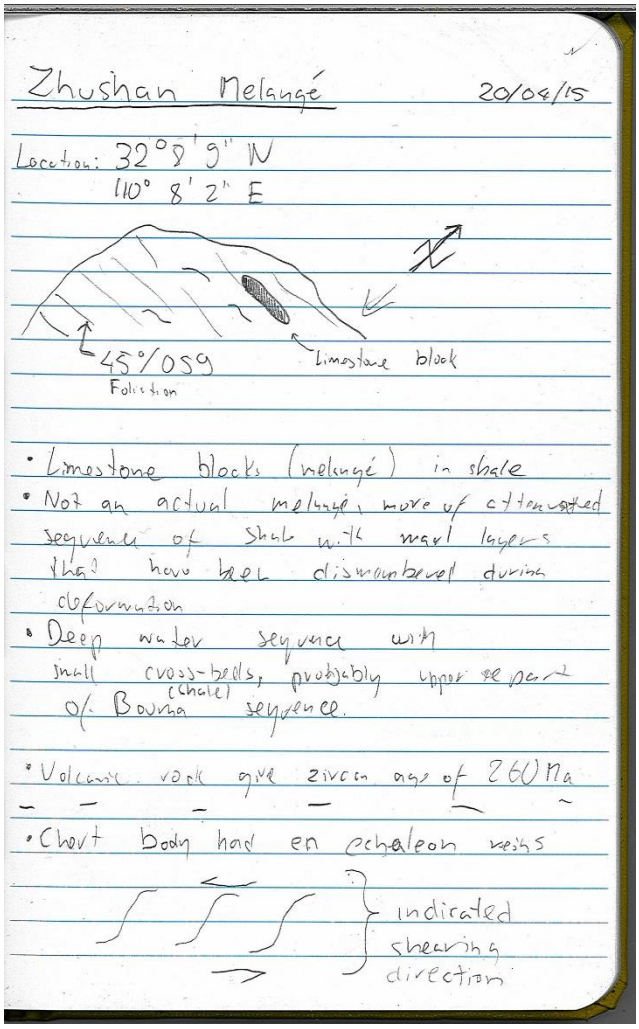

Date: 21/04/2015

Miaoya Deposit

Coordinates: 32°29’31”N 109°52’18”E

Lithologies: Carbonatite

Metals mined: Rare Earth Elements (REE)

Notes:

- REE hosted in alkaline carbonatite veins
- They have been dated at ~230 Ma
- The carbonatite veins might have formed during Triassic volcanism when magma intruded through limestones incorporating or melting them. Alternatively might be related to subduction of limestones that were observed in abundance in previous days

Date: 22/04/2015

Damogou Deposit

Coordinates: 32°14’05”N 109°30’17”E

Lithologies: Alkaline basalt, phyllite

Metals commodities: Zn & F

Notes:

- Fluorite and Zn mine
- Minerals hosted in phyllite that has been intruded by alkaline basalt as a sill and was dated at 250 Ma
- Mineralization fluids intruded the rocks at ~220 Ma and brought up sulphides, fluorite and barite
- Phyllite has been dated at Ordovician-Silurian from fossils

Date: 24/04/2015

Road Outcrops near Bajiao (8 Bananas)

Coordinates: 32°27’33”N 108°26’44”E

Lithologies: diorite, sedimentary rocks

Notes:

- Diorite body present at given location, its zircons have been dated at 440 Ma, what is oldest age in detrital zircons in sedimentray rocks in this region. This suggests that this diorite was a main source area for the sedimentary rocks further away.
- Diorite body was interpreted as part of island arc that was eroding into the fore-arc

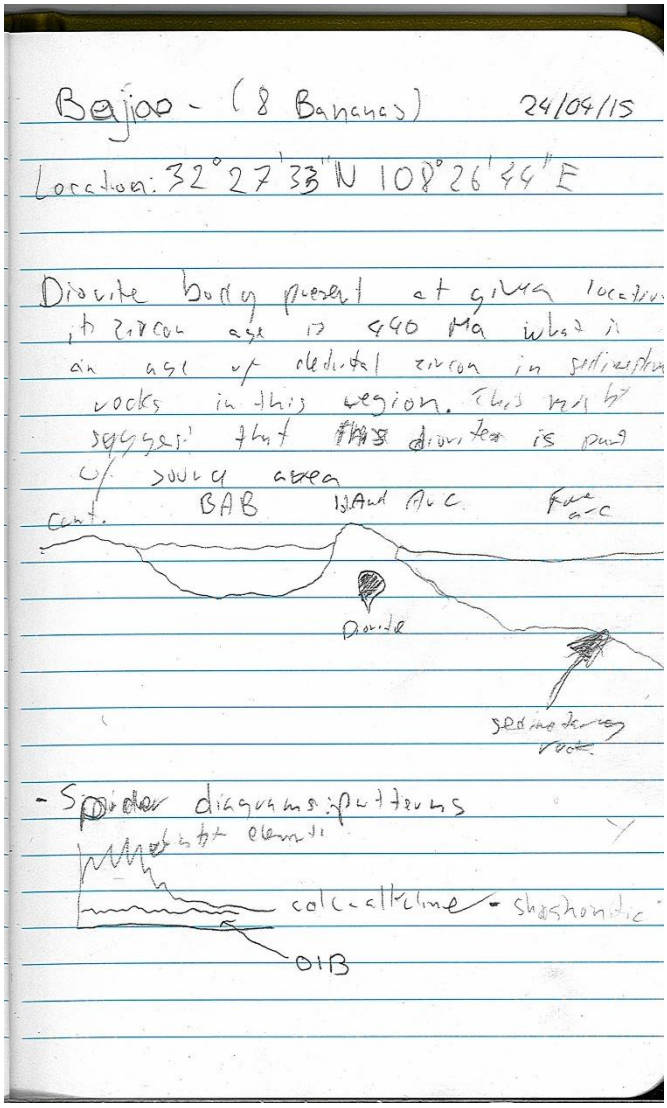

Date: 25/04/2015

Outcrops near Wu Li Town

Coordinates: 32°45’52”N 108°55’25”E

Lithologies: schist, sandstone, chert

Notes:

- Schist and chert contact could be a fault or unconformity
- Schist was originally thought to be Neoproterozoic but some pollen fossils were found that indicate Permian age
- Schist has volcanic protolith
- Schist strongly deformed, but not chert as it is rigid

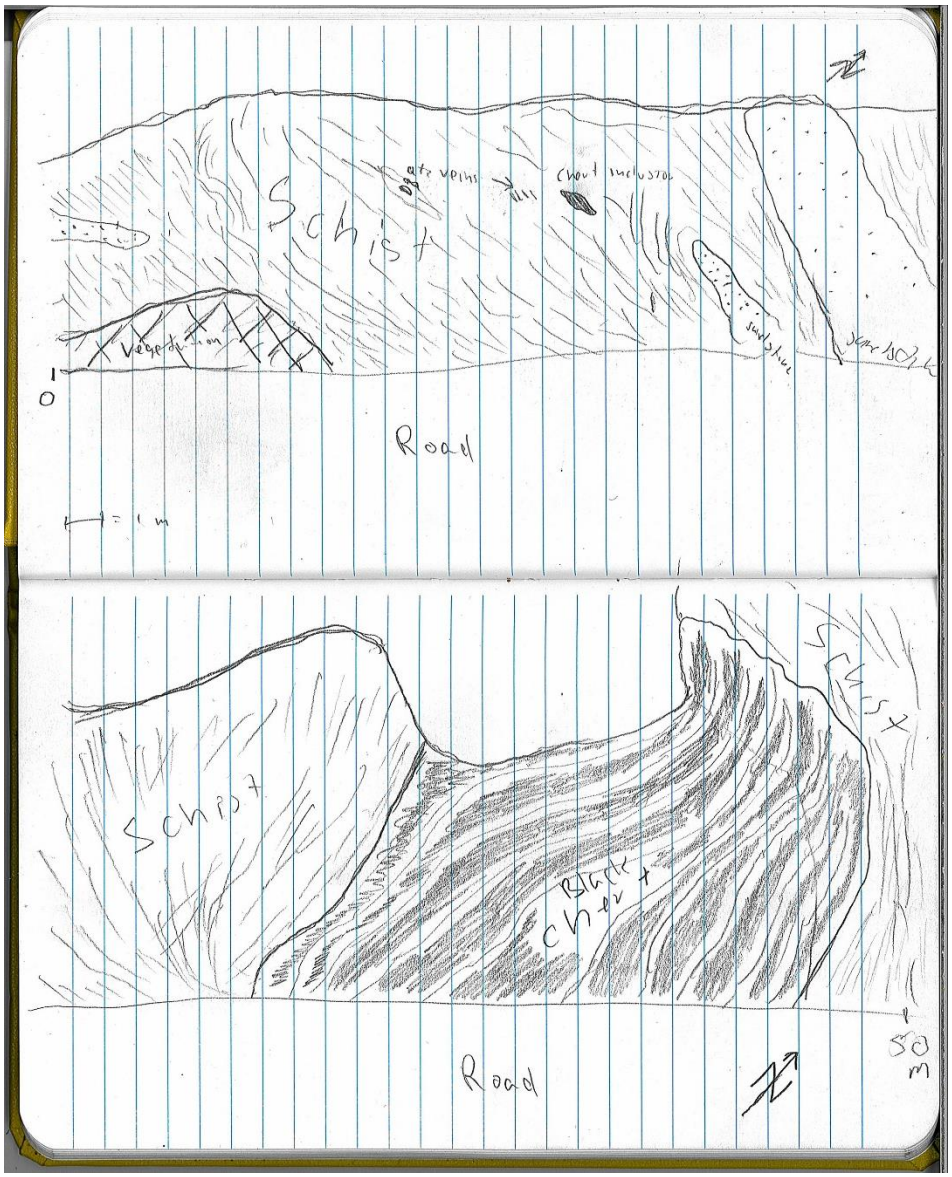

Appendix B – Hand Specimen Descriptions

Qinling – Kanfenggou Site in Shaanxi Province

Sample: 15KF4_1 Eclogite

Source: Outcrop

Location: 33° 50' 2"N 110° 51' 27"E

Mineralogy and Description

Sample has porphyropblastic texture of garnet that is abundant and mainly appears in clusters scattered throughout the sample. Pyroxenes are fine grain and make up the groundmass. The another highly visible mineral within the sample is phengite (white mica) that exists as small lenses or thin discontinues layers that define degree of deformation through amount of foliation developed within the rock. Some garnet clusters are surrounded by thin rim or “tail” following the direction of strain that is composed of amphiboles and plagioclase what indicates breakdown of HP minerals during retrogression event. The quartz mainly appears as thin veins cutting through the sample indicating that later stage event took place, and it is not part of equilibrated mineral assemblage.

Sample: 15KF4_2 Eclogite

Source: Outcrop

Location: 33° 50' 2"N 110° 51' 27"E

Mineralogy and Description

This sample exhibits exactly the same mineral assemblage as sample 15KF4_1. However quartz veining is not present but quartz crystals are still visible, especially among garnet clusters. It also very well displays retrogression rims around larger garnet porphyroblasts.

Sample: 15KF4_3 Eclogite with quartz vein

Source: Outcrop

Location: 33° 50' 2"N 110° 51' 27"E

Mineralogy and Description

This sample displays the same mineral assemblage as the previous ones but it is of a finer grain texture and displays stronger deformation. The garnet grains are the largest and most pronounced along the contact with the quartz vein. This sample is of a particular importance as it is a small fragment of larger rock collected for zircon extraction. Therefore two populations of zircons can be expected, one from eclogite itself and other from intruding vein that may not be very well related to the eclogite.

Sample: 15KF4_4 Eclogite pebble

Source: Pebble

Location: 33° 50' 2"N 110° 51' 27"E

Mineralogy and Description

This sample has the same mineralogical assemblage as all eclogite samples collected, it displays close to granoblastic texture with garnets approaching porphyroblastic margin; the foliation is clearly visible in cross-section. Sample was collected from the local river during the search for the *in situ* samples from the outcrop

Sample: 15KF4_5 Eclogite fragment

Source: Outcrop

Location: 33° 50' 2"N 110° 51' 27"E

Mineralogy and Description

The mineral assemblage remains the same, but more strain on minerals is visible as all grains are elongated in direction of strain. The garnet clusters or larger porphyroblasts seem to be disseminated or parted by their retrogression products.

Sample: 15KF1 Gneiss

Source: Outcrop

Location: 33° 50' 2"N 110° 51' 27"E

Mineralogy and Description

This sample was taken from the host rock of eclogite body. It generally has granoblastic texture with two observable minerals being quartz and biotite. This gneiss/gneissic schist has sedimentary protolith within which sandy layers persisted during metamorphism forming harder less ductile bands as shown in the picture, where cavities were formed as strain was applied to the rock. Whereas clay-rich layers formed mica-rich layers that are more ductile and therefore display more deformation. This sample shows well defined foliation as well as secondary source of strain causing crenulation, which forms wavy pattern that can be seen.

Qinling – Road-cuttings outcrops in North Western Hubei Province

Sample: MD01 Metamorphosed Dyke

Source: Road cutting outcrop near Gongjiayuan

Location: 32° 42' 51.48"N 110° 34' 39.36"E

Mineralogy and Description

The field context of the rock from which this sample was collected indicates intrusive dyke relationship, as it was cutting across highly deformed phyllite. The sample has porphyroblastic texture of euhedral garnet crystals. The groundmass is hard to define as it is very fine, but general green colouration of the rock with fine white crystals suggests presence of plagioclase and chlorite and/or epidote. Such mineral assemblage suggest that this may have been mafic dyke that was subjected to amphibolite facies metamorphism and then underwent retrogression or alteration event.

Sample: MD02 Metamorphosed Dyke

Source: Road cutting outcrop near Zhuang Wuyuan

Location: 32° 43' 18.228"N 110° 35' 0.96"E

Mineralogy and Description

This sample similarly to MD01 is also a metamorphosed dyke, it also displays overall green colouration and fine plagioclase crystals within groundmass. This sample generally has very fine texture with occasional garnet porphyroblasts. Its porphyroblastic texture it is not well define as garnet porphyroblasts are smaller and not as abundant as in previous sample. This sample also has rust filled cubic pits what may suggest that pyrite crystals are present within the sample.

Appendix C
EDS Spectra

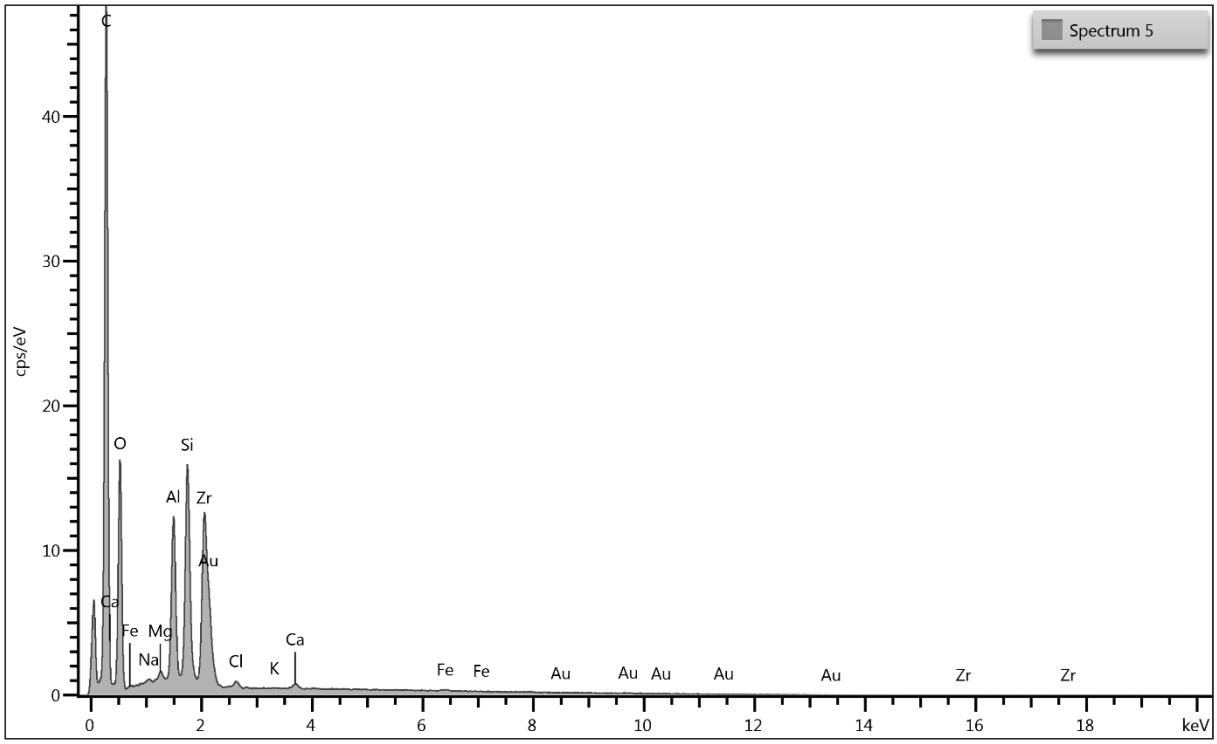
Spectrum 5
cps/eV
keV
C
O
Si
Al
Zr
Au
Ca
Fe
Mg
Na
Cl
K
Fe
Fe
Au
Au
Au
Au
Au
Zr
Zr

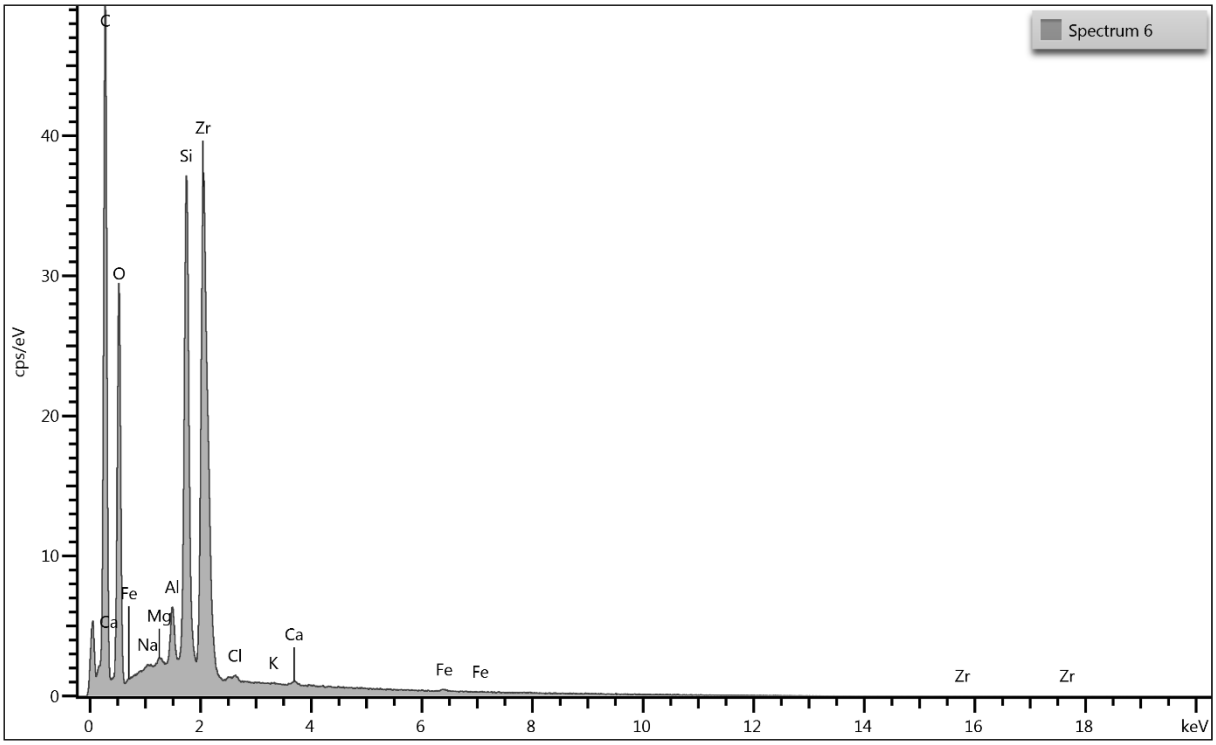
Spectrum 6
cps/eV
keV
C
Zr
Si
O
Fe
Al
Ca
Mg
Na
Cl
K
Ca
Fe
Fe
Zr
Zr

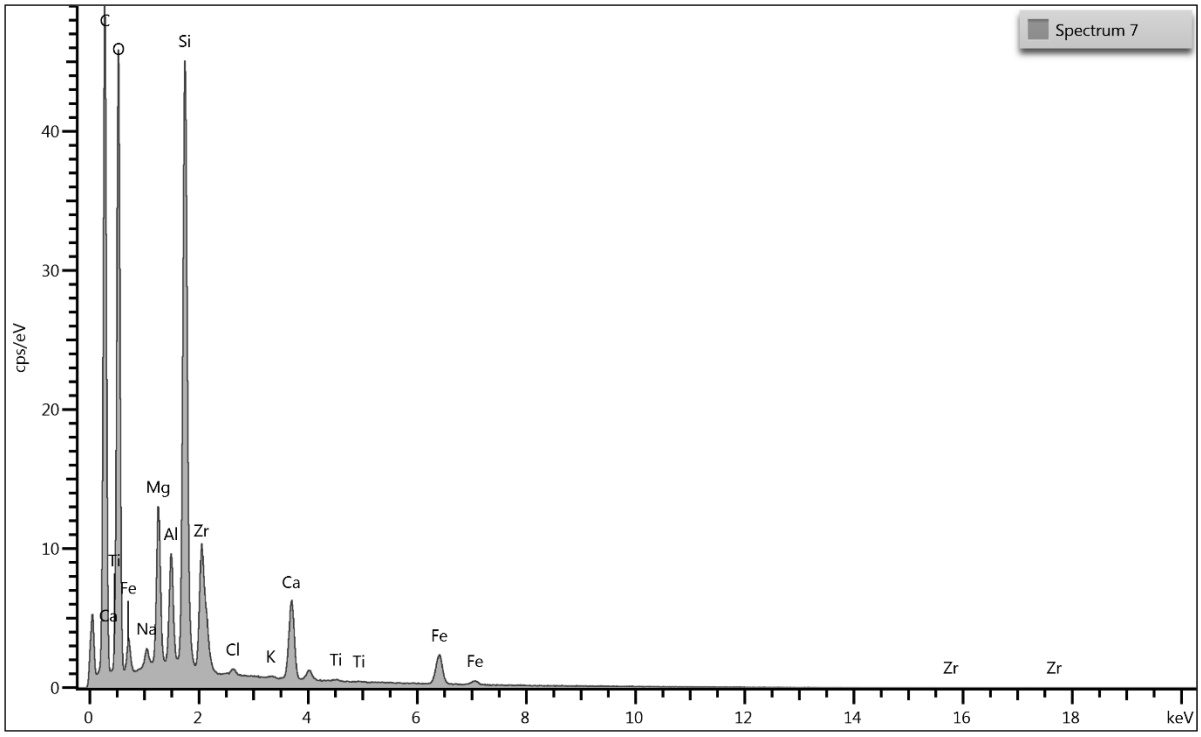
Spectrum 7
C
O
Si
Mg
Al
Zr
Ti
Fe
Ca
Na
Cl
K
Ti
Ti
Fe
Fe
Zr
Zr
cps/eV
keV

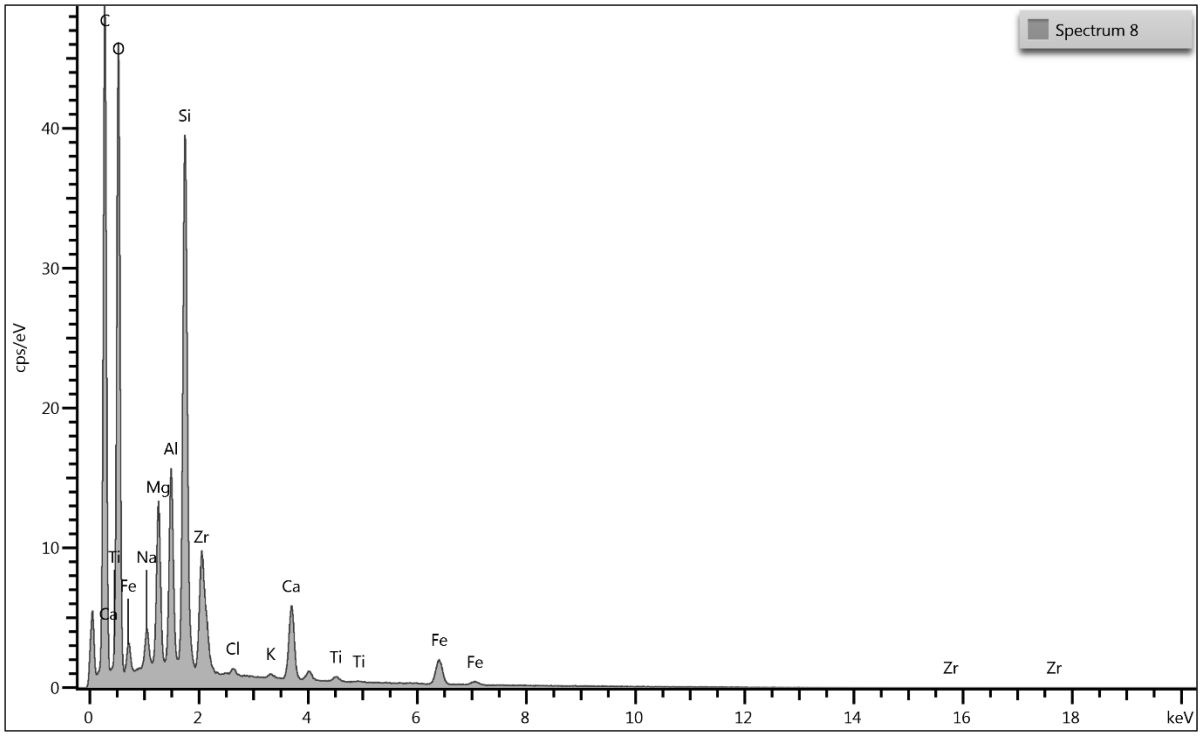
Spectrum 8
C
O
Si
Al
Mg
Zr
Ti
Na
Fe
Ca
Cl
K
Ti
Ti
Fe
Fe
Zr
Zr
cps/eV
keV

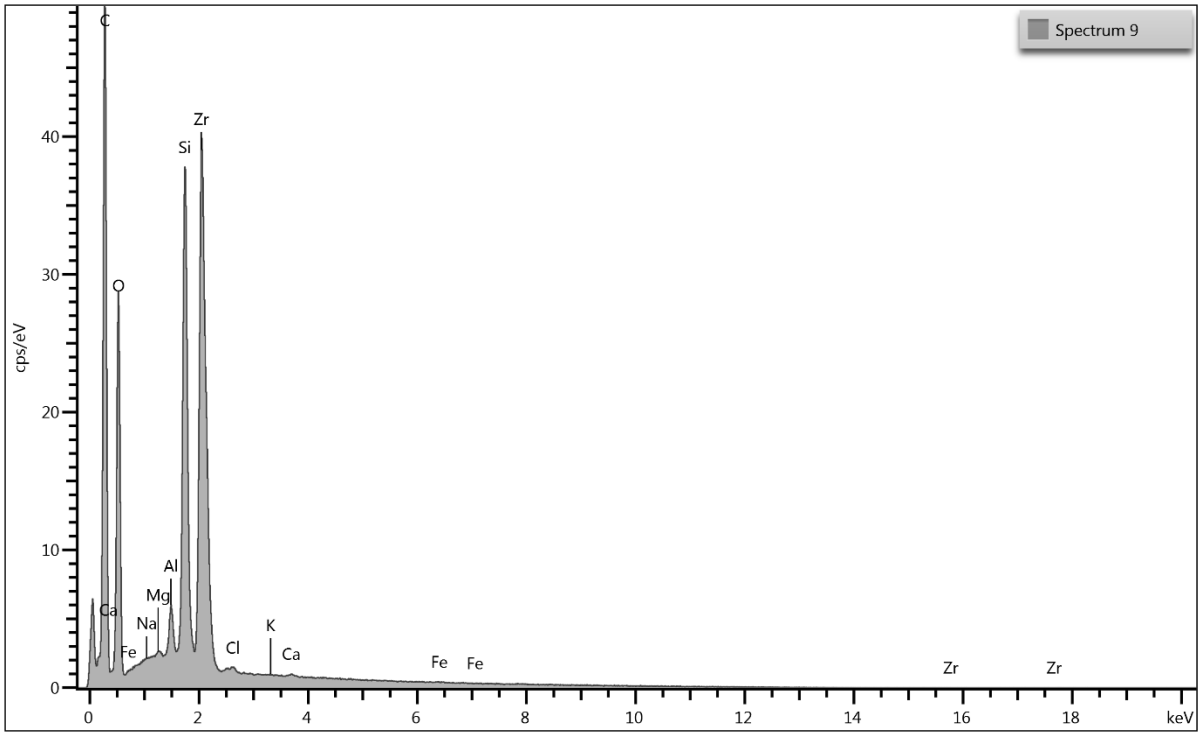
Spectrum 9
C
O
Zr
Si
Al
Mg
Ca
Na
Fe
Cl
K
Ca
Fe
Fe
Zr
Zr
cps/eV
0
10
20
30
40
0
2
4
6
8
10
12
14
16
18
keV

Result Type	Weight %

Spectrum Label	Spectrum 5	Spectrum 9	Spectrum 8	Spectrum 7	Spectrum 6
C	23.87	21.89	21.64	21.65	21.93
O	68.35	65.30	66.10	66.11	65.41
Na	0.04	0.00	0.36	0.16	0.03
Mg	0.07	0.03	1.25	1.21	0.05
Al	1.37	0.32	1.42	0.79	0.37
Si	1.74	2.96	3.83	4.32	2.99
Cl	0.08	0.05	0.06	0.06	0.05
K	0.00	0.00	0.05	0.03	0.00
Ca	0.09	0.03	1.21	1.30	0.06
Ti			0.12	0.04	
Fe	0.09	0.00	1.51	1.79	0.10
Zr	4.00	9.42	2.44	2.54	9.03
Au	0.29				
Total	100.00	100.00	100.00	100.00	100.00

Statistics	C	O	Na	Mg	Al	Si	Cl	K	Ca	Ti	Fe	Zr	Au
Max	23.87	68.35	0.36	1.25	1.42	4.32	0.08	0.05	1.30	0.12	1.79	9.42	0.29
Min	21.64	65.30	0.00	0.03	0.32	1.74	0.05	0.00	0.03	0.04	0.00	2.44	0.29
Average	22.20	66.25	0.12	0.52	0.85	3.17	0.06	0.02	0.54		0.70	5.49	
Standard Dev.	0.94	1.23	0.15	0.65	0.53	0.98	0.01	0.02	0.66		0.88	3.47	

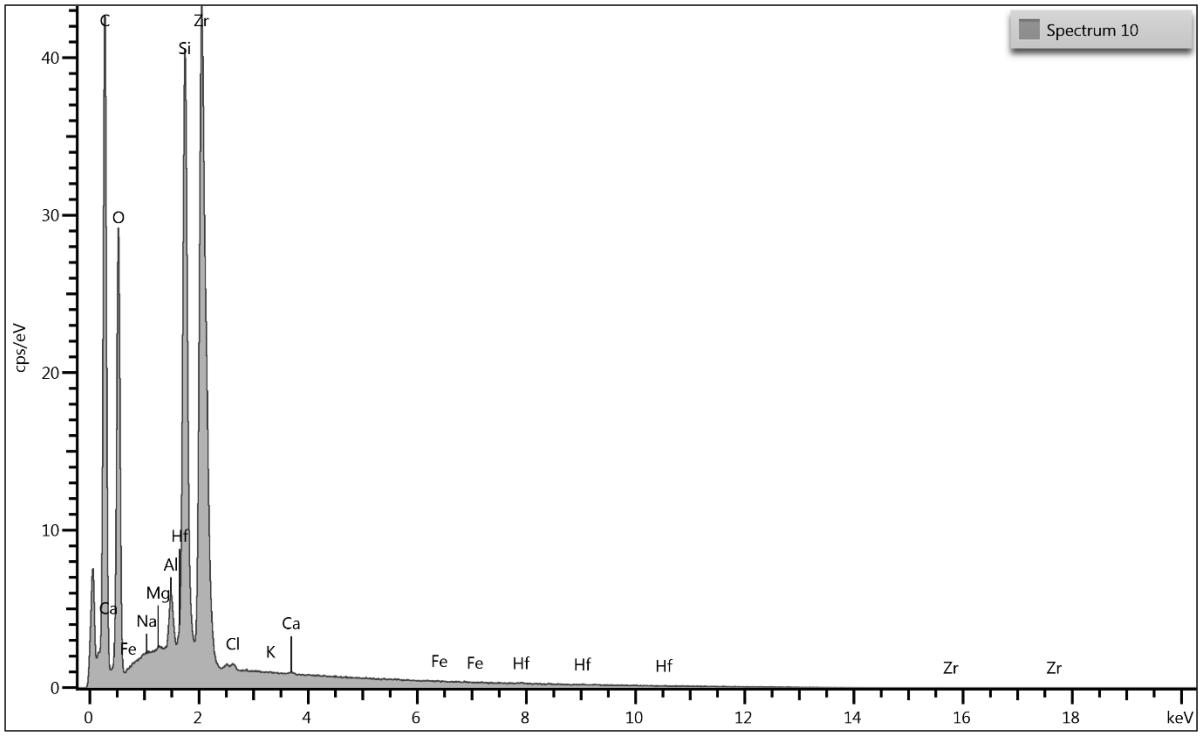
Spectrum 10
cps/eV
keV
C
Zr
Si
O
Hf
Al
Mg
Ca
Na
Fe
Cl
K
Ca
Fe
Fe
Hf
Hf
Hf
Zr
Zr

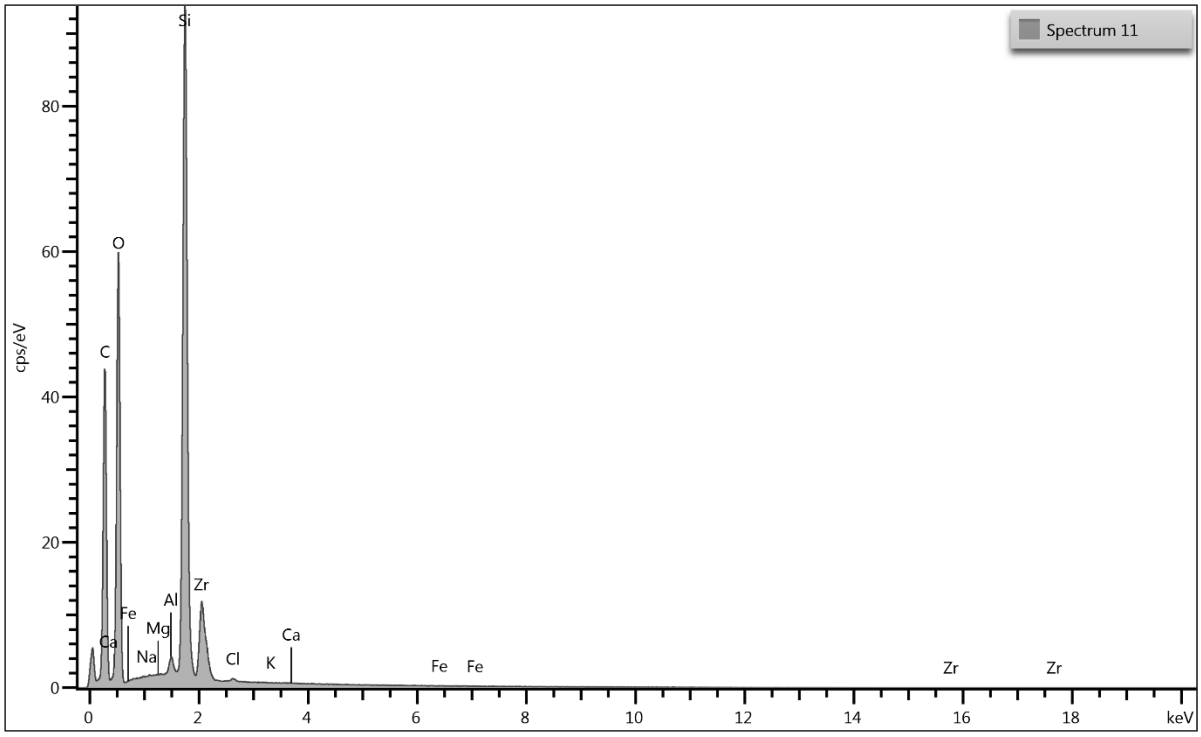
Spectrum 11
cps/eV
keV
Si
O
C
Zr
Fe
Al
Mg
Ca
Na
Cl
K
Ca
Fe
Fe
Zr
Zr

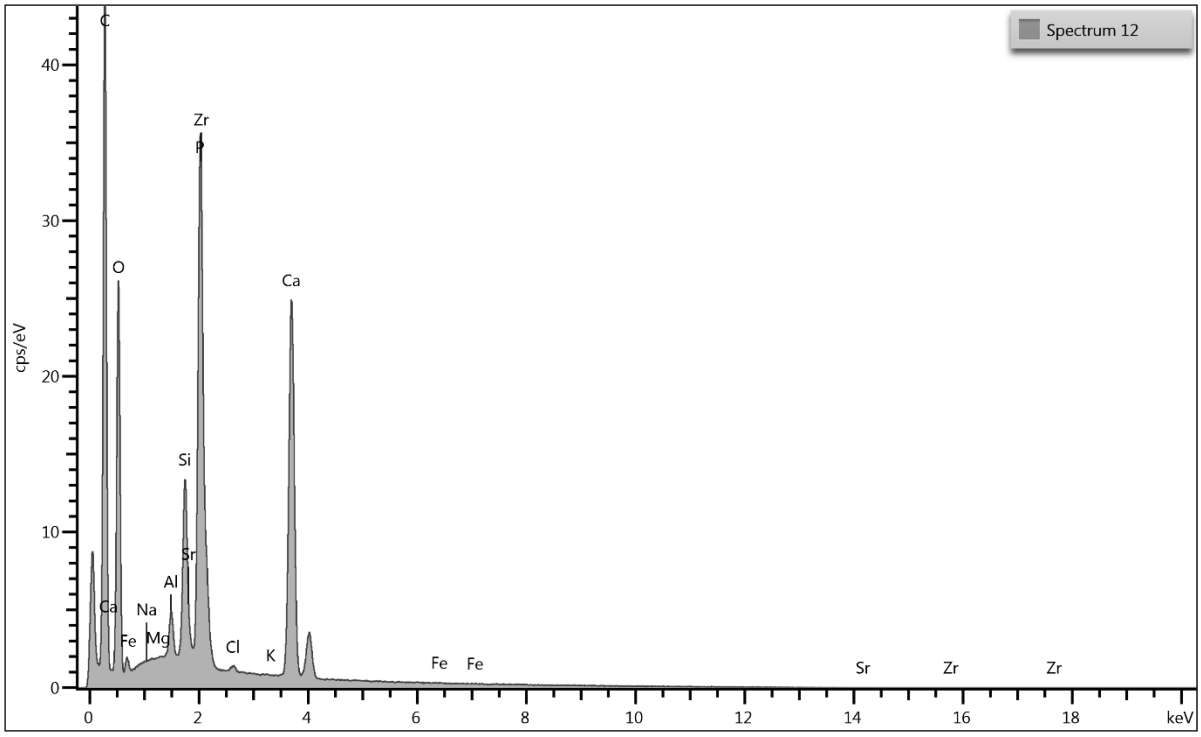
Spectrum 12
cps/eV
keV
C
O
Zr
Ca
Si
Sr
Al
Na
Mg
Fe
Cl
K
Fe
Fe
Sr
Zr
Zr

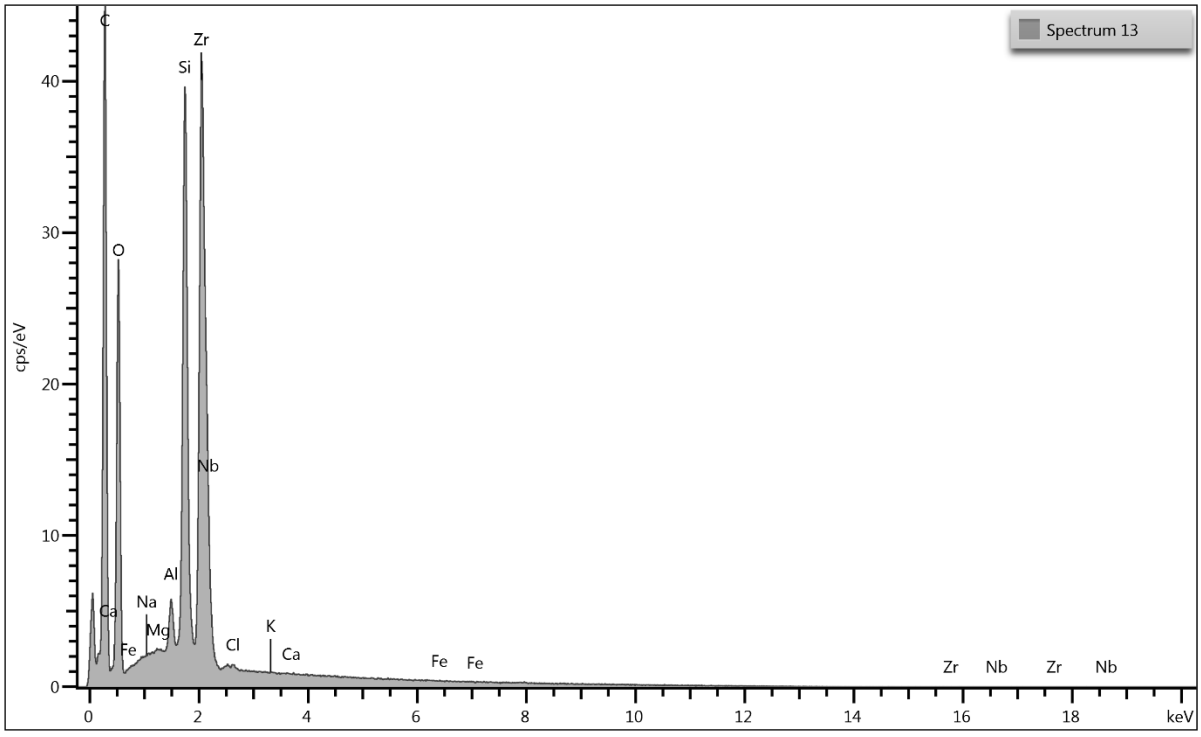
Spectrum 13
cps/eV
keV
C
Zr
Si
O
Nb
Al
Na
Ca
Mg
Fe
Cl
K
Ca
Fe
Fe
Zr
Nb
Zr
Nb

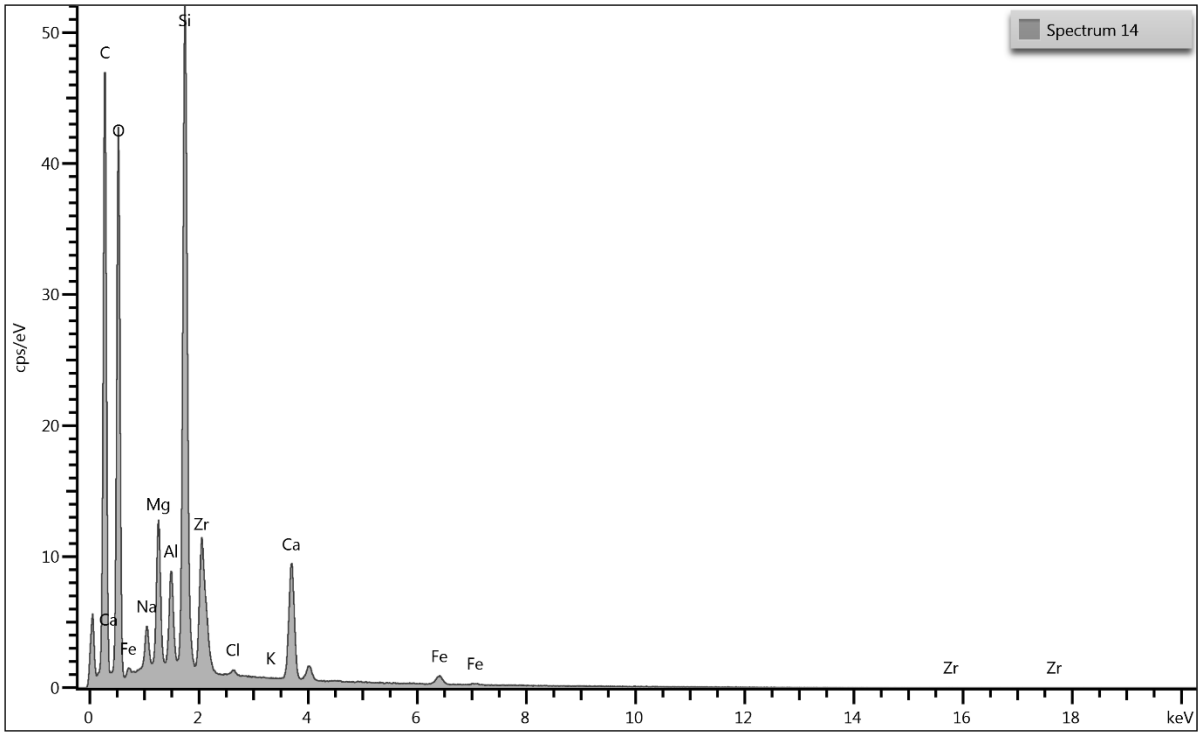
Spectrum 14
cps/eV
keV
C
O
Si
Mg
Al
Zr
Ca
Na
Ca
Fe
Cl
K
Fe
Fe
Zr
Zr

Result Type	Weight %

Spectrum Label	Spectrum 10	Spectrum 14	Spectrum 13	Spectrum 12	Spectrum 11
C	21.10	21.35	21.47	21.01	21.12
O	64.16	65.98	64.71	64.96	67.20
Na	0.00	0.42	0.00	0.00	0.00
Mg	0.00	1.17	0.00	0.00	0.00
Al	0.33	0.71	0.30	0.31	0.20
Si	3.35	4.91	3.15	1.14	8.55
P				2.96	
Cl	0.05	0.06	0.03	0.06	0.05
K	0.00	0.00	0.00	0.00	0.00
Ca	0.03	2.03	0.00	5.82	0.00
Fe	0.00	0.54	0.00	0.00	0.00
Sr				0.21	
Zr	10.81	2.84	10.07	3.53	2.86
Nb			0.27		
Hf	0.17				
Total	100.00	100.00	100.00	100.00	100.00

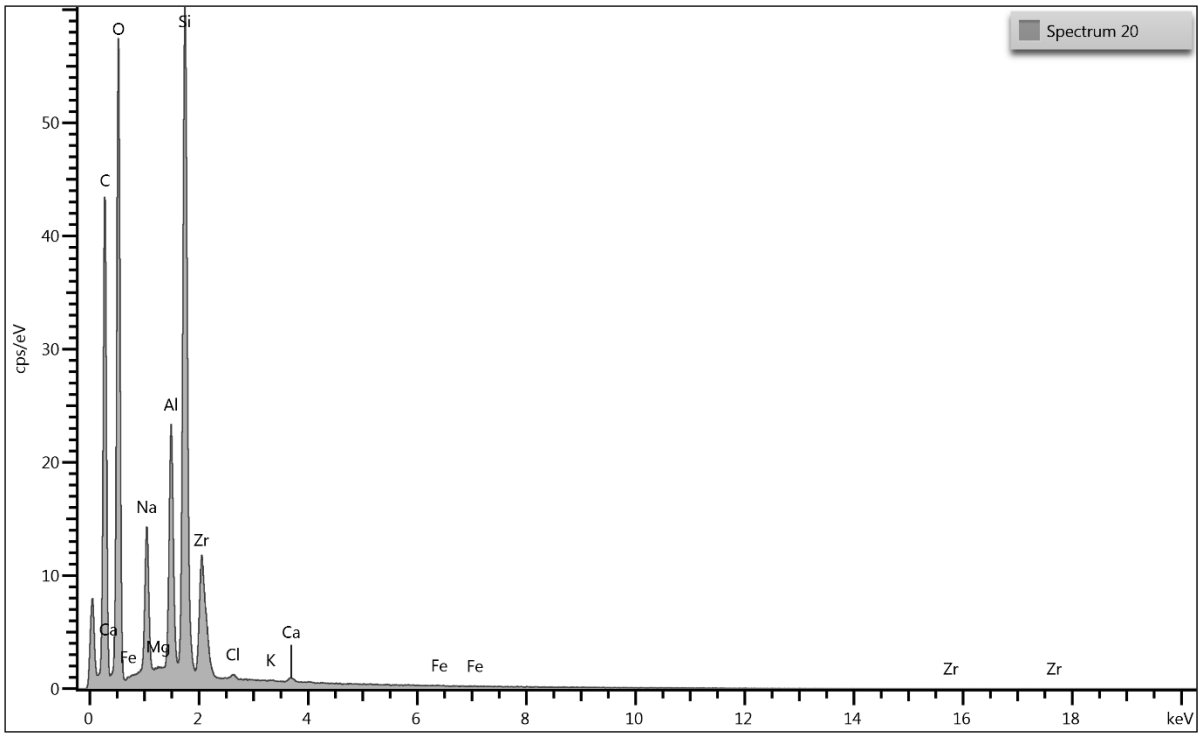
Spectrum 20
cps/eV
keV
O
Si
C
Al
Na
Zr
Ca
Fe
Mg
Cl
K
Ca
Fe
Fe
Zr
Zr

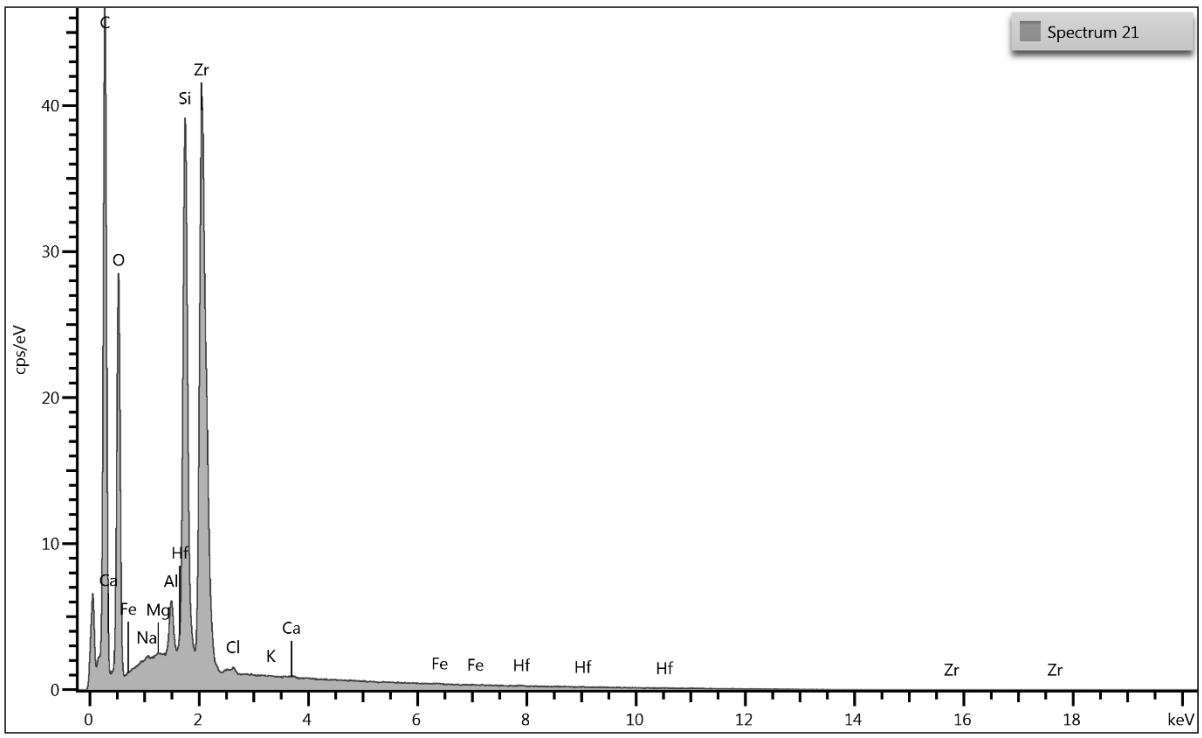
Spectrum 21
cps/eV
keV
C
Zr
Si
O
Hf
Al
Ca
Fe
Mg
Na
Cl
K
Ca
Fe
Fe
Hf
Hf
Hf
Zr
Zr

Result Type	Weight %

Spectrum Label	Spectrum 20	Spectrum 21
C	21.13	21.57
O	66.30	64.87
Na	1.67	0.00
Mg	0.00	0.00
Al	2.08	0.34
Si	5.72	3.18
Cl	0.06	0.05
K	0.00	0.00
Ca	0.08	0.00
Fe	0.00	0.00
Zr	2.96	9.87
Hf		0.13
Total	100.00	100.00

Statistics	C	O	Na	Mg	Al	Si	Cl	K	Ca	Fe	Zr	Hf
Max	22.13	66.30	1.67	0.00	2.08	5.72	0.06	0.00	0.08	0.00	9.87	0.29
Min	21.13	64.87	0.00	0.00	0.31	2.82	0.04	0.00	0.00	0.00	2.96	0.13
Average	21.67	65.49	0.42	0.00	0.76	3.67	0.05	0.00	0.02	0.00	7.74	
Standard Deviation	0.43	0.62	0.84	0.00	0.88	1.37	0.01	0.00	0.04	0.00	3.22	

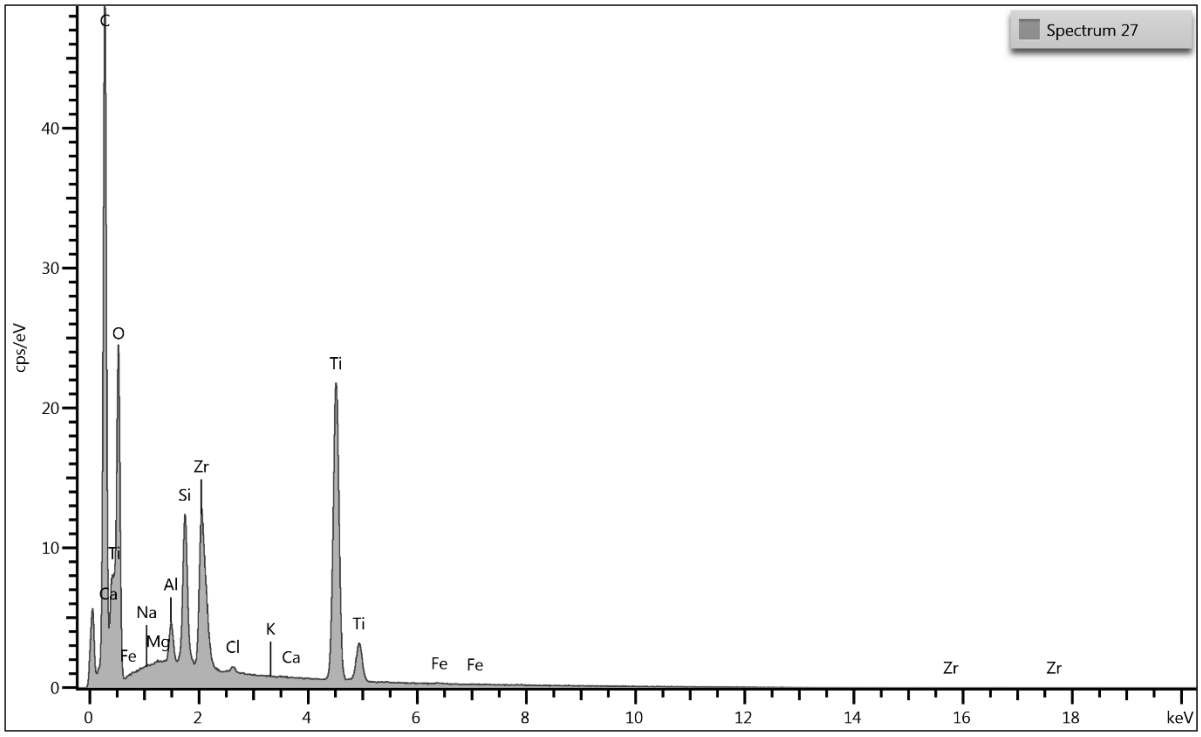
Spectrum 27
cps/eV
keV
C
O
Ti
Ca
Na
Al
Mg
Si
Zr
Fe
Cl
K
Ca
Ti
Fe
Fe
Zr
Zr

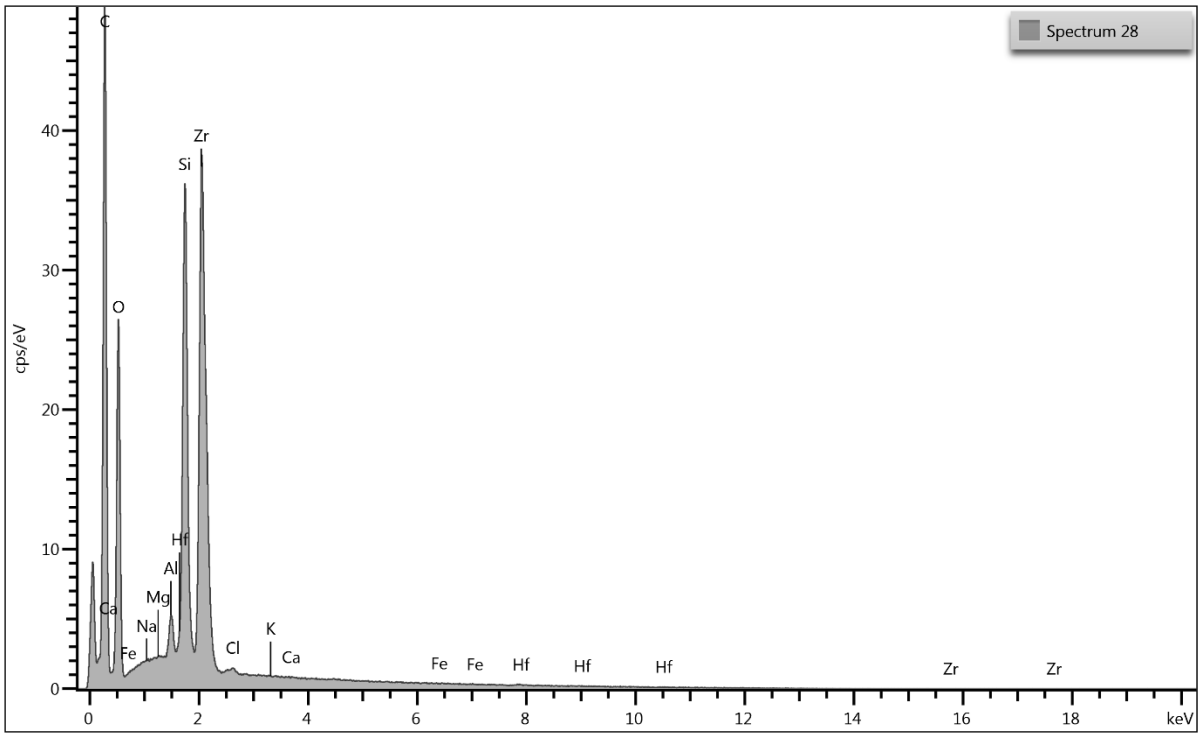
Spectrum 28
cps/eV
keV
C
O
Zr
Si
Hf
Al
Mg
Ca
Na
Fe
Cl
K
Ca
Fe
Fe
Hf
Hf
Hf
Zr
Zr

Result Type	Weight %

Spectrum Label	Spectrum 27	Spectrum 28
C	21.07	21.94
O	64.92	65.29
Na	0.00	0.00
Mg	0.00	0.00
Al	0.33	0.28
Si	1.15	2.91
Cl	0.07	0.05
K	0.00	0.00
Ca	0.00	0.00
Ti	8.87	
Fe	0.05	0.00
Zr	3.56	9.25
Hf		0.28
Total	100.00	100.00

Statistics	C	O	Na	Mg	Al	Si	Cl	K	Ca	Ti	Fe	Zr	Hf
Max	21.94	65.29	0.00	0.00	0.33	2.91	0.07	0.00	0.00	8.87	0.05	9.25	0.28
Min	21.07	64.92	0.00	0.00	0.28	1.15	0.05	0.00	0.00	8.87	0.00	3.56	0.28
Average	21.50	65.11	0.00	0.00	0.30	2.03	0.06	0.00	0.00		0.03	6.40	
Standard Deviation	0.61	0.27	0.00	0.00	0.03	1.25	0.01	0.00	0.00		0.04	4.03	